(Endo)fullerene functionalization : from material science to biomedical applications

Kalman Toth

UNIVERSITY OF STRASBOURG

(Endo)Fullerene functionalization: from material science to biomedical applications

A dissertation presented
by

Kalman Toth

Submitted to

the Doctoral school of Physiscs and Physical Chemistry
University of Strasbourg
In partial fulfilment of the requirements for the degree of

Doctor of Philosophy

Organic Chemistry and Material Science

25th September 2012

The Institute of Physics and Chemistry of Materials of Strasbourg
Department of Organic Materials
CNRS UMR 7504

Members of the committee:
Dr. Teresa Sierra, reporter, University of Zaragoza, Spain
Prof. Robert Deschenaux, reporter, University of Neuchâtel, Switzerland
Dr. Jean Weiss, internal examiner, University of Strasbourg, France
Prof. André-Jean Attias, external examiner, UPMC, Paris, France
Dr. Daniel Guillon, thesis director, ECPM/IPCMS, France
Dr. Delphine Felder-Flesch, thesis co-director, IPCMS, UMR 7504 -CNRS, France

UNIVERSITE DE STRASBOURG

Fonctionnalisation d' (endo)fullerène: de la science des matériaux aux applications biomédicales

Thèse présentée à
L'Ecole Doctorale de Physique et Chimie-Physique
de l'Université de Strasbourg

par

Kalman Toth

Pour l'obtention du grade de

Docteur en Science

Chimie Organique Moléculaire et Chimie des Matériaux

25 Septembre 2012

Institut de Physique et Chimie des Matériaux de Strasbourg
Département des Matériaux Organiques
CNRS UMR 7504

Le jury est composé de :
Dr. Teresa Sierra, rapporteur, Université de Zaragoza, Espagne
Prof. Robert Deschenaux, rapporteur, Université de Neuchâtel, Suisse
Dr. Jean Weiss, examinateur interne, Université de Strasbourg, France
Prof. André-Jean Attias, examinateur externe, UPMC, Paris, France
Dr. Daniel Guillon, directeur de thèse, ECPM/IPCMS, France
Dr. Delphine Felder-Flesch, co-directeur de thèse, IPCMS, UMR 7504 -CNRS, France

Abstract

Nanostructured carbonaceous materials such as empty cage fullerenes and endohedral metallofullerenes (EMFs) offer great potential and play an increasingly important role in applications such as photovoltaic and electronic devices, biocompatible medical diagnostic materials. Among all the possible applications, organic photovoltaics are the most widely studied due to the excellent electron acceptor abilities of most members of the fullerene family. Moreover, the HOMO-LUMO levels of EMFs can be fine-tuned by the choice of encapsulated metal(s) which provides further advantages in solar cell application. Biomaterials development arose from their high stability and the unique properties provided by the encapsulated metal species in case of EMFs.

Our approach to create π-conjugated oligomer-fullerene donor-acceptor (D-A) dyads led to the formation of two different families of photovoltaic materials, based on either oligo(phenylenevinylene) (OPV) or oligo(phenyleneethynilene) (OPE). The liquid crystalline (LC) behaviour, showed by all of the compounds was expected to improve photovoltaic efficiency via ambipolar charge transport. The structure of the mesophases and the supramolecular organization of the ensembles were studied by means of polarized optical microscopy (POM), differential scanning calorimetry (DSC), and small angle X-Ray scattering (SAXS). Apart from the C_{60} based compounds, OPE-Y_3N@C_{80} dyad was also synthesized as the first mesomorphic D-A EMF derivative. Photophysical measurements were conducted to reveal the charge or energy transfer scenarios between the subunits. A light harvesting antenna effect was observed for all OPE-based compounds that resulted in the photosensitization of the fullerene unit. Thus, these liquid crystalline compounds are presumably best used as a blend with appropriate semiconducting polymers for the development of photovoltaic cells and are expected to be able to control the morphology of the prepared film. Preliminary Grazing-incidence small-angle scattering (GISAXS) results confirmed that annealing and/or varying film thickness can induce molecular self-assembly in thin films.

Icosahedral $Gd_3N@C_{80}$ was derivatized with a tetraethylene glycol dendron to provide a safe and more efficient alternative to today's commercially available MRI contrast enhancement agents. The fullerene exohedral reactivity differed tremendously when the structure of the dendron was changed.

Acknowledgments

I want to express my gratitude to my supervisors Dr. Delphine Felder-Flesch and Dr. Daniel Guillon for giving me the opportunity to conduct my PhD research at the IPCMS Department of Organic Materials (DMO) in Strasbourg and for all their help, guidance and encouragement during my stay. I would also like to thank Delphine for her flexible attitude to research projects and for giving me the freedom to carry out research which was a great asset to me.

Also, I would like to thank Prof. José L. Serrano, project coordinator, for allowing me to participate in the "Dendreamers" project, to Dr. Jean-Louis Gallani, department leader, and to Dr. Jean-Pierre Bucher, director of the "Ecole Doctorale de Physique et Chimie-Physique" of the Strasbourg University, for allowing me to perform the work in the DMO laboratories and to carry out my PhD studies at the doctoral school.

I cannot exaggerate enough my gratefulness to Dr. Benoît Heinrich for all his contributions to the liquid crystalline part of the thesis, which has enabled me to broaden my knowledge in this area and for being available day and night, literally. I have to say thank you to Prof. Paola Ceroni and Jennifer Molloy from the Univerity of Bologna in Italy for the fruitful collaboration, for revealing the exciting photophysical properties of the compounds and for being available for discussions.

I would also like to thank Prof. Thomas Heiser, Nicolas Zimmermann and Peter Lienerth at INESS for allowing me to use different instruments in their institute, for testing my materials and for being always friendly and welcoming. I am grateful to Dr. Stephan Haacke and Thomas Roland at IPCMS-DON for performing experiments on my materials and for the discussions on photophysics.

I would also like to thank my committee members: Dr. Teresa Sierra, Prof. Robert Deschenaux, Prof. Jean Weiss and Prof. André-Jean Attias.

I would like to thank the assistance provided by Didier Burger (DCMI) for the TGA measurements and for the expertise of Jean-Marc Strub (ECPM) in MALDI-ToF analysis.

I thank the technical stuff of the DMO: first of all, Emilie Voirin for her help around the lab and for synthesizing a few intermediates to me, and also Emilie Couzigne, Nicolas

Beyer and Rose-Marie Weller for helping me in the everyday life at IPCMS-DMO. I thank also my colleagues, PhD students and Postdocs of the department: Antonio for always being happy, Edith and George for helping with the HPLC, Cynthia for advice in organic chemistry, Marie, P.O., Audrey, Carlos, Christina…

Many thanks to my partner (and colleague), Zsuzsa, who continuously supported me, helping me in different research problems and most importantly stuck with me for many years now.

I am very grateful to John R. Fyson, also known as Monty, for accepting to correct my "Franglais" and for spending so much of his free time with it.

I thank all of my family and friends.

And finally, I thank everyone else who did not try to hinder me (or at least not too much) in my research work.

Table of Content

List of Abbreviation

[60]Fullerene	C_{60}
AIBN	Azobisisobutyronitrile
Ac	Acetone
BHJ	Bulk heterojunction
tBuOK	Potassium-tert-butoxide
Col	Columnar phase
D-A	Donor-acceptor
DBU	1,8-Diazabicycloundec-7-ene
o-DCB	o-Dichlorobenzene
DCC	N,N'-Dicyclohexylcarbodiimide
DCM	Dichloromethane
DCU	N,N'-Dicyclohexylurea
DIPEA	N,N-Diisopropylethylamine
DMA	9,10-dimethylanthracene
DMF	Dimethylformamide
DPTS	4-(Dimethylamino)pyridinium 4-toluenesulfonate
DSC	Differential scanning calorimetry
EA	Elemental analysis
EMF	Endohedral metallofullerene
EPR	Electron paramagnetic resonance
Et_3N	Triethylamine
EtOAc	Ethyl acetate
EtOH	Ethanol
ex-TTF	π-extended tetrathiafulvalenes
Fc	Ferrocene
G	Glassy state
GISAXS	Grazing-incidence small-angle scattering
GPC	Gel permeation chromatography
HOMO	Highest occupied molecular orbital

HPLC	High pressure liquid chromatography
I	Isotropic liquid
I_h	Icosahedral
IPR	Isolated pentagon rule
K	Crystalline
LC	Liquid crystal
LUMO	Lowest unoccupied molecular orbital
$M_3N@C_{80}$	M_3N cluster in the interior of the C_{80} cage, where M is a metal
MeOH	Methanol
MRI	Magnetic Resonance Imaging
N	Nematic phase
NBS	*N*-bromosuccinimide
NMR	Nuclear magnetic resonance
OPE	Oligo(phenyleneethynylene)
OPV	Oligo(phenylenevinylene)
P3HT	Poly(3-hexylthiophene)
PCBM	Phenyl-C_{61}-butyric acid methyl ester
POM	Polarized optical microscopy
4-ppy	4-Pyrrolidinopyridine
RT	Room temperature
SAXS	Small-angle X-ray scattering
Sm	Smectic phase
TBAF	Tetra-*n*-butylammonium fluoride
$TBAPF_6$	Tetrabutylammonium hexafluorophosphate
TBDMS	T*ert*-Butyldimethylsilyl
TBDMSCl	tert-Butyldimethylsilyl chloride
TEG	Tetra(ethylene glycol)
TGA	Thermogravimetric analysis
THF	Tetrahydrofuran
TLC	Thin layer chromatography
TNT	Trimetallic nitride template

TsCl	Tosyl chloride
TTF	Tetrathiafulvalenes
UV-Vis	Ultraviolet-Visible
XRD	X-Ray diffraction

Chapter I

General Introduction

This chapter gives an overview of empty cage fullerenes and endohedral metallofullerenes (EMF), which are fullerenes that encapsulate metals in their interior. Their intriguing photophysical and electrochemical properties are discussed and special attention is devoted to their derivatization which is usually necessary for practical applications.

It is also an introduction to thermotropic liquid crystals (LCs), together with the structural classification of the mesophases and the techniques used for their identification, namely polarized optical microscopy (POM), differential scanning calorimetry (DSC) and small angle X-Ray scattering (SAXS).

I.1) Fullerenes

Fullerenes were discovered in 1985 by H. W. Kroto, R. F. Curl and R. E. Smalley [1], who were awarded the Nobel Prize in Chemistry for this work in 1996. After graphite and diamond it is the third form of carbon; furthermore it is the first known molecular form of carbon. While the two former varieties are solid state structures with two and three dimensional networks of undefined atoms, fullerenes are spherical, hollow molecular allotropes of carbon. The first synthesized and still the most stable and abundant member, C_{60}, has the shape of a football ball (soccer ball in the US). It is also called Buckminsterfullerene, named after the architect Buckminster Fuller, whose geodesic domes it resembles (Figure 1). The homologous series of fullerenes is continued with the discovery of smaller and higher fullerenes: constituted of 28 to hundreds of carbon atoms. Furthermore, its discovery led to other important breakthroughs in carbon nanoscience, including the discovery of carbon nanotubes and graphene (i.e. a single layer graphite sheet). Thus, unlike other states of carbon, the molecular nature of fullerenes focuses the imagination of chemists on specific and delineated forms. The ability to synthesize thousands of molecules with interesting properties seemed exciting. Nevertheless, the scientific and technological developments related to the study of fullerenes would be made possible by the development of a method of synthesis of these new carbon allotropes, and in macroscopic quantities.

Figure 1, Buckminster Fuller in front of a geodesic dome.

Fullerenes consist of fused pentagons and hexagons. Most stable allotropes follow the isolated pentagon rule (IPR): all pentagons are surrounded and isolated by hexagons. Fused pentagons cause local steric strain, therefore destabilize fullerenes, as it was explained by Kroto[2]. For example, C_{60} is made of 12 pentagons and 20 hexagons and obeys the IPR rule. The geometry of the molecule is that of a regular truncated icosahedron, where all the carbon atoms are equivalent (Figure 2, Figure 3). On the other hand, the bonds at the junctions of two hexagons – [6,6] bonds – are shorter than the ones at the pentagon-hexagon – [5,6] bonds – junctions, because the [6,6] bonds have more double-bond characteristics. For that reason, C_{60} is not a super aromatic compound although all the carbon atoms are conjugated.
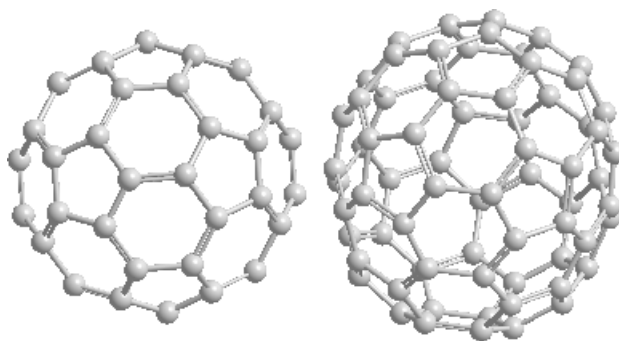
Figure 2, Ball and stick model of C_{60} and C_{70}, the most abundant fullerene homologues.
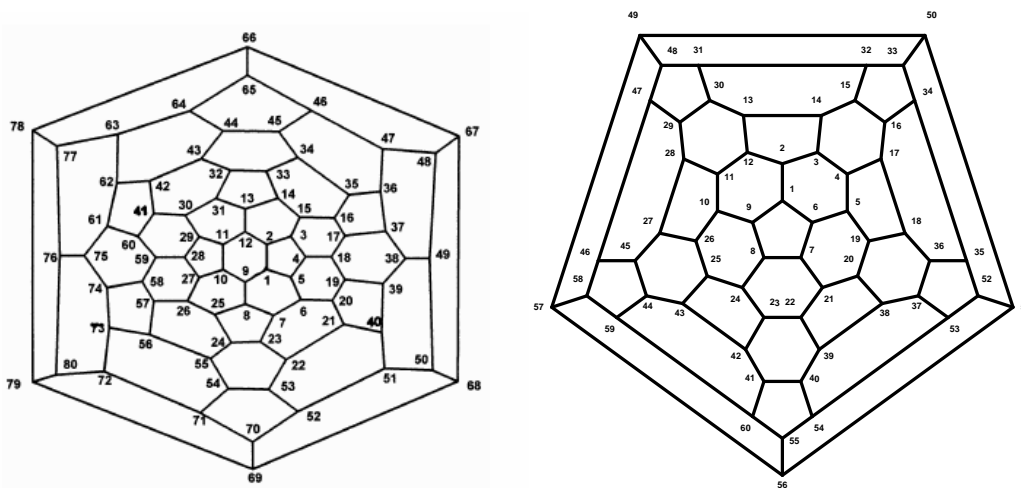
Figure 3, Schlegel diagram of I_h C_{60} (left) and I_h C_{80} (right) cages.

The hollow internal space of fullerene molecules is suitable for encapsulating a wide range of atoms, molecules and even otherwise instable species, clusters. We call these molecules endohedral fullerenes. Their discovery soon followed the discovery of C_{60}; the

4

mass signal of La@C_{60}[3], prepared by the laser vaporization of a $LaCl_2$ impregnated graphite rod, was observed. The first isolated endohedral fullerene was La@C_{82} in 1991[4]. The symbol @ is used to indicate the atoms in the interior of the fullerene cage. Since then, a large variety of endohedral fullerenes have been prepared and their unique properties, arising from the interaction between encaged species and the cage, have been investigated[5,6]. It is possible to encage non-metals, including noble gases[7], nitrogen[8] and phosphorus[9] in a C_{60} cage, which encapsulated elements stabilized in their atomic forms. Endohedral metallofullerenes (EMFs) can be created by encapsulating metal species. These materials have been extensively studied, because the encaged metal species directly interact with the surrounding cage and change its electronic structure. EMFs can be classified according to the number and type of the encaged metal species: mono-, di- and cluster EMFs.

- Mono EMFs are the simplest type, with only one metal atom encaged in the internal vacancy of fullerene. The most abundant examples can be described with the M@C_{82} formula. The single metal moves off-center and coordinates strongly to the cage affecting the charge density and causes cage curvature anisotropy[10].
- Di EMFs are filled with two freely rotating metals[11] inside the cage which usually consists of 80 carbons.
- Cluster EMFs. Metallic oxide[12], carbide-[13] or nitride clusters[14] encapsulated in the interior of the fullerene constitute another class of EMF. The latter type, often referred as a trimetallic nitride template (TNT) EMF, became the most popular due to its high stability and abundance in fullerene soot. The first TNT EMF was prepared by Dorn and coworkers[15] in 1999 by enclosing Sc_3N cluster into a I_h C_{80} cage (Figure 4). Neither the metallic nitride cluster nor the I_h C_{80} carbon cage have been prepared independently, but together they form a very stable molecule as a consequence of mutual stabilization.

EMFs, these novel metal-carbon hybrid materials, offer a broad range of properties of potential use in different fields such as materials science, photovoltaics and biomedicine. Gadolinium based EMFs have been widely studied due to their magnetic contrast-enhancing properties and thus have potential applications in magnetic resonance imaging (MRI)[16]. Paramagnetic or radioactive elements can be entrapped into the relatively inert carbon cage thus allowing EMFs to be used as radiotracers[17,18] or chemotherapeutics[18,19]. On the other

hand, their intriguing electronic properties combined with their low and tunable HOMO-LUMO gaps can be exploited in molecular electronics and donor-acceptor photovoltaic systems[20,21,22]. The potential use of EMFs for material science and as MRI contrast agents will be discussed in more details in Chapters II and III, respectively.
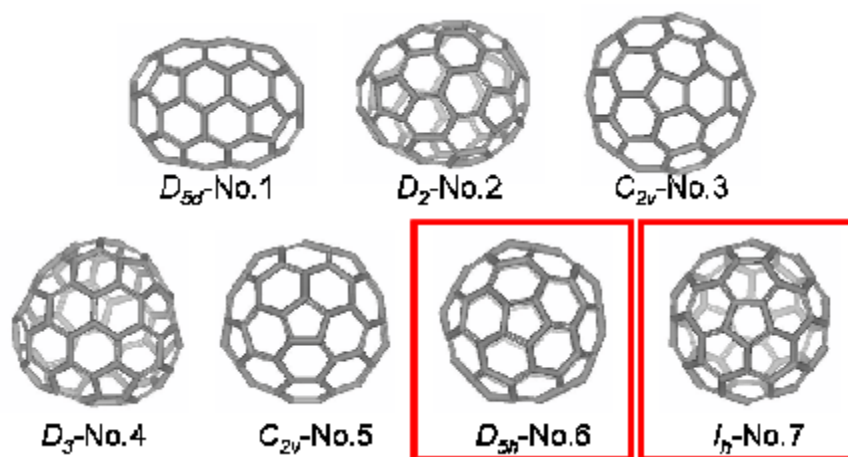
Figure 4, Empty-cage IPR constitutional isomers of C_{80} arranged by thermodynamic stability. Red boxes surround cage isomers that have been experimentally found to encapsulate trimetallic nitride clusters from which the I_h cage is more abundant[23]. (Bevan Craig Elliott PhD Thesis, 2008, Clemson University)

I.1.1)   Fullerene production

Fullerenes were produced in bulk quantities from 1990 by the Hufmann–Krätschmer arc-discharge method[24] (Figure 5), in which graphite electrodes are evaporated via resistive heating in a helium atmosphere of 100-200 mbar. A modified version of this apparatus[25] uses arc-discharge for the vaporization of graphite and appeared to be slightly more efficient for producing fullerenes. The resulting soot can contain only up to 10-15% in weight of fullerenes, but these can be easily isolated from the rest of the soot by extraction with organic solvents.
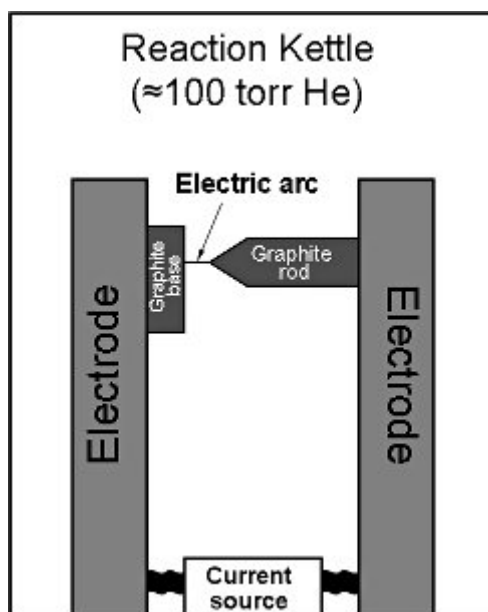
Figure 5, Schematic diagram of the contact-arc apparatus used to generate macroscopic quantities of C_{60}[26].

The combustion process[27] produces fullerenes in optimized sooting flames. Notable amounts of C_{60} and C_{70} fullerenes were produced, in varying amounts, from premixed laminar benzene/oxygen/argon flames operated under different pressures, temperatures and carbon-to-oxygen ratios. Further optimization of this flame-based technology is most suited for the mass production of fullerenes, since it is a continuous process and uses inexpensive hydrocarbons as starting materials, which is similar to that employed in a commercial carbon black production process. Fullerene yield in the resulting soot is now around 20%, which demonstrates that the combustion method is a practical technology for fullerene-soot production. This remarkable development has led to the ton scale production and plunging prices of fullerenes, so thus made them available for commercial use.

The organic synthesis of C_{60} is also possible via pyrolytic dehydrogenation or dehydrohalogenation of naphthalene, corannulene, 7,10-bis(2,2'-dibromovinyl)fluoranthene, and 11,12-benzofluoranthene[28]. These polyarenes can be submitted to flash vacuum pyrolysis at 1100 °C or high energy laser to form fullerenes (Figure 6), but the yields are low and this process is not suitable for mass production.
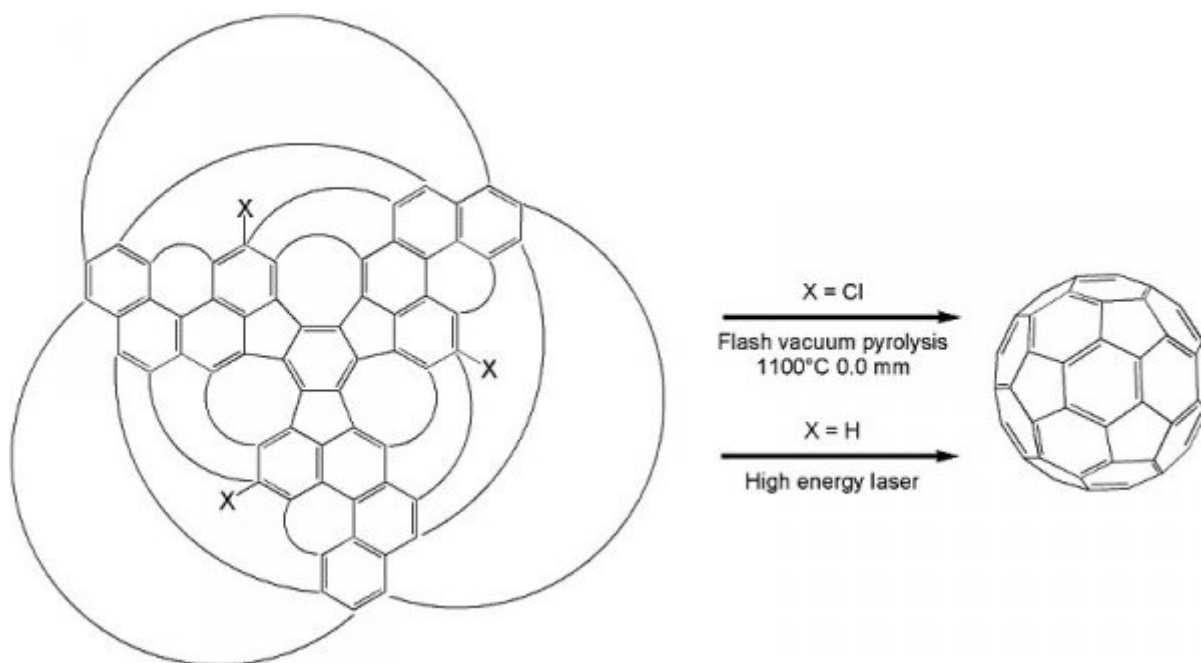
Figure 6, Final step in the synthesis of C_{60}. Curved lines indicate where the new bonds are formed[26].

Recently, researchers have discovered a method that produces the buckyball C60 configuration with nearly 100% conversion efficiency from aromatic precursor materials using a highly efficient surface-catalyzed cyclodehydrogenation process[29]. When depositing polycyclic aromatic precursors onto a platinum surface by chemical vapor deposition (CVD) technique and heating to 750 K, the precursors are transformed into the corresponding fullerene and triazafullerene molecules (C_{60} and $C_{57}N_3$, respectively) with close to 100% yield.

The process for producing EMF's is not very different from that of empty cage fullerenes. The most commonly used technique is the Hufmann–Krätschmer arc-discharge method equipped with metal oxide or metal alloy packed graphite rods as anodes. It has been discovered, that the presence of nitrogen gas in the arcing atmosphere gives rise to the formation of TNT EMFs, including $Sc_3N@C_{80}$[15] (Figure 7), which became the third most abundant member of the fullerene family after C_{60} and C_{70}.
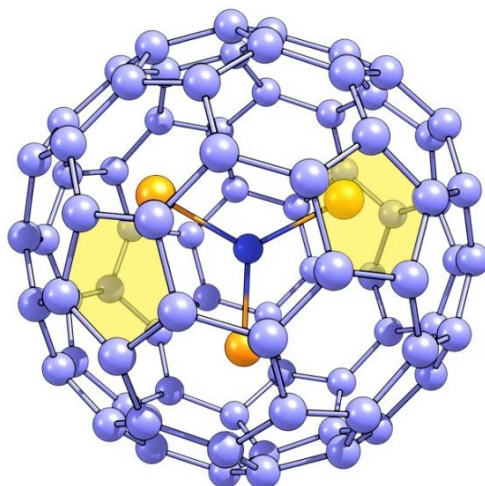
Sc₃N@Iₕ-C₈₀

Figure 7, Molecular structure of I_h Sc$_3$N@C$_{80}$.

I.1.2) Isolation and purification

The raw outcome of most production techniques is soot, meaning a mixture of C_{60}, C_{70}, higher fullerene homologues, nanotubes[30] and amorphous carbon. Fullerenes containing less than 100 carbon atoms can be extracted[24,31] with toluene. Repeated chromatography on neutral alumina allows separation of C_{60}, C_{70} and higher fullerenes, which are subjected to high pressure liquid chromatography (HPLC) afterwards. At the end of the purification process, C_{60} and C_{70} are the major compounds obtained from the soot in 73 and 23% yield, respectively, a variety of molecules larger than C_{60} and C_{70} representing a total amount of 3 to 4% by weight. The whole separation and isolation protocol is summarized in Figure 2.
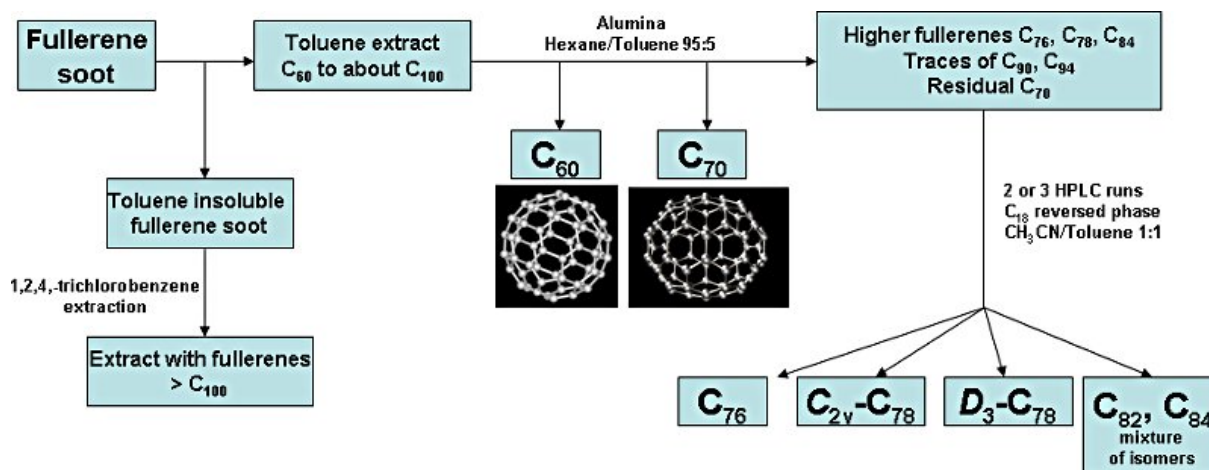
Figure 8, Separation and isolation protocol of fullerene soot[32].

The purification of EMF's requires multistage HPLC separation method (usually equipped with special (ie. Buckyprep columns), due to their low abundance relative to C_{60} and C_{70}, and the presence of numerous structural isomers in the soot with similar retention factors. To make the process less costly and time consuming, several elegant methods have been developed for the selective separation of EMFs from the soot based on a cyclopentadiene-functionalized resin[33], amine-functionalized silica gel[34] or the selective oxidation of the different isomers[35].

I.1.3)   Photophysical properties

The UV-Vis spectrum of pristine C_{60} extends from the UV to the near IR and covers the entire visible region with low intensity bands. A strong band region exists between 200 and 350 nm, containing three intense bands with maxima at 211, 256 and 328 nm. These are the orbitally allowed transitions of C_{60}, from the HOMO to the LUMO+1 and from the HOMO−1 to the LUMO energy levels. A spectral region extending from 350 to 430 nm containing weaker bands with most of the intensity generated by transitions to the lowest (LUMO) state (still allowed state). Above 430 nm up to 640 nm, a series of very weak, symmetry forbidden bands can be observed associated with the lowest energy HOMO to LUMO transition.[36]

The main characteristics of mono- and multiadducts are the following: between 200 and 410 nm there are orbitally allowed transitions of C_{60}, from the HOMO to the LUMO+1

and from the HOMO−1 to the LUMO, only slightly different from C_{60} due to symmetrical deviations. A second region around 430 nm is characterized by a sharp band whose assignment is still uncertain. This band is absent in the pristine C_{60} spectrum and it is typical of most mono- and multiadducts. At 440–510 nm and 510–570 nm there are two broad features related to the regions of the C_{60} UV-Visible spectrum. In the long-wavelength region between 600 and 710 nm there are several weak absorption bands or shoulders, interpreted as vibronic components belonging to the lowest HOMO–LUMO transition[37]. Thus, the UV-Vis spectra of pristine C_{60} and its derivatives are usually very similar in the UV-region. The main perturbing effect on the electronic structure of additions to the C_{60} can be observed above 380 nm due to sp^2 to sp^3 hybridization on the fullerene cage. When TNT EMFs are studied, these differences can be assigned to regioaddition on the I_h-C_{80} cage[38].

Upon photoexcitation, the singlet excited state decays are dominated by intersystem crossing to the lower lying triplet excited state. Consequently, C_{60} is a faint fluorophore, with a very low fluorescence quantum yield of $3.2*10^{-4}$ and a fluorescence maximum of around 705 nm at room-temperature in toluene[39]. The C_{60} triplet excited state sensitizes the formation of singlet molecular oxygen, the population of which can be followed by monitoring its phosphorescence emission at 1268 nm^{-1} in solution[40]. In deoxygenated media however, the triplet excited state of C_{60} is deactivated by slow non-radiative decay - including intersystem crossing, self-quenching, and triplet-triplet annihilation - back to the singlet ground state[41].

Due to the low reorganization energy of the rigid fullerene core in electron transfer reaction, C_{60} accelerates charge separation and retards charge recombination compared to planar electron acceptors. The covalent binding of fullerene, as a feasible electron acceptor (see next section), to electroactive donor molecules, such as conjugated oligomers and polymers or even their simple physical mixture, can lead to the development of photovoltaic devices.

Optical limiting is an optical nonlinear phenomenon which implies the increase of optical absorption as the incident radiation intensity increases. One of the possible mechanisms is the reverse saturable absorption, which is characteristic of materials with singlet and triplet excited states absorbing more strongly than the ground state. The excited states (especially the triplet excited state) of C_{60} show stronger absorption in the visible

region than its ground state. This effect combined with the relatively long excited state lifetimes and efficient intersystem crossing indicate that fullerenes are good candidates for optical limiting applications[42] (Figure 9).
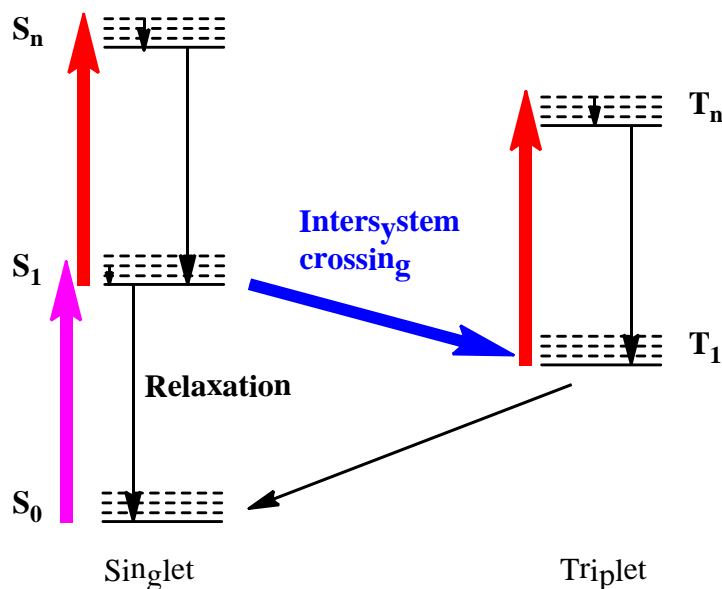
Figure 9, Efficient intersystem crossing and strong absorption of the triplet excited state makes C_{60} useful material as optical limiter.

I.1.4)   Electrochemical properties

I.1.4.1)   Empty cage fullerenes

Theoretical calculations suggested that the LUMO and LUMO + 1 levels of C_{60} are low-energy, triply degenerated molecular orbitals[43] (Figure 10). Thus, C_{60} was predicted to be a fairly electronegative molecule that is able to accept up to six electrons. Indeed, cyclic voltammetry studies exhibited six, stepwise, reversible reduction waves, which correspond to the formation of the mono- to hexaanion[44] (Table 1). The higher fullerene homologue C_{70} shows analogous behavior; indeed six reduction waves at comparable potentials have been reported[45]. The electrochemistry of higher fullerenes was also investigated[44], but they show complicated reduction waves due to the presence of different isomers.

The good electron accepting abilities of empty cage fullerenes fostered their incorporation into devices in materials science. Indeed, the development of fullerene based

bulk heterojunction (BHJ) or donor-acceptor (D-A) photovoltaic devices have been in the focus of scientific interest for the past two decades.
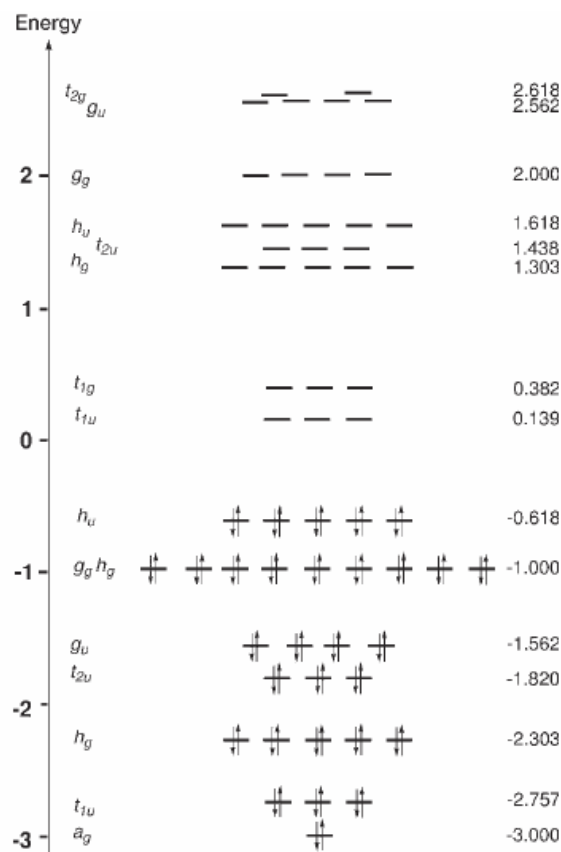
Figure 10, Molecular orbital energy diagram of C_{60}.

Table 1, Half-wave reduction potentials ($E_{1/2}$) of C_{60} in acetonitrile-toluene mixture with $TBAPF_6$ as supporting electrolyte at -10°C at 100 mV s^{-1} scan rate. a) V vs Fc^+/Fc

Reduction step	Reduction potential[a]
C_{60}/C_{60}^-	-0.98
C_{60}^-/C_{60}^{2-}	-1.37
C_{60}^{2-}/C_{60}^{3-}	-1.87
C_{60}^{3-}/C_{60}^{4-}	-2.35
C_{60}^{4-}/C_{60}^{5-}	-2.85
C_{60}^{5-}/C_{60}^{6-}	-3.26

The anodic behavior of C_{60} is usually less pronounced, as its irreversible one-electron oxidation potential is highly positive (E_0 ox = 1.26 V vs Fc/Fc^+ in trichloroethane and E_0 ox = 1.76 V vs SCE in benzonitrile), thus the use of very strong oxidants are required to oxidize 60[Fullerene][46].

I.1.4.2) TNT EMFs

It has been proven, that electron transfer from the cluster to the C_{80} cage stabilizes TNT EMFs[47,48]. Despite the high negative charge on the cage (-6), all $M_3N@C_{80}$ could be reduced in at least three irreversible steps and oxidized in two distinct steps, from which the first is reversible even at low scan rates in o-dichlorobenzene (o-DCB). However, the nature of the cluster metal has a notable influence on the reduction potentials and a less-marked influence on the oxidation potentials (see Table 2). The case of $Sc_3N@C_{80}$ seems unique, since this compound has a significantly lower reduction potential than the others. The electron paramagnetic resonance (EPR) spectrum of the $Sc_3N@C_{80}$ radical anion[49], together with quantum calculations suggested a major contribution of the cluster to the LUMO[50]. For the other TNT EMFs, presumably there is no significant contribution from the cluster to either the LUMO or the HOMO[48,50a].

Interestingly, the electrochemical behavior of TNT EMF monoadducts dramatically depends on the addition site. It has been found, that most [5,6] adducts exhibit reversible, while [6,6] adducts irreversible cathodic electrochemical behavior similar to the $M_3N@C_{80}$ precursor[51].

Table 2, Relevant redox potentials (in V versus Fc^+/Fc) of I_h $M_3N@C_{80}$ compounds and some of their cycloadducts[52].

Compound	$E_{1/2}$ ox$_1$[a]	E_p red$_1$[a]	E_p red$_2$[a]	ΔE_{gap}[a]	reference
$Sc_3N@C_{80}$	0.57-0.62	-1.22 to -1.29	-1.56 to -1.62	1.84-1.88	51, 53
$Y_3N@C_{80}$	0.64	-1.41	-1.83	2.05	51
$Lu_3N@C_{80}$	0.64	-1.40		2.04	54
$Er_3N@C_{80}$	0.63	-1.42	-1.80	2.05	51
$Gd_3N@C_{80}$	0.58	-1.44	-1.86	2.02	55

[5, 6]-pyrrolidino-Sc$_3$N@C$_{80}$	0.62[b]	-1.18	-1.57	51
[5, 6]-Diels-Alder-Sc$_3$N@C$_{80}$	0.62[b]	-1.16	-1.54	51
[5, 6]-pyrrolidino-Y$_3$N@C$_{80}$		-1.30	-1.65	51
[6, 6]-pyrrolidino-Y$_3$N@C$_{80}$	0.65[b]			51
Gd$_3$N@C$_{80}$-[C(CO$_2$Et$_2$)]	0.58[b]	-1.39	-1.83	56
Gd$_3$N@C$_{80}$-[C(CO$_2$Et$_2$)]$_2$	0.59[b]	-1.40	-1.88	56

[a] E_p denotes the peak potential and $E_{1/2}$ half-wave potential. $\Delta E_{gap} = E_{1/2}$ ox$_1$- E_p red$_1$.
[b] Based on the endohedral cage.

I.1.5) Chemical reactivity of fullerenes

Not only their unusual appearance, but also the intriguing physical, photophysical and electrochemical properties of fullerenes have moved them into the focus of scientists' interest. But C$_{60}$, and other members of the family are difficult to handle due to their sparing solubility in most organic solvents. For that reason, their exohedral functionalization while maintaining their electrochemical and photophysical properties became more and more important. A major driving force of fullerene chemistry is the relief of strain energy accomplished by sp^2 to sp^3 hybridization of cage carbons at the addition site[57]. It is therefore reasonable to assume that additions preferably take place at sites with the highest degree of pyramidalization[57,58]. The electrochemical properties of empty cage fullerenes predict easy reduction of the carbon sphere with electropositive metals such, as alkali and alkaline earth metals, and suggest the possibility of nucleophilic addition to the fullerene cage. The most common and most popular techniques for derivatization of fullerenes are summarized in the forthcoming subchapters.

I.1.5.1) Cyclopropanation: the Bingel reaction

The Bingel procedure[59] describes the formation of methanofullerene from fullerene and bromomalonate in the presence of a base via an addition-elimination reaction. The first step is the deprotonation of bromomalonate by the base, and then the resulting α-halomalonate anion attacks the electron deficient fullerene double bond (typically a [6,6]

bond in case of C_{60} and other empty cage fullerenes). The last step is an intramolecular nucleophilic substitution of the halide by the anionic center generated on the fullerene core to give the cyclopropanated product (Scheme 1A). Slightly modified procedures introduced by A. Hirsch and F. Diederich take advantage of the *in situ* generation of the halomalonate in the presence of iodine[60] or CBr_4[61] and a base (usually 1,8-Diazabicyclo[5.4.0]undec-7-ene (DBU)) (Scheme 1B). The Bingel reaction is one of the most wildly used methods for the functionalization of fullerenes due to the relatively mild conditions and high achievable yields.
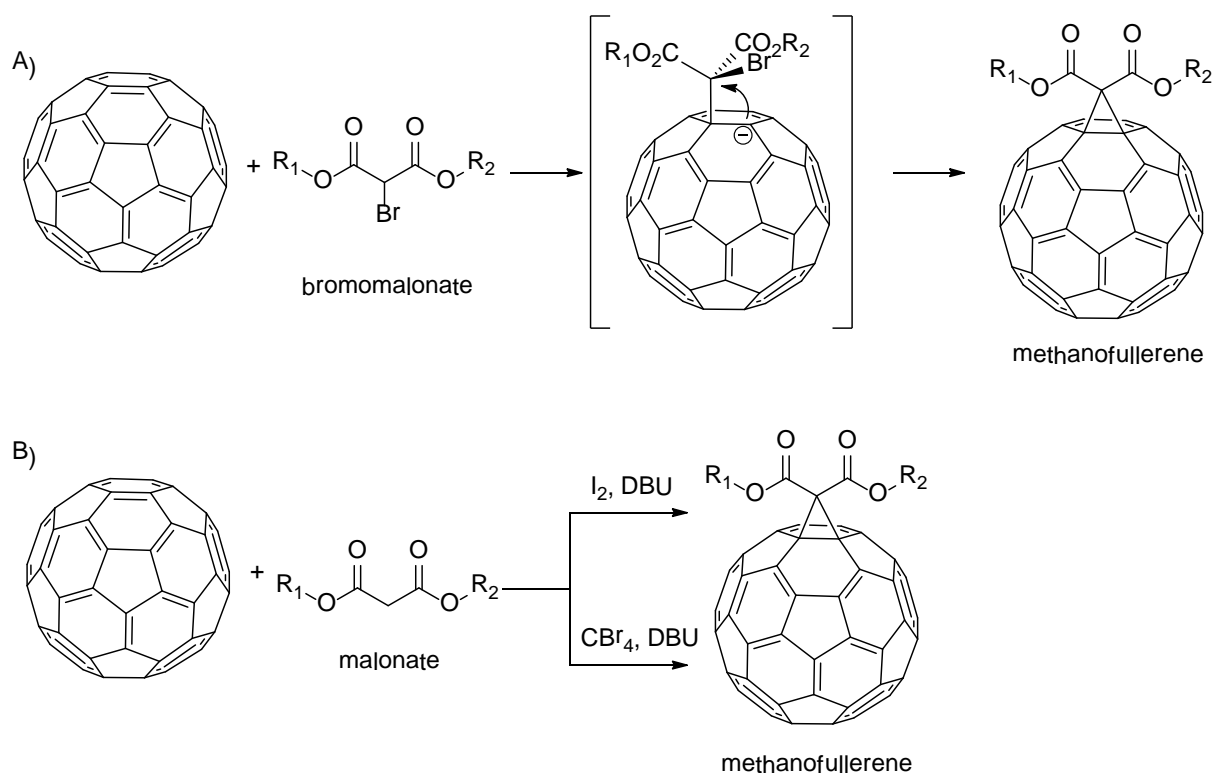
Scheme 1A, Bingel reaction mechanism. **B,** "One pot" synthesis of methanofullerene through Bingel type cyclopropanation.

Exhaustive electrolytic reduction at constant potential can eliminate the methanoaddend(s) to give back the starting materials. This method is called the retro-Bingel reaction[62].

I.1.5.2)   [4+2] Cycloadditions: Diels–Alder Reaction

The [6,6] double bonds of [60]fullerene are excellent dienophiles and therefore, C_{60} can react with different dienes by Diels–Alder cycloaddition reaction[63]. The conditions for cycloadduct formation strongly depend on the reactivity of the diene. Most [4+2] cycloadditions with C_{60} are accomplished under thermal conditions, but photochemical and microwave irradiated[64] reactions have also been reported. Equimolar amounts of cyclopentadiene and C_{60} react even at room temperature to give the monoadduct in good yield[65], while the reaction with anthracene requires an excess of the diene in refluxing toluene[65b] for successful isolation of the monoadduct (Scheme 2).
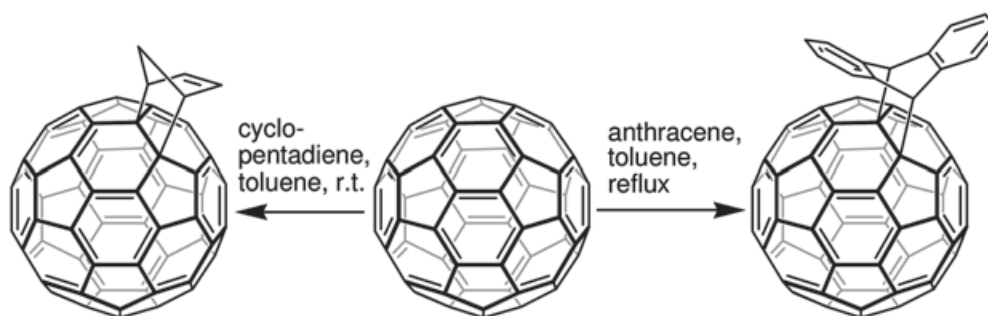
Scheme 2, Diels-Alder cycloadduct formation of C60 with different dienes: cyclopentadiene and anthracene, respectively[66].

The main drawback of Diels-Alder reactions is the low thermal stability of the products and their easy decomposition to the starting materials in the so called retro-Diels-Alder reaction. It was shown that an addition-elimination equilibrium during [4+2] cycloaddition reactions results in low yields in some cases[67]. Contrarily, reacting C_{60} with in situ generated ortho-quinodimethanes leads to products with great thermal stability. Therefore, the different o-quinodimethane-generating precursors[68] became very popular additives for this type of cycloaddition reaction (Scheme 3).
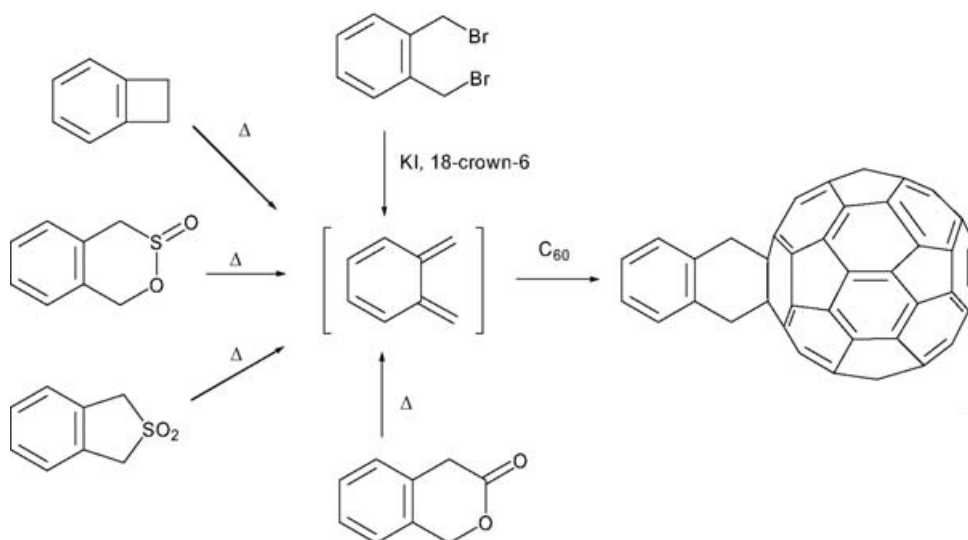
Scheme 3, Different o-quinodimethane-generating precursors used for [4+2] cycloaddition of C_{60}[63].

I.1.5.3)   [3+2] Cycloadditions: the Prato Reaction

The first fulleropyrrolidine adducts have been synthesized by Prato and Maggiani[69] via a [3+2] cycloaddition reaction, also known as 1-3-dipolar cycloaddition, and soon become the most frequently prepared fullerene derivatives. In this reaction an azomethine ylide, generated in situ by the decarboxylation of immonium salts derived from the condensation of α-amino acids with aldehydes or ketones, reacts with fullerene. The reaction of sarcosine, formaldehyde and C_{60} provided the first [3+2] cycloadduct: N-methylfulleropyrrolidine[69], as depicted on Scheme 4.
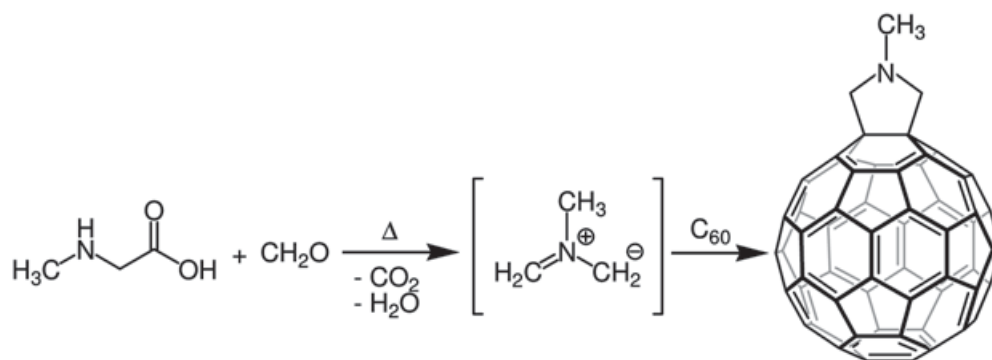
Scheme 4, N-methyl fulleropyrrolidine synthesis via the formation of azomethine ylide[66].

The popularity of the Prato reaction relies on the fact, that it tolerates a wide variety of addends and functional groups and it is possible to incorporate different substituents into three different positions (two of them simultaneously) on the pyrrolidine ring depending on the carbonyl compound (aldehyde or ketone) and substituted the amino acid used (Scheme 5). It has to be kept in mind that the functionalization of the carbon adjacent to the nitrogen leads to the formation of a racemic mixture of diastereomers[70].
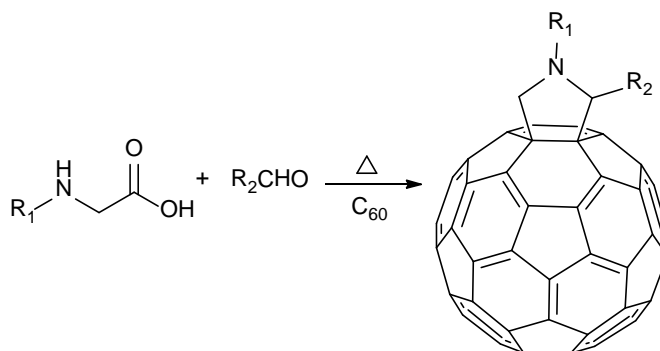
Scheme 5, General synthesis method of substituted fulleropyrrolidine with different functional groups appended to the nitrogen and the adjacent carbon.

I.1.5.4)   [2+2] Cycloadditions

The addition of benzyne - generated in situ by diazotization of anthranilic acid with isoamyl nitrite - to C_{60} leads to the formation of [2+2] cycloadducts[71]. Adduct formation occurs in the 1,2-position, resulting in the corresponding [6,6] closed fullerene structure. It is important to note, that this reaction usually leads to the formation of a series of multiadducts as well.
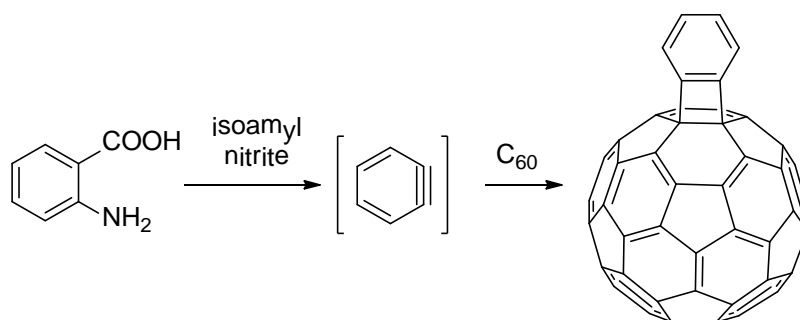
Scheme 6, [2+2] cycloaddition reaction of C_{60} with benzyne generated from anthranilic acid[71].

I.1.5.5)   Multiaddition Reactions

For a second attack to a [6,6]-bond of a C_{60} monoadduct, eight different sites are available (Figure 11). For that reason, the formation of eight regioisomeric bisadducts, which are difficult to separate, is possible. Product distributions are not statistical; different procedures and precursors used for the functionalization result in various regioadduct distributions[72]. In most cases e-isomers followed by the trans-3-isomers are the preferred reaction products while cis-1 isomers are rarely formed due to steric hindrance[66].
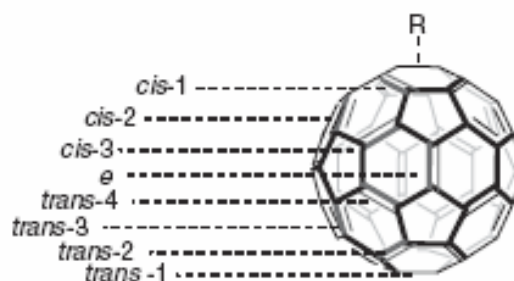
Figure 11, The relative positional relationship between [6,6] bonds. Instead of IUPAC nomenclature, the relative position of addends is indicated, as proposed by A. Hirsch.

The geometry plays a crucial role in the properties of fullerene adduct and for that reason the regioselective synthesis of fullerene multiadducts is of great importance for the preparation of advanced functional materials. The regiocontrol over bisadditions to fullerenes was achieved by an elegant procedure, introduced by F. Diederich[73], which involved tether-directed remote functionalization (Scheme 7).
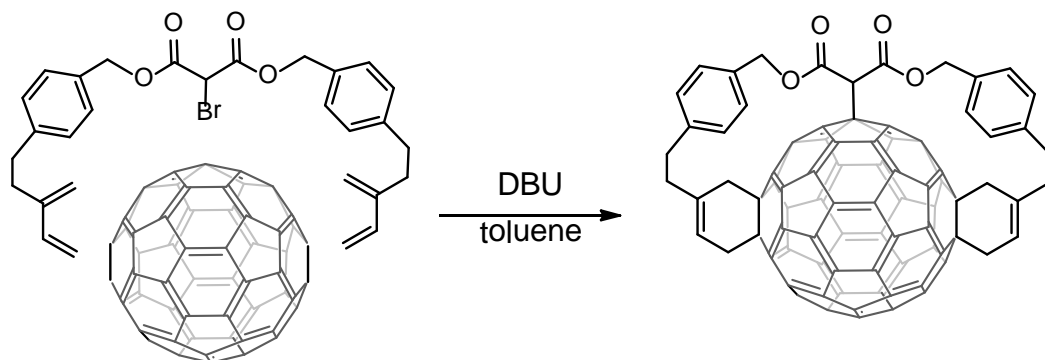
Scheme 7, C_{60} tris adduct, synthesized by tether directed method.

A 9,10-dimethylanthracene (DMA) template mediated approach was also developed by A. Hirsch[74] for the regioselective multiaddition to C_{60}. DMA binds reversibly to C_{60} and can be replaced by the precursor material during the cycloreaction, leading to T_h symmetrical hexakisadducts with an all e addition pattern (Scheme 8).
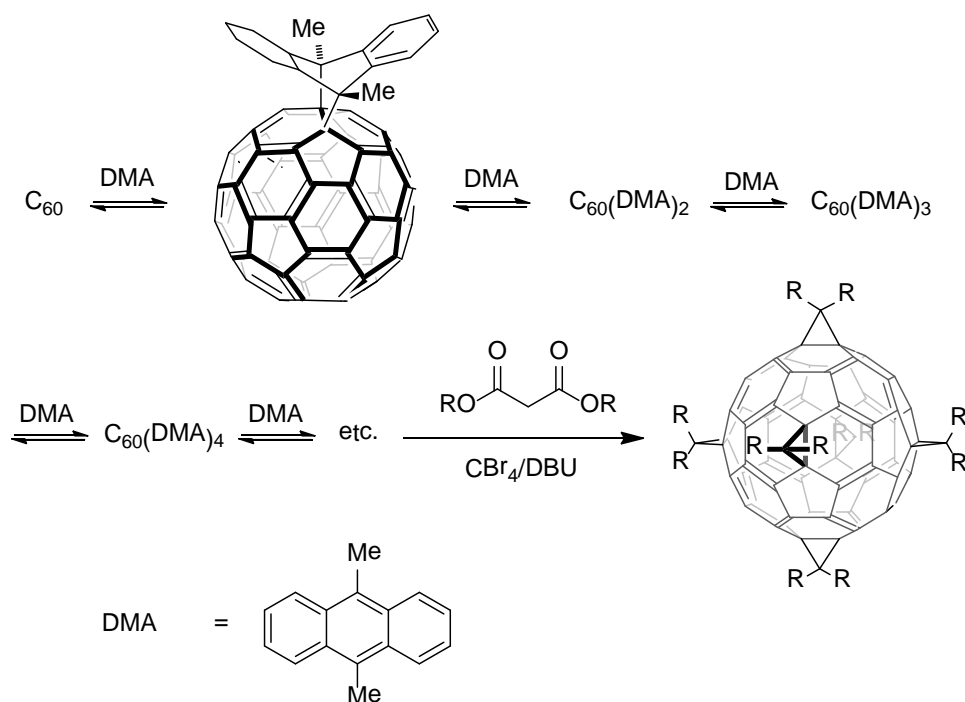
Scheme 8, Template mediated synthesis method leading to the hexakisadduct of C_{60} with an "all e" addition pattern.

I.1.5.6) Reactivity of higher fullerenes

Most of the additions in C_{70} take place exclusively on [6,6] bonds and give rise to many regioisomers even in the case of monoaddition, because the cage of C_{70} contains four

different [6,6] double bonds. The reactivity of each double bond largely depends on the degree of pyramidalization[75]. The covalent chemistry of the higher fullerenes has been excellently reviewed by Diederich and co-workers[76]. Different symmetry C_{76}, C_{78} and C_{84} cages also have been successfully derivatized[77].

I.1.6) Reactivity and regioselectivity of TNT fullerenes and their comparison with C_{60}

The exohedral reactivity of the icosahedral (I_h) $M_3N@C_{80}$ carbon cage differs enormously from the I_h C_{60} and other empty caged fullerenes that comply with the isolated pentagon rule. TNT endohedral fullerenes can be described with an ionic model ($M_3N^{6+}@C_{80}^{6-}$) and can be imagined as a non-dissociable salt due to the formal transfer of six electrons from the metal cluster towards the fullerene cage which results in a closed shell structure and consequently decreased reactivity. The chemical reactivity of TNT EMFs depends on the encapsulated cluster, metal species, carbon cage size and symmetry. More information about the chemistry, electrochemistry and potential applications of EMFs can be found in recent reviews[52,78].

Herein, we summarize recent results on $M_3N@C_{80}$ carbon cages with icosahedral (I_h) symmetry, mainly focusing on the role of the encapsulated cluster and metal species in cycloaddition reactions and the most important differences from their C_{60} analogues.

I.1.6.1) Reactive sites

It is found that the cycloaddition reaction takes place on the [6,6] site of pristine C_{60} with remarkable regioselectivity. Experimental results have proved that both the [5,6] and [6,6] double bonds can be reactive sites of TNT fullerenes, although the regioselectivity is usually very high. In order to understand this difference, we have to closely examine the double bonds of C_{60} and C_{80}. The cage of C_{60} consists of pyracylene type sites: [6,6] double bonds are abutted by two pentagons (Figure 12, type A) and corannulane-type sites: [5,6] bonds are abutted by two hexagons (Figure 12, type D). Due to the high symmetry of I_h C_{80}

cage there is also only two different accessible [1,2] addition sites. One of them is the same corannulane-type [5,6] bond, but unlike C_{60}, the I_h C_{80} cage does not have any of the reactive pyracylene type [6,6] double bonds. Instead, there is a different [6,6] bond abutted by a pentagon and a hexagon (Figure 12, type B).
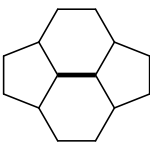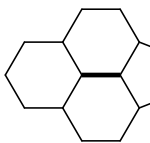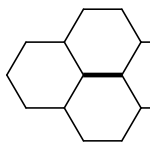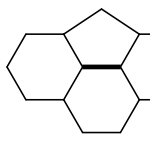
[6,6] bond types			[5,6] bond type
Pyracylene-type	abutted by a pentagon and a hexagon	Pyrene-type	Corannulane-type
A	B	C	D

Figure 12, All different types of C–C bonds in IPR fullerenes (**A-D** types)[79].

The preferred sites for cycloaddition can be characterized by high double bond character and pyramidalization angle which are favourable for nucleophilic attack. DFT calculations performed by Poblet and co-workers were carried out to obtain information about reactivity and preferred cycloaddition site of C_{80} cages on the basis of bond length, bond order and pyramidalization angle[79]. (Here to give a simpler, but still useful image, we use the assumption that bond length and π electron density are directly and inversely proportional respectively). The bond length and pyramidalization angle data of I_h C_{60} and I_h C_{80} are summarized in Table 4 andTable 5, respectively. It has been already discussed in this Chapter, that the [5,6] and [6,6] sites of [60] fullerene have the same bond angle, but the [6,6] site has more double bond character. In other words its [6,6] bond lengths are significantly shorter than the [5,6] ones. Even if the kinetically favoured [5,6] open structure forms initially, in most of the cases it rearranges to the thermodynamically more stable [6,6] closed methanofullerene[80].

Smaller pyramidalization angles and longer bond lengths typify the carbon-carbon bonds of C_{80} relative to the reactive pyracylene type site of C_{60}. It means, that there are corroborating electronic and geometric effects behind the lower exohedral reactivity of C_{80} cages. Further investigation of the data can reveal the reactivity of the different sites. The type B site has only a slightly higher double bond character and its pyramidalization angle is even smaller than the corannulane type site (Type D). By way of explanation, the small

difference in π character is more or less compensated with the bond angle difference making the reactivity of the [6,6] and [5,6] double bonds comparable. (The pyrene type (Type C) site is not present in I_h C_{60} and I_h C_{80} cages).

Table 3, Description of the C–C bonds of the I_h-C_{60}:**1** IPR fullerene divided into 2 non-equivalent sets[79].

I_h C_{60}	Bond length (Å)	Θ_p (°)
Type A	1.397	11.67
Type D	1.452	11.67

Table 4, Description of the C–C bonds of the I_h-C_{80}:**7** IPR isomer divided into 2 non-equivalent sets[79].

I_h C_{80}	Bond length (Å)	Θ_p (°)
Type B	1.428	9.62
Type D	1.438	10.58

Possible characterization techniques to differentiate between regioisomers:

- X-Ray crystallography can give unambiguous information about addition site and an open or closed cage structure.
- NMR spectroscopy: the protons and carbons close to the addition site can appear as equivalent or non-equivalent according to their symmetry, which differ by the type of the addition site.
- UV/Vis spectroscopy: Earlier studies of C_{60} derivatives revealed that, the UV-Vis spectra are independent of the nature of the addend but characteristic of the regiochemistry for each isomer[81]. It seems to be the case for TNT EMF fullerene adducts, as well[38]. The fulleroid character can also be identified, because it shows similar spectra to its precursor fullerene due having the same number of p orbitals[82].

- Electrochemistry: In most of the cases [5,6] and [6,6] adducts exhibit reversible and irreversible cathodic behaviour, respectively[53b].

$M_3N@C_{80}$ cages have been successfully derivatized by different methods, including disilylation[53a,83], Diels-Alder, Prato, Bingel, radical[84], polyhydroxylation[85] and other miscellaneous reactions[86].

I.1.6.2)   Diels-Alder reaction

The first functionalized TNT EMF was a Diels-Alder adduct of $Sc_3N@C_{80}$ prepared by Dorn and co-workers in 2002 (Scheme 9)[87]. Refluxing the endofullerene in the presence of ^{13}C labelled 6,7-dimethoxyisochroman-3-one, as dienophile yielded the desired monoadduct. NMR investigation showed evidence of a plane of symmetry which bisected the cyclohexene ring perpendicularly suggesting that the functionalization took place at the [5,6] ring junction which was later unambiguously confirmed by X-ray crystallographic data[88]. The same reaction was also performed on $Gd_3N@C_{80}$ and a bis-adduct was isolated, but its regiochemistry was not studied[89].
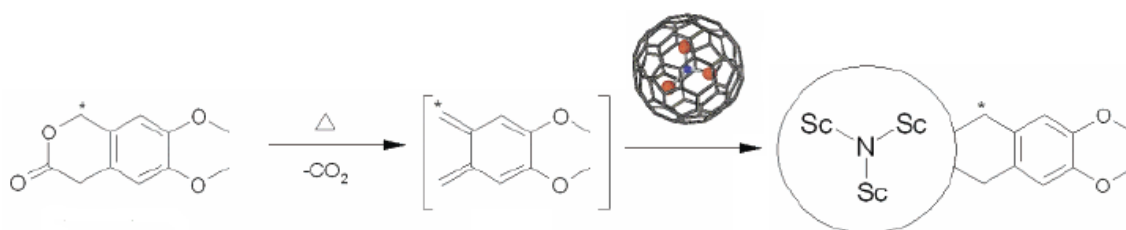
Scheme 9, The first Diels-Alder cycloadduct of $Sc_3N@C_{80}$[87]. * denotes ^{13}C label.

I.1.6.3)   Prato reaction (1-3 dipolar cycloaddition)

1-3 dipolar cycloaddition of $Sc_3N@C_{80}$ with huge excess of N-ethylglycine and ^{13}C labelled formaldehyde in o-DCB gave the first TNT fulleropyrrolidine (Scheme 10). Similarly to the Diels-Alder adduct, the selective formation of [5,6] regioisomer was confirmed by NMR techniques (ie. equivalent methylene carbons, but non-equivalent germinal protons appeared on ^{13}C and ^1H NMR spectra, respectively)[90]. Surprisingly, the same reaction

performed on $Y_3N@C_{80}$ yielded exclusively the [6,6] regioisomer[91], with non-equivalent pyrrolidine methylene carbons and germinal protons which are equivalent, but different from those attached to the opposite carbon. The unexpected reaction behavior is clearly attributed to the trimetallic nitride cluster which seems to be controlling the regioselectivity. Further studies revealed that the [6,6] regioisomer of $Y_3N@C_{80}$ is merely a kinetically favored derivative which isomerizes quantitatively into the thermodynamically more stable [5,6]-adduct upon heat treatment. During the synthesis of N-tritylpyrrolidino derivative of I_h $Sc_3N@C_{80}$ both [5,6] and [6,6] monoadduct and a bisadduct were formed. The kinetically favored [6,6] regioisomer can be thermally converted to the thermodynamically more stable [5,6] adduct[38]. A combined experimental and theoretical investigation on the regiochemistry of a series of TNT endohedral fullerenes $Sc_xGd_{3-x}N@C_{80}$ (x = 0-3) in 1,3-dipolar cycloadditions with N-ethylazomethine ylide demonstrated that the regioselectivity of the TNT EMF derivatives depended remarkably on the size of the encaged cluster. Functionalization of $Sc_3N@C_{80}$ provided almost exclusively the [5,6] regioisomer, while the same reaction performed on $Gd_3N@C_{80}$ gave the [6,6] regioisomer, as the major product[92]. It has be suggested that the large cluster size of $M_3N@C_{80}$ (M = Y, Gd, and other lanthanides) distorts the cage and promotes the reactivity of [6,6] double bonds (type B site).
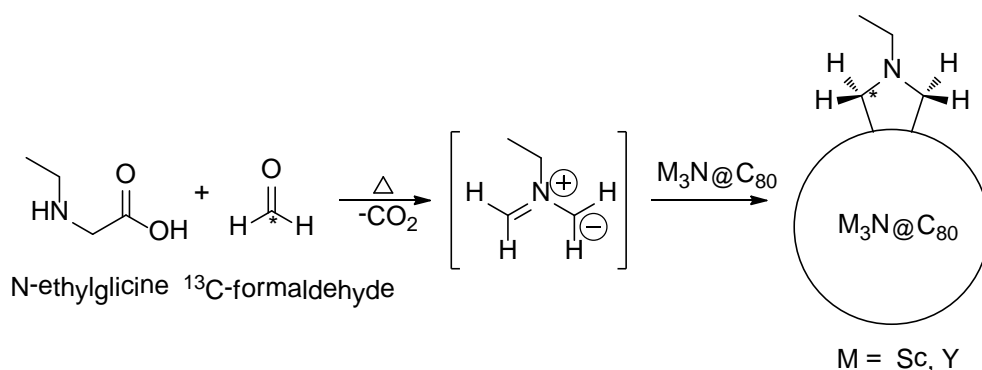
Scheme 10, 1,3-Dipolar cycloaddition of $M_3N@C_{80}$ (M = Sc, Y) with huge (25 and 125 fold) excess of N-ethylglycine and ^{13}C labeled formaldehyde.

TNT D-A fulleropyrrolidines based on a ferrocene electron donor and $Sc_3N@C_{80}$[20] (Scheme 11) or $Y_3N@C_{80}$ acceptor moieties yielded the [5,6] and [6,6] regioisomers, respectively. Surprisingly, instead of isomerisation, retro-cycloaddition was observed upon heat treatment of the adduct obtained for $Y_3N@C_{80}$[21]. The photophysical and electrochemical properties of these materials will be discussed in Chapter II.
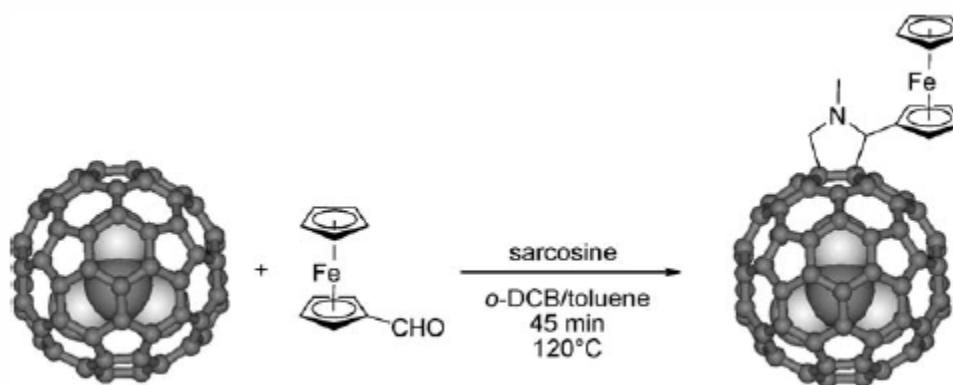
Scheme 11, 1,3-Dipolar cycloaddition reaction of I_h-Sc$_3$N@C$_{80}$ with ferrocene carboxaldehyde and sarcosine[20].

Table 5, Cycloaddition reaction vs reactivity site of different M$_3$N@C$_{80}$ (M=Sc, Y, Lu, Gd).

Addition type	Sc$_3$N@C$_{80}$	Y$_3$N@C$_{80}$	Lu$_3$N@C$_{80}$	Gd$_3$N@C$_{80}$
[4+2] addition (Diels-Alder reaction)	[5,6][87,88]	-	-	not studied[89]
[3+2] cycloaddition (Prato reaction)	[5,6][90,91,21]	[6,6][a,91]	-	[6,6][c,92]
	[5,6], [6,6] mixture[a,38]	[6,6][b,21]		
[2+1] cycloaddition (Bingel reaction)	[6,6][d,94]	[6,6][82,91]	[6,6][d,94]	[6,6][56]
			[6,6][e,22,95]	
2+2 cycloaddition	[5,6], [6,6] mixture[97]	-	-	-

a) can be converted to the thermodynamically more stable [5,6] adduct b) undergo retro-cycloaddition upon heat-treatment c) [6,6] adduct is the major product, but minor amount of [5,6] is also present d) under general reaction conditions (big excess of bromomalonate and DBU in oDCB) the product is not formed; the use of NaH and/or more polar environment is necessary for successful derivatization e) these cyclopropanated methanofullerene derivatives were not prepared by the Bingel reaction

I.1.6.4) Modified Bingel-Hirsch reaction ([2+1] cycloaddition)

The first cyclopropanation reaction of $Y_3N@C_{80}$[91] and $Er_3N@C_{80}$[51] with an excess of diethyl bromomalonate and DBU in o-DCB led to the selective formation of the [6,6] monoadduct (Scheme 12). Using the same reaction conditions for the functionalization of $Sc_3N@C_{80}$ failed to give any recoverable product and proved that the internal cluster has a tremendous impact on the reactivity toward the Bingel reaction[91]. The presence of a stronger base (ie. NaH) and/or the addition of a polar co-solvent promotes the cycloadduct formation (Scheme 13). Theoretical calculations[93] suggested that the energy barrier of reaction rate controlling process during the Bingel reaction, which leads to the elimination of the halide, is strongly affected by the solvent polarity. Indeed, Echegoyen and co-workers have found that the addition of a polar co-solvent (eg. DMF) favored the cyclopropanation reaction without the formation of undesired byproducts in contrast to the use of NaH which led to the inevitable formation of hydrolysis-decarboxylation compounds. The successful functionalization of $Lu_3N@C_{80}$ also required the use of the aforementioned reaction conditions[94].
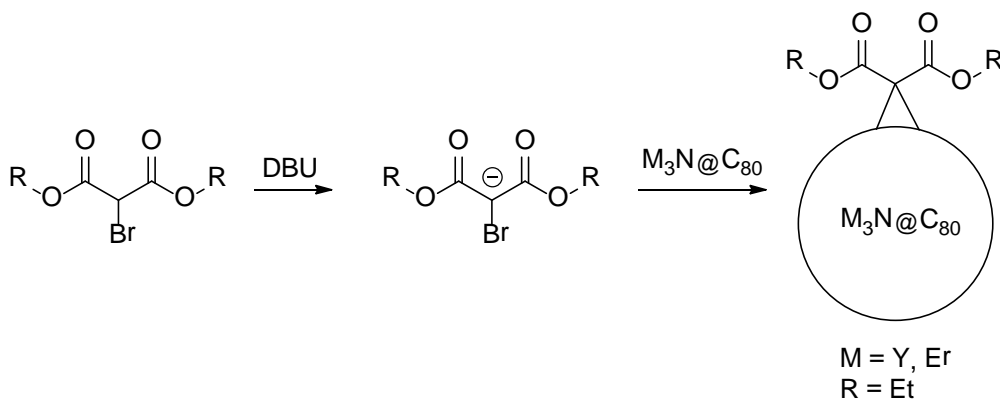
Scheme 12, Cyclopropanation of $M_3N@C_{80}$ (M = Y, Er) with bromodiethylmalonate (30-fold excess) in the presence of DBU (50-fold excess) gives the relevant cycloadduct in good yields (84% in case of $Y_3N@C_{80}$).
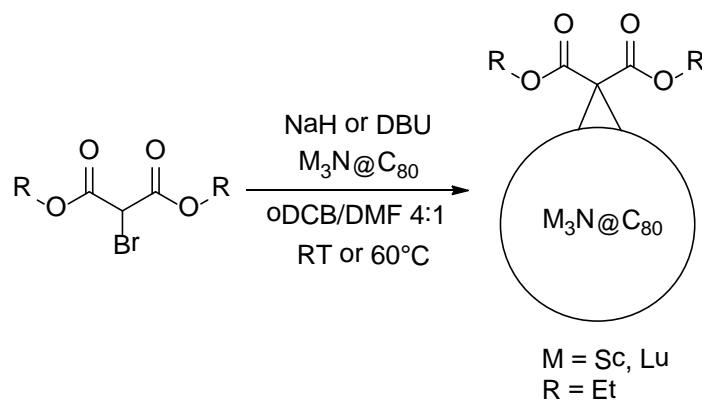
Scheme 13, The cyclopropanation of $Sc_3N@C_{80}$ and $Lu_3N@C_{80}$ required modified reaction conditions (bromomalonate in 4-32x access, ~40% yield in both cases).

The resulting Bingel-Hirsch adducts proved to be remarkably stable. No isomerisation or retrocycloaddition took place upon heat treatment at high temperature for prolonged time (ie. $Y_3N@C_{80}$-$C(CO_2Et)_2$ remained stable after heating it for 21h at 180°C) or exhaustive reduction by controlled potential electrolysis. The X-Ray diffraction pattern of the sample(s) revealed a fulleroid character, where the C-C bond at the site of the addition was broken or open.

Gd_3N in different cage sizes has also been studied, as well as the influence of the cage size on reactivity towards cyclopropanation. Mono and bisadducts were obtained for $Gd_3N@C_{80}$, whereas only a monoadduct was observed for $Gd_3N@C_{84}$ (non IPR fullerene cage), and no reaction occurred with $Gd_3N@C_{88}$. Their different reactivity was explained as a function of the pyramidalization degree of the double bonds, with C_{80} having the highest degree of pyramidalization while C_{88} the lowest[56].

Cyclproanated TNT EMF adducts were also prepared by other methods than the generally applied Bingel-Hirsch reaction. The methano derivative of $Lu_3N@C_{80}$ was synthesized via an electrosynthetic route; electrochemically generated $[Lu_3N@C_{80}]^{2-}$ dianions reacted with the electrophile $PhCHBr_2$. $Sc_3N@C_{80}$ did not provide the desired product under the same reaction conditions probably due to the fact that its HOMO is more localized on the inside cluster, as was shown by DFT calculations[95]. By analogy with the organic electron acceptor, C_{60}-PCBM, the $Lu_3N@C_{80}$-PCBX family of derivatives (X = methyl, butyl, hexyl and octyl) have been synthesized by modified Hummelen method[96] to replace the former in BHJ organic photovoltaic devices (see Chapter II for more details).

I.1.6.5)   2+2 cycloaddition

Recently, the addition of benzyne to $Sc_3N@C_{80}$ provided an adduct with a four-membered ring attached to the cage surface with different ring fusions. Surprisingly and contrarily to C_{60}, a mixture of 5,6 and 6,6 regioisomers was obtained (Figure 13). Both of the purified compounds show reversible cathodic behaviour, thus in this case electrochemical analysis is not sufficient to distinguish between regioisomers[97].

[5,6]-regioisomer   [6,6]-regioisomer   n = 1-10
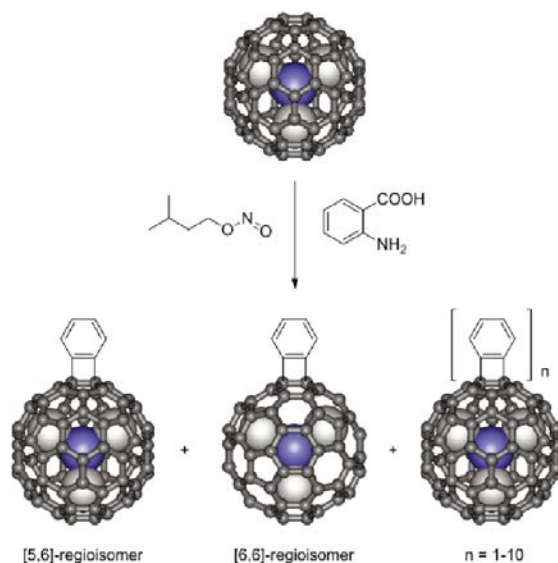
Figure 13, [2 + 2] Cycloaddition Reaction to I_h $Sc_3N@C_{80}$[97].

TNT endofullerenes with cage size and cage symmetry different from I_h C_{80} have been also derivatized by different type of reactions, but these are not detailed here.

I.1.7)   Solvation

Fullerenes are barely soluble in any apolar solvent and practically insoluble in polar solvents. TNT EMFs are even less soluble than C_{60}. Their most common solvent is o-DCB, but chlorobenzene and toluene can be also used. In order to generate processable materials for potential applications their chemical functionalization is necessary.

TNT EMFs are also less reactive than C_{60}. The usual reaction conditions for 60[Fullerene] derivatization results in low yields and the formation of unidentifiable byproducts if applied to TNT EMFs. A big excess of reactants is generally added to the

reaction mixture and sometimes only harsher reaction conditions or the use of polar co-solvent leads to successful cycloaddition. Most EMFs are prone to oxidation, thus the halomalonate cannot be formed in situ in the Bingel reaction.

Here we would like to mention, that the $Y_3N@C_{80}$ derivative **42** (see Chapter II for details) is soluble in most organic solvents due to the attached long alkyl chains, making it one of the most soluble TNT EMF derivatives prepared to date (Figure 14).

R = -C_{12}H_{25}
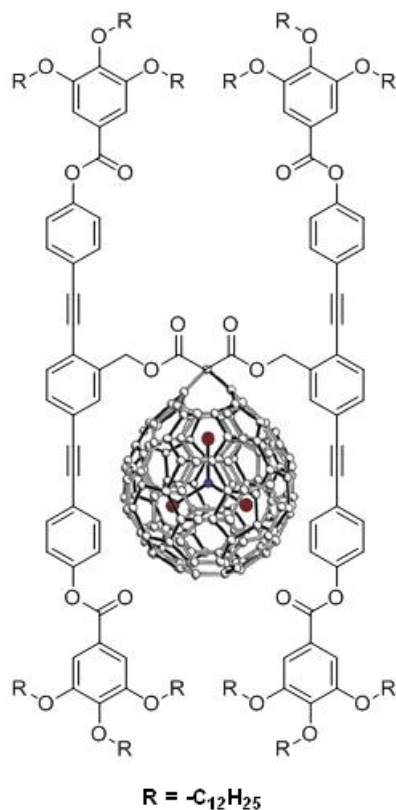
Figure 14, The functionalization of $Y_3N@C_{80}$ leads to well soluble derivative **42**.

I.2)   Liquid crystals

Liquid crystals (LCs) have intermediate physical properties between conventional solid and liquid phases. The study of liquid crystals began in 1888 when an Austrian botanist named Friedrich Reinitzer observed that the crystals of cholesterol benzoate had two distinct melting points. The crystals melted at 145.5 °C to give a milky fluid, which turned into a perfectly clear liquid at 178.5 °C[98]. This observation led to the assumption of a new

thermodynamically stable state of matter, and soon the term "flowing crystal" and later "liquid crystal" has appeared in scientific publications. The generally accepted classification of matter of states (ie. solid, liquid and gaseous) seems to be incomplete, as many organic substances do not exhibit a phase transition between single crystal and liquid states, but a series of transitions showing different states whose physical properties are intermediate between those of the crystal and the liquid. These statements improperly called it "liquid crystal", but the term has passed into common parlance. It can be more aptly labeled "mesomorphic" (from the Greek mesos (middle) and morph (form)), as it was introduced by O. Lehmann[99] or "mesophase"[100]. Thus, today we call LCs or mesogens all organic materials which exhibit intermediate fluid phases between an ordered crystalline phase and an isotropic liquid. For instance, a liquid crystal may flow like a liquid, but its molecules may be oriented in a crystal-like way. These phases can be characterized by anisotropic (ie. directionally dependent) physical properties due to orientational and varying degrees of positional ordering of the constituent molecules. Positional order refers to the extent to which an average molecule or group of molecules shows translational symmetry (as a crystalline material shows). Orientational order represents a measure of the tendency of the molecules to align along the director on a long-range basis. It is sometimes difficult to determine whether a material is in a crystal or liquid crystal state. Crystalline materials demonstrate long range periodic order in three dimensions. By definition, an isotropic liquid has no orientational order. Substances that show fluid-like behavior, but aren't as ordered as a solid, yet have some degree of alignment are properly called liquid crystals.

Laptop computers and most new televisions have flat screens with LC displays. The same technology has been used for years in calculators, mobile phones, and digital watches exploiting the anisotropic properties of mesomorphic materials.

The mesophases are currently identified by the combination of three techniques: polarized optical microscopy (POM), differential scanning calorimetry (DSC) and small angle X-ray diffraction (SAXS). The first allows us to view the characteristic birefringent textures, the second provides information on the enthalpy changes during the various transitions and the third provides structural information on the organization of the molecules in the mesophase.

The two main types of liquid crystals are:

- Lyotropic liquid crystals[101], which are amphiphilic molecules, surfactants consisting of two distinct parts: a polar, often ionic, head and a nonpolar, often hydrocarbon tail. The molecules self-associate in a solvent at a precise concentration and temperature range (Figure 15).
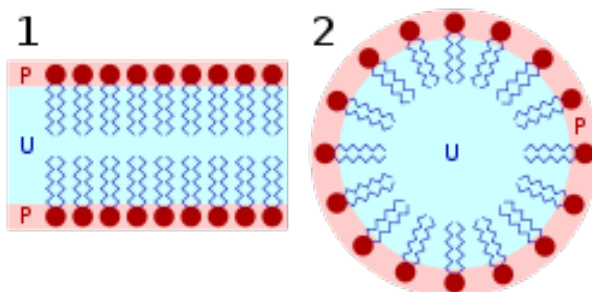
Figure 15, Lyotropic liquid crystals with apolar tail (blue) and polar head groups (red).
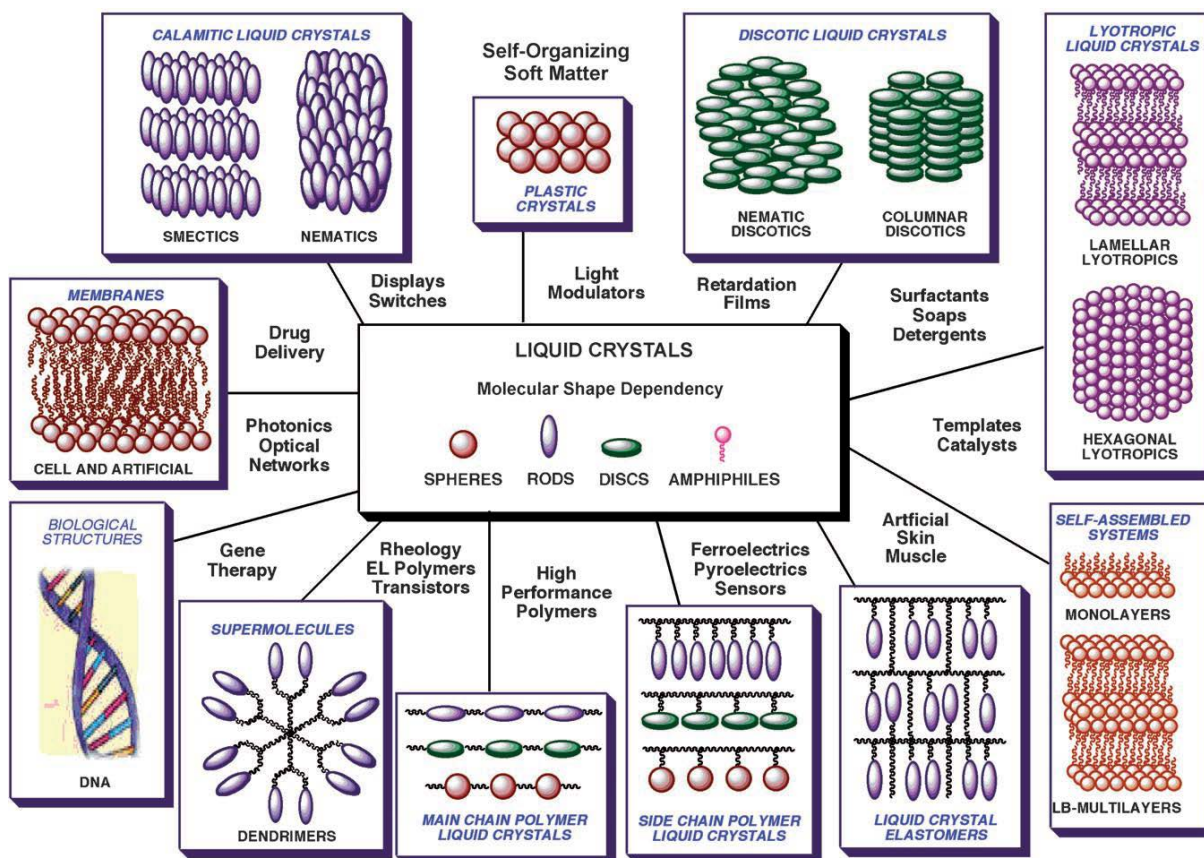
Figure 16, World of liquid crystals[102].

- Thermotropic liquid crystals show mesomorphic behavior in a certain temperature range by heating them from the crystalline state or cooling from the liquid (isotropic) state (Figure 16).

Only thermotropic liquid crystals are the subject of the present work.

I.2.1) Mesophases of thermotropic liquid crystals

I.2.1.1) Nematic phase

The nematic phase is the least ordered mesophase, where the molecules have no positional order, but they have long range orientational order, as the molecules tend to align roughly parallel to each other (Figure 17). Therefore, the molecules flow just like in a liquid due to easy sliding of the molecules over each other, while retaining their orientation. Most nematics are uniaxial with a one dimensional structure, but some examples of biaxial nematics also exist. In addition to orienting along their director axis these molecules orient along a secondary axis.
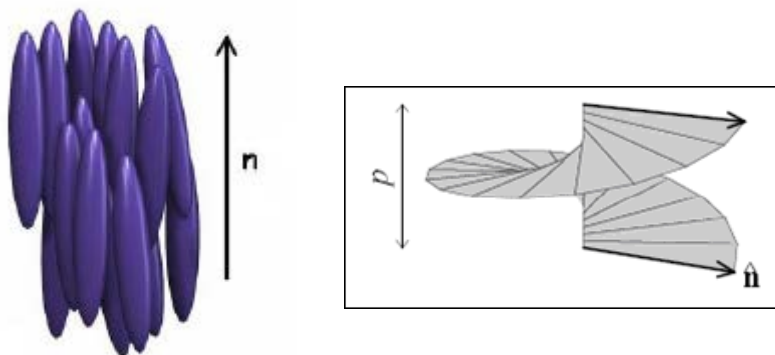
Figure 17, (Left) Nematic organization of calamitic molecules along the director axis (n). (Right) Helical rotation of the molecular director caused by the chiral center of the mesogens.

The chiral nematic or cholesteric phase, built up from the helical arrangement of chiral molecules, is a special case of the nematic phase. This phase exhibits a twisting of the molecules perpendicular to the director, with the molecular axis parallel to the director (Figure 17).

34

I.2.1.2) Smectic phase

The smectic phases form well-defined lamellar layers that can slide over one another due to their loose associations; as a result they show mechanical properties similar to that of soap. The main difference between nematics and smectics is that the latter also organized into layers in addition to the orientational order. There are several smectic phases, but the most common ones are Smectic A (SmA) and Smectic C (SmC) (Figure 18). The layers of these last two phases can be described by a sinusoidal wave, where the density maxima define the layers. In the SmA phase, the molecules are oriented along the layer normal ie. the director is perpendicular to the layer planes, while in the SmC phase they are tilted away from the layer normal (ie. the director is tilted to the layer planes). Inside the plane, perpendicular to the wave vector, there is only short-range ordering of the molecules. For that reason, these phases are liquid-like within the layers.
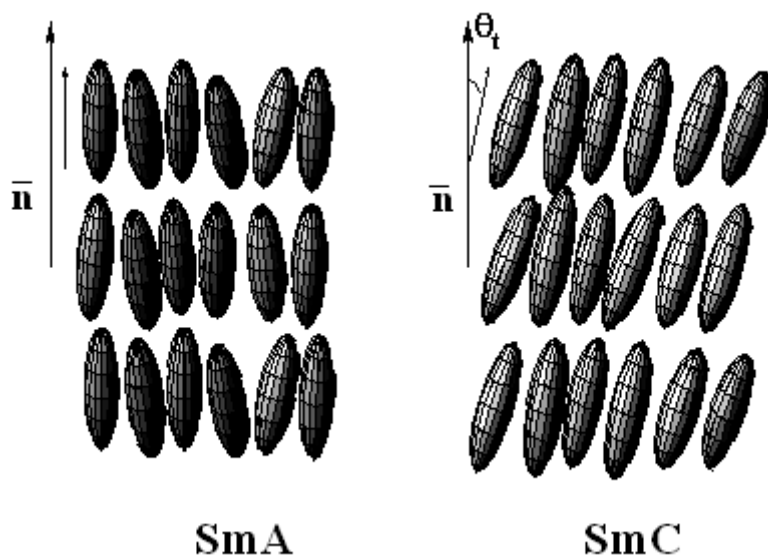
Figure 18, The molecular alignments of SmA and SmC phases. n: director, Θ_t: tilt angle.

I.2.1.3) Columnar phases

Columnar phases consist of the periodic assembly of columns resulting in a two dimensional lattice generally defined over a large correlation length. The different types of columnar phases are characterized by the 2D lattice symmetry of the columnar packing, that can be hexagonal (Col_h), rectangular (Col_r) or oblique (Col_o) (Figure 19).
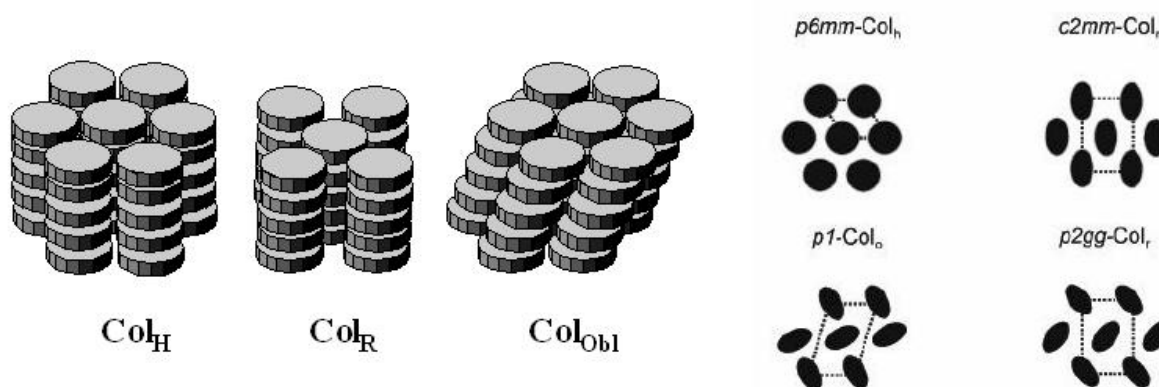
Figure 19, Columnar phases with different lattice symmetries.

These mesophases are usually made up of discoid molecules or disc-like molecular aggregates, but are also exhibited by many non-discotic molecules such as polycatenar mesogens[103]. The latter ones are generally composed of long, rod-like, rigid cores ending in two half-disk-like moieties, which are aromatic rings bearing several flexible chains (Figure 20). Polycatenar mesogens are a class of molecules whose structural and mesogenic properties are intermediates between conventional calamitic (ie. rod shaped) and discotic liquid crystals.
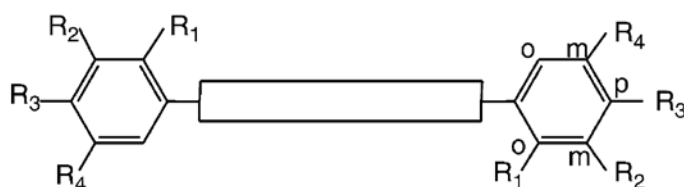
a Hexacatenars *3mpm-3mpm* or phasmids: R_1 = H; R_2 = R_3 = R_4
b Tetracatenars *2mp-2mp* or biforked mesogens: R_1 = R_4 = H; R_2 = R_3

R = alkoxy chain in general
o = *ortho* position; *m* = meta position; *p* = para position

Figure 20, General "biforked" structure of polycatenar mesogens[103e].

I.2.1.4)   Cubic phases

The cubic phase is very common in lyotropic liquid crystals, but was only reported much later for thermotropic mesophases. Due to the cubic symmetry, the phases are isotropic and show no birefringence when observed under an optical microscope between a crossed polarizer and analyzer. The molecules constitute long-range, 3D ordered mesophases. To date, these have been observed in dendrimers[104], spheroidal systems[105], as well as amphiphilic, calamitic molecules[106].

These phases are distinguished according to their space group. They may be continuous 3D arrays of micelles (micellar cubic phases), or bicontinuous phases (Figure 21), formed by two mutually interpenetrating networks with different symmetries.

a   b   c
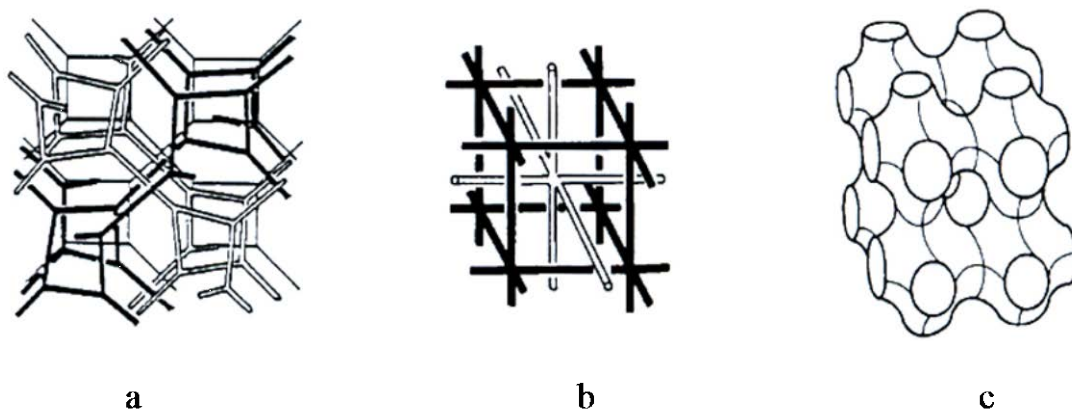
Figure 21, Schematic representation of bicontinuous cubic phases with different symmetries: a) Ia3d, b) Im3m and c) Pn3m.

I.2.1.5)   Techniques to study mesomorphic properties and supramolecular organization

First thermogravimetric analysis (TGA) was used to determine the thermal stability of the compounds as it is usually required before using differential scanning calorimetry, which contains several heating and cooling cycles.

TGA is a technique in which the loss of mass of a substance is monitored as a function of temperature or time under a controlled temperature program in a controlled

atmosphere, and the degradation temperature is determined from the onset of weight loss temperature curve.

Polarized optical microscopy - POM

Light with transverse wave vibrations that possess direction is called polarized light. Light from an ordinary light source (natural light) that vibrates in random directions is called non-polarized light. In contrast, while light with vertical vibrations that travels within a single plane is called linearly polarized light; circularly polarized light and elliptically polarized light are types of light in which the vibration plane rotates with time. Liquid crystals are birefringent or in other words they have a double refraction which can be observed if irradiated with polarized light. When plane-polarized light enters a birefringent material, it is refracted into two individual rays: extraordinary (slow) and ordinary (fast) rays, each polarized in mutually perpendicular planes. These light components travel at different velocities, which vary with the propagation direction through the sample. When the rays exit the material and pass through the analyser they recombine with constructive and destructive interference (due to the phase difference) and image contrast will be created.

A polarized light microscope (Figure 22) is designed to observe samples that are visible primarily due to their optically anisotropic character. These microscopes are equipped with both a polarizer, positioned in the light path before the sample, and an analyzer (a second polarizer) placed in the optical pathway between the objective rear aperture and the observation tubes or camera port. In the absence of liquid crystal material, if the polarizer and analyser are parallel the light passes through but if they are perpendicular to each other no light can be observed.
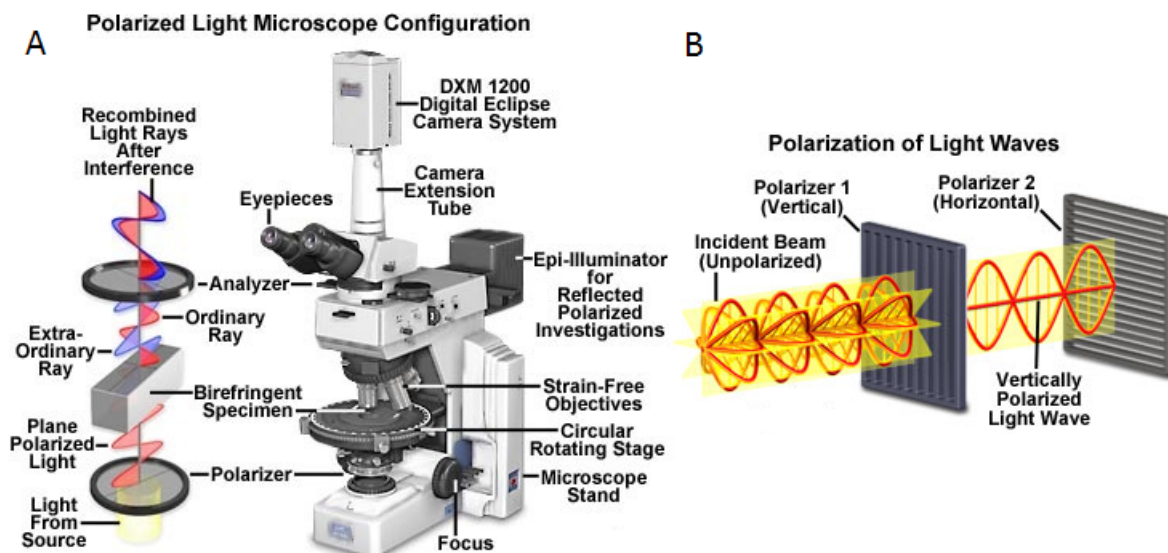
Figure 22, Configuration of polarized light microscope.

Differential scanning calorimetry (DSC) is used as a complimentary technique to POM and X-Ray diffraction to confirm whether the changes observed by POM, arise from phase transitions. This is a technique allows the study of the thermal transition of a material by measuring the amount of energy (heat), which is proportional to the enthalpy of the transition (ΔH), absorbed or released by a sample as it is heated, cooled or held at a constant temperature[107]. The sample is measured against a reference sample with well-defined heat capacity. During a phase transition the sample needs less or more heat to be applied, to maintain the sample at the same temperature of the reference compound, depending on whether the reaction is exothermic (e.g. melting) or endothermic (e.g. crystallization). The transition is defined by the free energy which can be expressed as:

$$\Delta G = \Delta H - T\Delta S$$

where ΔH is the change of enthalpy of the system, ΔS is the change of the entropy and T is the absolute transition temperature (usually the onset temperature). At the transition ΔG = 0, so ΔS can be determined and a peak will be present on the DSC profile which is represented by curves of heat flux versus temperature or versus time. Integration of the peak corresponding to a given transition gives the enthalpy of this transition and usually referred to as latent heat. When phase transitions occur without a change in entropy they are referred to as second order and are accompanied by a discontinuity in heat capacity (ΔC_p) which is the second derivative of G with respect to T at constant pressure. *Glass Transition* (Tg) temperature is associated with a change in the baseline. In liquid crystals,

transitions between phases are referred to as weakly first order, however second order transitions are not uncommon (eg. SmC-SmA). Large enthalpies always correspond to first order transitions eg. *melting transition* (crystal-to-mesophase or to-isotropic liquid) and in some cases at the *clearing transition* (mesophase-to-isotropic liquid). When a crystal melts to an isotropic liquid at T_I, but on cooling crystallizes at lower temperature T_K, ($T_K < T_I$), the liquid is called *supercooled* and is the result of kinetic stabilization. If a material exhibits a mesophase during the heating process, when the entropy of the system increases due to loss of positional and orientational ordering, and also on cooling, then this phase is thermodynamically stable. Such a phase is described as *enantiotropic* and the enthalpies are reproducible. If a mesophase only appears on cooling (thermally less stable), due to the hysteresis at the crystallization temperature, which is the product of kinetic stabilization, it is described as *monotropic* (Figure 23). In this case the clearing point is reversible. When materials exhibit a number of different mesophases, involving an increase of entropy of the system, they are called *polymorphic*. Except for the first phase transition temperature, which might be supercooled, the transitions are reversible.
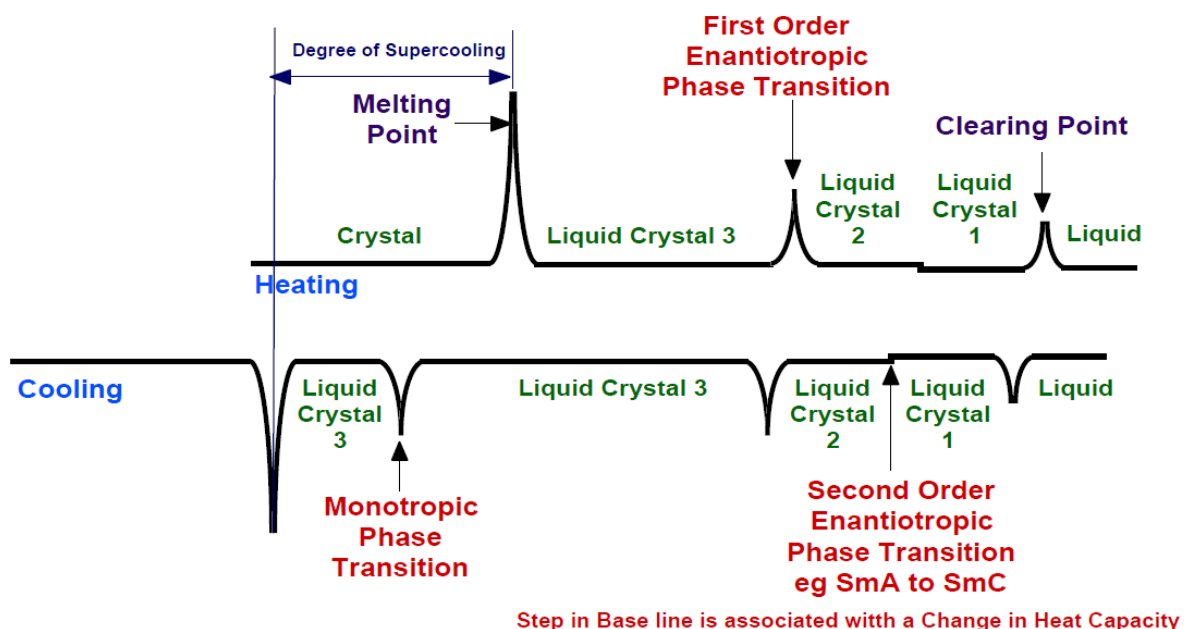

Figure 23, An example DSC of Liquid Crystalline Phases.

When information is collected from a DSC trace, the transition temperature is indicated at the temperature of the onset of the change and the Tg is taken as the mid-point of the change.

Small Angle X-ray Scattering (SAXS)

X-rays are a form of electromagnetic radiations, with typical wavelength λ < 1nm. The X-ray scattering power of atoms is proportional to the atomic number *Z*. X-ray diffraction picks out any periodically repeating features of a structure, e.g. if a lamellar liquid crystal was positioned with its layers roughly parallel to the incident beam, a series of spots would be observed[108]. These result from Bragg reflections of the smectic layers. Bragg's law for X-ray diffraction, which is anticipated from crystal structures, can be used to determine the supramolecular arrangement of the liquid crystals, but not the atomic position because the mesophase exhibits some disorder. Small angle X-ray diffraction ($2\Theta \leq 30°$) can be used to determine mesophase ordering (low order reflections, large distances). Bragg's law indicates that constructive interference between rays reflected by successive planes will only occur when the path difference, $2d\sin\Theta$, equals an integral number of wavelengths[109] of the radiation:

$$2dsin\theta = n\lambda$$

where *d* is the spacing between planes, Θ is the angle of incidence, *n* is an integer and λ is the wavelength. The reciprocal relationship between scattering angle and spacing allows us to interpret the X-ray diffraction from LCs as the following: small distances result in a large scattering angle; long range (crystal-like) order results in sharp peaks and short range (liquid-like) order results in diffuse peaks (halo), e.g. the diffuse maxima of the molten and/or rigid disordered aliphatic chains are generally observed at 4.5 Å. For a nematic phase, diffuse maxima are seen at both small and large scattering angles. For smectic phases, a number of equally-spaced low angle (00*l*) pseudo-Bragg peaks can be observed, but only the first one, two or three have observable intensity. Distinguishing a SmA from a SmC phase is difficult as the only difference is that the layer distance is smaller in SmC but the variation of the d-spacing can be observed during a temperature change due to the tilt angle variation. Most commonly, columnar phases are typical for the molecular arrangement of discotic liquid crystals and the phases are ordered in at least two dimensions. The

positional order along the columns can be short range (Col$_h$, disordered) or long range (Col$_o$, ordered). However, it has been shown that polycatenar molecules also exhibit columnar phases[102e,110]. In this case, the sublayer formed by the rigid cores undergoes undulations when its thickness is at a maximum, in order to keep the aliphatic part efficiently excluded from the sublayers of the rigid cores. When the maximum of the undulations reaches the whole thickness of the sublayer, it breaks into columns, separated by the aliphatic chains.

I.3)   Objectives

The aim of this thesis is to develop fullerene derivatives for both materials science and biomedical applications and to present their detailed characterization and properties.

Materials science

The great electron acceptor properties and small reorganization energy of fullerenes motivated their use as the active material of photovoltaic devices. The performance of devices based on a blend or covalent linking of fullerenes and an organic electron donor material is moderate relative to that of inorganic solar cells, but their potentially low production cost and processability can make them viable alternatives.

One of the main drawbacks of blended photovoltaic devices is the uncontrolled macroscopic phase separation of their components, which deteriorates device performances. In order to avoid such unwanted event, donor-acceptor (D-A) dyads, molecules that are built up via the covalent linking of donor molecules (conjugated oligomers in our case) to fullerenes, emerged as a possible alternative for creating stable bicontinuous network. The ensembles of different liquid crystalline conjugated oligomers, namely oligo(phenylenevinylene) (OPV) and oligo(phenyleneethynilene) (OPE) and fullerenes with different characteristics, namely C_{60} and $Y_3N@C_{80}$ were studied. Supramolecular self-assembly of D-A molecules into well-defined networks, initiated by mesogenic promoters, is a highly appealing strategy to actualize ambipolar charge transport (ie. the simultaneous transport of electrons and holes) between the electrodes and thus to improve photovoltaic performances.

Biomedical applications

Most commercially available magnetic resonance imaging (MRI) contrast agents are gadolinium chelates. Gd (III) ion is used due to it having the largest electron spin quantum number of all elements and its large magnetic moment, while its main limitation is the release of metal ions in vivo during metabolic processes and the subsequent toxicity. Eliminating toxicity, besides further improving the proton relaxation rate enhancement of these biomaterials, evokes researcher's interest. Water soluble $Gd_3N@C_{80}$ derivatives fulfil both of the aforementioned requirements and have great potential as magnetic resonance enhancement agents. The mass production of the pristine metal cluster fullerene and its functionalization are still challenging areas on this field. Focusing on the latter problem, the aim was to find suitable reaction conditions for the functionalization of the gadofullerene with dendritic tetraethylene glycol ligands. The dendritic branches are expected to retain water in their cavities and positively influence the proton relaxivity both in vivo and in vitro environments.

[1] H. W. Kroto, J. R. Heath, S. C. O'Brien R. F. Curl, R. E, Smalley, *Nature,* **1985**, *318*, 162-163.

[2] H. W. Kroto, *Nature*, **1987**, *329*, 529-531.

[3] J. R. Heath, S. C. O'Brien, Q. Zhang, Y. Liu, R. F. Curl, H. W. Kroto, F. K. Tittl and R. E. Smalley, *J. Am. Chem. Soc.*, **1985**, *107*, 7779-7780.

[4] Y. Chai, T. Guo, C. Jin, R. E. Haufler, L. P. F. Chibante, J. Fure, L. Wang, G. M. Alford and R. E. Smalley, *J. Phys. Chem.*, **1991**, *95*, 7564-7568.

[5] H. Shinohara, *Rep. Prog. Phys.*, **2000**, *63*, 843-892.

[6] Guha, S., Nakamoto, K., *Coord. Chem. Rev.*, **2005**, *249*, 1111-1132.

[7] (a) M. Saunders and H. A. Jiménez-Vázquez, R. J. Cross, R. J. Poreda, *Science*, **1993**, *259*, 1428--1430; (b) M. Saunders, H. A. Jimenez-Vazquez, R. J. Cross, S. M. L. Gross, D. E. Giblin and R. J. Poreda, *J. Am. Chem. Soc.*, **1994**, *116*, 2193-2194; (c) M. S. Syamala, R. J. Cross and M. Saunders, J. Am. Chem. Soc., **2002**, *124*, 6216-6219.

[8] H. Mauser, N. van Eikema Hommes, T. Clark, A. Hirsch. B. Pietzak, A. Weidinger and L. Dunsch, *Angew. Chem., Int. Ed. Engl.*, **1997**, *36*, 2835-2838.

[9] J. A. Larsson, J. C. Greer, W. Harneit and A. Weidinger, *J. Chem. Phys.*, **2002**, *116*, 7849-7854.

[10] (a) K. Kobayashi and S. Nagase, *Chem. Phys. Lett.*, **1998**, *282*, 325–329; (b) E. Nishibori, M. Takata, M. Sakata, M. Inakuma and H. Shinohara, *Chem. Phys. Lett.*, **1998**, *298*, 79–84; (c) M. Yamada, T. Wakahara, Y. F. Lian, T. Tsuchiya, T. Akasaka, M. Waelchli, N. Mizorogi, S. Nagase and K. M. Kadish, *J. Am. Chem. Soc.*, **2006**, *128*, 1400–1401.

[11] T. Akasaka, S. Nagase, K. Kobayashi, M. Walchli, K. Yamamoto, H. Funasaka, M. Kako, T. Hoshino and T. Erata, *Angew. Chem., Int. Ed. Engl.*, **1997**, *36*, 1643–1645.

[12] (a) S. Stevenson, M. A. Mackey, M. A. Stuart, J. P. Phillips, M. L. Easterling, C. J. Chancellor, M. M. Olmstead and A. L. Balch, *J. Am. Chem. Soc.*, **2008**, *130*, 11844–11845; (b) B. Q. Mercado, M. A. Stuart, M. A. Mackey, J. E. Pickens, B. S. Confait, S. Stevenson, M. L. Easterling, R. Valencia, A. Rodriguez-Fortea, J. M. Poblet, M. M. Olmstead and A. L. Balch, *J. Am. Chem. Soc.*, **2010**, *132*, 12098–12105; (c) B. Q. Mercado, M. M. Olmstead, C. M. Beavers, M. L. Easterling, S. Stevenson, M. A. Mackey, C. E. Coumbe, J. D. Phillips, J. P. Phillips, J. M. Poblet and A. L. Balch, *Chem. Commun.*, **2010**, *46*, 279–281.

[13] (a) C. R. Wang, T. Kai, T. Tomiyama, T. Yoshida, Y. Kobayashi, E. Nishibori, M. Takata, M. Sakata and H. Shinohara, *Angew. Chem., Int. Ed.*, **2001**, *40*, 397–399; (b) Y. Iiduka, T. Wakahara, T. Nakahodo, T. Tsuchiya, A. Sakuraba, Y. Maeda, T. Akasaka, K. Yoza, E. Horn, T. Kato, M. T. H. Liu, N. Mizorogi, K. Kobayashi and S. Nagase, *J. Am. Chem. Soc.*, **2005**, *127*, 12500–12501

[14] L. Dunsch. S, Yang, *Small*, **2007**, *3*, 1298-1320.

[15] S. Stevenson, G. Rice, T. Glass, K. Harish, F. Cromer, M. R. Jordan, J. Kraft, E. Hadju, R. Bible, M. M. Olmstead, K. Maitra, A. J. Fisher, A. L. Balch, H. C. Dorn, *Nature* **1999**, *401*, 55 – 57.

[16] R. D. Bolskar, *Nanomedicine*, **2008**, *3*, 201-213.

[17] M. D. Diener, J. M. Alford, S. J. Kennel, and S. Mirzadeh, J. Am. Chem. Soc., 2007, 129, 5131-5138.

[18] Shultz, M. D.; Duchamp, J. C.; Wilson, J. D.; Shu, C.-Y.; Ge, J.; Zhang, J.; Gibson, H. W.; Fillmore, H. L.; Hirsch, J. I.; Dorn, H. C.; Fatouros, P. P., *J. Am. Chem. Soc.*, **2010**, *132*, 4980–4981.

[19] (a) Chen, C. Y.; Xing, G. M.; Wang, J. X.; Zhao, Y. L.; Li, B.; Tang, J.; Jia, G.; Wang, T. C.; Sun, J.; Xing, L.; Yuan, H.; Gao, Y. X.; Meng, H.; Chen, Z.; Zhao, F.; Chai, Z. F.; Fang, X. H., *Nano Lett.*, **2005**, *5*, 2050-2057; (b) X. J. Liang, H. Meng, Y. Z. Wang, H. Y. He, J. Meng, J. Lu, P. C. Wang, Y. L. Zhao, X. Y. Gao, B. Y. Sun, C. Y. Chen, G. M. Xing, D. W. Shen, M. M. Gottesman, Y. Wu, J. J. Yin and L. Jia, *Proc. Natl. Acad. Sci. U. S. A.*, **2010**, *107*, 7449–7454.

[20] J. R. Pinzon, M. E. Plonska-Brzezinska, C. M. Cardona, A. J. Athans, S. S. Gayathri, D. M. Guldi, M. A. Herranz, N. Martin, T. Torres, L. Echegoyen, *Angew. Chem. Int. Ed.*, **2008**, *41*, 4173 – 4176.

[21] J. R. Pinzon, C. M. Cardona, M. A. Herranz, M. E. Plonska- Brzezinska, A. Palkar, A. J. Athans, N. Martin, A. Rodriguez- Fortea, J. M. Poblet, G. Bottari, T. Torres, S. S. Gayathri, D. M. Guldi, L. Echegoyen, *Chem. Eur. J.*, **2009**, *15*, 864 – 877.

[22] R. B. Ross, C. M. Cardona, D. M. Guldi, S. G. Sankaranarayanan, M. O. Reese, N. Kopidakis, J. Peet, B. Walker, G. C. Bazan, E. Van Keuren, B. C. Holloway and M. Drees, *Nat. Mater.*, **2009**, *8*, 208–212.

[23] B.C. Elliott, PhD Thesis, **2008**, Clemson University, USA

[24] W. Krätschmer, L. D. Lamb, K. Fostiropoulos, D. R. Huffman, *Nature*, **1990**, *347*, 354-358.

[25] R. E. Haufler, J. Conceicao, L. P. F. Chibante, Y. Chai, N. E. Byrne, S. Flanagan, M. M. Haley, S. C. O'Brien, C. Pan and R. E. Smalley, *J. Phys. Chem*., **1990**, *94*, 8634-8636.

[26] Langa, F., Nierengarten, J-F. (editors), **2012**, *Fullerenes: Principles and Applications* (2ⁿᵈ ed.), RSC, Cambridge,   Felder-Flesch D., *Chapter1: (Endo)fullerenes: From Production to Isolation*.

[27] J. B. Howard, J. T. McKinnon, Y. Makarovsky, Y. Lafleur and M. E. Johnson, *Nature*, **1991**, *352*, 139-141.

[28] (a) R. Taylor, G. J. Langley and H. W. Kroto, *Nature*, **1993**, *366*, 728-731.; (b) R. Taylor, G. J. Langley and H. W. Kroto, *Mol. Mat.*, **1994**, *4*, 7-14; (c) R. Taylor and G. J. Langley, *Recent Adv. Chem. Phys. Fullerenes and Rel. Mater.*, **1994**, 94-24, 68; (d) C. J. Crowley, H. W. Kroto, R. Taylor, D. R. M. Walton, M. S. Bratcher, P.-C. Cheng and L. T. Scott, *Tetrahedron Lett.,* **1995**, 9215-9218; (e) L. T. Scott, *Angew. Chem. Int. Ed.*, **2004**, *43*, 4995-5007.

[29] G. Otero, G. Bissau, C. Sanchez-Sanchez, R. Caillard, M. F. Lopez, C. Rogero, F. J. Palomares, N. Cabello, M. A. Basanta, J. Ortega, J. Mendez, A. M. Echavarren, R. Perez, B. Gomez-Lor and J. A. Martin-Gago, *Nature*, **2008**, 865-868.

[30] (a) S. Iijima, Nature 1991, 354, 56-58; (b) T. W. Ebbesen and P. M. Ajayan, *Nature*, **1992**, *358*, 220-222.

[31] (a) H. Ajie, M. M. Alvarez, S. J. Anz, R. D. Beck, F. Diederich, K. Fortiropoulos, R. Huffman, W. Krätschmer, Y. Rubin, K. E. Schriver, D. Sensharma and R. L. Wetten, *J. Phys. Chem*., **1990**, *94*, 8630-8633; (b) R. L. Wetten, M. M. Alvarez, S. J. Anz, K. E. Schriver, R. D. Beck, F. Diederich, Y. Rubin, R. Ettl, C. S. Foote, A. P. Darmanyan and J. W. Arbogast, *Mater. Res. Soc., Symp. Proc.*, **1990**, *206*, 639-650; (c) A. S. Koch, K. C. Khemani and F. Wudl, *J. Org. Chem.*, **1991**, *56*, 4543-4545; (d) R. E. Haufler, Y. Chai, L. P. F. Chibante, J. Conceicao, C. Jin, L. S. Wang, S. Maruyama and R. E. Smalley, *Mater. Res. Soc. Symp. Proc.*, **1991**, *206*, 627-638. (e) D. H. Parker, K. Chatterjee, P. Wurz, K. R. Lykke, M. J. Pellin, L. M. Stock and J. Hemminger, *Carbon*, **1992**, *30*, 1167-1182.

[32] C. Thilgen, F. Diederich and R. L. Whetten, *Buckminsterfullerenes*, W. E. Billups, M. A. Ciufolini, Eds. VCH Weinheim, **1993**.

[33] Ge, Z. X.; Duchamp, J. C.; Cai, T.; Gibson, H. W.; Dorn, H. C., *J. Am. Chem. Soc.*, **2005**, *127*, 16292–16298.

[34] Stevenson, S.; Harich, K.; Yu, H.; Stephen, R. R.; Heaps, D.; Coumbe, C.; Phillips, J. P., *J. Am. Chem. Soc.*, **2006**, *128*, 8829-8835.

[35] Elliott, B.; Yu, L.; Echegoyen, L., *J. Am. Chem. Soc.*, **2005**, *127*, 10885–10888.

[36] (a) S. Leach, M. Vervloet, A. Despres, E. Breheret, J. P. Hare, T. J. Dennis, H. W. Kroto, R. Taylor and D. R. M. Walton, *Chem. Phys.*, **1992**, *160*, 451-466. (b) G. Orlandi and F. Negri, *Photochem. Photobiol. Sci.*, **2002**, *1*, 289-308.

[37] S. Ceola, L. Franco, M. Maggini and C. Corvaja, *Photochem. Photobiol. Sci.*, **2006**, *5*, 1177-1182.

[38] Cai, T., Slebodnick, C., Xu, L., Harich, K., Glass, T. E., Chancellor, C., Fettinger, J. C., Olmstead, M. M., Balch, A. L., Gibson, H. W. and Dorn, H. C., *J. Am. Chem. Soc.*, **2006**, *128*, 6486– 6492.

[39] Ma, B.; Sun, Y.-P., *J. Chem. Soc., Perkin Trans. 2*, **1996**, 2157-2162.

[40] Khan, A.U. and Kasha, M., *Proc. Natl. Acad. Sci. USA*, **1979**, *76*, 6047-6049.

[41] Fraelich, M. R. and Weisman, R. B., *J. Phys. Chem.*, **1993**, *97*, 11145-11147.

[42] G. Brusatin and R. Signorini, *J. Mater. Chem.*, **2002**, *12*, 1964–1977.

[43] (a) Haddon, R. C.; Brus, L. E.; Raghavachari, K., *Chem. Phys. Lett.*, **1986**, *125*, 459-464; (b) Satpathy, S., *Chem. Phys. Lett.*, **1986**, *130*, 545-550; (c) Hale, P. D., *J. Am. Chem. Soc.*, **1986**, *108*, 6087-6088.

[44] L. Echegoyen, L. E. Echegoyen, *Acc. Chem. Res.*, **1998**, *31*, 593-601.

[45] Q. Xie, E. Perez-Cordero, L. Echegoyen, *J. Am. Chem. Soc.*, **1992**, *114*, 3978-3980.

[46] (a) Xie, Q.; Arias, F.; Echegoyen, L., *J. Am. Chem. Soc.*, **1993**, *115*, 9818-9819; (b) Dubois, D.; Kadish, K. M.; Flanagan, S.; Wilson, L. J., *J. Am. Chem. Soc.*, **1991**, *113*, 7773-7774.

[47] J. M. Campanera, C. Bo, J. M. Poblet, *Angew. Chem. Int. Ed.*, **2005**, *44*, 7230 – 7233.

[48] M. N. Chaur, R. Valencia, A. Rodrguez-Fortea, J. M. Poblet, L. Echegoyen, *Angew. Chem. Int. Ed.*, **2009**, *48*, 1425 – 1428.

[49] P. Jakes, K.-P. Dinse, *J. Am. Chem. Soc.*, **2001**, *123*, 8854 – 8855.

[50] (a) A. A. Popov, L. Dunsch, *J. Am. Chem. Soc.*, **2008**, *130*, 17726 – 17746; (b) J. M. Campanera, C. Bo, M. M. Olmstead, A. L. Balch, J. M. Poblet, *J. Phys. Chem. A*, **2002**, *106*, 12356 – 12364.

[51] C. M. Cardona, B. Elliott, L. Echegoyen, *J. Am. Chem. Soc.*, **2006**, *128*, 6480 – 6485.

[52] Chaur, M. N.; Melin, F.; Ortiz, A. L.; Echegoyen, L., *Angew. Chem., Int. Ed.*, **2009**, *48*, 7514-7538.

[53] (a) Y. Iiduka, O. Ikenaga, A. Sakuraba, T. Wakahara, T. Tsuchiya, Y. Maeda, T. Nakahodo, T. Akasaka, M. Kako, N. Mizorogi, S. Nagase, *J. Am. Chem. Soc.*, **2005**, *127*, 9956 – 9957; (b) M. Krause, L. Dunsch, *ChemPhysChem*, **2004**, *5*, 1445 – 1449.

[54] T. Cai, L. Xu, M. R. Anderson, Z. Ge, T. Zuo, X. Wang, M. M. Olmstead, A. L. Balch, H.W. Gibson, H. C. Dorn, J. *Am. Chem. Soc.*, **2006**, *128*, 8581 – 8589.

[55] M. N. Chaur, F. Melin, B. Elliott, A. J. Athans, K. Walker, B. C. Holloway, L. Echegoyen, *J. Am. Chem. Soc.*, **2007**, *129*, 14826 – 14829.

[56] M. N. Chaur, F. Melin, A. J. Athans, B. Elliott, K. Walker, B. C. Holloway, L. Echegoyen, *Chem. Commun.* **2008**, 2665 – 2667.

[57] R. C. Haddon, *Science*, **1993**, *261*, 1545-1550.

[58] (a) J. M. Hawkins, A. Meyer, *Science*, **1993**, *260*, 1918-1920 (b) R. C. Haddon, G. E. Scuseria, R. E. Smalley, *Chem. Phys. Lett.*, **1997**, *272*, 38-42 (c) J. M. Hawkins, A. Meyer, M. A. Solow, *J. Am. Chem. Soc.*, **1993**, *115*, 7499-7500.

[59] Bingel, C.; *Chem. Ber.*, **1993**, *126*, 1957 – 1959.

[60] (a) J.-F. Nierengarten, V. Gramlich, F. Cardullo and F. Diederich, *Angew. Chem. Int. Ed. Engl.*, **1996**, *35*, 2101-2103; (b) J.-F. Nierengarten and J.-F. Nicoud, *Tetrahedron Lett.*, **1997**, *38*, 7737-7740.

[61] X. Camps and A. Hirsch, *J. Chem. Soc., Perkin Trans. 1*, **1997**, *11*, 1595-1596.

[62] R. Kessinger, J. Crassous, A. Hermann, M. Ruttimann, L. Echegoyen and F. Diederich, *Angew. Chem. Int. Ed. Engl.*, **1998**, *37*, 1919-1922.

[63] Hudhomme, P., *C. R. Chimie*, **2006**, *9*, 881-891.

[64] (a) F. Langa, P. de la Cruz, A. de la Hoz, A. Dıaz-Ortiz and E. Diez-Barra, *Contemp. Org. Synth.*, **1997**, 373-386 ; (b) F. Langa, P. de la Cruz, E. Espildora, J. J. Garcia, M. C. Perez, A. de la Hoz, *Carbon*, **2000**, *38*, 1641-1646.

[65] Rotello, V. M.; Howard, J. B.; Yadav, T.; Conn, M. M.; Viani, E.; Giovane, L. M.; Lafleur, A. L., *Tetrahedron Lett.*, **1993**, *34*, 1561-1562 (b) M. Tsuda, T. Akayuki, T. Nagami, S. Kurano and M. Ohashi, *J. Chem. Soc., Chem. Commun.*, **1993**, 1296-1298.

[66] Hirsch, A.; Brettreich, M., *Fullerenes: Chemistry and Reactions*, Wiley-VCH, New York, **2005**.

[67] (a) J. A. Schluter, J.M. Seaman, S. Taha, H. Cohen, K. R. Lykke, H. H. Wang and J.M. Williams, *J. Chem. Soc., Chem. Commun.*, **1993**, 972-974; (b) K. Komatsu, Y. Murata, N. Sugita, K. Takeuchi and T. S. M. Wan, *Tetrahedron Lett.*, **1993**, *34*, 8473-8476.

[68] J. L. Segura and N. Martın, *Chem. Rev.*, **1999**, *99*, 3199-3246.

[69] Maggini, M.; Scorrano, G.; Prato, M., *J. Am. Chem. Soc.*, **1993**; *115*, 9798-9799.

[70] Maggini, M.; Prato M., *Acc. Chem. Res.*, **1998**, *31*, 519-526.

[71] S. H. Hoke II, J. Molstad, D. Dilettato, M. J. Jay, D. Carlson, B. Kahr, R. G. Cooks, *J. Org. Chem.*, **1992**, *57*, 5069-5071.

[72] (a) K. D. Kampe, N. Egger and M. Vogel, *Angew. Chem*. Int. Ed., **1993**, *32*, 1174-1176; (b) J. M. Hawkins, A. Meyer, T. A. Lewis, U. Bunz, R. Nunlist, G. E. Ball, T. W. Ebbesen and K. Tanigaki, *J. Am. Chem. Soc.*, **1992**, *114*, 7954-7955; (c) C. C. Henderson, C. M. Rohlfing, R. A. Assink and P. A. Cahill, *Angew. Chem. Int. Ed. Engl.*, **1994**, *33*, 786-788; (d) Y. Nakamura, N. Takano, T. Nishimura, E. Yashima, M. Sato, T. Kudo and J. Nishimura, *Org. Lett.*, **2001**, *3*, 1193-1196.

[73] L. Isaacs, R.F. Haldimann and F. Diederich, *Angew. Chem. Int. Ed.*, **1994**, *33*, 2339-2342.

[74] A. Hirsch, I. Lamparth, T. Grösser, H. R. Karfunkel, *J. Am. Chem. Soc,.* **1994**, *116*, 9385.

[75] C. Thilgen, A. Herrmann and F. Diederich, *Angew. Chem., Int. Ed.Engl.*, **1997**, *36*, 2269.

[76] C. Thilgen and F. Diederich, *Top. Curr. Chem.*, **1999**, *199*, 135-171.

[77] (a) A. Herrmann, F. Diederich, C. Thilgen, H.-U. Ter Meer and W. H. Muller, *Helv. Chim. Acta,* **1994**, *77*, 1689-1706; (b) A. Herrmann and F. Diederich, *J. Chem. Soc., Perkin Trans. 2*, **1997**, 1679-1684.

[78] X. Lu, T. Akasaka and S. Nagase, *Chem. Commun.*, **2011**, *47*, 5942–5957.

[79] Campanera, J. M.; Bo, C.; Poblet, J. M., *J. Org. Chem.*, **2006**, *71*, 46-54.

[80] (a) Diederich, F., Thilgen, C., *Science*, **1996**, *271*, 317-324 (b) Hall, M. H.; Lu, H.; Shevlin, P. B., *J. Am. Chem. Soc.*, **2001**, *123*, 1349-1354.

[81] (a) Kordatos, K.; Bosi, S.; Da Ros, T.; Zambon, A.; Lucchini, V.; Prato, M., *J. Org. Chem.*, **2001**, *66*, 2802-2808. (b) Ishi-i, T.; Nakashima, K.; Shinkai, S., *Chem. Commun.*, **1998**, 1047-1048. (c) Taki, M.; Sugita, S.; Nakamura, Y.; Kasashima, E.; Yashima, E.; Okamoto, Y.; Nishimura, J., *J. Am. Chem. Soc.*, **1997**, *119*, 926-932.

[82] O. Lukoyanova, C. M. Cardona, J. Rivera, L. Z. Lugo-Morales, C. J. Chancellor, M. M. Olmstead, A. Rodriguez-Fortea, J. M. Poblet, A. L. Balch and L. Echegoyen, *J. Am. Chem. Soc.*, **2007**, *129*, 10423–10430.

[83] T. Wakahara, Y. Iiduka, O. Ikenaga, T. Nakahodo, A. Sakuraba, T. Tsuchiya, Y. Maeda, M. Kako, T. Akasaka, K. Yoza, E. Horn, N. Mizorogi, S. Nagase, *J. Am. Chem. Soc.*, **2006**, *128*, 9919 – 9925.

[84] (a) N. B. Shustova, A. A. Popov, M. A. Mackey, C. E. Coumbe, J. P. Phillips, S. Stevenson, S. H. Strauss, O. V. Boltalina, *J. Am. Chem. Soc.*, **2007**, *129*, 11676 – 11677 (b) C. Shu, T. Cai, L. Xu, T. Zuo, J. Reid, K. Harich, H. C. Dorn, H.W. Gibson, *J. Am. Chem. Soc.,* **2007**, *129*, 15710 – 15717.

[85] (a) E. B. Iezzi, F. Cromer, P. Stevenson, H. C. Dorn, *Synth. Met.*, **2002**, *128*, 289 – 291; (b) P. P. Fatouros, F. D. Corwin, Z. J. Chen, W. C. Broaddus, J. L. Tatum, B. Kettenmann, Z. Ge, H. W. Gibson, J. L. Russ, A. P. Leonard, J. C. Duchamp and H. C. Dorn, *Radiology*, **2006**, *240*, 756–764; (c) J. F. Zhang, P. P. Fatouros, C. Y. Shu, J. Reid, L. S. Owens, T. Cai, H. W. Gibson, G. L. Long, F. D. Corwin, Z. J. Chen and H. C. Dorn, *Bioconjugate Chem.*, **2010**, *21*, 610–615; (d) M. Mikawa, H. Kato, M. Okumura, M. Narazaki, Y. Kanazawa, N. Miwa and H. Shinohara, *Bioconjugate Chem.*, **2001**, *12*, 510–514; (e) G. M. Xing, H. Yuan, R. He, X. Y. Gao, L. Jing, F. Zhao, Z. F. Chai and Y. L. Zhao, *J. Phys. Chem. B*, **2008**, *112*, 6288–6291.

[86] C. Shu, C. Slebodnick, L. Xu, H. Champion, T. Fuhrer, T. Cai, J. E. Reid, W. Fu, K. Harich, H. C. Dorn, H.W. Gibson, *J. Am. Chem. Soc.*, **2008**, *130*, 17755 – 17760.

[87] E. B. Iezzi, J. C. Duchamp, K. Harich, T. E. Glass, H. M. Lee, M. M. Olmstead, A. L. Balch and H. C. Dorn, *J. Am. Chem. Soc.*, **2002**, *124*, 524–525.

[88] H. M. Lee, M. M. Olmstead, E. B. Iezzi, J. C. Duchamp, H. C. Dorn, A. L. Balch, *J. Am. Chem. Soc.*, **2002**, *124*, 3494 – 3495.

[89] S. Stevenson, R. R. Stephen, T. M. Amos, V. R. Cadorette, J. E. Reid, J. P. Phillips, *J. Am. Chem. Soc.*, **2005**, *127*, 12776 – 12777.

[90] C. M. Cardona, A. Kitaygorodskiy, A. Ortiz, M. A. Herranz, L. Echegoyen, *J. Org. Chem.*, **2005**, *70*, 5092 – 5097.

[91] C. M. Cardona, A. Kitaygorodskiy, L. Echegoyen, *J. Am. Chem. Soc.*, **2005**, *127*, 10448 – 10453.

[92] N. Chen, E.-Y. Zhang, K. Tan, C.-R. Wang, X. Lu, *Org. Lett.,* **2007**, *9*, 2011 – 2013.

[93] X. Gao, K. Ishimura, S. Nagase, Z. Chen, *J. Phys. Chem. A*, **2009**, *113*, 3673 –3676.

[94] J. R. Pinzon, T. M. Zuo and L. Echegoyen, *Chem.–Eur. J.*, **2010**, *16*, 4864–4869.

[95] Li, F. F.; Rodríguez-Fortea, A.; Poblet, J. M.; Echegoyen, L. J., Am. Chem. Soc., **2011**, 133, 2760-2765.

[96] J.C. Hummelen, B.W. Knight, F. Lepeq, F. Wudl, J. Yao, and C.L. Wilkins, *J. Org. Chem.*, **1995**, *60*, 532-538.

[97] F. F. Li, J. R. Pinzon, B. Q. Mercado, M. M. Olmstead, A. L. Balch and L. Echegoyen, *J. Am. Chem. Soc.*, **2011**, *133*, 1563–1571.

[98] Reinitzer F., *Monatsh.Chem.*, **1888**, *9*, 421-441.

[99] Lehmann O., *Z. für Physik. Chemie 4*, **1889**, 462-472.

[100] Friedel G., *Annales de Physique*, **1922**, *18*, 273-474.

[101] A. Skoulios, *Annales de Physique*, **1978**, *3*, 421-450.

[102] Goodby, J. W.; Saez, I. M.; Cowling, S. J.; Görtz, V.; Draper, M.; Hall, A. W.; Sia, S.; Cosquer, G.; Lee, S.-E.; Raynes, E. P., *Angew. Chem., Int. Ed.*, **2008**, *47*, 2754-2787.

[103] (a) J. Malthête, A. M. Levelut, H. T. Nguyen, *J. Phys. Lett.*, **1985**, *46*, 875-880; (b) H. T. Nguyen, C. Destrade, J. Malthête, *Adv. Mater.*, **1997**, *9*, 375-388; (c) J. Malthête, H. T. Nguyen, C. Destrade, *Mol. Cryst. Liq. Cryst.*, **1993**, *13*, 171; (d) H. Gasparoux, F. Hardouin, C. Destrade, H. T. Nguyen, *New. J. Chem.*, **1992**, *16*, 295; (e) M. Gharbia, A. Gharbi, H. T. Nguyen and J. Malthete, *Curr. Opin. Colloid Interface Sci.*, **2002**, *7*, 312–325.

[104] V. S. K. Balagurusamy, G. Ungar, V. Percec, G. Johansson, *J. Am. Chem. Soc.*, **1997**, *119*, 1539-1555.

[105] D. Felder, B. Heinrich, D. Guillon, J.–F. Nicoud, J.-F. Nierengarten, *Chem. Eur. J.*, **2000**, *6*, 3501-3507.

[106] P. Fuchs, C. Tschierske, K. Raith, K. Das, S. Diele, *Angew. Chem. Int. Ed. Engl.*, **2002**, *41*, 628-631.

[107] D. W. Bruce, Differential Scanning Calorimetry and Liquid Crystals, *Lecture on Liquid Crystal Workshop*, **2011,** Hull, UK

[108] R. M. Richardson, X-ray Diffraction from Liquid Crystals, , *Lecture on Liquid Crystal Workshop*, **2011,** Hull, UK

[109] D. Demus, J. Goodby, G.W.Gray; H.-W. Spiess, V. Vill, *Handbook of Liquid Crystals,* **1998**, Weinheim, Wiley – VCH

[110] D. Guillon, B. Heinrich, A.C. Ribeiro, C. Cruz, H. T. Nguyen, *Mol. Cryst. Liq. Cryst.*, **1998**, *317*, 51-64.

Chapter II

LC fullerene derivatives for improved photovoltaic devices

This chapter gives a brief overview of liquid crystalline (LC) fullerene derivatives, fullerene based donor-acceptor (D-A) systems with special attention to C_{60}-π conjugated oligomer ensembles and their combinations (ie. liquid crystalline donor-acceptor fullerenes). It summarizes our efforts to create such a system from design to materialization. Two D-A dyads have been synthesized using an asymmetric or symmetric oligo(phenyleneethynylene) based malonate precursor. They display smectic A and columnar phases, respectively, and demonstrate the energy transfer process with unitary efficiency. Herein, we also describe the synthesis and analysis of the first LC, D-A, trimetallic nitride template (TNT) endohedral metallofullerene (EMF), prepared by the functionalization of $Y_3N@C_{80}$ with an oligo(phenyleneethynylene) derivative.

Four oligo(phenylenevinylene) based electron donor units, each comprising three and four monomeric units, were covalently bonded to one C_{60} acceptor unit. Thus, D-A ensembles with multiple electron donors were created. The preliminary results suggest the occurrence of mesophase for the dyads and the quenching of the luminescence of the OPV moieties imply excited state communication between the donor and acceptor moieties.

These findings are important for the design of photovoltaic and optoelectronic devices with well-defined morphology at the nanometer level.

II. 1)   Introduction

II. 1. 1)   LC fullerenes

Functionalization of C_{60} with mesogenic promoters can lead to mesomorphic fullerene derivatives. There are two main approaches to achieve fullerene-containing liquid crystals based on covalent and non-covalent[1] methods. Herein, only the covalent method will be discussed.

The incorporation of a fullerene into such a system requires careful tailoring of the compound, because grafting a mesogen on the periphery of the C_{60} core does not always promote self-organization. Failure to promote self-organization happens if the mesogen is not large/strong enough to prevent the steric effects generated by the bulky fullerene or the cross-sections of the two building blocks are not adequate to induce an LC phase. Decoupling the anisotropic unit(s) from the bulky C_{60} (eg. via the introduction of a flexible spacer) promotes self-organization due to the free interaction between mesogenic side-groups of neighboring molecules.

Usually dendrimers or cholesterol units, as mesogens, have been attached to the fullerene through methano- or pyrrolidine bridges. To date, a large number of LC fullerene derivatives with smectic[2], columnar[3], nematic[4] and chiral nematic[5] phases have been prepared and reported. The properties of the materials are mostly dominated by the anisotropic moiety[6] ie. the supramolecular organization of functionalized fullerenes closely resembles that of the corresponding mesogenic precursor mainly because these materials are often made with low C_{60} content.

The first mesomorphic derivative of C_{60} bearing two mesogenic cholesterol subunits (Figure 1) was synthesized in 1996 by R. Deschenaux and T. Chuard[7]. It displays a monotropic smectic A (SmA) mesophase between 146 °C and 190 °C, which is a significantly limited mesomorphic behavior when compared to that of the malonate precursor. It has been concluded that this is a consequence of the presence of the fullerene moiety which acts as a bulky spacer and greatly disturbs the interactions between mesogen units.
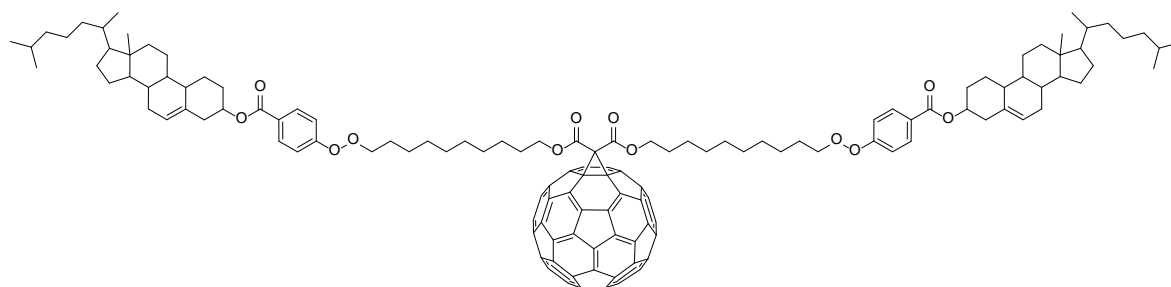
Figure 1, The first liquid crystalline [60]fullerene derivative that gives rise to SmA phase[7].

The use of dendritic mesomorphic precursors often facilitates the formation of mesophases via the avoidance of C_{60} aggregation and unfavorable steric effects[6]. For example, a methanofullerodendrimer built up from fourth generation dendrimers containing cyanobiphenyl units as liquid-crystalline promoters at the periphery, display similar mesomorphic properties (ie. SmA phase) and supramolecular organization to the corresponding malonate precursor[2f]. Most of the analogue fullerodendrimers with dendrimer generation numbers between 0 and 4 show a similar behavior as a consequence of the C_{60} being buried within the dendritic branches and the large number of mesogenic groups that can compensate for the influence of the fullerene.
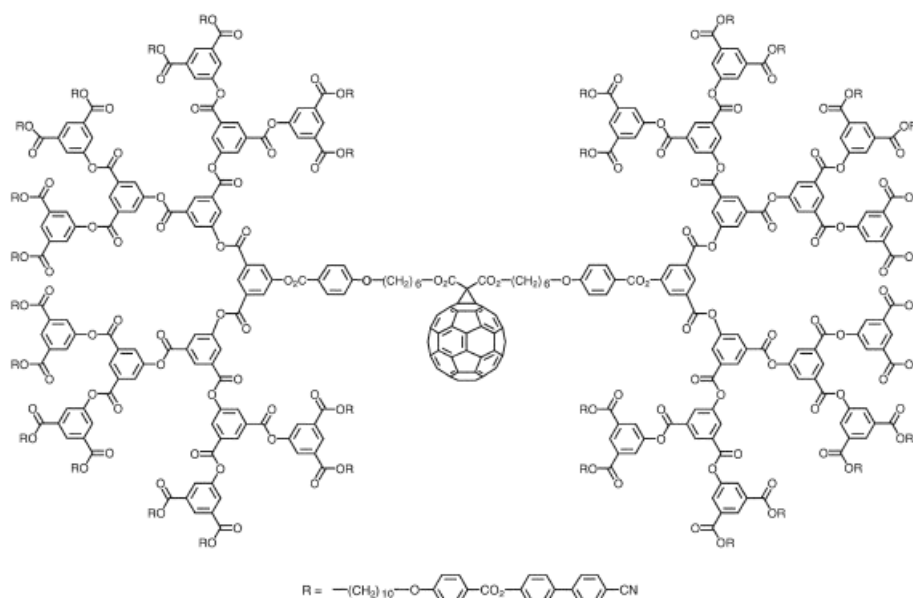

Figure 2, Fullerodendrimer derivatized with fourth generation mesomorphic dendrimers containing cyanobiphenyl subunits at the periphery[2f].

Hexaaddition was considered to be another possible approach to circumvent the undesirable effect of C_{60} on the optical anisotropy. Several hexakisadducts have been synthesized by numerous groups [4a,c,8,]. In this case, C_{60} can be considered as a versatile hard nanocore to build up globular systems due to its tunable valency (1 to 6) and regioselective polyaddition where the fullerene core plays the role of a scaffold to build supermolecular structures. Hexaaddition appears to be sufficient to achieve the preparation of thermotropic [60]fullerene-based liquid-crystals, even starting from weak or non-mesogenic promoters[4a,c] (Figure 3) and to prevent the aggregation of C_{60}, but the electronic properties of the fullerene are usually greatly altered.
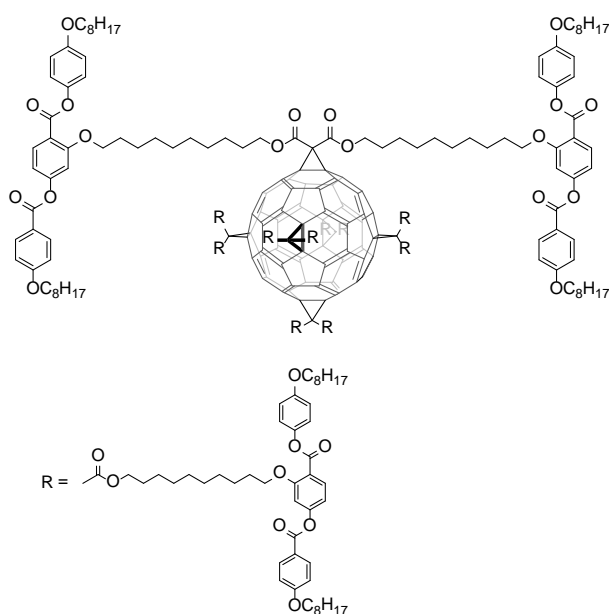

Figure 3, Structure of a liquid crystalline hexakisadduct built up of non-mesomorphic promoters[4a].

Bis-addition was also studied in order to retain the photo- and electrochemical properties of the fullerene. Different regioisomers (trans-2, trans-3 and equatorial) of LC fullerene bisadducts containing cyanobiphenyl mesogenic promoters[9] (Figure 4) have been prepared and their LC properties were compared to their corresponding monoadduct. All bisadducts displayed SmA phases in a similar way to their precursor. The supramolecular organization of the monoadduct was governed by steric factors and as a consequence, the molecules are organized into a head-to-tail fashion forming a bilayered structure. On the other hand, the molecular organization of bisadducts was governed only by the dendritic mesogens and the C_{60} had no influence on it. All regioisomeric bisadduct derivatives were

organized into a monolayered SmA phase and the position of the second addition did not seem to seriously alter the supramolecular organization.
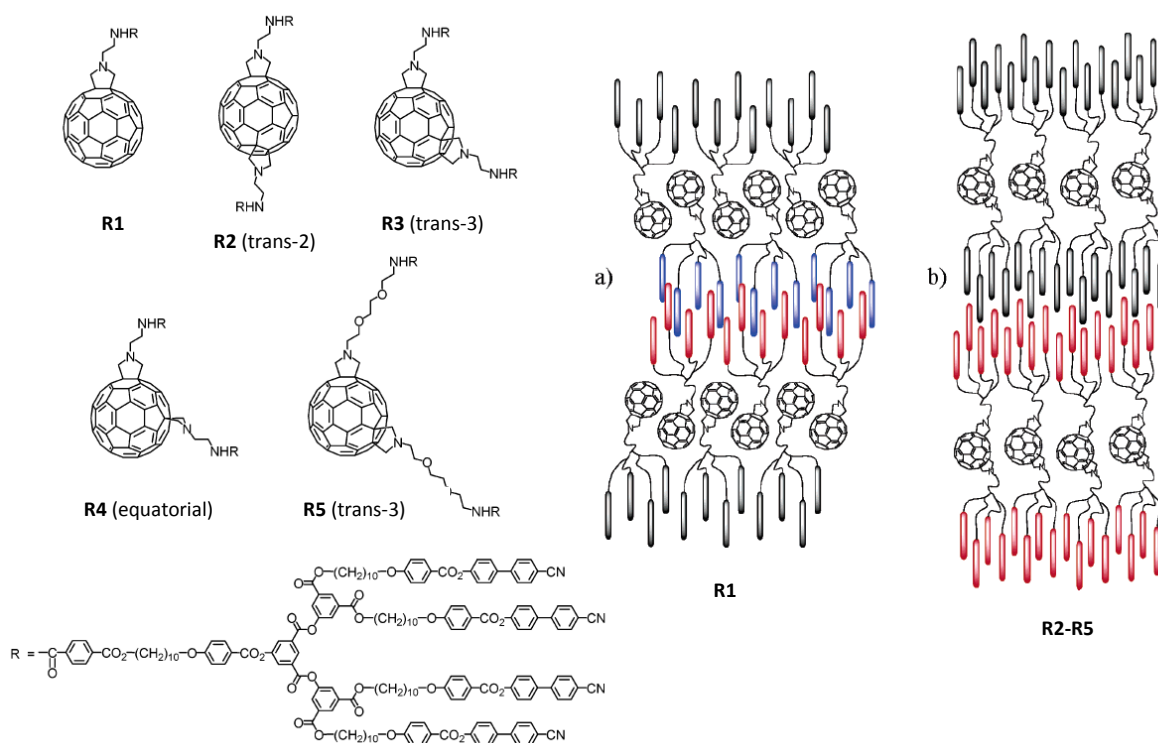

Figure 4, (left) Structure of mono- and regioisomeric bisadducts containing cyanobiphenyl mesogenic promoters. (Right) supramolecular organization of a) monoadduct and b) bisadducts[9].

II. 1. 2) Photovoltaics, fullerene and endofullerene based photovoltaic devices

Fossil energy resources are limited and produce several forms of pollution in our environment. Hence, there is an urgent need for renewable energy sources which come from natural resources such as sunlight, wind, rain, tides, and geothermal heat. There is roughly 174 petawatts of incoming solar radiation on the Earth, which could potentially satisfy and even exceed many times the world's energy requirements if harnessed efficiently.

The photovoltaic effect is the conversion of light energy into electric energy, which was first observed in 1839 by the French physicist, Alexandre-Edmond Becquerel[10], who witnessed the generation of a photocurrent when light irradiated silver-chloride coated

platinum plates were placed in a weakly conducting acidic solution. Since then, the photovoltaic effect has been broadly studied and a vast number of different photovoltaic devices have been created. Today's solar cell market is dominated by inorganic silicon based n-p junction semiconducting materials due to their relatively high efficiency (Figure 5).

In these Si cells, n-type and p-type doped Si are brought in contact to form a junction. The doping in the n-type Si results in an excess of electrons in the crystal lattice while the doping of the p-type yields electron deficient sites (holes). When they come into contact, the energy difference between these two materials results in band bending that can induce spontaneous flow of excited electrons in the conduction band. Upon irradiation, the absorbed light induces photoexcitation and promotes electrons to the conduction band which then flow along the bent band and are collected as photocurrent.
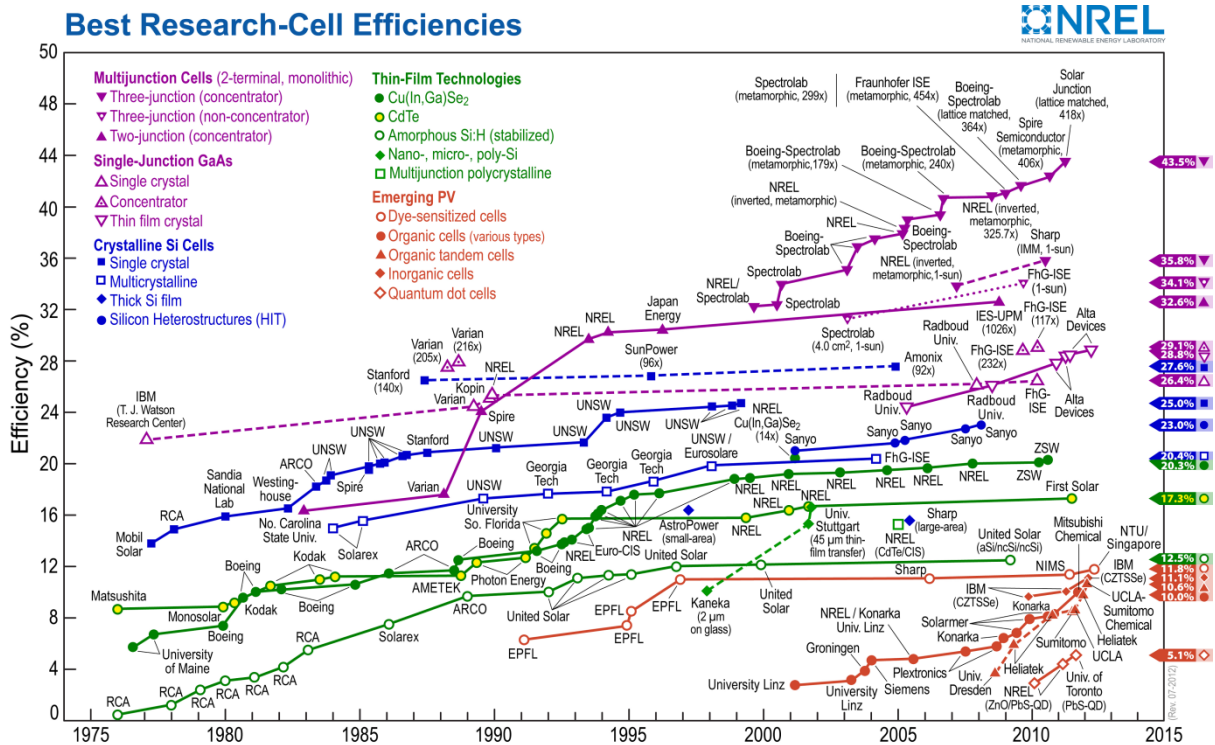

Figure 5, Best research photovoltaic cell efficiencies (National Center for Photovoltaics).

Much less attention has been paid to the development of organic photovoltaic devices due to their lower efficiency (Figure 5). Still, these devices can be considered as viable alternatives because of their potential low production cost (no high temperature and high vacuum is required in contrast to inorganic solar cells), incorporation into flexible devices, light weight and fairly good performances shown under low light conditions[11].

Two main approaches can be considered to build such devices:

- bulk heterojunction (BHJ) solar cells consists of the blend of organic semiconducting – p-type donor and n-type acceptor – materials.
- covalent linking of the donor to the acceptor creates donor-acceptor (D-A) molecular dyads sometimes also called molecular heterojunction devices.

II. 1. 2. 1)BHJ organic solar cells

The efficiency of BHJ organic solar cells remained low until the mid 1980s. The p-n junction approach in organic photovoltaic cells, introduced in 1986 by Tang[12], was a significant step towards higher efficiency device fabrication. A double-layer solar cell was prepared by thermal evaporation of sequential layers of copper phthalocyanine (CuPc) and 3,4,9,10- perylenetetracarboxylic bis-benzimidazole (PTCBI) sandwiched between silver and ITO-coated glass substrates and had an efficiency of 0.95%. However, the effective interaction between electron-donor and electron-acceptor was limited and only active at the interfaces, thus yielded low photovoltaic performances.

The bulk heterojunction concept[13] (Figure 6) was introduced to overcome the aforementioned problem and became another major breakthrough towards efficient photovoltaic devices. It is an interpenetrating network of a p-type organic donor and an n-type organic acceptor material blend. Thus, effective donor-acceptor interaction can take place over a much larger interface area and, as a consequence, the performance of the device improves. Soon after the discovery of fullerenes, C_{60} became the most widely used electron acceptor in organic photovoltaic devices due to its electron deficient cage and small reorganization energy; whilst conjugated polymers emerged as the primary electron donor materials of BHJ cells. In order to improve hole mobility usually a hole transporting poly(3,4-ethylenedioxythiophene)-poly(styrenesulfonate) (PEDOT-PSS) layer is placed between the transparent ITO electrode and the photoactive layer blend. The most important drawback of such devices is the tendency, especially for pristine C_{60}, to phase separate on a macroscopic scale and through this, deteriorate device performances. Thus, the more easily processable [6,6]-phenyl C_{61}-butyric acid methyl ester (PCBM), a relatively

simple C_{60} derivative, was synthesized and is widely used as electron acceptor material. Nowadays, most organic BHJ solar cells are prepared from PCBM either based on C_{60} or C_{70}[14].
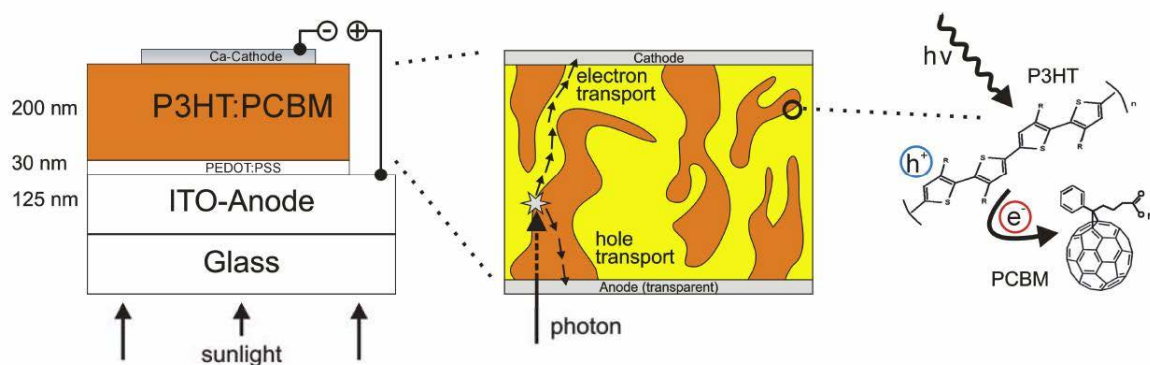

Figure 6, *General structure and basic principle of the BHJ solar cells. Electron donor* poly(3-hexylthiophene) *(P3HT) and acceptor (PCBM) are blended together to maximize the interface where the exciton dissociation into electrons and holes takes place. For an efficient photocurrent, each material must provide a continuous path for electron and hole transport to the respective contact*[15].

The process in BHJ photovoltaic devices, which converts light energy to chemical energy, is the following:

1)   light absorption (exciton generation),

2)   exciton diffusion (a few nanometers),

3)   charge separation and

4)   charge transport.

There are different molecular and morphological requirements for the photoactive layer to obtain high-performance organic solar cell. Effective light absorption and charge separation depend on the molecular structures, the HOMO and LUMO levels of the donor and acceptor materials and the donor/acceptor interface area, layer thickness and roughness. While effective/optimal charge transport relies on the charge carrier mobility and the development of a suitable nanomorphology i.e. bicontinuous interpenetrating phase structures within the blend films[16,17].

Numerous donor polymers and acceptor fullerene derivatives were synthesized and different film formation methods were tested. A lot of research efforts have been aimed at improving the spectral absorption of donor polymers[18] to achieve a better match with the

solar radiation spectrum. But one can also find interesting examples of fullerene derivatives as possible replacements or additives of the very popular PCBM (vide infra).

Endohedral fullerenes. The $Lu_3N@C_{80}$-PCBX family of TNT EMF derivatives (X = methyl, butyl, hexyl and octyl) have been synthesized[19] by a modified Hummelen method[20] to replace C_{60}-PCBM in BHJ organic photovoltaic devices (Figure 7). The $Lu_3N@C_{80}$ derivatives have a higher LUMO level than their C_{60} analogue, thus when paired with the same donor (P3HT) the $Lu_3N@C_{80}$-PCBX family demonstrates reduced energy losses in the charge transfer process and increased open circuit voltages. This study demonstrates that reducing the donor/acceptor LUMO offset, by using TNT EMF derivatives as acceptor materials, can lead to more efficiently harnessed photoexcited electrons and higher overall power conversion efficiency (PCE).
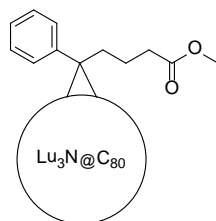

Figure 7, $Lu_3N@C_{80}$-PCBM.

Multiadducts. The performance of C_{60}-PCBM and its bis- and trisadduct were also compared. A BHJ photovoltaic device of P3HT:bisPCBM[21] showed a higher PCE due to the increased LUMO level, even though the regioisomeric mixture of bisadducts was used for device fabrication. Despite the even higher LUMO level, trisPCBM demonstrated poor performance as a consequence of the deteriorated charge carrier properties[22].

Light-harvesting and energy funnel fullerenes. Light harvesting fullerene additives were designed to cover the visible and near-IR region of the solar spectrum. A silicon phthalocyanine (SiPc) interface additive was tested in a P3HT:PCBM device and revealed improved PCE. This result suggested that SiPc molecules located at the interface have a double role: a) a light harvesting photosenzitizer and b) an energy funnel for P3HT excitons. Thus, SiPc can harvest excitons efficiently through long-range energy transfer[23].
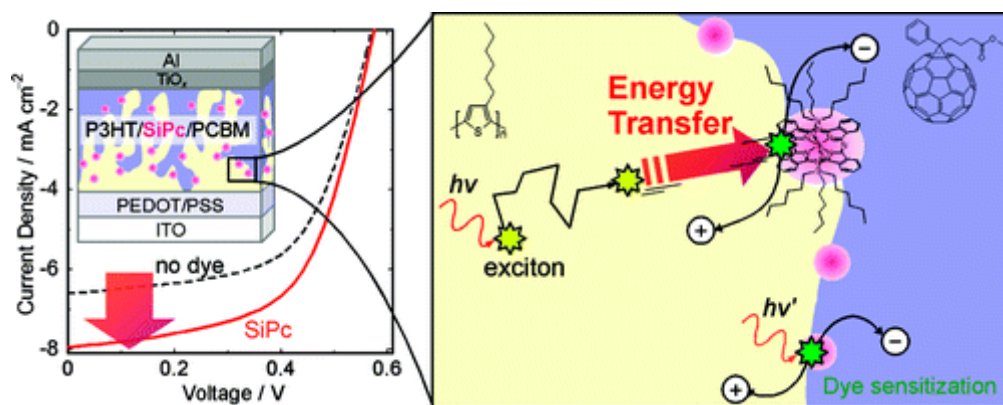
Figure 8, Introduction of silicon phthalocyanine derivative (SiPc) at the donor-acceptor interface increased the short-circuit current density and hence improved the PCE[23].

A phthalocyanine-fullerene (Pc-C_{60}) D-A dyad was designed (Figure 9) not only to extend the absorption range of the active layer, but also to contribute to the charge separation process. The absorption spectrum of poly [2-methoxy-5-(30,70-dimethyloctyloxy)-1-4-phenylene vinylene] (MDMO-PPV), which was used as an antenna system for energy transfer to the dyad, covered another significant part of the solar radiation spectrum. Three different active layers were investigated: Pc-C_{60}; MDMO-PPV:Pc-C_{60}; and MDMO-PPV:Pc-C_{60}:PCBM. Low PCE (0.02 %) was observed when solely the D-A dyad was used for device fabrication[24]. In the other two cases, an energy transfer from MDMO-PPV to the dyad was found to take place, but the low short-circuit currents indicated charge transport problems within the device[25].
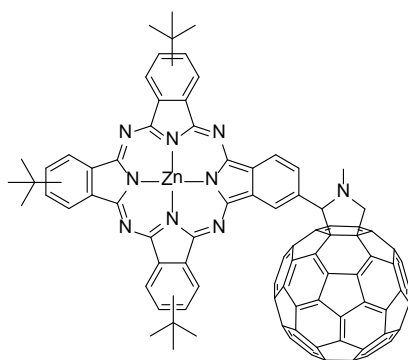

Figure 9, Structure of Pc-C_{60} D-A dyad.

A series of perylene-3,4:9,10-bis(dicarboximide) (PDI)-C_{60} dyads were synthesized and examined as the acceptor material of the active layer. Almost quantitative photoinduced energy transfer was observed from the PDI to the C_{60} moiety and the relationship between the electrochemical properties of the dyad and the photovoltaic device efficiency of the P3HT:C_{60}–PDI blend was demonstrated[26].
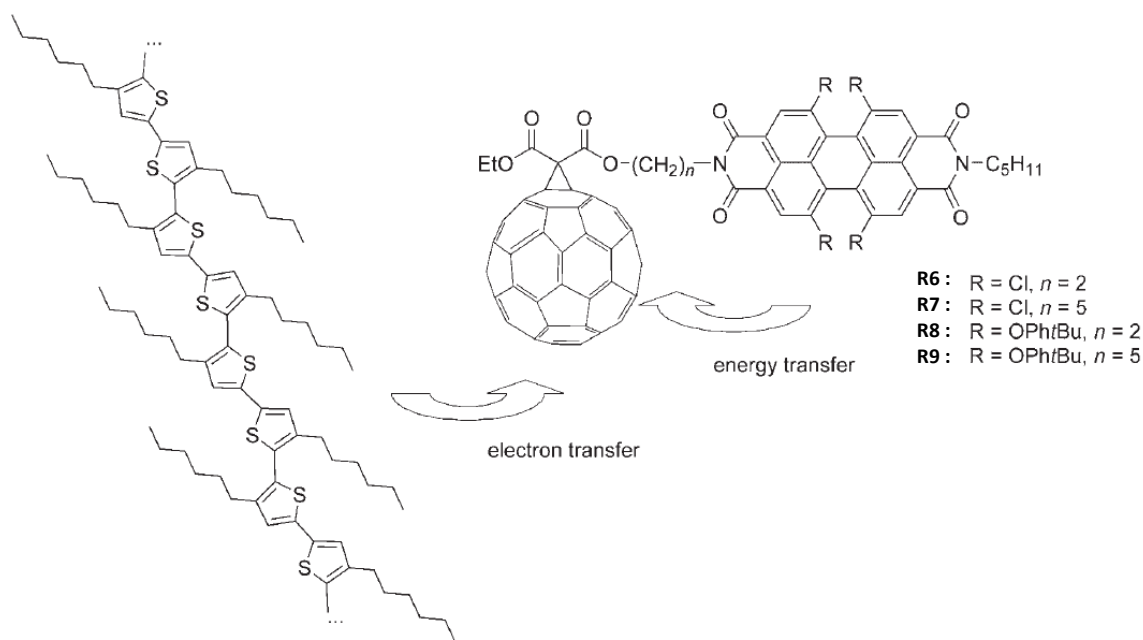
Figure 10, Representation of the photoactive layer of an organic solar cell incorporating the p-type P3HT polymer donor and the C_{60}–PDI dyad as electron acceptor, where PDI act as a light harvesting antenna[26].

II. 1. 2. 2) D-A ensembles

Molecular heterojunction devices consist of an electron donating moiety (D) covalently (or non-covalently via complexation) attached to an electron acceptor (A), which is often fullerene. These devices attempt to mimic the natural process of photosynthesis, where a sequence of electron transfer events takes place between electron donating chromophores and electron acceptors to give a long distance and long lived (~1 ms) charge separated state. The photovoltaic process in artificial D-A ensembles also resembles that of BHJ photovoltaic devices. This approach has emerged as a solution for the uncontrolled phase separation of donor and acceptor components which is observed in BHJ solar cells and results in deteriorated device performances. In D-A dyads both energy and electron transfer processes can take place between the photoexcited donor moiety and the fullerene. Researchers usually focus on the optimization of the electron transfer efficiencies.

Although, a lot of effort has been made, and many different D-A ensembles have been prepared[27], the devices' performance cannot yet reach that of natural photosynthesis (and not even that of BHJ solar cells), where the same fundamental effects occur.

Photosynthesis begins with the excitation of a chlorophyll molecule, followed by an electron transfer cascade in which a charge separated state is generated. The early events have near 100% quantum efficiency, as energy-wasting charge recombination is reduced by having the electron shuttled away a long distance from its point of origin, and by a low reorganization energy[28]. The main challenges in artificial D-A dyads are charge separation due to competition between energy and electron transfer processes and the lifetime of the charge separated state due to charge recombination.

Two different types of electron donors have been paired with fullerenes: photoactive and non-photoactive donors.

Non-photoactive electron donors:

a) Tetrathiafulvalenes (TTF), π-extended tetrathiafulvalenes (ex-TTF) (Figure 11): TTF is a nonaromatic molecule that adopts aromatic character with the formation of a radical cation and dication. Its main advantage is the ability to stabilize a charge separated state in a D-A ensembles, but its donating capabilities have to be improved to induce electron transfer.
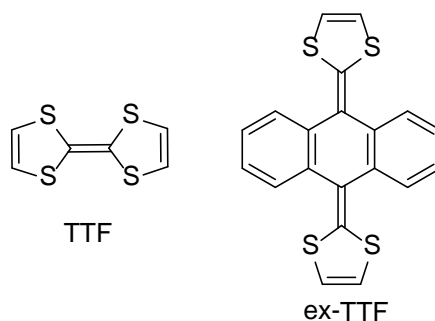

Figure 11, Chemical structure of TTF and ex-TTF.

b) Ferrocenes, ruthenocenes[29] (Figure 12): Organometallic "sandwich" compounds with low oxidation potentials. Ferrocenes are more widely used[30,33g] due to their reversible and tunable redox chemistry (and lower price).
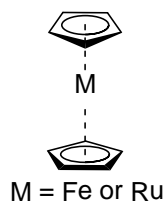
M = Fe or Ru

Figure 12, Structure of ferrocene and ruthenocenes.

Photoactive electron donors:

a) Porphyrins and phthalocyanines (Figure 13) are heterocyclic, aromatic macrocycles that can bind metals in their cavities to form complexes. They are widely investigated donor units, due to their excellent light absorption in the visible and near-IR region. D-A systems built up from a fullerene and one of the aforementioned compounds[3c,d,27a,31] (for example see Figure 9) display among the longest charge separated lifetimes in the µs-ns range.
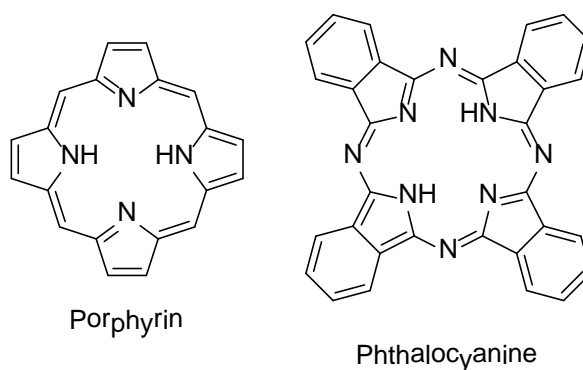

Porphyrin

Phthalocyanine

Figure 13, General structure of porphyrins and phthalocyanines.

b) Conjugated oligomers: As we discussed previously, conjugated polymer - PCBM blends are the most popular active layers of BHJ organic solar cells. The development of conjugated oligomers was initiated by the demand to understand the basic electronic properties and other features of more complex and polydisperse polymer correspondents (eg. polyphenylenevinylenes and polythiophenes) and through this to increase the photovoltaic efficiency. Furthermore, it was found, that these components have several benefits making them promising candidates for photovoltaic applications. They are monodisperse, can be attached to fullerenes by various ways and it is also presumed, that nanosegragation could be induced which would give rise to a well-ordered bicontinuous interpenetrating network of covalently linked D-A systems and

therefore no macroscopic segregation occurs. This bicontinuous network ensures the unrestricted transport of electrons and holes to the appropriate electrodes (although at least one blocking layer is usually applied to avoid charge flow in reverse direction) . Their most prominent and most widely studied members are: oligophenylenevinylenes (OPV), oligophenyleneethynylenes (OPE), and oligothiophenes[32].

II. 1. 2. 2. 1)   OPE-based ensembles

OPEs are rigid, triple bonded compounds which can be considered as 1D nanorods with freely rotating benzene rings along the molecular axis. The use of OPE as an electron donating unit in D-A systems has been studied by the group of Nierengarten[33] and several other groups[34]. The majority of the studies were done on 2,5-dialkoxysubstituted OPE based fulleropyrrolidines[33a-e, 34a].

The effect of varying the length of the OPE backbone and the terminal groups (tri-isopropylsilane and N,N-di-n-butylaniline) was probed. It has been found that the terminal group has a bigger influence on the energy/electron transfer process than the oligomeric length[33c-e] (Figure 14). The conclusion was that the donating ability of the OPE unit, the energy level of the charge separated state and the charge carrier mobility can be highly influenced by the terminal group.
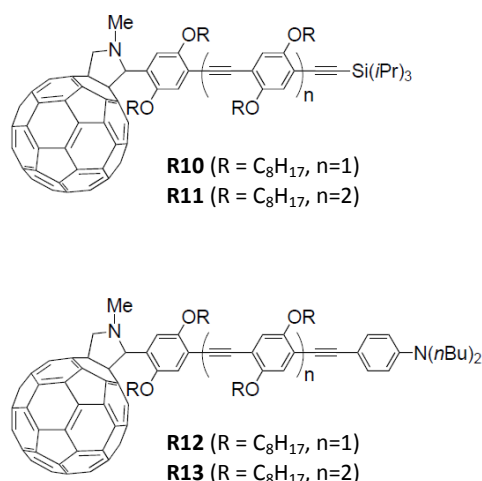

R10 (R = C_8H_{17}, n=1)
R11 (R = C_8H_{17}, n=2)

R12 (R = C_8H_{17}, n=1)
R13 (R = C_8H_{17}, n=2)

Figure 14, Series of OPE-C_{60} D-A dyads with different oligomeric length and terminal groups. Due to the presence of the aniline group the donating ability of the second set (bottom) is increased and shows better photovoltaic performance[33d].

Two sets of isomeric OPE-based dendritic branches linked to C_{60} through a pyrrolidine ring were also studied. There was ultrafast energy transfer from the OPE dendrons to the fullerene moiety[33f], but the different isomers demonstrated different light harvesting abilities.
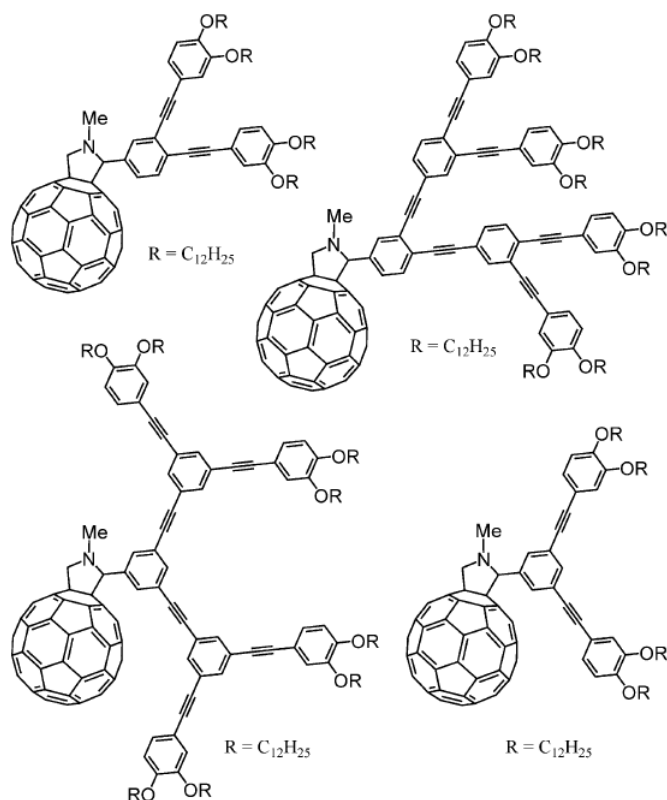

Figure 15, Very efficient energy transfer from dendritic OPE units to C_{60} was observed with two sets of isomeric OPE-C_{60} D-A dyads[33f].

Dyads, tryads, and polyads consist of multiple donor and acceptor units, thus a series of electron transfer processes takes place, which makes them even more similar to natural photosynthesis. Numerous donor-bridge-acceptor type triads[35] have been made, where OPE is used as a bridge for electronic communication because of the cylindrical symmetry of the acetylene units which maintain the π-electron conjugation at any degree of rotation. Connecting two C_{60} moieties via an OPE bridge leads to ultrafast energy transfer[34a] and poor device performance[33b] , if the compound is used as the active layer of a photovoltaic device. Porphyrin-OPE-fullerene donor-bridge-acceptor systems, display variable extent of charge electron transfer as a function of the polarity of the media; in polar media the lifetime of the

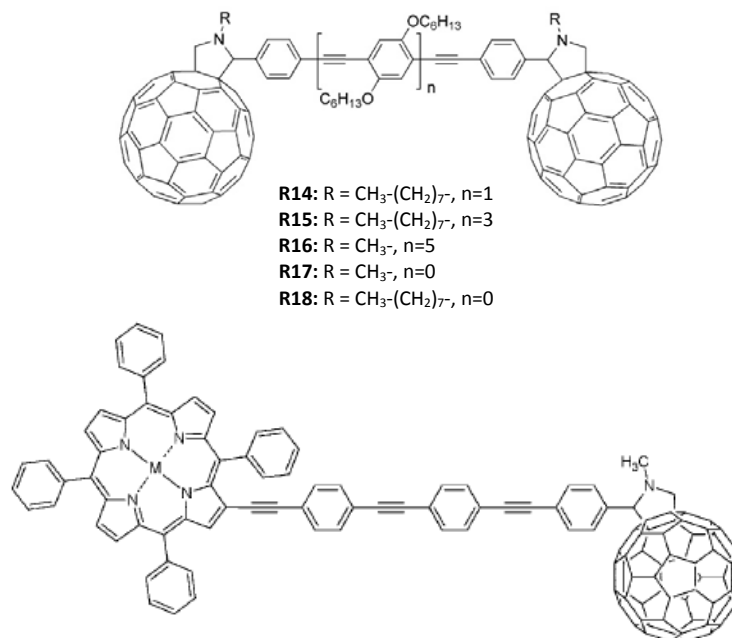charge separated state can reach 700ns, while in apolar solvents energy transfer is the predominant process[34b].

R14: R = CH$_3$-(CH$_2$)$_7$-, n=1
R15: R = CH$_3$-(CH$_2$)$_7$-, n=3
R16: R = CH$_3$-, n=5
R17: R = CH$_3$-, n=0
R18: R = CH$_3$-(CH$_2$)$_7$-, n=0

Figure 16, OPE used as a bridge for electronic communication (top) between two C$_{60}$ moieties and (bottom) between the electron donating porphyrin and electron acceptor fullerene units[33].

OPV can also play the role of a nanowire. C$_{60}$-OPV-ferrocene tryads bearing a fulleropyrrolidine and a ferrocene (Fc) unit connected via different lengths of OPV bridges have been prepared[33g]. The time resolved fluorescence and transient absorption spectroscopy analyses of the C$_{60}$-OPV-Fc arrays suggest that different energy transfer processes compete with charge separation.
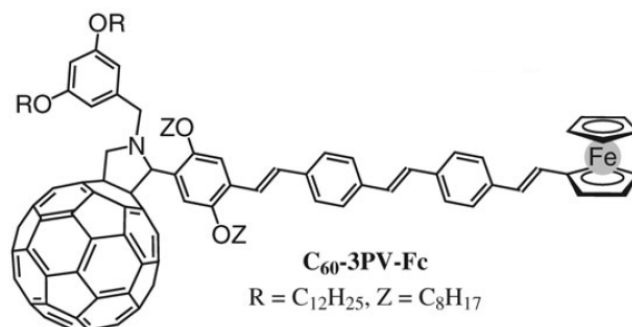
Figure 17, Example of C_{60}-OPV-ferrocene array[33g].

II. 1. 2. 2. 2)   OPV-based ensembles

A great deal of attention has been devoted to the construction of OPV-C_{60} D-A assemblies from the end of the last century. Nierengarten and co-workers have synthesized[36] OPE-C_{60} fulleropyrrolidines derivatives with varying oligomeric length and the number of attached oligomer arrays (Figure 18), which were the first examples of OPV-based D-A dyads. The transient absorption spectroscopy study revealed that a singlet-singlet energy transfer from the excited OPV moiety to the fullerene occurs followed by intersystem crossing to the fullerene triplet excited state. The use of polar solvents did not change the observed behaviour. Thus, all the absorbed light energy was conveyed to the fullerene by energy transfer and the charge separated state was not populated due to its high energy level relative to the fullerene singlet excited state.
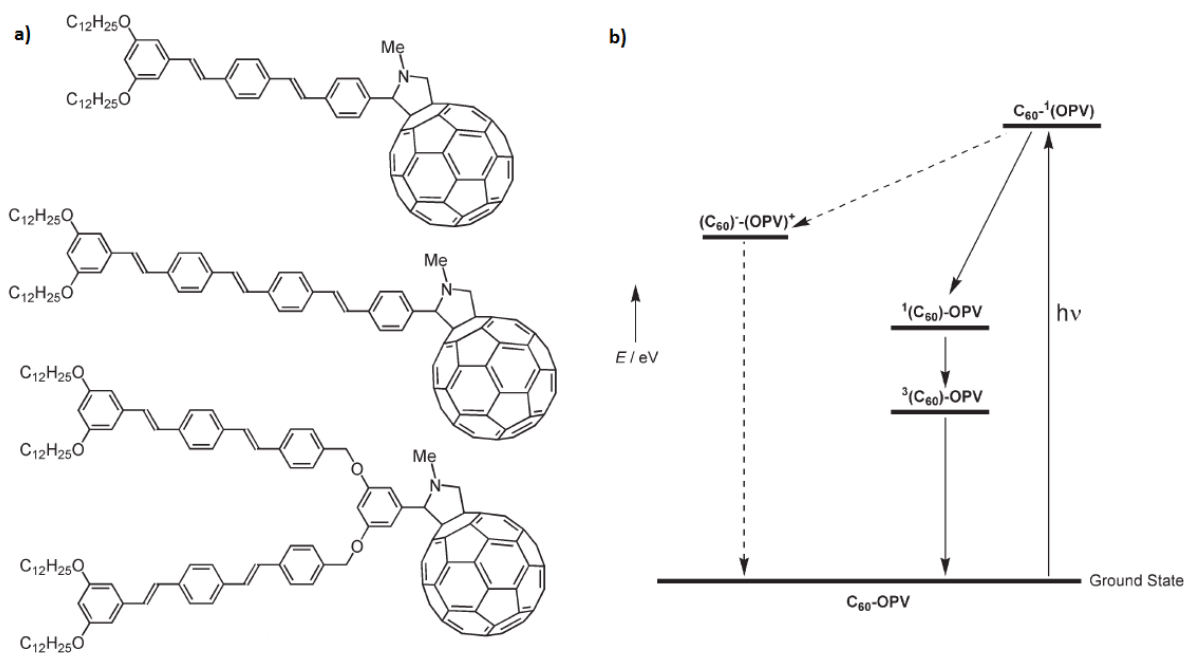
Figure 18, a) The first OPV-C_{60} conjugates. b) Energy level diagram of the dyads[36].

The electron transfer from the OPV moiety to the fullerene comes from varying the structure of the grafted OPV unit[37] (Figure 19). Solvent dependent charge or energy transfer processes have been observed for several OPV-based dyads[36]. Photoexcitation of the OPV moiety in apolar solvents resulted in ultrafast energy transfer from the OPV unit to the fullerene. While in polar solvents the energy level of the charge separated state drops below the fullerene singlet excited state, thus the electron transfer process takes place.
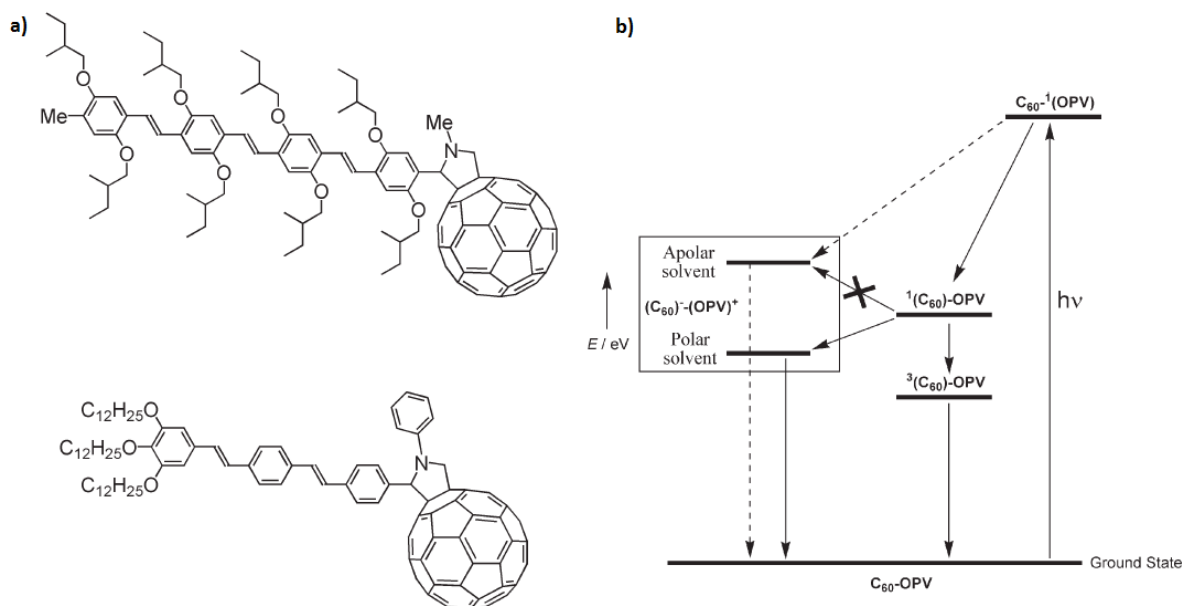
Figure 19, The structures of some of the OPE-C_{60} D-A dyads that show solvent dependent charge separation[37].

The photophysical analysis of different OPV-C_{60} D-A dyads, that are end-capped with diethyl amino groups[38] (Figure 20), revealed the existence of a charge separated state independent from the polarity of the solvent (i.e. it was observed in both toluene and benzonitrile). The lifetime of the charge separated state is found to be several nanoseconds. The authors presumed that longer lifetime of the charge separated state could be observed in the solid state, though it was not tested. These findings indicate that the energy level of the charge separated state is below of that of the fullerene triplet excited state in any solvent. It has been concluded, that the excellent donating abilities of these OPE moieties promoted electron transfer upon photoexcitation of the dyad.
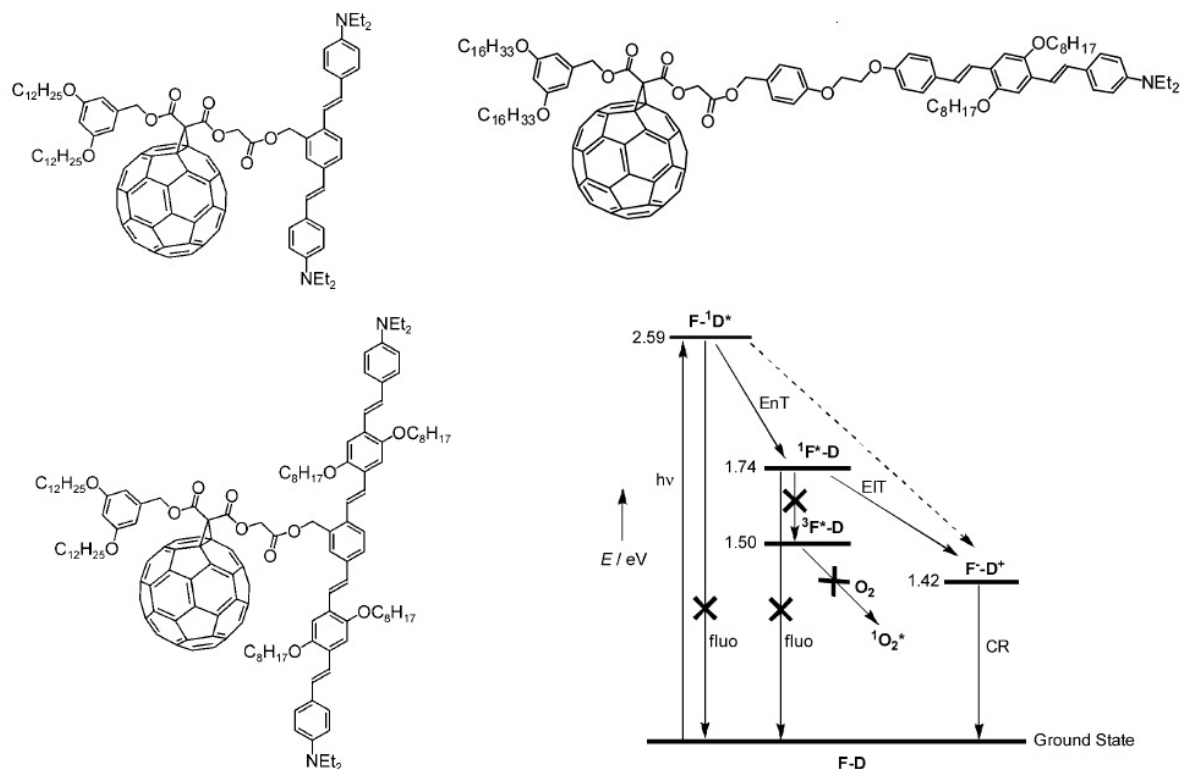
Figure 20, The formation of a charge separated state was observed for diethyl amino end-capped OPV-C_{60} dyads.

Efficient light-harvesting fullerodendrimers can be obtained by grafting dendritic OPV branches to a fullerene core[39] (Figure 21) in a similar way to OPE-based fullerodendrimers. The energy of the light absorbed by the OPV arrays can be channeled to the central C_{60} core thus mimicking the natural light-harvesting complex in which antenna molecules collect the sunlight and transfer the energy to a single reaction center.
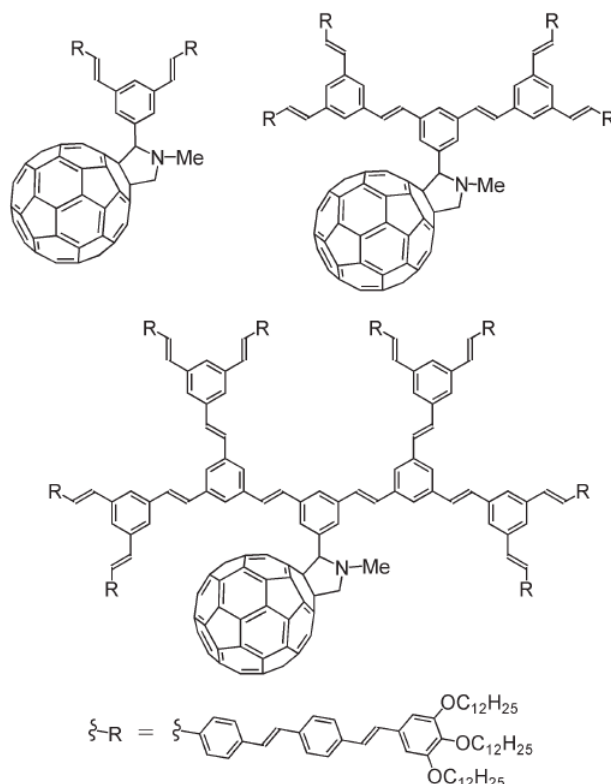
Figure 21, OPV based fullerodendrimers[39] as light harvesting molecular devices.

A detailed review on OPV-C_{60} D-A assemblies has been reported by Nierengarten et al. in 2007[40].

II. 1. 2. 2. 3)   D-A dyads with TNT EMFs as electron acceptor

TNT EMFs possess larger extinction coefficients than C_{60} in the visible region of the absorption spectrum and have a low band gap, while preserving a remarkable electron accepting ability, similar to that of C_{60}[41]. These properties inspired researchers to investigate their potential use in D-A systems.

The first D-A dyad with the incorporation of a TNT EMF as electron accepting moiety was a I_h $Sc_3N@C_{80}$-ferrocene ensemble synthesized by Echegoyen and coworkers in 2008[42] (Figure 22a). The photophysical properties of the dyad revealed electron transfer between the subunits. More importantly the stability of the charge separated state was pronouncedly better than in the C_{60} analogue. (The chemical properties of the material were discussed in Chapter I.)

A stable D-A dyad has been prepared via [2+1] cycloaddition reaction using $Sc_3N@C_{80}$ and a zinc porphyrin derivative[43] (Figure 22b). Upon photoexcitation of the donor chromophore the formation of $Sc_3N@C_{80}^{\cdot-}$- zinc porphyrin$^{\cdot+}$ radical ion pair was observed and monitored by transcient absorption spectroscopy.
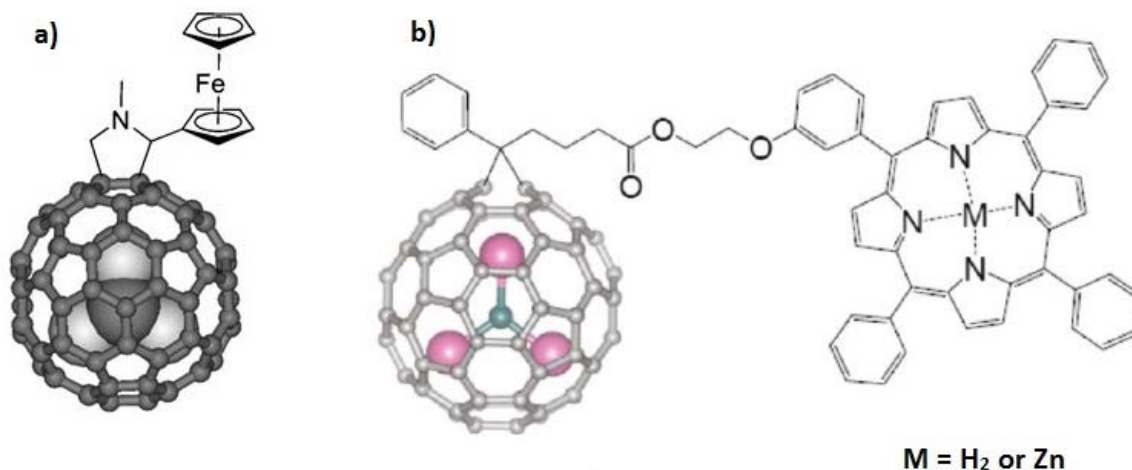

Figure 22, a) $Sc_3N@C_{80}$-ferrocene[42] and b) $Sc_3N@C_{80}$-porphyrin D-A dyads.

Two constitutional isomers of I_h-$Sc_3N@C_{80}$-triphenylamine (TPA) electron donor-acceptor conjugates, containing TPA as the donor, were synthesized[44] (Figure 23). It was found that when the donor is connected to the pyrrolidine nitrogen atom, the resulting dyad produces a significantly longer lived radical pair and better thermal stability than the corresponding 2-substituted isomer. It is also important to note, that both $Sc_3N@C_{80}$ based dyads have longer lived charge separated states than their corresponding C_{60} derivatives.
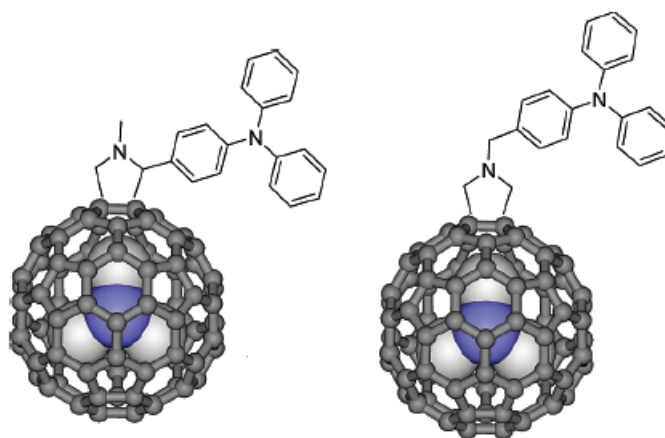

Figure 23, Two different constitutional isomers of $Sc_3N@C_{80}$-triphenylamine D-A conjugate[44].

Arising from the exceptional stability of the malonate fulleroids, two $Y_3N@C_{80}$ D-A dyads have been designed and synthesised, using exTTF or phthalocyanine as electron donors, respectively. Surprisingly, these compounds did not present the high stability of open caged cycloadducts, but rather on the contrary decomposed within a few hours[45]. In another example, instead of the expected [6,6] to [5,6] isomerisation, retro-cycloaddition was observed upon heat treatment of the $Y_3N@C_{80}$-ferrocene D-A adduct[45]. The compound was found to be sensitive to light and temperature and decomposition was observed in a similar way to the aforementioned conjugates.
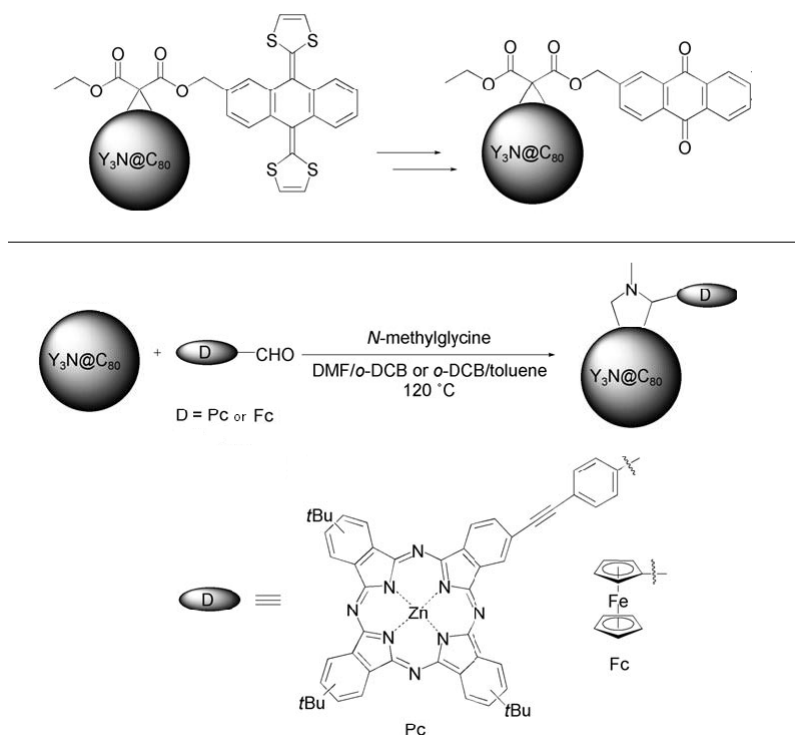

Figure 24, (top) The oxidative decomposition of exTTF-$Y_3N@C_{80}$ D-A dyads to an anthraquinone derivative. (bottom) The $Y_3N@C_{80}$ based fulleropyrrolidines derivatized by either ferrocene or phthalocyanine were sensitive to light and temperature[45].

II. 1. 2. 2. 4)   Supramolecular assemblies of D-A dyads

Well controlled morphology plays a crucial role in high power conversion efficiencies of organic photovoltaic devices. The maximized PCEs can be achieved via a bicontinuous network with a large donor/acceptor interface and separate electron- and hole-transporting channels (vide supra). To control the morphology at the nanometer level, self-assembling

electroactive materials are required that can form long-range ordered supramolecular structures. Self-assembling liquid crystal materials appear to be the obvious choice to fill this role as they supposedly self-organize into nanosegregated D-A supramolecular networks with ambipolar transporting properties.

The synthesis of LC D-A materials for controlled morphology requires careful tailoring in order to maintain the electro- and photochemical properties of the components. For that reason, one can find only scarce examples of the successful formation of supramolecular D-A heterojunction structures, most of them being porphyrin-C_{60} and phthalocyanine-C_{60} ensembles.

Two phthalocyanine-C_{60} D-A dyads have been synthesized with a rigid and a flexible spacer being introduced between the electroactive moieties[3d]. The molecule with the rigid spacer (Figure 25, left) was not mesomorphic, but was able to form columnar mesophases when blended with equimolar amount of a mesomorphic phthalocyanine. On the other hand, the one with the flexible spacer (Figure 25, right) self-assembled to a columnar phase. The regular arrangement of C_{60} units was not observed in either of the two cases.
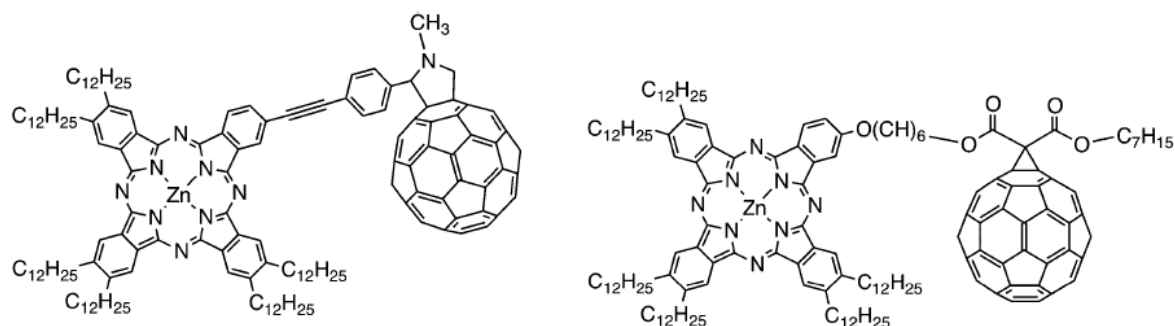

Figure 25, Phthalocyanine-C_{60} D-A dyads (left) with rigid and (right) flexible spacers between the donor and acceptor units[3d].

Another phthalocyanine-C_{60} D-A dyad has been designed and synthesized by Imahori and co-workers with six 4-dodecyloxyphenoxy groups grafted to the periphery of the phthalocyanine[31c] (Figure 26, left). The formation of a columnar rectangular phase was deduced from the analysis of the XRD patterns obtained by SAXS (Figure 26, right). Due to the strong π–π interaction between the C_{60} molecules the fullerene moieties are also arranged linearly, showing a helical alignment along the zinc phthalocyanine 1D columns.

The nanosegregated phthalocyanine-C_{60} D-A channels exhibited very efficient ambipolar charge transfer properties.
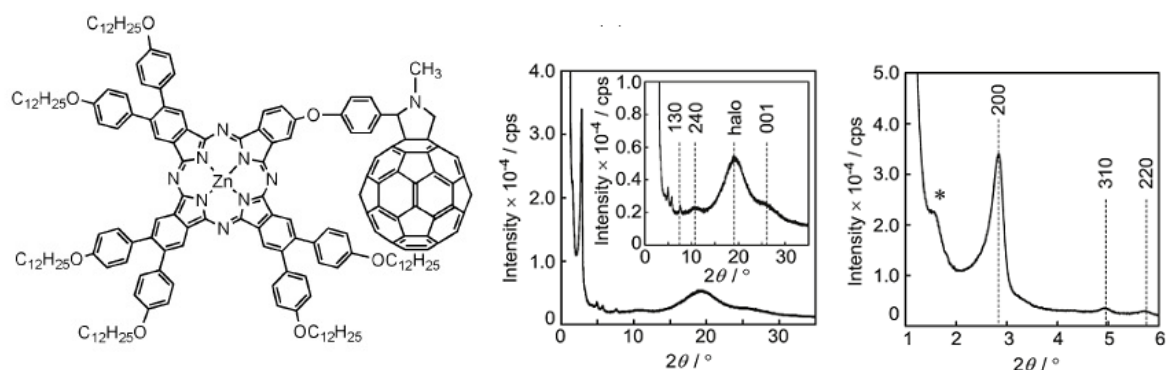

Figure 26, (left) Structure of zinc phthalocyanine-C_{60} D-A dyad. (right) XRD patterns of the dyad, where the asterisk marks the peak arising from a helical pitch of C_{60} molecules along the ZnPc column[31c].

A chiral amphiphilic porphyrin-C_{60} assembly[46] displayed highly efficient charge transport over a large length scale via the self-organization into bundles of long nanowires. It is important to note, that the enantiopure sample showed a far better charge-carrier mobility than the racemic mixture.
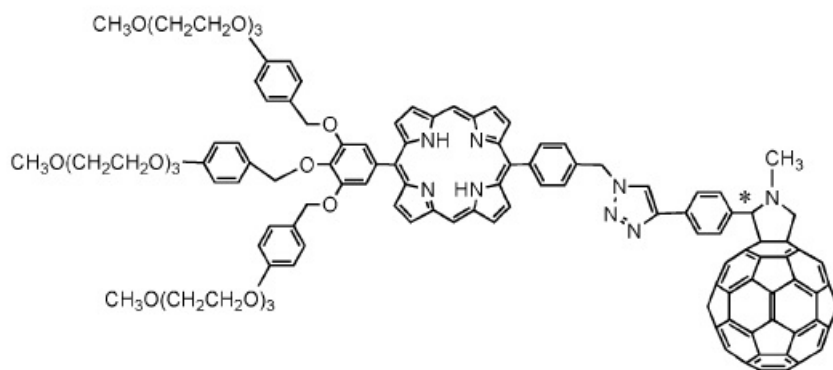

Figure 27, The chiral amphiphilic porphyrin-C_{60} dyad self-organizes into bundles of long nanowires[46].

In another example, the porphyrin-fullerene dyad (PFD1) (Figure 28) self-assembles into a well-defined 3D structure with alternating arrangements of separate domains of porphyrin and C_{60} in the solid state[47]. The compound was tested as the acceptor material of a BHJ solar cell blend, using poly[(4,4'-bis(2-ethylhexyl)dithieno[3,2-b:2',3'-d]silole)-2,6-diyl-alt-(4,7-bis(2-thienyl) 2,1,3-benzothiadiazole)-5,5'-diyl] (SiPCPDTBT) as the donor polymer. The comparison of the electron diffraction patterns of the pure PFD1 and the

SiPCPDTBT:PFD1 thin film blend after annealing suggests that their supramolecular organization is identical. The device fabricated with SiPCPDTBT:PFD1 showed a higher open circuit voltage (V_{oc}) and short circuit current (J_{sc}) (the latter being the result of improved charge carrier mobility due to the self-assembly of PFD1 within the film) than the reference device with a SiPCPDTBT:PCBM active layer. Although, its overall PCE was somewhat lower than that of the reference device (3.35% vs 4.03%), the authors suggest that further optimization of the morphology may lead to higher PCEs.
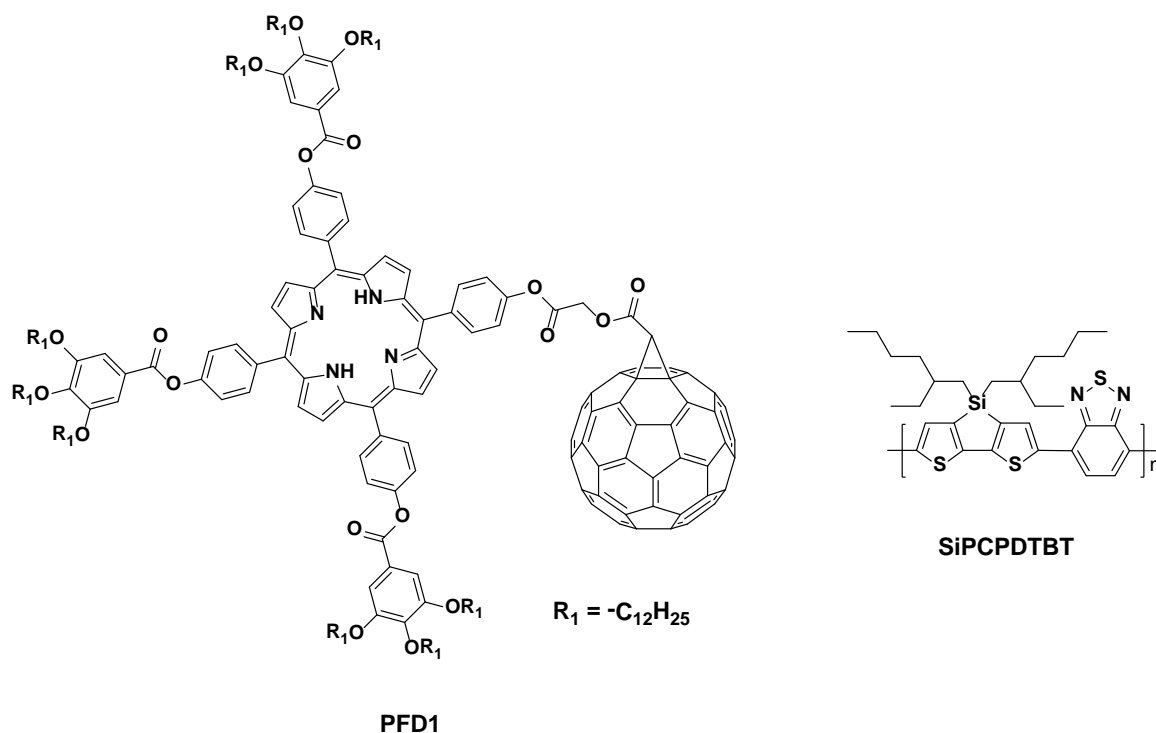

Figure 28, The BHJ solar cell with PFD1 as acceptor dyad and SiPCPDTBT as donor polymer showed 3D supramolecular organization with high V_{oc} and J_{sc}[47].

Oligothiophene-C_{60} photoconductive LC dyads with bicontinuous arrays of densely packed donor and acceptor components have been reported[48]. The molecular structures of two synthesized compounds were identical except for the terminal wedges, which were either lipophilic or hydrophilic. Both dyads self-assembled into a SmA phase, but the one with the hydrophilic terminals exhibited a much better photoconducting character and a long-range conducting pathway.
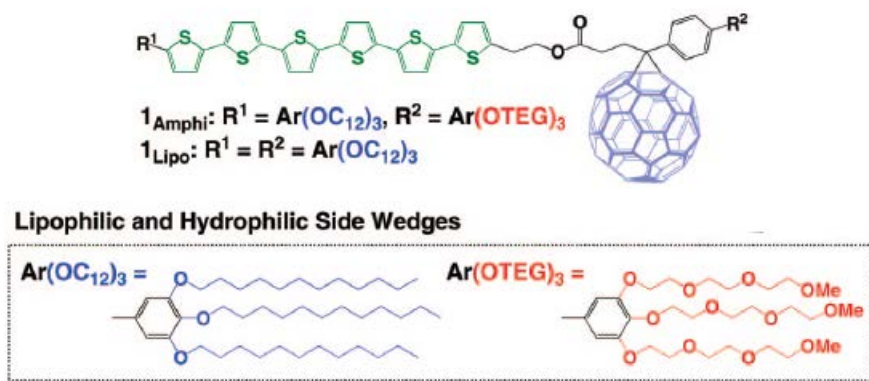
Figure 29, Oligothiophene-C_{60} photoconductive LC dyads with terminal wedges of different chemical nature[48].

An OPV-C_{60} dyad, with poly(benzyl ether) dendritic branches at the periphery[3f], was specifically tailored to form a columnar phase which is presumed to be very advantageous to obtain materials with high charge carrier mobility[49] (Figure 30). Although the dyad exhibited very rich mesomorphism, its photovoltaic effect was limited due to the absence of well-defined charge transporting channels in the structure.
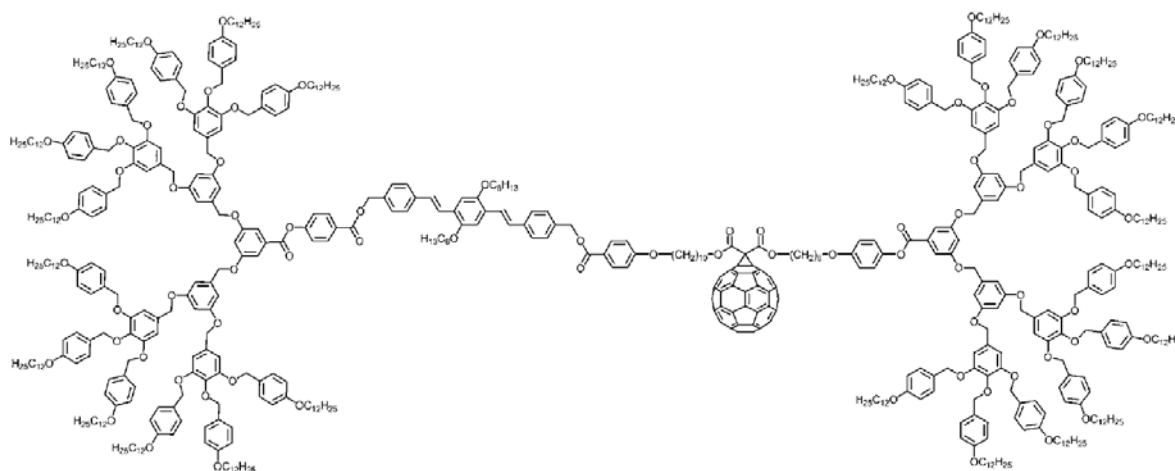

Figure 30, The OPV-C_{60} dyad with poly(benzyl ether) dendritic branches shows rich mesomorphism, but limited photovoltaic effect[3f].

II. 1 .3) Photovoltaics objectives

The use of LC OPE or OPV derivatives in the cyclopropanation reaction with [60]Fullerene leads to mesomorphic, photoactive monoadducts. Due to the covalent attachment of donor and acceptor moieties, the finest level of nanosegragation can be

obtained that can give rise to a well-ordered bicontinuous interpenetrating network between the two electrodes of a photovoltaic device. These D-A dyads could self-organize into well defined supramolecular structures and create separated charge transport channels of donor and acceptor moieties (eg. via columnar mesophase formation) with ambipolar charge transfer properties. It is anticipated that the photovoltaic devices, which are fabricated by using the dyads either as the active layer, or as the acceptor component of a BHJ solar cell blended with an appropriate donor polymer, show improved performance due to the tailored nanomorphology.

The design of the OPE moiety follows the architecture of the typical hexacatenar (phasmidic) mesogens with a small lateral group attached to the middle benzene ring. As for the construction of the OPE-based D-A dyads, different structural factors have been considered in our study:

- **The chemical nature of the donor moiety**. Lyophilic (2 to 1 ratio of D/A units) and amphiphilic (1 to 1 ratio of D/A units) malonates with OPE-based donor moieties (Figure 31) were prepared and used for the derivatization of C_{60}. The lyophilic precursor contained two OPE donor oligomer units, and in order to build up amphiphilic compounds one of the OPE units was replaced with a hydrophilic dendron.

- **The characteristics of the fullerene acceptor**. Two different fullerene acceptors, namely C_{60} (Figure 31, left) and $Y_3N@C_{80}$ (Figure 32) were connected to the same donor unit in order to investigate their influence on the photophysical properties and supramolecular organization of the photoactive dyad.
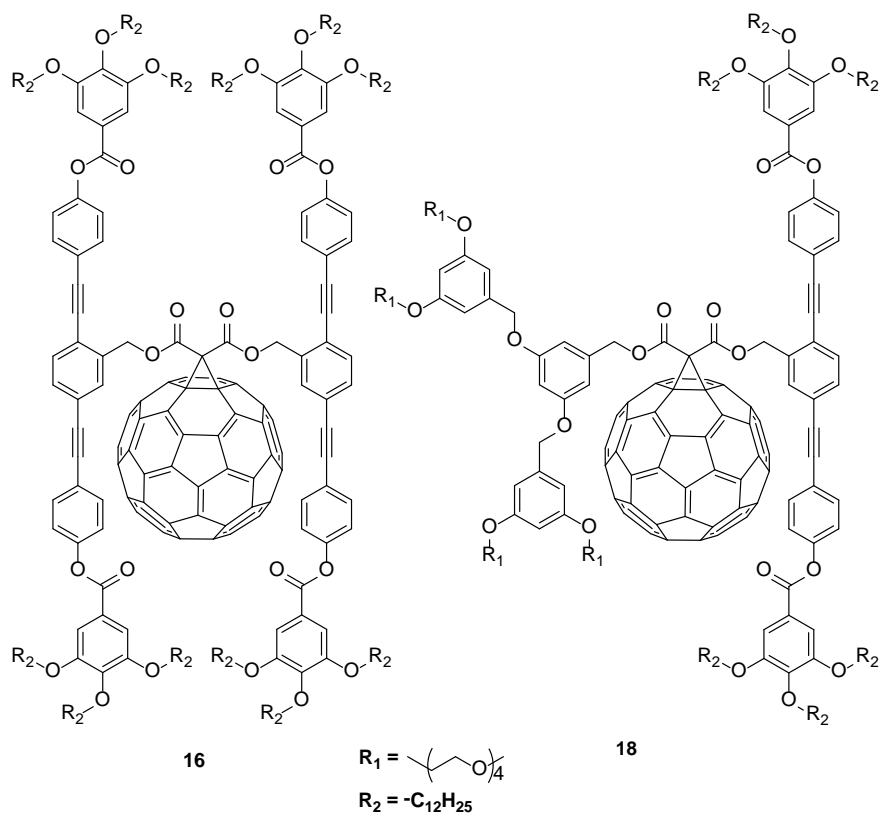
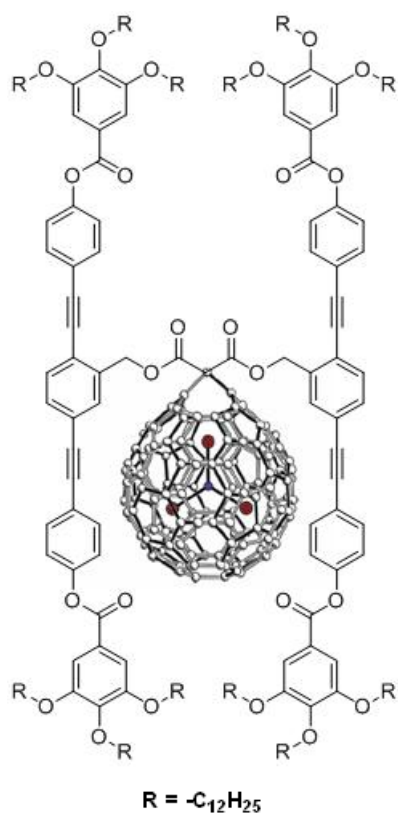**Figure 31**, OPE base D-A dyads.

Figure 32, The first LC D-A TNT EMF.

The OPE-$Y_3N@C_{80}$ D-A dyad is the first mesomorphic TNT EMF which also exhibits photoactive properties (Figure 32), according to our knowledge. Therefore special attention has been paid to the analysis of this compound and unusual properties have been revealed (eg. high $Y_3N@C_{80}$ fullerene core emission of the excited dyad in deareated solutions) which will be discussed in detail.

Two OPV based D-A dyads with a ratio of the OPV donors to the C_{60} acceptor moieties of 4 : 1 have been synthesized. The oligomeric length of the grafted π-conjugated oligomer donors was varied between 3 and 4 (ie. each oligomeric array consisted of three or four phenylenevinylene monomer units) while keeping the donor to acceptor ratio constant (4 : 1) (Figure 33) and its effect on the mesophase formation and the photophysical properties was studied.
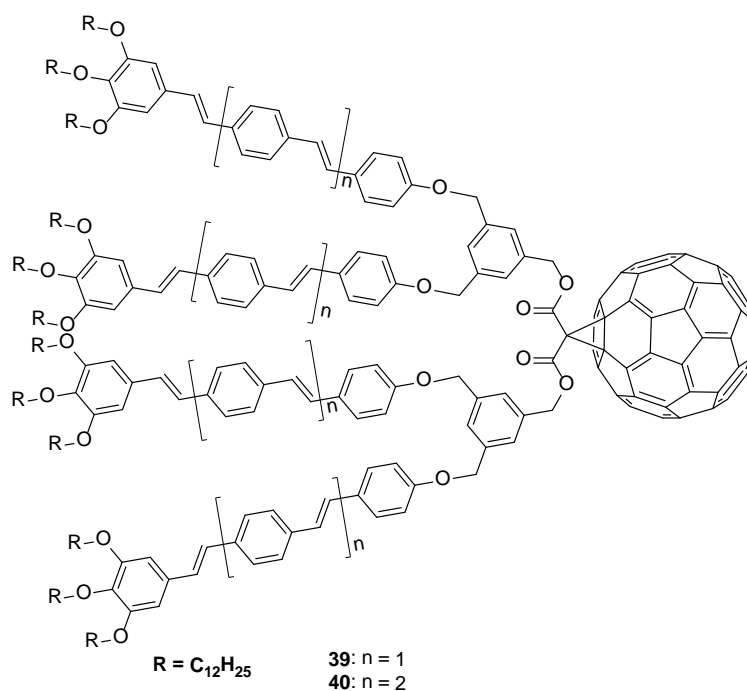

Figure 33, OPV based D-A "rockets".

We describe, herein, the synthesis, structural analysis, liquid crystalline properties, supramolecular organization, electrochemical and photophysical properties of the aforementioned OPE and OPV based photoactive LC dyads and their main intermediates.

## II. 2)   Results and discussion of OPE derivatives

II. 2. 1)   Synthesis

We designed a highly convergent synthetic route for the synthesis of an oligo(phenylene ethynylene) derivative (**OPE)** where each step provided the desired product in good yield. The summary of the reaction steps of **OPE** is depicted on Scheme 1. Firstly, 2,5-diidobenzoic acid was reduced with BH_3-THF complex in THF to give **1b** in 94% yield. **1b** was reacted with trimethylsilyl acetylene in a Sonogashira coupling reaction to give **2**, and the deprotection of trimethylsilyl group with TBAF gave **3** afterwards. We also prepared **4** with tangling alkyl chains by Williamson etherification reaction of methyl gallate and 1-bromododecane in the presence of 18-crown-6 catalyst, similarly to literature procedure[50]. Then, the methyl ester moiety was reduced to give **5** with a focal carboxylic acid group. Esterification of **5** with 4-iodophenol gave **6**, a compound suitable for the coupling reaction with **3** to give **7** a polycatenar mesogen (i.e., a molecule with a long rod-like rigid core ending in two half-disc moieties). The synthesis of the malonate half ester **8** was accomplished with the reaction of **7** and Meldrum's acid at 110°C. It is also important to mention that the ester bond of **6** and **7** is very susceptible to certain reaction conditions (eg. pH) and can be easily cleaved followed by an undesired esterification reaction of the OH group of **OPE** and the carboxyl group of the cleaved **5**. Using our pathway the cleavage of this ester bond is negligible.
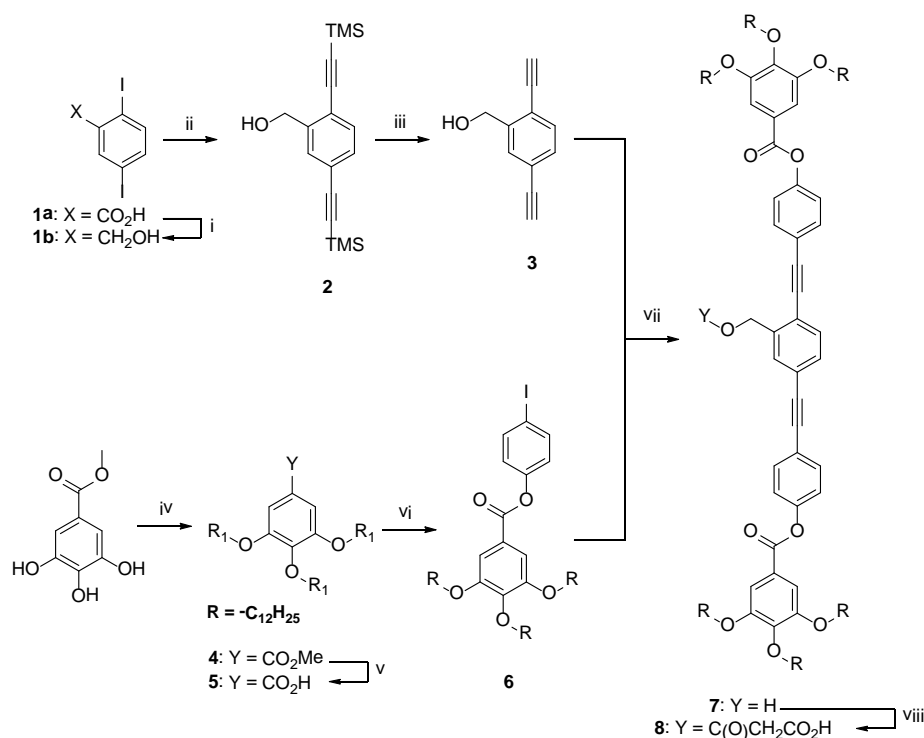
Scheme 1, The summary of the synthetic steps of OPE electron-donating moiety. Reagents and conditions : (i) BH_3-THF, THF, 0°C to RT, 21h (94%); (ii) TMS-Ac, $PdCl_2(PPh_3)_2$, CuI, DIPEA, toluene, RT, 23h (90%); (iii) TBAF, THF, 0°C to RT, 24h (92%); (iv) $C_{12}H_{25}Br$, K_2CO_3, KI, 18-crown-6, acetone, 60°C, 24h (96%); (v) KOH, MeOH, THF, H_2O, 80°C, 24h (99%); (vi) 4-iodophenol, DCC, DPTS, 4-ppy, DCM, RT, 24h (94%); (vii) $PdCl_2(PPh_3)_2$, CuI, DIPEA, DCM, RT, 42h (65%); (viii) Meldrum's acid, 110°C, 4h, (100%).

In order to obtain an amphiphilic fullerene derivative which could demonstrate induced organization through Langmuir film formation, we decided to prepare a Janus compound bearing an apolar OPE unit and a very polar second generation dendron with tetraethylene glycol moieties. Tosylated tetraethyleneglycol monomethyl ether **9** can be easily prepared in one step following literature procedures[51] (Scheme 2). Methyl 3,5-dihydroxybenzoate was reacted with **9** to afford the water soluble methyl ester **10**. In the next steps, the methyl ester moiety was reduced to alcohol **11** which was subsequently converted to a more reactive bromide group **12**. The second generation dendron **13** was synthesized by a Williamson etherification reaction between **12** and methyl 3,5-dihydroxybenzoate and consecutive reduction of this compound gave **14** in 43% overall yield. The synthetic procedure is summarized in Scheme 3.
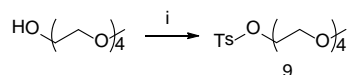
Scheme 2, TEG monomethyl ether tosylation.
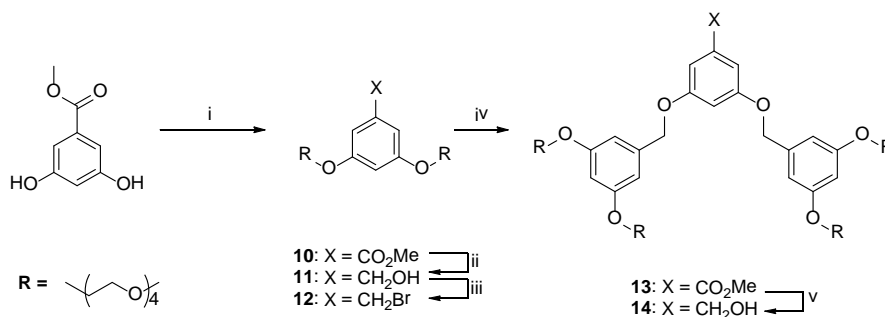
Scheme 3, Synthetic routes to second generation TEG-based dendron. Reagents and conditions : (i) 9, K_2CO_3, KI, 18-crown-6, acetone, 65°C, 4 days (99%); (ii) LiAlH$_4$, THF, RT, 3h (92%); (iii) TMS-Br, CHCl$_3$, 0°C to RT, 48h (71%); (iv) Methyl-3,5-dihydroxybenzoate, K_2CO_3, KI, acetone, 65°C, 24h (87%); (v) LiAlH$_4$, THF, 0°C to RT, 4h (96%).

The symmetric malonate **15** was built up from two polycatenar OPE units **7** which were connected through a malonate bridge. A subsequent Bingel reaction[52] gave methanofullerene **16**, the combination of two of the same electron donor- and one electron acceptor units, as shown in Scheme 4. A modified Steglich esterification reaction between **8** and **14** afforded the asymmetric and amphiphilic malonate ester **17** in 32% yield. In this step the malonate **15** was also obtained as a byproduct in similar yield. It has to be mentioned that much lower yields were achieved (0 to 6% only) when the malonyl group was attached to **14** (See Annex x for details). Finally, the D-A dyad **18** was obtained through a cyclopropanation reaction of C$_{60}$, as depicted in Scheme 5.
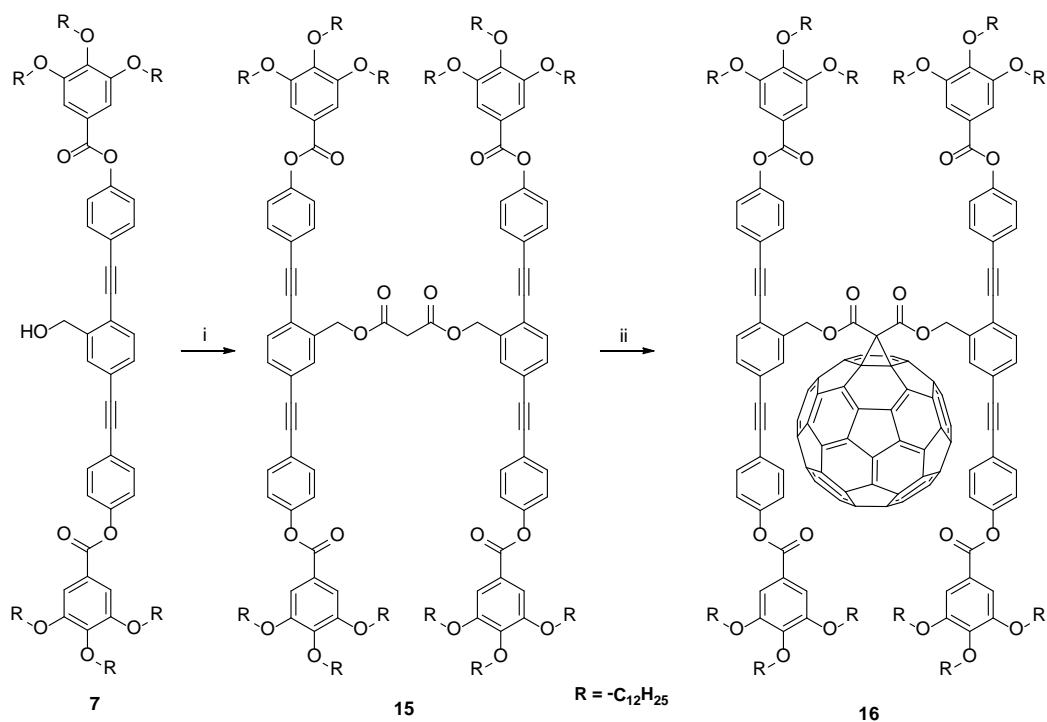
Scheme 4, Synthetic steps of dOPE-C60 D-A dyad. Reagents and conditions: (i) malonyl dichloride, *N,N*-Diisopropylethylamine, 4-Dimethylaminopyridine, CH$_2$Cl$_2$, RT, 20h (76%); (ii) C$_{60}$, 1,8-Diazabicycloundec-7-ene, I$_2$, toluene, RT, 3days (84%).
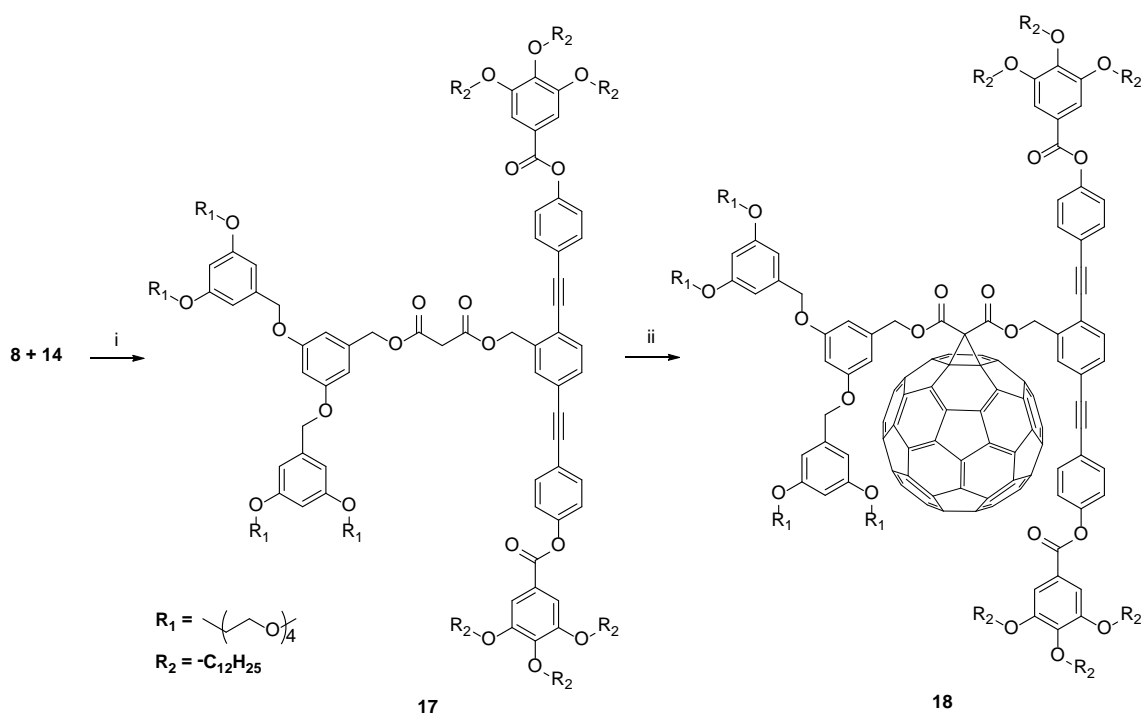
Scheme 5, The summary of the synthetic steps of OPE-TEGd2-C60 D-A dyad. Reagents and conditions: (i) *N,N'*-Dicyclohexylcarbodiimide, 4-(dimethylamino)pyridinium 4-toluenesulfonate, 4-pyrrolidinopyridine, CH$_2$Cl$_2$, RT, 48h (32%; 60% based on unreacted **14**); (ii) C$_{60}$, 1,8-Diazabicycloundec-7-ene, I$_2$, toluene, RT, 3days (87%).

While D-A dyad **16** was stable during storage at room temperature under air over 6 months period, **18** has decomposed under the same conditions.
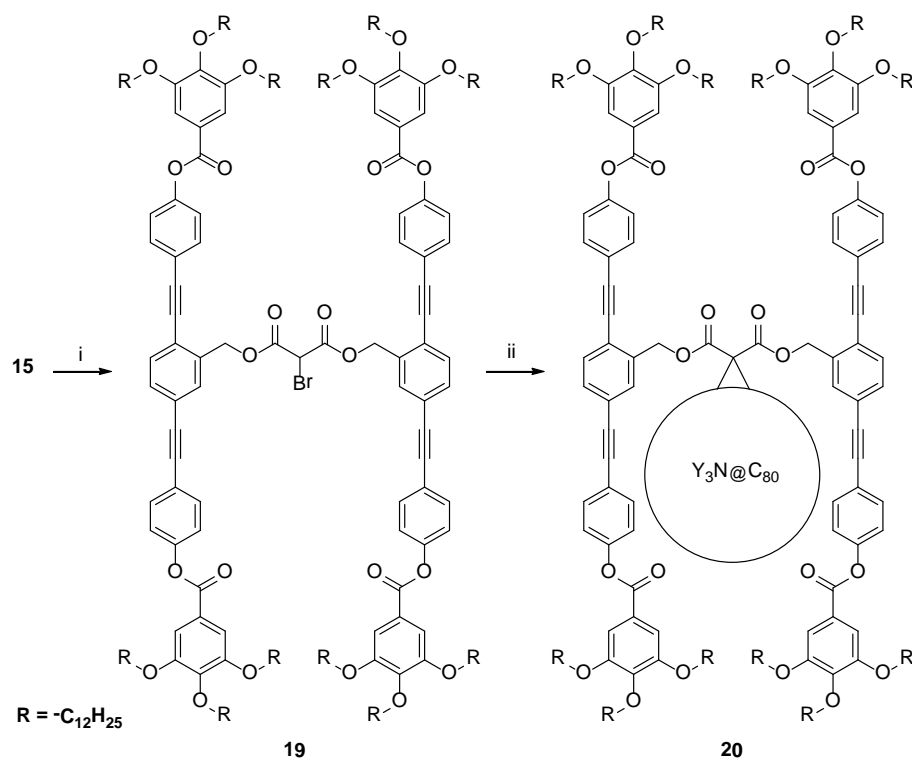
Scheme 6, Synthesis of dOPE-$Y_3N@C_{80}$ ensemble. Reagents and conditions: (i) CBr_4, DBU, CH_2Cl_2, 0^oC to RT, 2h, (32%); (ii) $Y_3N@C_{80}$, DBU, chlorobenzene, RT, 2h, (20%).

The general Bingel conditions cannot be applied for the functionalization of TNT EMFs, as we discussed in Chapter I. Therefore, bromomalonate **19** was prepared from malonate **15** with CBr_4 and it was subjected to a cyclopropanation reaction in the presence of $Y_3N@C_{80}$ to give a OPE-TNT EMF D-A ensemble **20**. To date, this is the first liquid crystalline D-A dyad based on TNT EMF (for mesomorphic properties see: Section II. 2. 3) for photophysical properties: Section II. 2. 5)). Purification of this class of molecules is rather difficult, and we successfully adopted preparative thin layer chromatography techniques, which were first eluted with CS_2 to remove unreacted $Y_3N@C_{80}$ which elutes with the solvent front, then with DCM/cyclohexane 3/2 solvent mixture to separate the product.

II. 2. 2)   Structural analysis

II. 2.2.1) NMR spectroscopic features of OPE-C_{60} based compounds

In this section, the general ^{1}H- and ^{13}C-NMR features of fullerene monoadducts will be detailed; also the spectra of the methanofullerene monoadducts and malonate precursors will be compared, so that a universal trend could be deduced. For this purpose we chose the OPE based D-A dyad **16** and its precursor malonate **15**, as an example. Apart from that, only unexpected results of some compounds will be presented and analyzed.
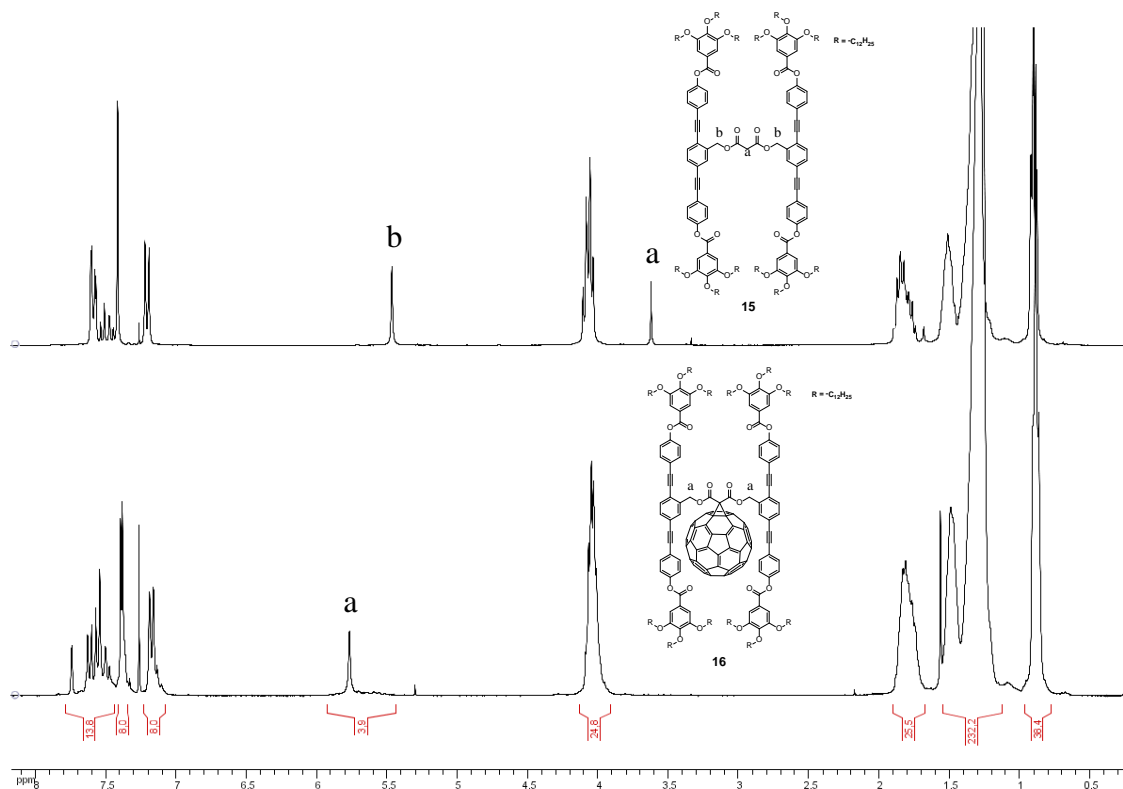

Figure 34, ^{1}H-NMR spectra (300 MHz, CDCl$_3$) of methanofullerene **16** and its malonate precursor **15**.

The most important differences between the ^{1}H-NMR spectra of the D-A dyad and its precursor malonate are highlighted in Figure 34. The spectrum of malonate **15** contains two important singlets at 3.61 ppm and 5.46 ppm corresponding to the methanobridge H atoms. A good indication of the successful cyclopropanation reaction and the absence of starting material is the absence of the signal of the bridgehead protons around 3.61 ppm. Besides, this, the downfield shift of the remaining methanobridge protons and some degree of perturbation of the aromatic protons can be observed. On the spectrum of the dyad **16** the

singlet of the methanobridge protons is downfield shifted to 5.77 ppm and broadened, maybe due to some extent of hindered rotation after grafting the bulky C_{60}.
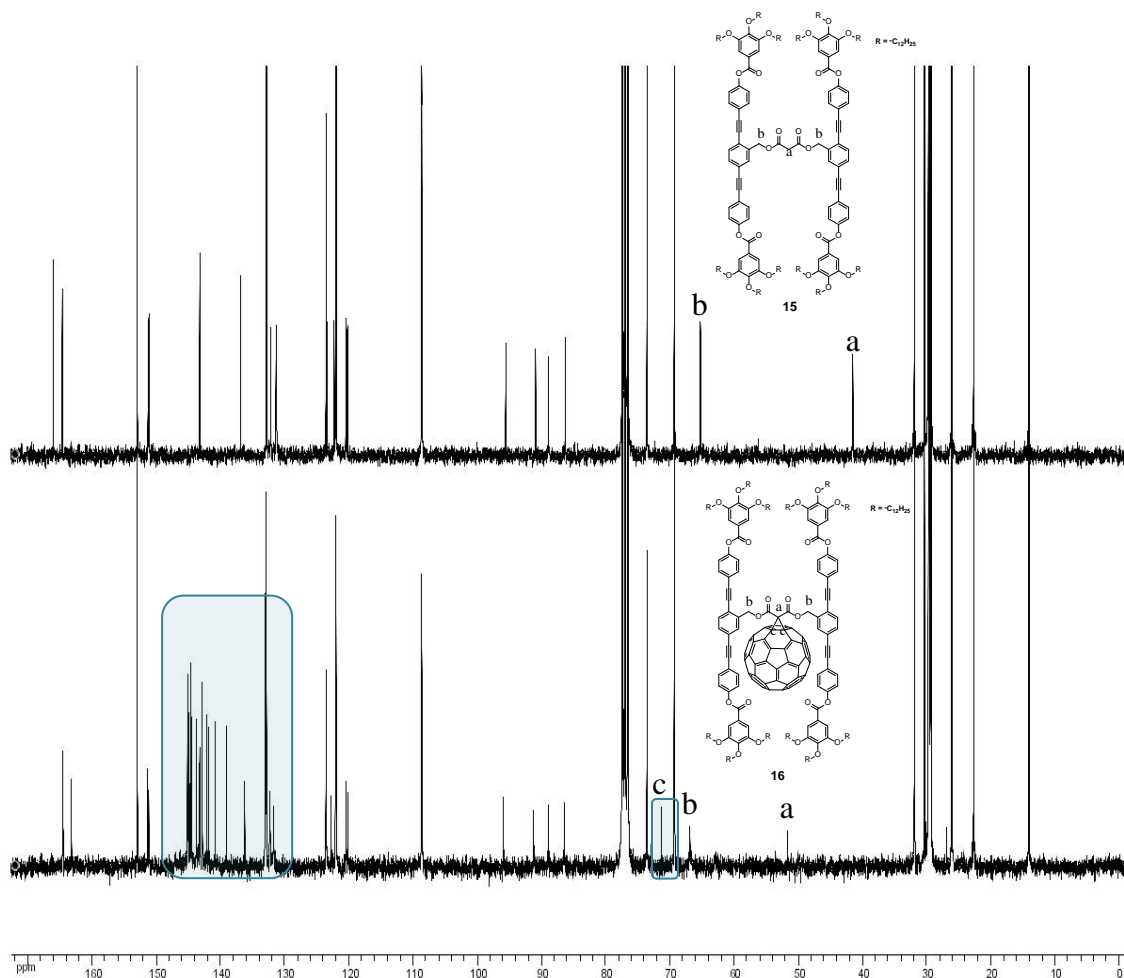

Figure 35, ^{13}C-NMR spectra (300 MHz, CDCl$_3$) of methanofullerene **16** and its malonate precursor **15**. The fullerene carbon signals are highlighted in turquoise rectangles.

The most conspicuous difference between the ^{13}C-NMR spectra of malonate **15** and methanofullerene **16** is the comb like manifestation of sp^2 hybridized fullerene carbon peaks between 130 and 150 ppm as the icosahedral symmetry of C_{60} ceases to exist (Figure 35). Also, the sp^3 hybridized carbon signals of C_{60} emerge at 71.39 ppm as a distinct signal. In The case of methanobridge carbons a downfield shift can be observed relative to the malonate precursor carbons (from 41.52 and 65.28 ppm to 51.76 and 66.91 ppm, respectively), similarly to the ^{1}H-NMR results.

Very similar results were obtained for other methanofullerenes and these results are in good agreement with literature data.
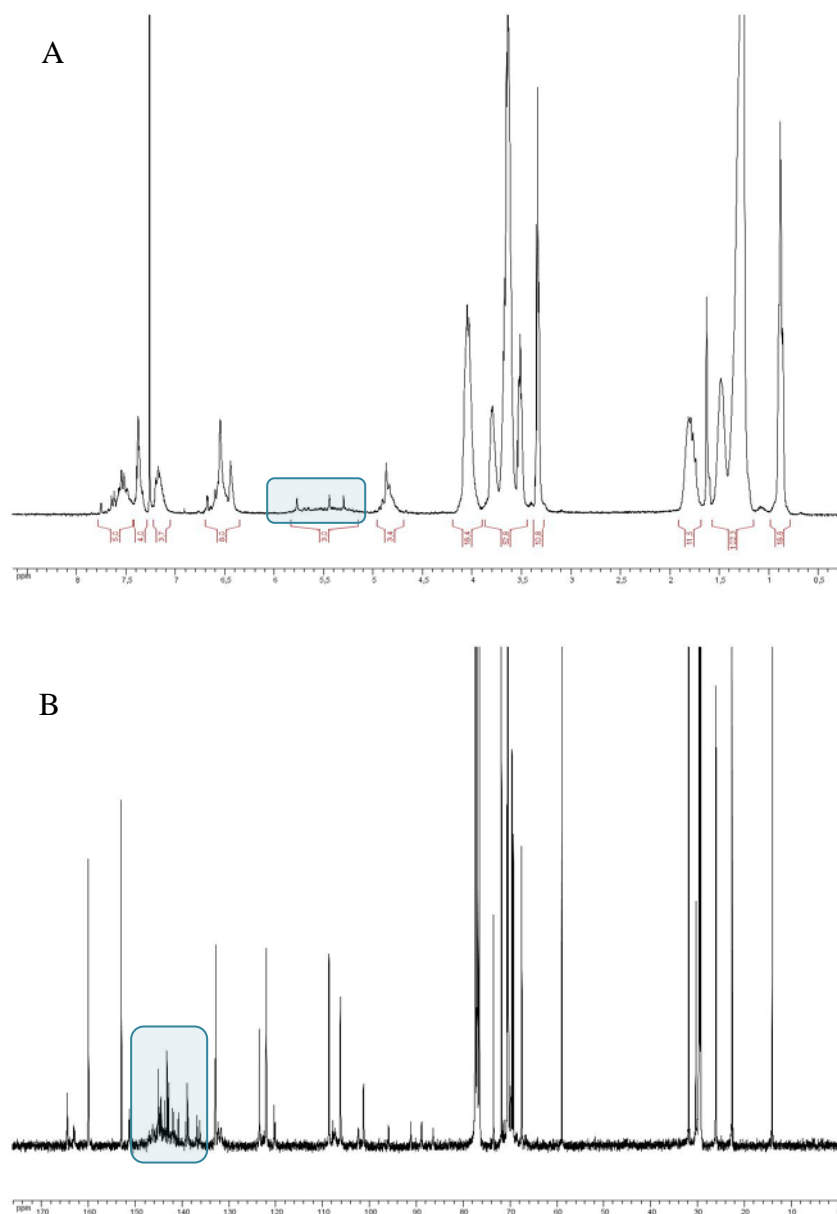
Figure 36, ^{1}H and ^{13}C-NMR spectra (300 MHz, CDCl$_3$) of methanofullerene **18**. The highlighted areas: A, The broad ^{1}H-NMR signal of malonate bridge protons B, Broad signal of fullerene sp^2 carbons.

The spectra of the OPE and TEG based fullerene derivative **18** is also presented, mainly because this compound decomposed over time (the timescale of the degradation is not known, but only minor amount of monoadduct remained after a few months), when stored under ambient conditions. The disappearance of the two methanobridge protons are hidden by the signals of the TEG chains, the other singlet of four protons smeared to a

broad multiplet, which can be a consequence of hindered rotation, the presence of certain amount of regioisomeric bisadducts or early decomposition. A variable temperature NMR study was not performed to corroborate the dynamic effect and rule out the other two options. As mentioned, the blunt, unsharpened signals on the ^{1}H-NMR spectrum could also indicate that the monoadduct is contaminated with regioisomeric bisadducts. This idea was also supported by the ^{13}C-NMR spectrum, as many small signals appear between 130 and 150 ppm apart from the comb-like feature of the monoadduct. The formation of a bisadduct during Bingel reaction would not be a surprise (we also observed it for the OPV4 derivative **41bis** and TEG based fullerodendrimer **49bis**), but TLC and mass spectra of the compound did not confirm its existence.

II. 2.2.2)   NMR spectroscopic features of OPE-Y$_3$N@C$_{80}$ dyad

NMR is a powerful technique to distinguish between [5,6] and [6,6] addition patterns as both I$_h$ C$_{80}$ double bonds are available reaction sites (see Chapter I). If the cycloaddition occurs at the [6,6] site, then all the OPE based protons at both sides of the malonate moiety are magnetically equivalent. On the other hand, addition at the corannulane type site provides an adduct with non-equivalent methylene (and other OPE based) protons adjacent to the malonate moiety, due to their different chemical environments (ie. in close proximity of either a five or six-member ring). It is important to note, that **20** can be easily solubilized in most of the organic solvents in contrast to the sparing solubility of most of the TNT EMF derivatives prepared to date. The ^{1}H-NMR and ^{13}C-NMR spectra of **20** were recorded in deuterated chloroform (Figure 37 and Figure 38). The protons of the two methylene groups attached to the malonate moiety are characterized by a singlet resonance at 5.77ppm (highlighted on Figure 37, bottom spectrum). Also, the chemical shift and the ratio of the areas of all the ^{1}H-NMR signals of **20** are consistent with the C$_{60}$ counterpart **16** suggesting a [6,6] addition pattern on the I$_h$ C$_{80}$ cage.
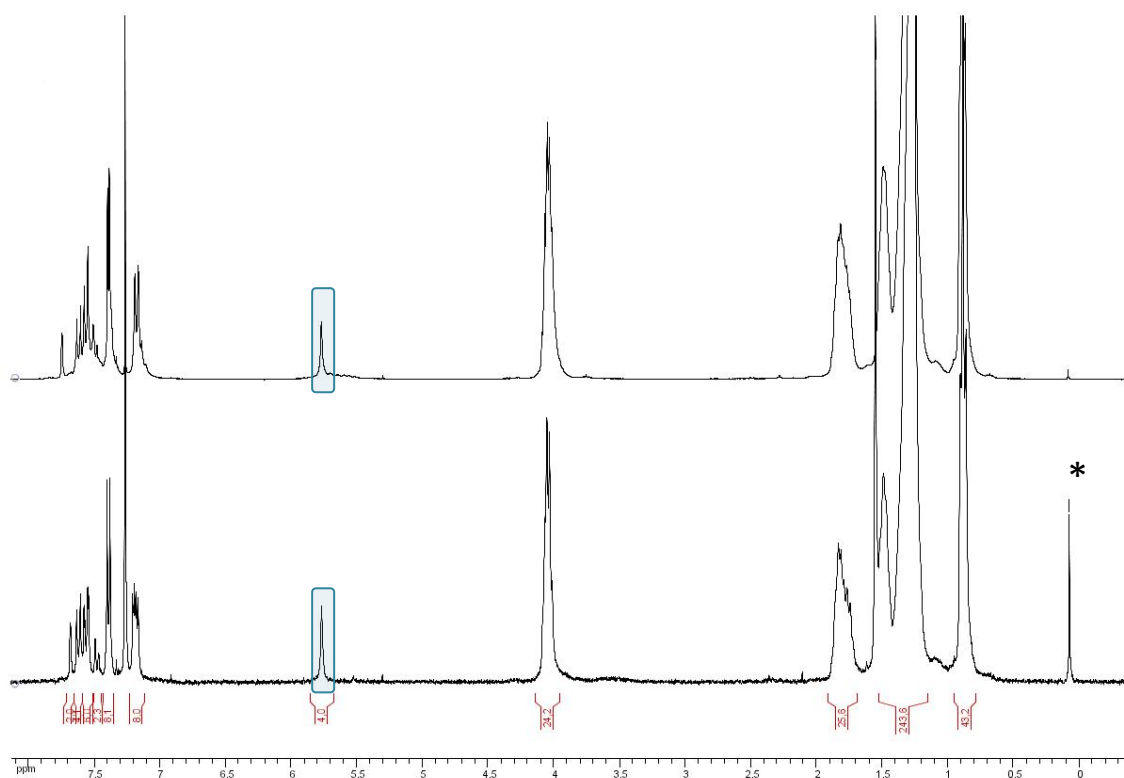
Figure 37, ^{1}H NMR spectra (300 MHz, CDCl$_3$) of **20** (bottom) and its C$_{60}$ counterpart **16** (top). The highlighted areas (on both spectra) are the methylene proton signals appended to the malonate moiety. (*) denotes grease.

On the basis of symmetry considerations, the observed ^{1}H NMR signals are consistent with a [6,6] addition pattern and the only question remains – from a structural point of view – whether the compound is an a cyclopropane derivative similarly to its C$_{60}$ analogue or an open cage fulleroid, as with some other TNT EMF adducts. The low solubility of most of the TNT EMF derivatives prevents their ^{13}C-NMR characterization or the use of ^{13}C labeled samples and solvent mixtures with CS$_2$ is required. Herein, we describe the full ^{13}C-NMR characterization of the Y$_3$N@C$_{80}$ derivative **20** in pure CDCl$_3$ solution. The ^{13}C-NMR spectrum of the dyad displays all the resonances we expect, but the methano bridge carbon signal is too weak to be observed. (The methano carbon resonance of the C$_{60}$ counterpart appears at 51.76 ppm.) The methylene carbons adjacent to the malonate moiety display only one resonance at 67.50 ppm - consistently with resonance of the C$_{60}$ analogue methylene carbons at 66.91 ppm – confirming that the addition occurred at the [6,6] site. All the other OPE related carbon resonances were detected, which are consistent with the

93

similar resonances of the C_{60} counterpart. Another very important feature of the spectrum is the missing sp^3 cage carbon contrarily to the observed sp^3 carbon resonance at 71.39 ppm of the C_{60} counterpart. This is an unambiguous proof of the open cage fulleroid character of dOPE-$Y_3N@C_{80}$ methano derivative. Noticeably, the number and position of sp^2 cage carbon resonances (highlighted areas between 125 and 155 ppm on Figure 37) are altered on the two spectra as an obvious consequence of the presence of different fullerene homologues (ie. C_{60} and C_{80}) and the fulleroid character of the I_h C_{80} derivative. The UV-Vis results also supported the NMR findings and suggest a high stability of the compound (vide infra).

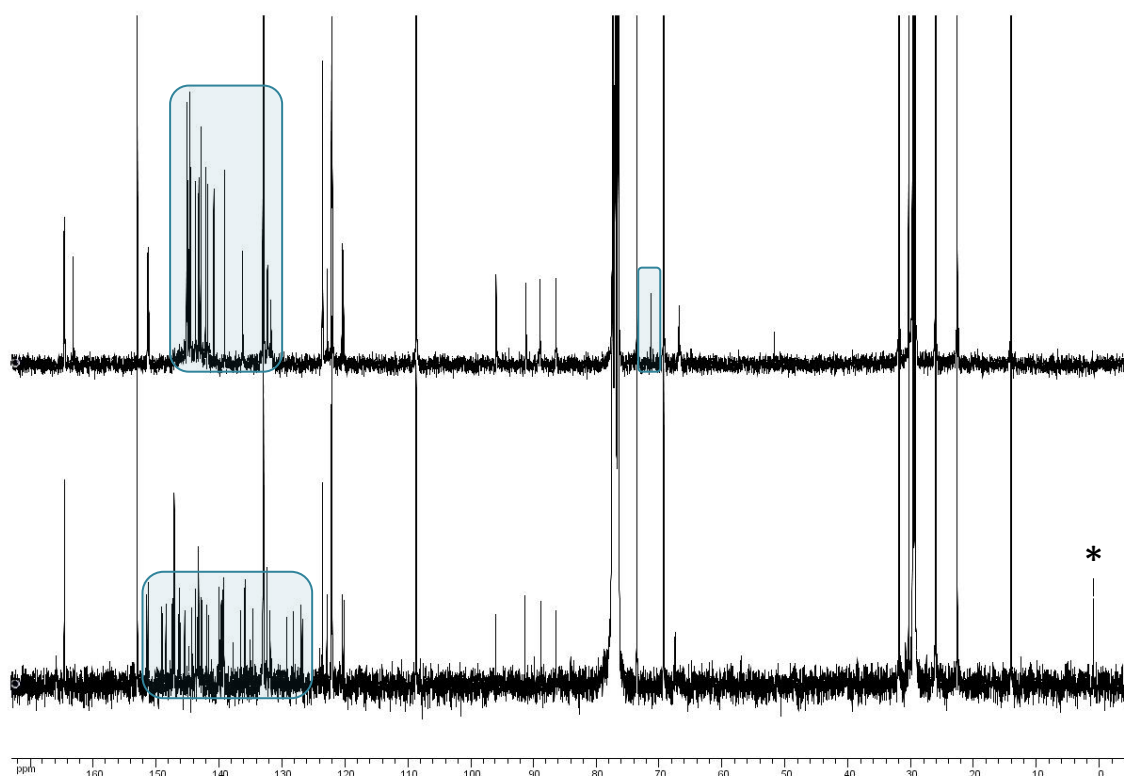**Figure 38,** ^{13}C-NMR spectra (300 MHz, CDCl$_3$) of fulleroid **20** (bottom) and its C_{60} counterpart **16** (top). The highlighted areas (on both spectra) are the sp^2 carbon signals of the carbon cage; and the sp^3 carbon signals of the C_{60} cage (spectrum at the top). There is no sp^3 cage carbon signal on the bottom spectra, indicating an open fulleroid character of C_{80} cage. (*) denotes grease.

II. 2.2.3)   Mass spectroscopy for the analysis of C_{60} derivatives

The MALDI-TOF spectrum of D-A dyad **16** is shown on Figure 39 as representative example. The peak with the highest m/z value corresponds to the product while peaks A-E can be assigned to different fragments of the compound.
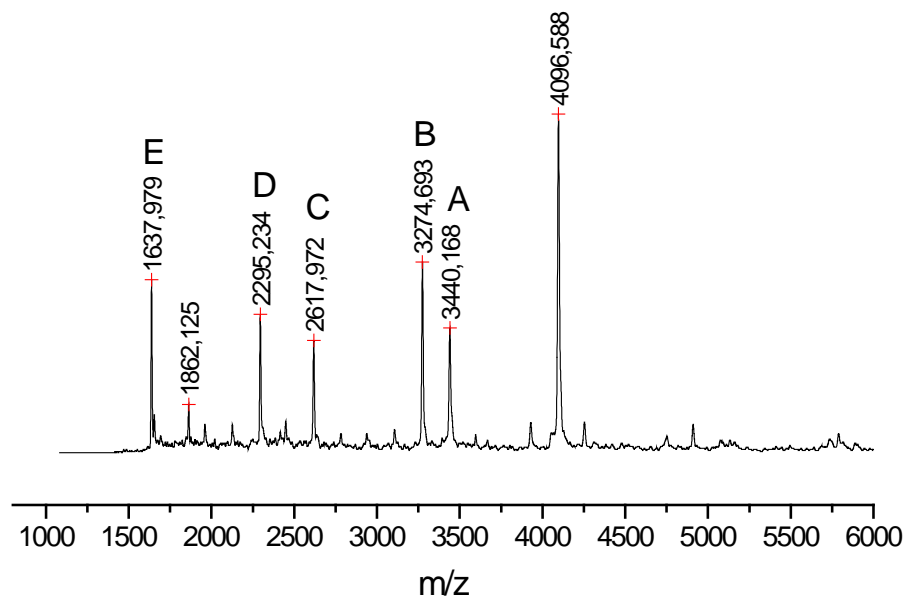
Figure 39, MALDI-TOF mass spectrum of **16** and its fragmentation.

A [M - $C_{43}H_{77}O_4$]
B [M - $C_{43}H_{77}O_4$ - $C_{12}H_{25}$]
C [M - 2*$C_{43}H_{77}O_4$ - $C_{12}H_{25}$]
D [M - $C_{109}H_{167}O_{10}$ - $C_{12}H_{25}$]
E [$C_{109}H_{167}O_{10}$]

$C_{43}H_{77}O_4$

$C_{109}H_{167}O_{10}$
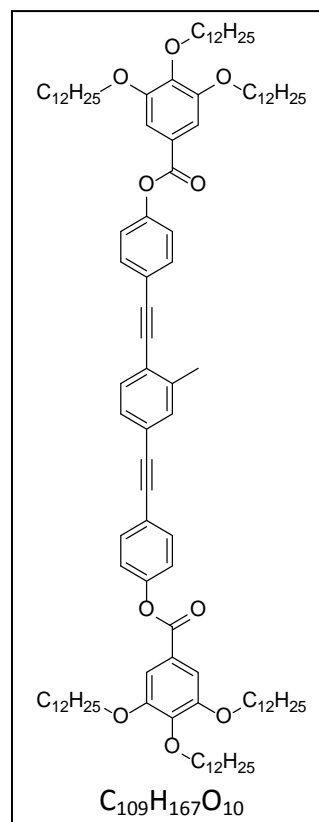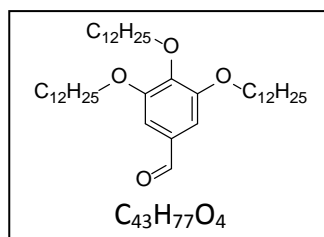
II. 2.2.4) Mass spectroscopy of OPE- $Y_3N@C_{80}$ dyad
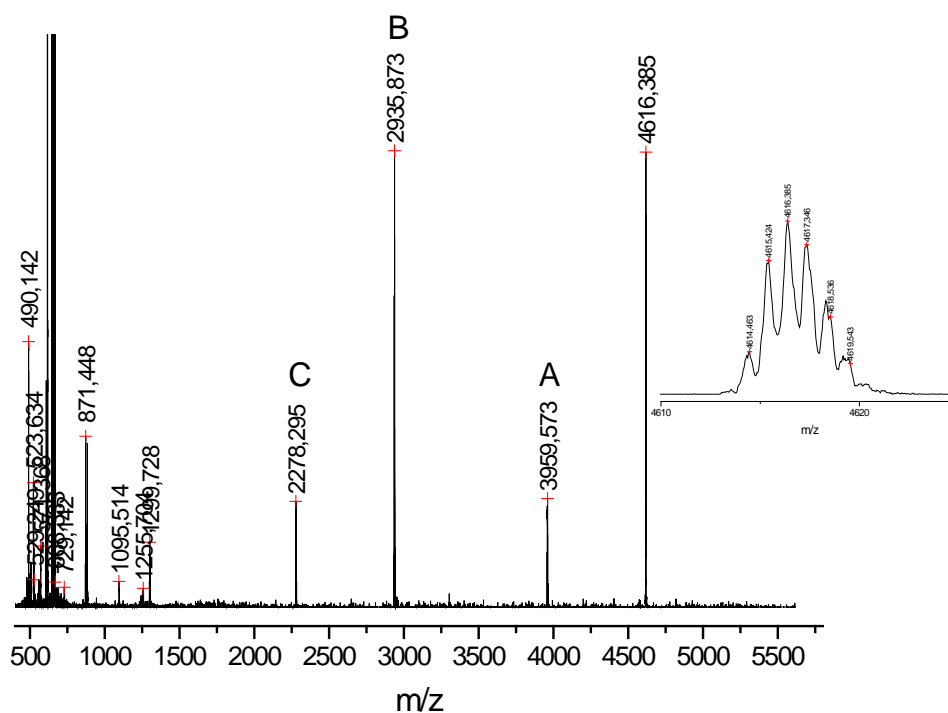
Figure 40, MALDI-TOF mass spectrum of **20**, its fragmentation, and the monoisotopic distribution (inset).

A [M - $C_{43}H_{77}O_4$]
B [M - $C_{110}H_{167}O_{12}$]
C [M - $C_{110}H_{167}O_{12}$ - $C_{43}H_{77}O_4$]

$C_{43}H_{77}O_4$
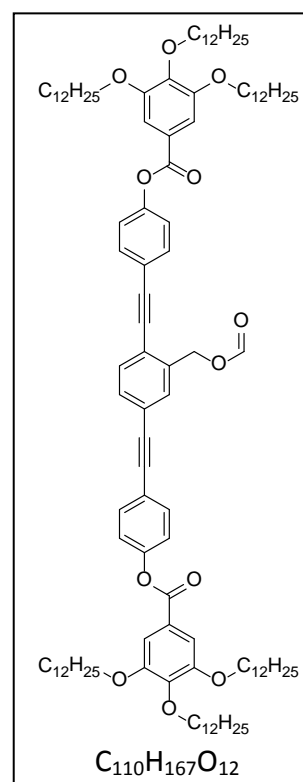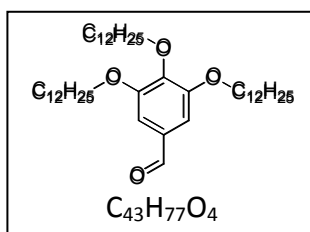
The peak with the highest m/z value corresponds to the product while peaks A-C can be assigned to different fragments of the compound (see above).


$C_{110}H_{167}O_{12}$

II. 2. 3)   LC properties (POM, DSC, X-rays)

The study of the liquid crystalline properties required the expertise of Benoit Heinrich, at CNRS IPCMS-DMO, Strasbourg, France.

The thermal behavior of all the compounds were studied by polarized optical microscopy with a heating stage (POM), differential scanning calorimetry (DSC), and temperature dependent wide- and small-angle X-ray diffraction (WAXS, SAXS). For the POM observation, samples were put between two glass plates and heated to the isotropic liquid phase at first and optical images were taken upon slowly cooling down to room temperature. The study was supported by thermogravimetric analysis (TGA) data if it was necessary.

The phase transition temperatures and enthalpies are reported in Table 1. The XRD data of most of the OPE-based compounds are collected in Table 2.

II. 2. 3. 1)POM and DSC results of OPE based D-A ensembles and their main building blocks

The POM observations on the first heating revealed that compound **7** is birefringent even at room temperature. This observation is consistent with the DSC traces (Figure 41), which do not contain any peak associated to a latent heat in the 100 J/g order of magnitude typical of melting. Moreover, two small transition peaks around 40°C and at 80°C precede the transition to the isotropic liquid at 87°C, evidencing the succession of several mesophases (labeled M_1, M_2 and M_3), whilst the unusually large enthalpy variation associated to the isotropization peak reveals the high degree of ordering involved in the mesophase organizations. A further indication for mesophases with crystal-like partial ordering consists in the exceptionally large delay of the reverse transition on cooling noticed for the upper transition between mesophases (exceeding 10°C). The lower transition is even not observed on the DSC trace but reproduces on further heating, which is presumably due a slow kinetics smearing off the signal in the background line, in consistency with the broad peak shape on heating.
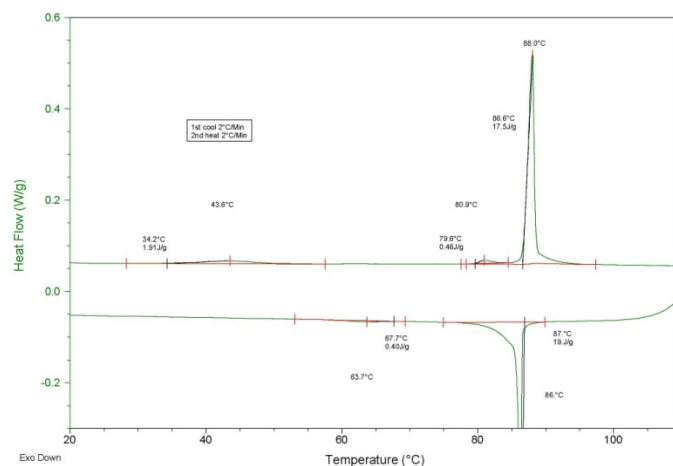
Figure 41, DSC heating-cooling cycle of OPE derivative **7**.

Symmetric OPE-malonate **15** behaves similarly to **7** from different aspects. There are two co-existing mesophases present on DSC solely or simultaneously over a wide temperature range (Figure 42). This material shows mesomorphic behavior only after the first heating, but retains those properties when cooling down to room temperature or even below. The identification of the mesophase structures of these two materials was difficult and required the recording of numerous XRD patterns (see next Section).
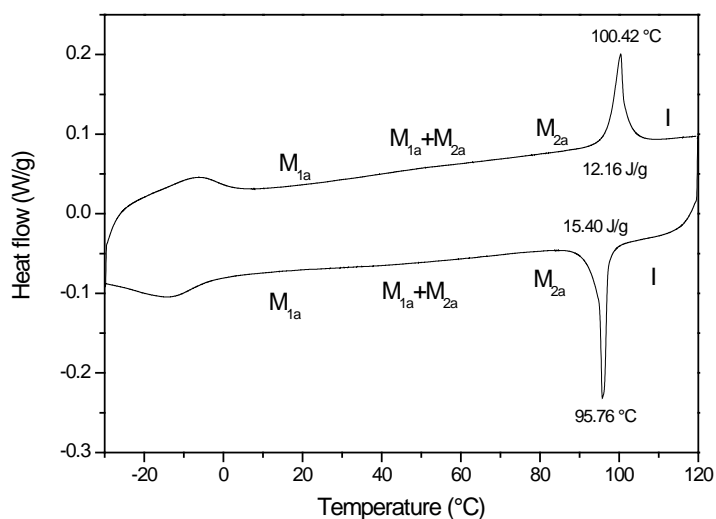
Figure 42, DSC heating-cooling curves of symmetric OPE-malonate **15**. M_{1a}: mesophase 1, M_{2a}: mesophase 2, I: isotropic phase.

POM image of asymmetric malonate **17** shows typical fan shaped focal-conic texture of smectic A phase (Figure 43). On repeated heating–cooling cycles, a stable and

reproducible behavior took place with crystal-to-smectic A phase transition at 38°C and smectic A to isotropic liquid transition at 81°C (Figure 44).
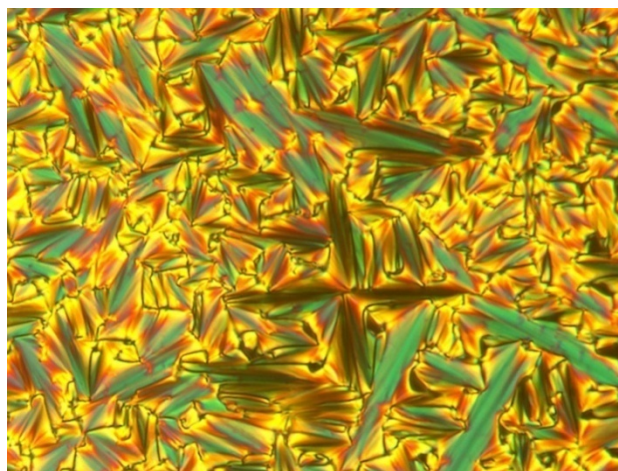
Figure 43, The polarized optical micrograph of **17**, observed on cooling from the isotropic liquid phase. Typical texture of SmA phase.
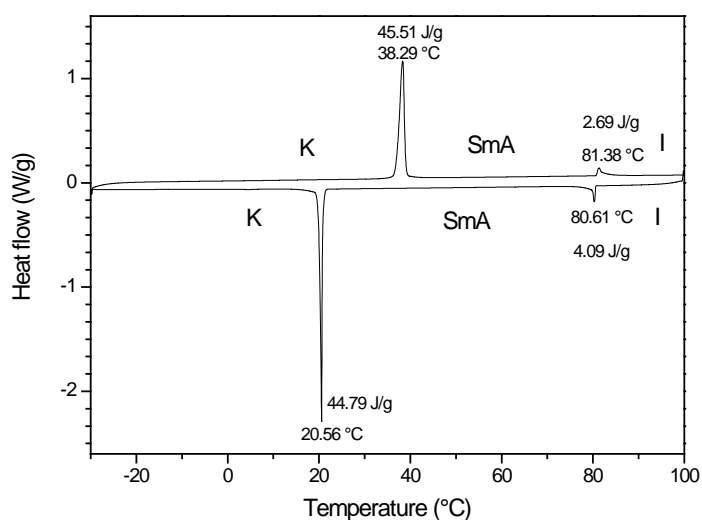
Figure 44, The DSC heating-cooling curves of asymmetric malonate **17**. K: crystal phase 1, SmA: smectic A phase, I: isotropic phase.

The POM and DSC analyses (Figure 45) suggest the presence of a mesophase for dyad **18** as there is a very broad, reproducible transition between 40 and 90°C on second heating cycle with very small enthalpy difference. The isotropization temperature was found to be around 100°C by POM observation.
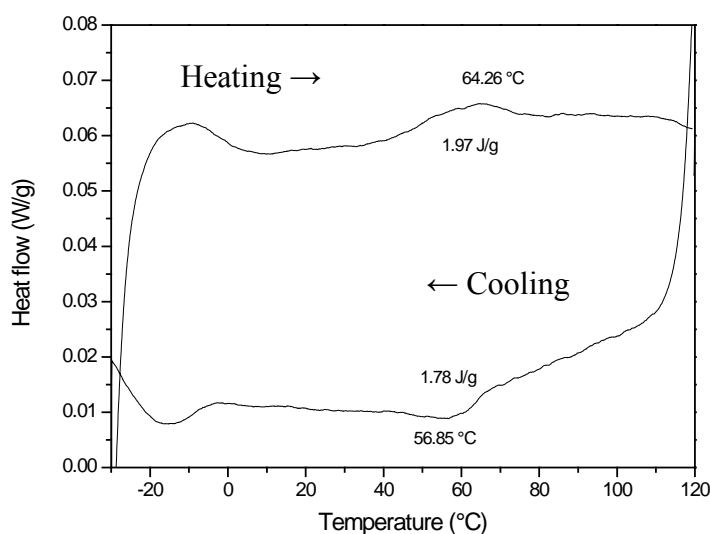
Figure 45, DSC heating-cooling curves of asymmetric D-A dyad **18**.

Observation of the OPE-C_{60} (**16**) and OPE-$Y_3N@C_{80}$ (**20**) D-A dyads under POM (Figure 46) did not allow us to assign the mesophase. Moreover, the isotropization peak in the DSC traces spreads over more than 10°C with tens of degrees delay on cooling (Figure 45), likely in relation with the high viscosity of the sample even beyond the isotropization, as appreciated from the polarizing microscopy (POM) observation. Although the peak separation from the baseline is delicate, the isotropization enthalpy is a few J/g, which is classical of mesophase to isotropic phase transitions.
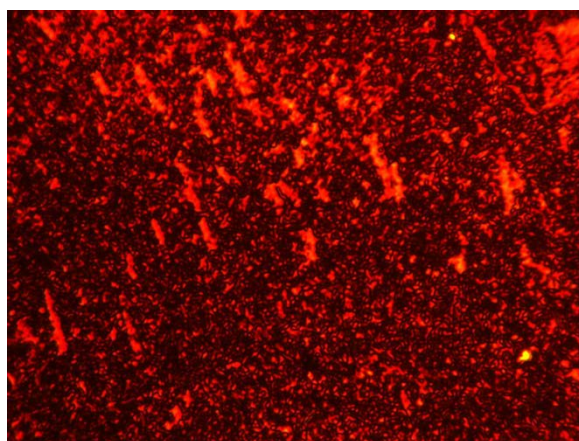
Figure 46, Polarized optical micrograph of **20**, birefringent texture observed at RT on cooling from the isotropic liquid phase.

Table 1, The phase transition temperatures and enthalpies of OPE based compounds.

compound	transition[a]	T(°C)	dH (J/g)
7	$M_1 - M_2$	~44*	1.9*
	$M_2 - M_3$	~81	0.5*
	$M_3 - I$	87	17.5
15	$M_{1a} - M_{2a}$	~40*	0.8*
	$M_{2a} - I$	97.1	13.2
16	$Col_r - I$	96.1*	3.8*
17	$K - SmA$	37.0	45.5
	$SmA - I$	80.8	2.7
18	$SmA - I$	~90-100*	2.0*
20	$Col_h - I$	~80	4.8*

[a] K: crystalline or semicrystalline solid, Col_r: columnar rectangular phase, SmA: smectic A phase, I: isotropic liquid. Temperatures are given as the onset values taken from the second heating run.

The transitions marked with asterisk are very broad transitions thus the enthalpy values were roughly estimated and the corresponding phase transition temperatures were determined from SAXS experiments.

II. 2. 3. 2)Supramolecular organization

Phasmidic building blocks

The XRD on powder patterns of **7** (Figure 47) confirms the mesophase sequence deduced from the DSC traces. The same three mesophases succeeding on heating (labeled M_1, M_2, M_3) are re-obtained on cooling, but with a substantial delay (about 10°C and 20°C hysteresis for the transitions M_3 to M_2 and M_2 to M_1). In the wide-angle region of patterns, the unique broad band centered at about 4.5 Å indicates that the lateral packing of mesogens and chain is liquid-like in the three phases, whilst the small-angle region evidences the different types of mesophase structures resulting from the segregation of mesogens and chains in separated micro-domains. Thus, the observation of numerous sharp reflections in the small angle region in the M_2 and M_3 phases suggests long range ordered 3D structures. Only a few reflections, moreover slightly broadened, subsist in the M_1 phase and are indexed in a Col_R lattice containing two columns. Actually, excepted the lateral CH_2OH group borne by the central ring, the architecture of the molecule is the typical "phasmidic" one, which is well known to give raise to columnar phase, by folding of the aliphatic tails in excess in between the mesogen sub-layers: these sub-layers break then into

one-dimensional ribbons forming the columns at the nodes of a bidimensional lattice[53]. For these reference systems, the hexagonal symmetry implies that the section of ribbons is randomized to a cylinder, but here a slight shrinking and the reduced contrast in the **a**-lattice vector direction indicates that preferential orientations of the mesogens within the ribbons are still preserved, as sometimes observed in polycatenar systems[54].
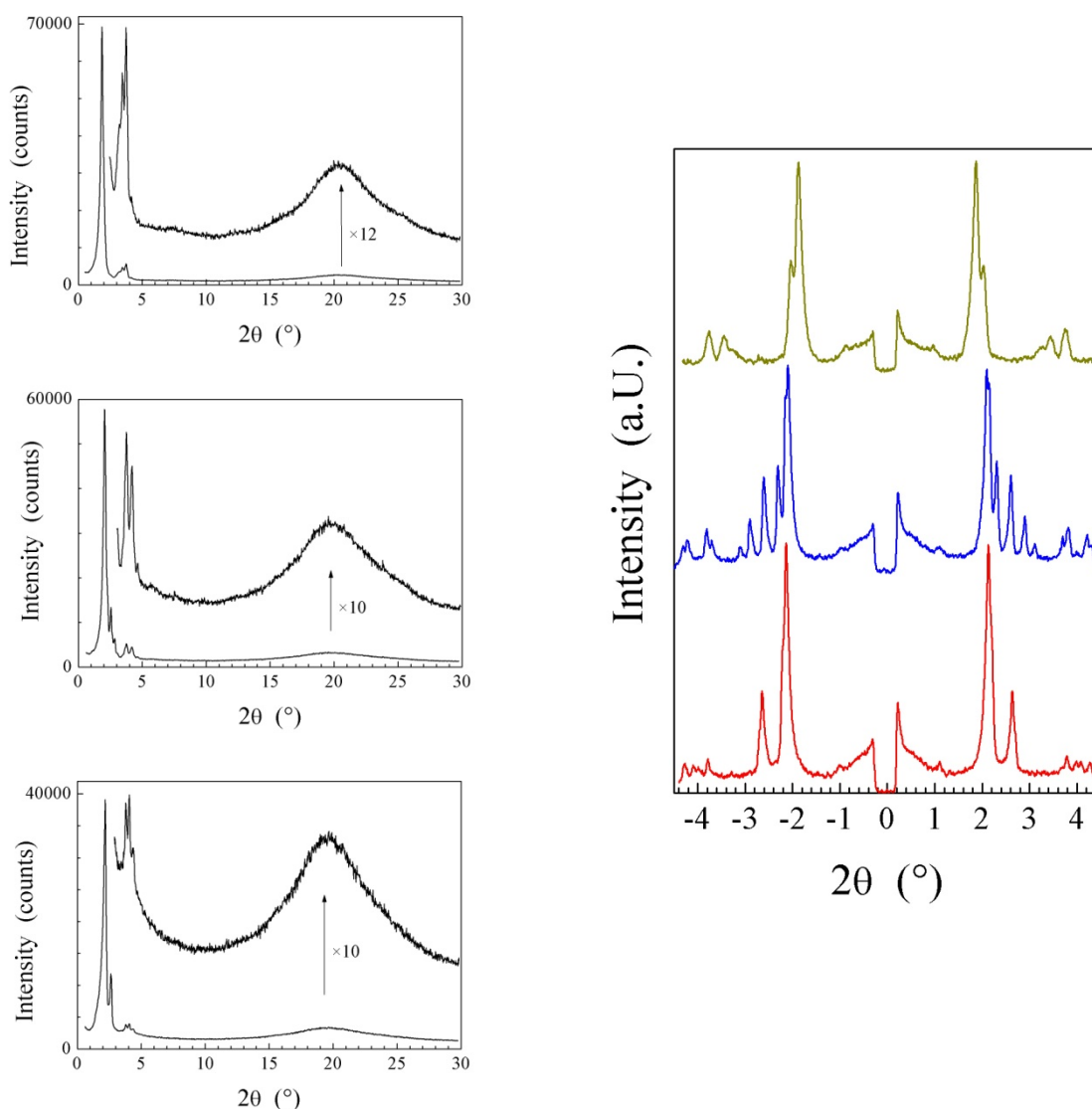
Figure 47, WAXS (left) and SAXS (right) patterns of **7** in the M_1 phase at 20°C, in the M_2 phase at 60°C and in the M_3 phase at 85°C (from top to bottom).

Remarkably, the bidimensional lattice is maintained in the M_2 and M_3 phases, becoming sub-lattices of the 3D-structure. Furthermore, the rectangular geometry is preserved in the M_3 phase and the patterns mainly differ from the M_1 phase by the

presence of an additional intense reflection and of several weak higher order reflections, from which the phase could be identified as monoclinic. The geometry and size of the cell in the M_2 phase are similar as in the M_3 phase, but the fundamental periodicity of the bidimensional sub-lattice (110) splits into a close (110) and (1-10) pair, resulting in a symmetry break toward an oblique sub-lattice and a triclinic cell.

The XRD on powder patterns of **15** (Figure 48) confirms the same sequence of mesophases that was observed in DSC thermograms (labeled M_{1a} and M_{2a} by increasing temperature). The diffuse scattering in the wide-angle region and the sharp reflections in the small angle region evidencing respectively the liquid-like lateral packing of mesogens and chains, and the structures resulting from their micro-segregation. The M_{2a} phase is very similar to the M_3 phase of **7**, consisting in a three-dimensional cell with a Col_R sub-lattice containing two strings of bundles. Patterns within the M_{1a} and M_1 phases are also similar and indicate for both phases a similar 2D-organization of continuous columns with reduced correlation length.
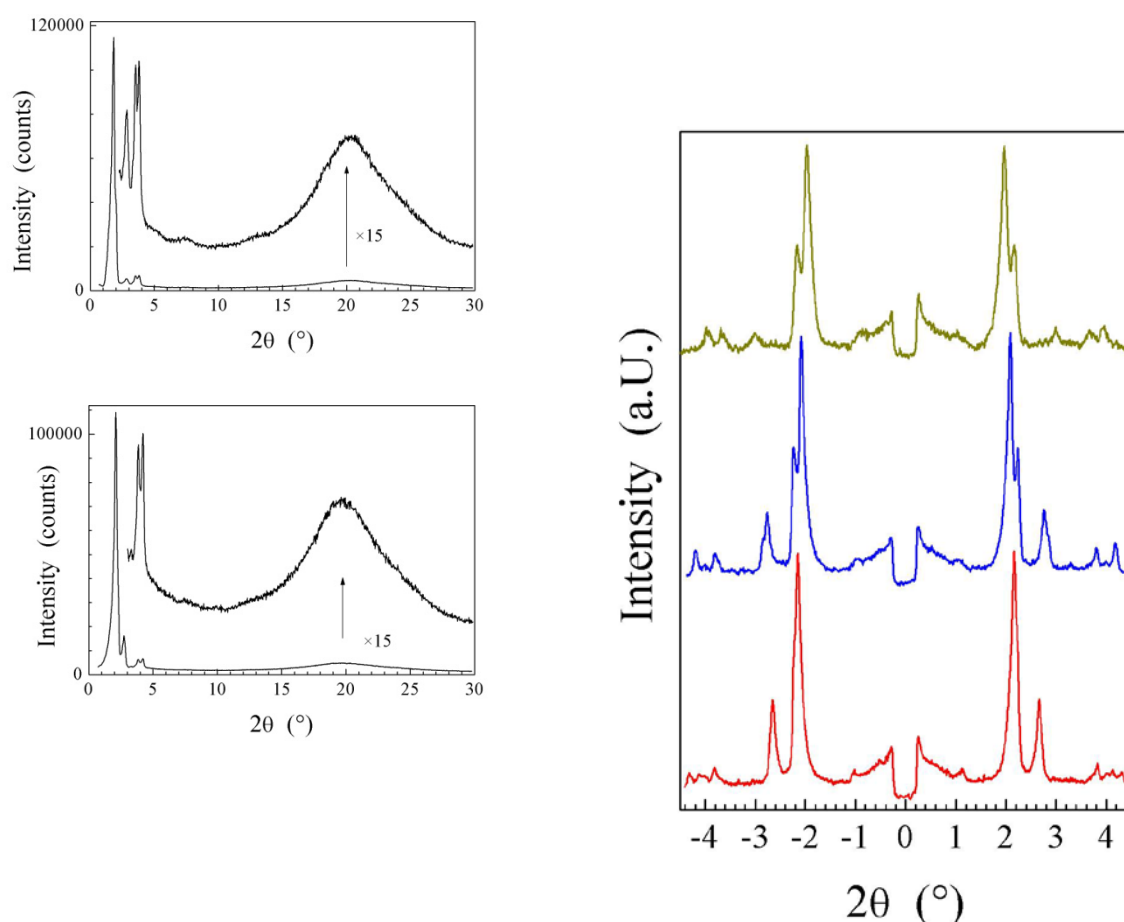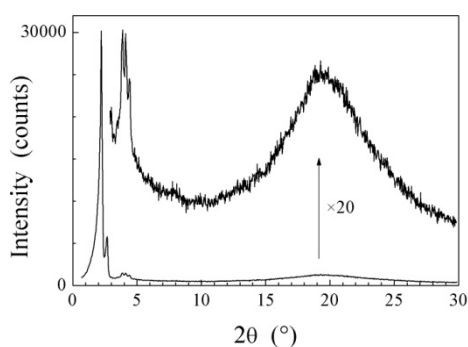
Figure 48, up: WAXS (left) and SAXS (right) patterns of **15** in the M_{1a} phase at 20°C, in the M_{2a} phase at 60°C and at 85°C (from top to bottom).

The observed molecular organization, which is different from that of typical phasmidic molecules, appeared to be a consequence of the presence of the lateral carbinol group (in case of **7**) or the malonate bridge (in case of **15**). However, the detailed supramolecular organization of the 3D mesophases of **7** and **15** are not discussed in this thesis.

Columnar phases

The grafting of a C_{60} fullerene or a C_{80}-endofullerene unit onto the central malonate bridge of **15** generates a triblock architecture which should lead to the micro-segregation of the fullerenes, the mesogens and the chains in different zones separated by interfaces constraining the organization. As a matter of fact, both adducts are amorphous in the pristine state and self-organize into a mesophase on heating (at 80°C for **16** and at 70°C for **20**). The mesophase is then kept up on cooling down to room temperature and is also recovered on cooling after a further heating beyond the isotropization temperature (located roughly around 100°C for **16** and 80°C for **20**). The self-organization and the transition to the isotropic state are best appreciated from XRD patterns (vide supra).

Fortunately, columnar mesophases are readily recognized from X-rays patterns, which are composed of the usual diffuse scattering at 4.5 Å indicative of the liquid-kike lateral packing, and of up to four sharp reflections in the spacing ratio $1:3^{0.5}:2:7^{0.5}$ in the small angle region indicative of a 2D-lattice with hexagonal geometry (the last reflection was not detected for **20**). As no further small-angle reflection is visible in the patterns of **20**, the mesophase is assigned to the Col_H phase. One additional weak signal located at twice the

spacing of the first reflection of the series is detected in patterns of **16** (Figure 49 andFigure 51) and the real lattice therefore includes several hexagonal cells, presumably under the effect of small shifts in orientation and/or position between neighboring columns[55]. The doubling of the hexagonal sub-lattice then generates a primitive rectangular lattice containing two columns per lattice area, assigned to a Col_R phase with pseudo-hexagonal geometry.
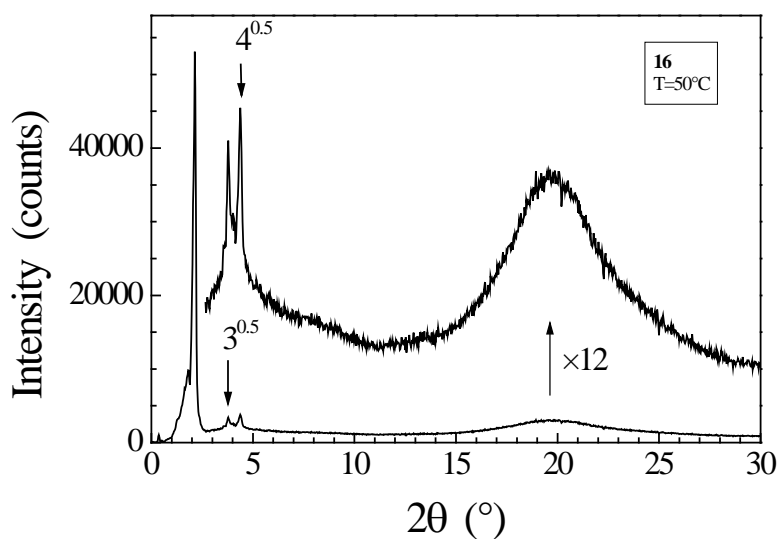
Figure 49, SAXS of **16**.
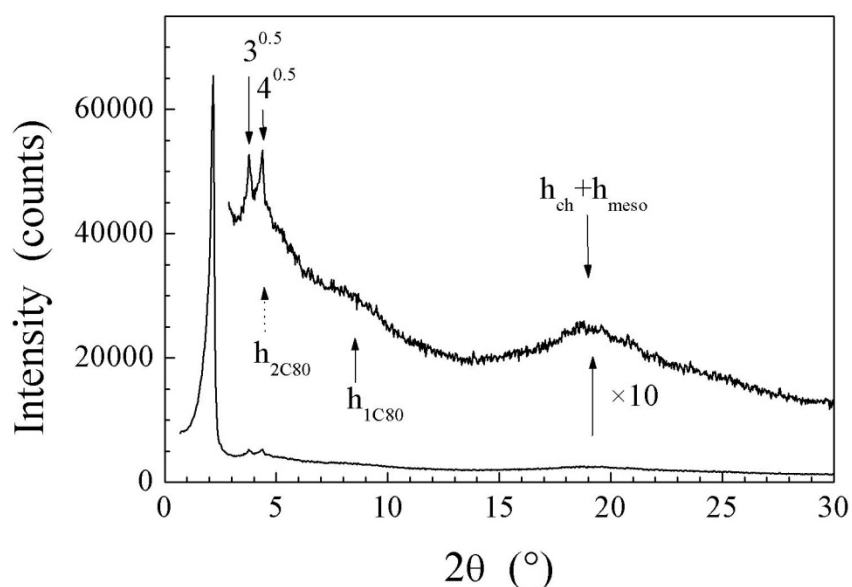
Figure 50, SAXS of **20**.
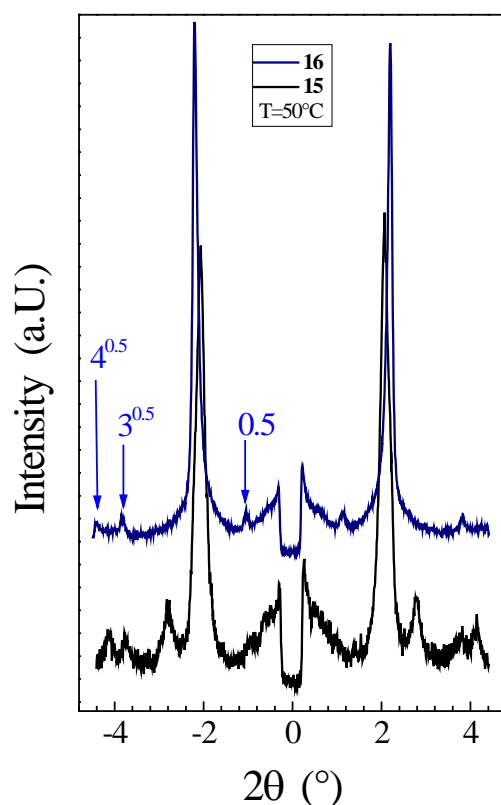
Figure 51, SAXS comparison of **15** and **16**.

The layer spacing dependence of **16** upon temperature is locked below 60 °C. Above 60 °C a decrease of around 0.07% per °C can be observed (Figure 52), which is typical value for columnar phases. The schematic views of the columnar packing of dyads **16** and **20** are given in Figure 53.
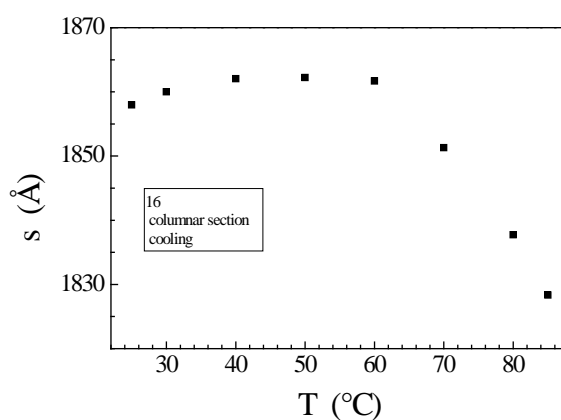
Figure 52, Layer spacing dependence upon temperature of **16** symmetric D-A dyad within a column section.
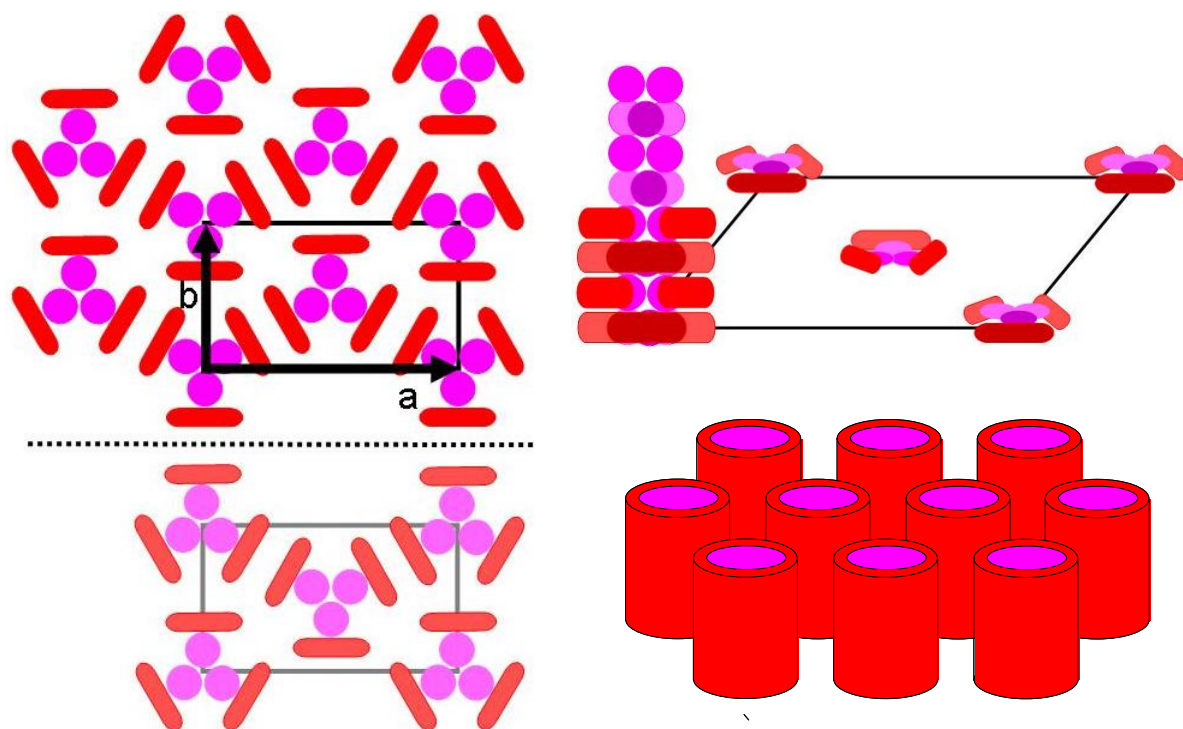
Figure 53, The core is constituted by the fullerenes and is mapped by a shell of mesogens, themselves surrounded by the continuum of aliphatic tails. The distribution of mesogens around the cores confers to the columns a cylindrical shape (left and right, top), preserving the pseudo-hexagonal geometry in **16**, despite the doubling of the lattice toward a rectangular columnar phase. The dotted line separates different slices of D_{C60} thickness parallel to the lattice plane. No correlations between column orientations subsist in **20** and the organization resumes to hexagonal columnar packing of concentric cylindrical columns (left, bottom).

Except the lattice doubling, both columnar structures appear very similar. In both cases, the micro-segregated regions are separated by regular and sharp interfaces, as shown by the presence of several sharp higher order reflections. The intensity decrease in the reflection series suggests that the (sub-)lattice contains only one peak of electronic density, implying that the high electronic density fragments (fullerene and mesogen) micro-segregate from the aliphatic periphery by forming mixed columns with micro-segregated regions of each fragment. The hexagonal geometry generally supposes that the cross-section of columns is averaged to a disc at the long-range correlation length scale, and both fragments should therefore respectively constitute the core and the shell of the average concentric columns. Actually, the molecular architecture imposes that the fullerenes constitutes the cores and the mesogens the shell, which corollary explains the high intensity

of the first order reflection of **20**, even though the electronic density of the endofullerene exceeds the one of the mesogen (partial molecular volume calculations leading to close electronic densities for C_{60} and mesogen).

A further similitude between both organizations consists in the size of columns: their similar cross-sections **S** (about 1.5% larger in **20** due to the presence of the approximately 40% greater fullerene cage volume compared with that of the C_{60} cage of **16**) lead to slice thicknesses $h_M=V_M/S$ comprised between 3.4 and 3.6 Å showing a slight increase with temperature. These values represent about the one third of the distance between first neighbor's fullerenes obtained from crystalline phases (about 10 Å and 11 Å, for C_{60} and C_{80}, respectively) and the column cross-sections contain therefore an average of three fullerenes. This suggest the naive image of successive molecular plates with a core of 3 interacting fullerenes stacked into columns with an alternating 120° rotation, according a strand of hexagonally close packed bowls (Figure 53). Such regularity is excluded by the absence of long-range ordered 3D structure in the patterns, but the image should appropriately represent the preferential local organization, as shown by the observation of additional diffuse signals in the patterns of **20**. Thus, endofullerenes are associated to electron density peaks, explaining the appearance of scatterings at 10.3 Å (correlation distance from Scherrer formula: $\xi \approx 30$ Å) and at 19 Å, respectively attributed to first and second neighboring distances between endofullerenes. There is no direct experimental information upon the orientation of the mesogens inside the shell, but the orientation in parallel to the core axis is excluded from a molecular point of view, especially as the core-shell interface area would be smaller than the projection area of the mesogens and moreover as the shell to periphery interface would not be rejected apart from the core. In contrast, mesogens oriented in perpendicular to the core axis would fulfill both criteria. So, with the geometrical parameters of **16** and **20**, the decoration of the internal interface with face-on mesogens would respectively lead to 90% and 100% surface coverage, whilst the grafting sites of alkyl tails would even be rejected a little beyond the diameter of the average interface cylinder between shell and periphery. In reality, the mesogens in the shell should adopt various orientations around a preferential one which lies therefore between both limit cases, but obviously closer to the perpendicular orientation. At the outer interface of the shell, the chain packing ratio largely exceeds unity

even for a cylindrical shape in consistency with the observed classical columnar mesomorphism.

Smectic phases

The X-Ray diffractogram of **17** registered at 50°C (Figure 54 andFigure 58) is consistent with the formation of a Smectic A phase. It reveals three reflections with varying intensities in the small angle region in the spacing ratio 1:2:4 indicative of the lamellar periodicity. By applying Bragg's law to these maxima, layer spacing of 46 Å was obtained. The very intense and broad wide angle diffusion is assigned to the molten chains at ca. 4.5 Å in the plane normal to the field, indicating short-range correlated in-plane ordering due to the liquid-like lateral packing of the molten aliphatic and oligo(ethylene oxide) chains.
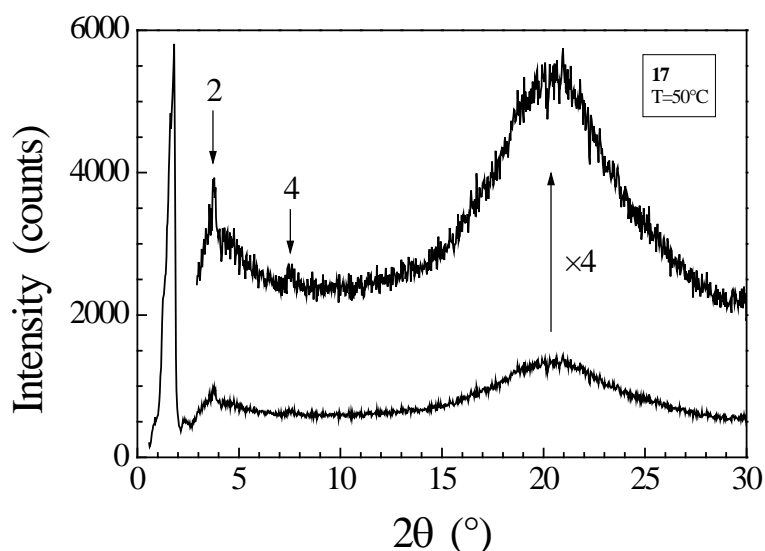
Figure 54, SAXS of **17**.

The layer spacing dependence upon temperature shows a decrease of 0.1% per °C, which is classical for SmA phase (Figure 55). The schematic view of the columnar packing of malonate precursor **17** is given in Figure 56.
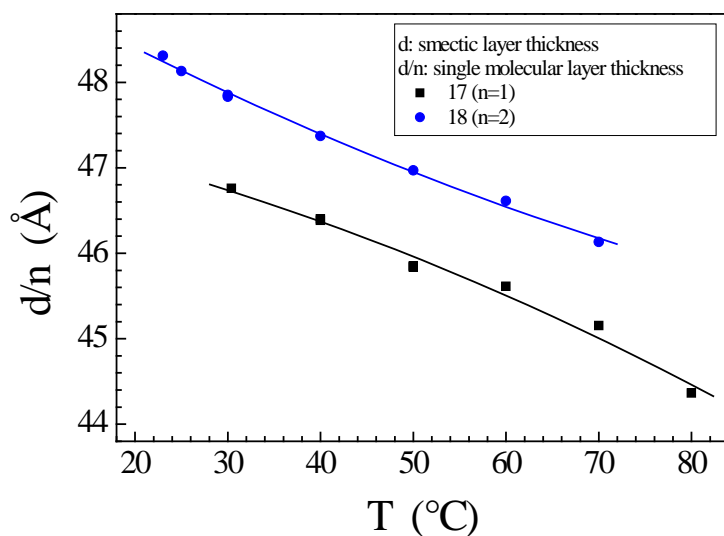
Figure 55, Layer spacing dependence upon temperature of **18** asymmetric D-A dyad and its precursor malonate **17**.
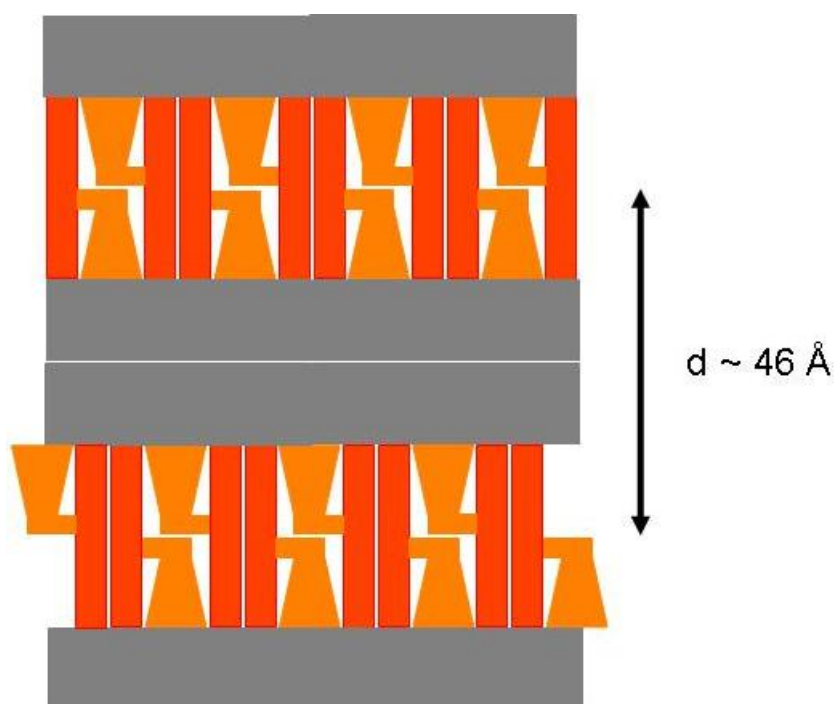
Figure 56, Schematic view of a likely molecular organization in the SmA phase of **17** (red: calamitic part; orange: :dendritic part; grey: aliphatic and oligo(ethylene oxide) chains).

The absence of reflections related to columnar superstructures and to ribbon periodicities indicates that vicinal mesogenic sublayers are not registered and that the space filling within these sublayers is statistical.

In order to assign the mesophase and understand the supramolecular organization of D-A dyad **18** it was X-Ray irradiated at different temperatures. The obtained diffraction patterns are in good accordance with the formation of smectic A phase even at room temperature (Figure 57 and Figure 58), similarly to that of the precursor **17**. At 80°C the sample decomposed during the XRD investigation. Choosing any pattern between room temperature and 80°C three reflections appear in the small angle region in the spacing ratio 1:2:4, which are typical of lamellar systems. The layer spacing dependence is also the same as that of precursor **17** (0.1% per °C) affirmative of SmA phase (Figure 55).
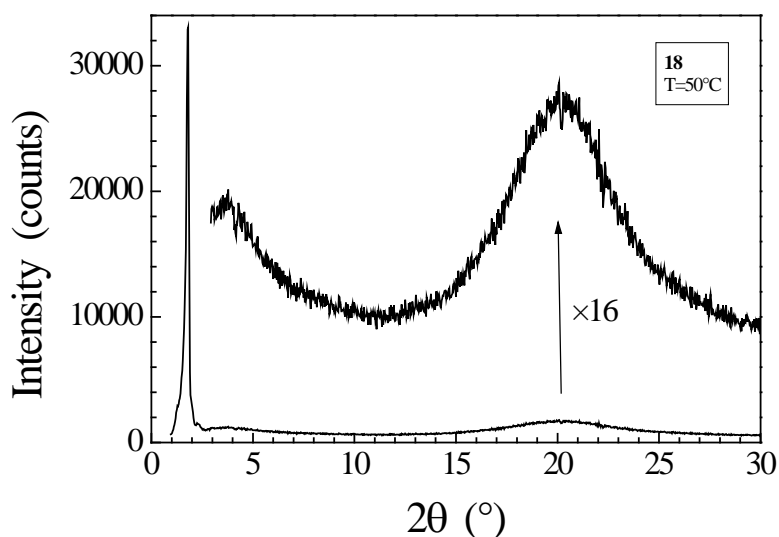
Figure 57, SAXS of **18**.
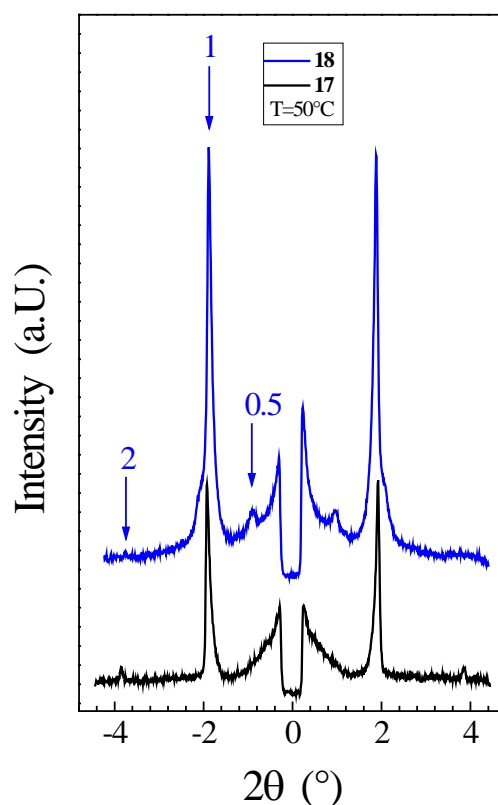
Figure 58, SAXS comparison of **17** and **18**.

Intensity variation in the series suggests double layer periodicity (Figure 59). Indeed, the lamellar distance is found to be 94 Å, the double of that of **17**. There is one, broad diffraction in the wide angle region due to the presence of molten aliphatic and oligo(ethylene oxide) chains at ca. 4.5 Å.

The layer doubling implies a shift along the layer normal between the electronic density profiles of adjacent mesogenic sublayers. This very likely occurs over layer undulations mechanisms, as the ones encountered for polycatenar compounds which prefigure the columnar lattices made of layers broken into ribbons[56]. However, beyond this layer doubling, neither reflections of ribbon periodicities nor columnar superstructures were detected in the patterns.

The XRD data of most of the OPE-based compounds are collected in Table 2.
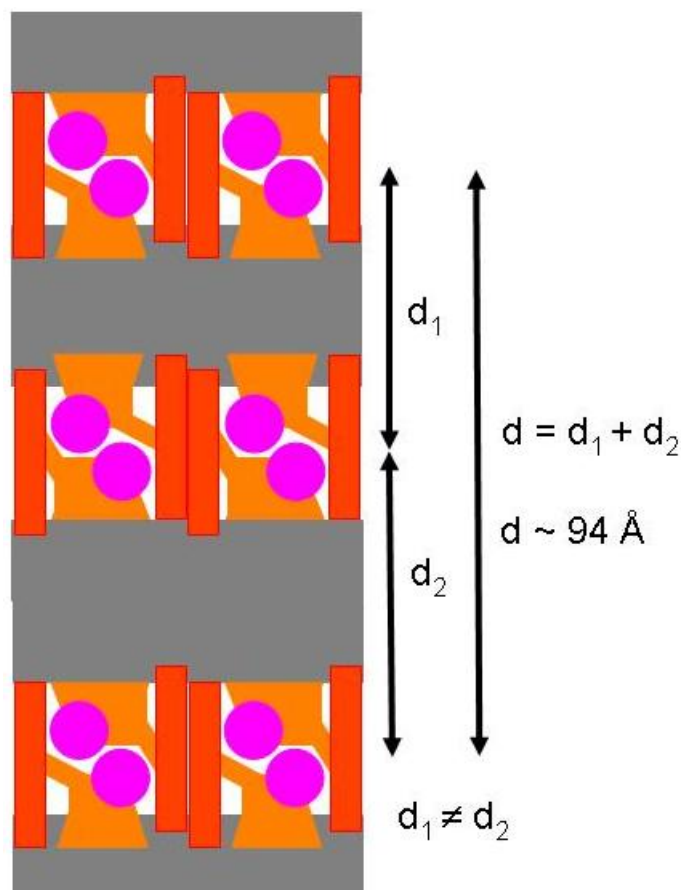
Figure 59, Schematic view of a possible molecular organization in the SmA phase of **18**. (red: calamitic part; orange: :dendritic part; grey: aliphatic and oligo(ethylene oxide) chains, pink: fullerenes).

Table 2, The X-Ray characterization of the mesophases of OPE based compounds.

Compound	$d_{meas.}$/Å[a]	hk(l)[b]	I[c]	$d_{theor.}$/Å[ad]	Parameters[d]
16	80.2	10	M (sh)	80.3	a = 80.2 Å
	40.1	20/11	VS (sh)	40.1	b = 46.3 Å
	23.1	31/02	M (sh)	23.2	S = 3713 Å^2
	20.0	40/22	M (sh)	20.1	V_{mol} = 6231 Å^3
	15.2	51/42/13	VW (sh)	15.2	h = 3.4 Å, Z = 2
	4.5	h_{ch}	VS (br)		n_{mol} ~ 3.0
17	45.9	001	VS (sh)	45.8	d = 45.83 Å
	22.9[e]	002	W (sh)	22.9	S = 104 Å^2
	11.6[e]	004	VW (sh)	11.45	V_{mol} = 4762 Å^3
	4.5	h_{ch}	VS (br)		S_{ch} = 20.8 Å^2
18	93.7	001	W(sh)	93.9	d = 93.9 Å
	46.8[e]	002	VS (sh)	46.95	S = 116 Å^2
	23.4[e]	004	VW (sh)	23.5	V_{mol} = 5469 Å^3
	4.5	h_{ch}	VS (br)		S_{ch} = 23.3 Å^2
20	40.4	10/1$\bar{1}$/01	VS (sh)	40.4	a = 80.3 Å
	23.4	10/2$\bar{1}$/$\bar{1}$2	M (sh)	23.4	b = 46.3 Å
	20.2	20/2$\bar{2}$/02	M (sh)	20.2	S = 3778 Å^2

19	h_{2C80}	VW (br)	V_{mol} = 6502 Å^3
10.3	h_{1C80}	V (br)	h = 3.6 Å, Z = 2
4.5	h_{ch}	VS (br)	n_{mol} ~ 3.0

[a] d_{meas} and d_{theor} are the measured and theoretical diffraction spacings, respectively. [b] [hkl] are the indexation of the reflections; h_{ch} is the liquid-like order of the molten chains. [c] Intensity of the reflections: VS: very strong, S: strong, M: medium, W: weak, VW: very weak; br: broad, sh: sharp. [d] d_{theo} is deduced from the lattice parameters a and b (Col$_r$) and layer spacing [d] (SmA) from the following mathematical expressions: i) for Col$_r$, S = a x b/2 and $<d_{hk}>$ = 1 / [(h^2/a^2 + k^2/b^2)$^{1/2}$] where N_{hk} is the number of hk reflections. S is the lattice area; ii) for SmA, S = V_{mol}/d and $<d_{hkl}>$ = d/l. Z is the aggregation number or the number of molecular equivalents per stratum of column. V_{mol} is the molecular volume: V_{mol} = V_{C60} + $V_{malonate}$ or V_{mol} = V_{C80} + $V_{malonate}$, where V_{C60} = 707 Å^3 (estimated from crystallographic data), V_{C80} = 974 Å^3 (estimated from crystallographic data), $V_{malonate}$ = (MW/0.6022) x (V_{CH2}(T)/V_{CH2}(T$_0$)), MW the molecular weight of the malonate and V_{CH2} = 26.5616 + 0.02023T. h is the theoretical intracolumnar repeating distance, deduced from the measured molecular volume and the columnar cross-section, h = V_{mol}/S/Z. [e] N_D: number of dendritic branches per stratum; n_{mol} is the number of molecules in a column segment of height: n_{mol} = D_{C60}/h, where D_{C60} = 10.0 Å (estimated from crystallographic data); S_{ch}: molecular area per chain, S_{ch} = S/n_{ch}, where n_{ch} is the number of chains. [e] The values cannot be precisely measured due to the weak signals.

II. 2. 3. 3)Self-assembly in thin films

Nanoscale molecular self-organization in thin films of **16** was studied by Grazing-incidence small-angle scattering (GISAXS). Two films were compared: the first one was a non-annealed, around 200 nm thick film and the second one was annealed at 85 °C for 1h and had around 120 nm thickness. In both cases, the 20/11 reflection of the pseudo-hexagonal lattice can be seen, but with a different scattering intensity distribution which evidences the different orientation of columnar domains. The scattering intensity of the 120 nanometer, annealed film is mainly concentrated in 3 spots separated by roughly 60°, with a reinforcement of the spot on the meridian. This clearly shows that columns lie in parallel to the substrate with the edge of the columnar lattice on the surface. Quite the contrary, the scattering intensity of the 200 nanometer, non-annealed film is distributed in a continuous ring, without visible reinforcement on the equator or meridian. This indicates that the columnar lattice is rather randomly oriented in the film.
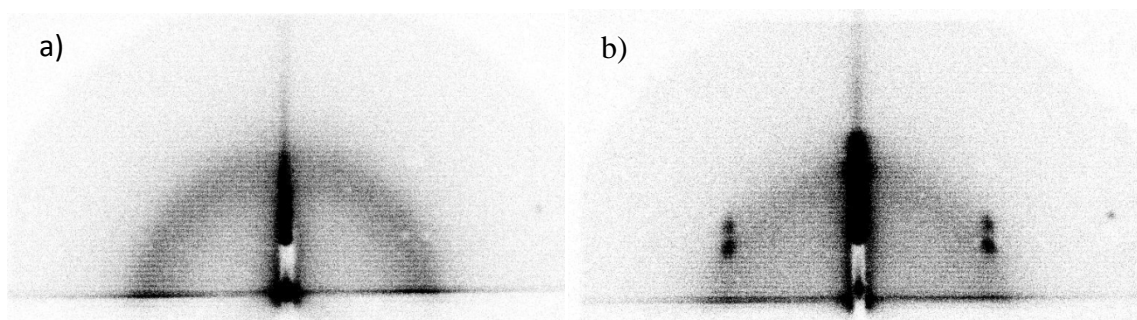
Figure 60, GISAXS patterns of a) non-annealed, 200 nm and b) annealed, 120 nm films of 16.

We can conclude, that either or both effects: annealing and film thickness change can induce molecular self-assembly in thin films. These preliminary results are very promising for the construction of electronic devices with separated donor and acceptor channels.

II. 2. 4)   Electrochemical studies

The photophysical and electrochemical measurements were performed in collaboration with the laboratory of Pr. Paola Ceroni, at the University of Bologna, Italy.

II. 2. 4. 1)General electrochemical properties of π-conjugated oligomer-fullerene D-A ensembles

As a general feature, all π-conjugated oligomer-fullerene D-A dyad preserve the electroactive features of their individual component units, which is also a good indication of the absence of ground state interaction between those two moieties. The first oxidation step corresponds to the one-electron loss of the π-conjugated acceptor unit (A/A^+), while the first reduction step is related to the one-electron gain of the fullerene (D/D^-).

The formation of sp^3 carbons on the C_{60} cage (eg. as a result of cycloaddition) shifts the C_{60} centred reduction potentials towards more negative values if it is compared to that of pristine C_{60}, in other words functionalized C_{60} derivatives are more difficult to reduce than pristine C_{60}. The nature of the link between the fullerene and the π-conjugated system (eg.

methano bridge, pyrrolidine- or pyrazoline ring etc.) also influences the redox behaviour of the D-A ensemble.

The oxidation potential of the π-conjugated acceptor (ie. the donor strength) can be influenced by the chemical structure of the laterally connected π-conjugated system and the conjugation length. Generally, the donor strength is increased (ie. the oxidation potential is decreased) with the increasing number of monomer units[27b].

II. 2. 4. 2) Cyclic voltammetry study of OPE-C_{60} dyads

The electrochemical properties of alcohol **7**, malonates **15** and **17** and their C_{60} counterparts **16** and **18** were investigated by cyclic voltammetry in dichloromethane with tetrabutylammonium hexafluorophosphate as supporting electrolyte. The internal reference for the experiment was ferrocene, which has an $E_{1/2}$ of 0.46 in dichloromethane solution. The values of the half wave potentials ($E_{1/2}$) of the investigated compounds are listed in Table 3.

Table 3, Half-wave potentials ($E_{1/2}$), unless otherwise noted for the investigated compounds in DCM/TBAPF$_6$ solutions at 298 K.

compound	2nd Ox	1st Ox	1st Red	2nd Red	3rd Red	4th Red
7		+ 1.71*	- 0.99*		-	-
15	+1.83*	+ 1.69*	- 0.96*		-	-
17		+ 1.70*	- 0.95*	-	-	-
16		+ 1.56*	-0.64	- 1.08*	-1.45	- 1.88
18		+1.83*	-0.66	- 1.04*	- 1.45	- 1.66
Malonate-C_{60}			-0.60	-0.98	- 1.43	
C_{60}**			-0.44	-0.82	-1.25	-1.72

*Chemically irreversible process; E_p value at 0.2 V/s.
**Adapted from ref 57.

The compounds **7**, **15** and **17** show a chemically irreversible process both in the anodic and in the cathodic region. The OPE malonate **15** also shows a second process in the

anodic region. The number of exchanged electrons cannot be determined because of the irreversibility of the process.

Measurements of the fullerene derivatives, **16** and **18** show the distinctive pattern for the fullerene core superimposed to that of the phenyleneethynylene moiety. An increase of the donor strength was observed when the number of grafted OPE moieties were increased from one, in case of dyad **18** (E^1_{ox} = 1.83) to two, in case of dyad **16** (E^1_{ox} = 1.56). The first reduction potential for each of the D-A assemblies occurs at ca. -0.66 Vs^{-1}, the second reduction potential, however, is almost identical in all five molecules and exhibits the irreversible reduction of the phenyleneethynylene core. The remaining two reductions correspond to the 2nd and 3rd reduction potential of the fullerene moiety occurring at -1.32 and -1.90 Vs^{-1} respectively.

The calculated electrochemical and optical band gap values of the OPE-based D-A dyads are summarized in Table 4.

Table 4, Electrochemical and optical band gaps of the OPE-based D-A dyads.

Compound	HOMO(eV)[a]	LUMO(eV)[a]	E_{gap}(el)(eV)[b]	Onset (nm)	E_{gap}(opt)(eV)[c]
16	-6.29	-4.09	2.20	715	1.94
18	-6.56	-4.07	2.49	715	1.94
20				760	1.63

[a]HOMO and LUMO values were estimated from the half-wave potentials; HOMO/LUMO = -e $E_{ox/red}$ + 4.73 (eV). [b]The electrochemical band gap was calculated from the HOMO and LUMO values; E_{gap}(el) = LUMO - HOMO (eV). [c]The optical band gap was calculated from the spectral onset; E_{gap}(opt) (eV) ≈ 1240/onset (nm).

II. 2. 5) Photophysical studies (Steady state absorption and fluorescence, time-resolved fluorescence)

The photophysical and electrochemical measurements were performed in collaboration with the laboratory of Pr. Paola Ceroni, at the University of Bologna, Italy.

II. 2. 1) Steady state UV-Vis absorption spectroscopy of OPE derivatives

The absorption spectrum of each compound was recorded in $1*10^{-5}$ M dichloromethane solution (for **15-18**). The central arene ring of unmodified OPEs can rotate through a very low potential energy barrier (~0.5 kcal/mol) between the fully planar and perpendicular structures[58]. It has a broad absorption band in the spectral region of 250-350 nm representing the time-averaged spectra of the various rotamers[59]. Indeed, the absorption spectrum of **7** contains a broad band with maximum at 326 nm, which is attributed to the phenyleneethynylene chromophore and also observed in the spectra of each of the other compounds. The precursor malonates **15** and **17** show no significantly different features indicating the existence of nearly freely rotating conformers with unaffected central arene π-orbitals[61]. The spectra of the fullerene derivatives **16** and **18** showed additional bands with maxima at approximately 260 nm as well as at 465 and 485. These bands were assigned to the fullerene itself.[60] The sharp band around 425nm is a characteristic feature of methanofullerene monoadducts, although this band is not so sharp in case of **16** possibly due to partial decomposition of the product. The remaining broad bands in the visible region are blue shifted and less structured if compared to pristine C_{60} and related to the forbidden transitions of C_{60}.
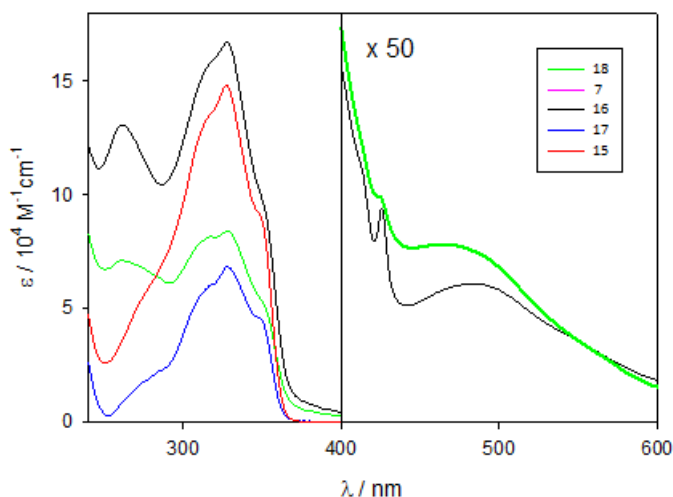

Figure 61, Absorption spectra of compound **7** and **15-18** in dichloromethane solution.

The existence or absence of ground state interaction between donor and acceptor moieties can be verified by the superimposed absorbance features of all elementary building

blocks. The absorption spectra of π-conjugated oligomers can be described with a high extinction coefficient band, typically located in the 250-500 nm range. On the other hand, typical fingerprints of C_{60} monoadducts reveal above 400 nm with low extinction coefficient (as it was detailed above). Therefore, the most important region for comparison is the 250-500nm region, where the most intense bands are located; we always investigated only this region (for the direct comparison of C_{60} fingerprints a simple monoadduct (eg. $C_{61}(COOEt)_2$) should be used instead of pristine C_{60}).
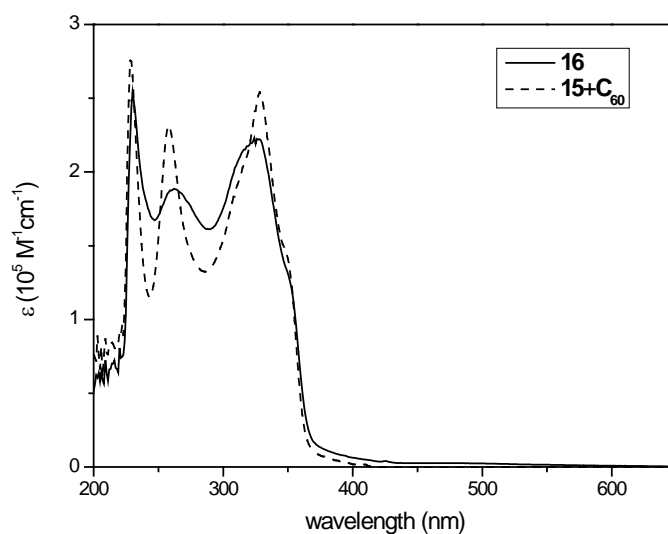
Figure 62, UV-Vis comparison of **16** with the sum of building blocks: **15** and C_{60}

The absorption spectrum of **16** is not the exact superimposition of the sum of its individual components: **15** malonate and C_{60}, as we can see on Figure 62, indicating the presence of ground state interaction between the electroactive moieties. The asymmetric OPE based donor-acceptor conjugate, **18** shows similar behaviour. Furthermore, similar effect has been found in the group of Nierengarten with a series OPE based dyads and suggested to be the reason of electronic perturbation of the OPE centred transition[33a,c,d,39]. Another explanation could be the change of isomeric configuration of the OPE moiety due to the attachment to the bulky fullerene core. But neither **16** nor **18** shows any sign of high rotation barrier along the carbon-carbon triple bond, as the shape of the broad band with maximum at 326 nm does not change significantly.

II. 2. 2) General steady state fluorescence features of fullerene derivatives based D-A ensembles

In general, π-conjugated oligomers are very strong chromophores with fluorescence that approaches unity quantum yields and high extinction coefficient in the visible region. Therefore, visible light irradiation of a fullerene based D-A system excites almost exclusively the oligomeric moiety. In such molecular architectures the fluorescence of the oligomers is strongly quenched, but its emission pattern remains the same and is not affected by the presence of fullerene. The fluorescence of C_{60} is much less intense, but noticeable with a maximum around 715 nm. Despite the different fluorescent quantum yields the fluorescence lifetime of π-conjugated system and fullerene moieties are comparable.

The fluorescence quenching of the oligomer moiety is a good indication of excited state communication between the building blocks. On the other hand, lot of information can be gained from the fullerene emission as well. Quenching of the fullerene related emission can be the consequence of charge separated state evolvement. Changing solvent polarity influences the energy levels of the fullerene singlet excited state and the charge separated state, therefore the fullerene quantum yield can deviate significantly in different solvents. The solvent dependence also denotes "through space" or "through bond" charge transfer processes. Monitoring its fluorescence lifetime can also provide evidence of electron or energy transfer scenario.

II. 2. 3) Steady state fluorescence spectroscopy of OPE derivatives

The photophysical properties of 1,4-bis(phenylethynyl)benzene and different OPE derivatives have been investigated by several groups[59,61-64]. In general, the emission spectra of these compounds can be described by a vibrationally structured band. It has been also shown that their normalized spectra are identical on exciting at different wavelengths which indicates the presence of a single emitting species[61]. Further studies revealed that rapid rotational relaxation (~60 ps)[62] occurs in the excited state followed by planarization. Semiempirical calculations[58, 61] also confirmed that rotational energy barrier of the arene rings along the molecular axis is higher in the excited state, limiting the number of conformers and leading to a structured emission. Therefore, the excited-state geometry of

OPE derivatives is strongly constrained to planar configuration in contrast to that of the ground state. Picosecond time-resolved resonance Raman spectroscopy revealed that photoexcitation does not bring any significant changes in the bond order of the acetylene group, ruling out any cumulenic or quinonoid character in its singlet excited state[63]. When investigating our components (**7**, **15-18, 20**), besides our own conclusions, we also wanted to know how they fit into the general trend.

Excited state properties of OPE-C$_{60}$ dyads

The excitation of each compound at 326 nm in the band of the phenyleneethynylene yielded the fluorescence spectra reported in Figure 63 which, for each compound, demonstrated a vibrationally structured band with maximum at 360 nm. The spectra were recorded for solutions having the same absorbance at the excitation wavelength, so that they are proportional to the relative emission quantum yields (Figure 63).
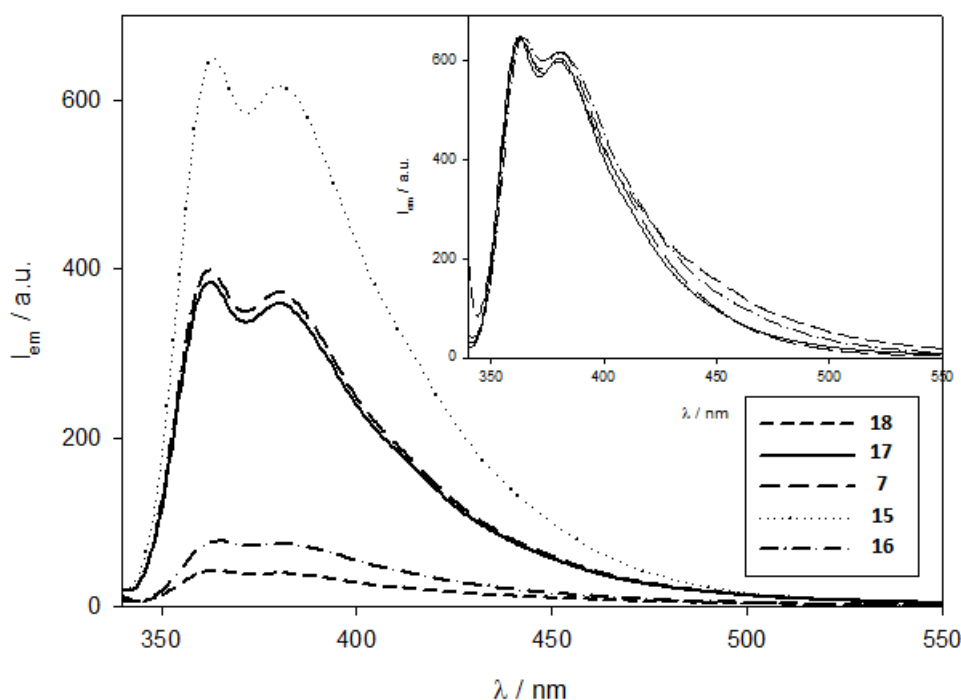

Figure 63, Fluorescence spectra of **7** and **15-18** in dichloromethane. The investigated solutions have the same absorbance (0.2) at λ_{ex} = 326 nm for the comparison of relative quantum yields.

In accordance with their molecular structure, compound **15** has a higher emission quantum yield than both **7** and **17**, which have the same emission quantum yield, within the experimental errors (see Table 5). For compounds **7**, **15** and **17** the emission quantum yields are lower than those expected for such a chromophore (in the literature emission quantum yields up to 0.8).[64]

The emission spectra of **16** and **18** have the same maximum, but with a tail at lower energy (inset in Figure 63) and a significantly lower intensity.

Upon excitation at 480 nm of **16** and **18**, the weak fluorescence typical of the fullerene was observed (Figure 64). The corresponding emission quantum yields are similar to that reported for fullerene derivatives (3×10^{-4}),[65] suggesting that the fullerene is not affected by the attachment to the phenyleneethynylene chain.
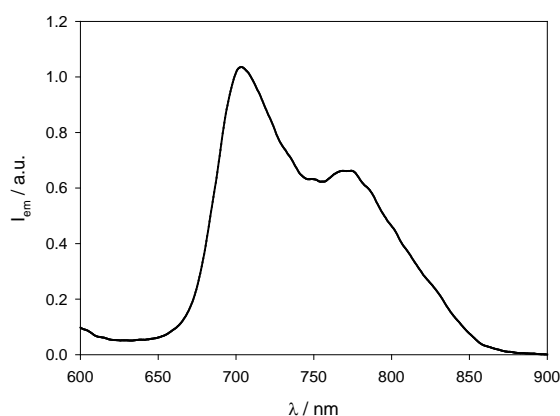

Figure 64, Fluorescence spectrum of compound **16** in dichloromethane at λ_{ex} = 480 nm for monitoring the fullerene luminescence.

Upon excitation at 275 nm, compounds **16** and **18** show a very weak emission band typical of the dimethoxybenzene unit. However, the small molar absorption coefficient of this chromophore compared to the phenyleneethynylene one prevents a quantitative discussion.

The emission of the fullerene containing compounds **16, 18** and **20** is significantly quenched either by energy or electron transfer compared to their precursory malonates **15** and **17**. Indeed, based on the electrochemical results (Section II. 2. 4), the photoinduced electron transfer from the trimethoxy unit to the fullerene moiety is thermodynamically allowed (ΔG ca. -1 eV). Energy transfer is the dominant pathway for quenching of the S_1 excited state of the phenyleneethynylene moiety and sensitization of the fullerene

emission. Indeed, the emission intensity of the fullerene at 705 nm by excitation of two isoabsorbing solutions of compound **16** at 326 nm, where most (>90%) of the light is absorbed by the phenyleneethynylene chromophore, and 480 nm, where light is absorbed only by the fullerene unit is the same, demonstrating a unitary efficiency of the energy transfer process (Scheme 7). The same result was obtained for compound **18**.
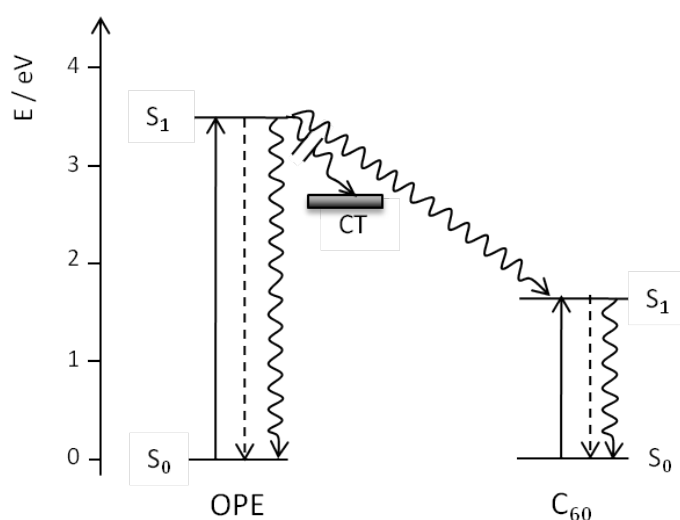
Scheme 7, Schematic energy level diagrams of compounds **16** and **18** showing absorption (solid line), emission (dashed line) and non-radiative deactivation processes (wavy lines).

The lifetime of the phenylenethynylene fluorescent excited state of all the investigated compounds was too short to be determined in dichloromethane solution at 298 K (instrument resolution 0.8 ns). The lifetime of the fullerene moiety in dichloromethane solution was found to be 1.5 ns and 1.6 ns for **16** and **18** respectively, which corresponds to the observed literature value of 1.2 - 1.6 ns for other fullerene derivatives suggesting no quenching of the fullerene emission.

Table 5, Most relevant photophysical data of compounds **7** and **15-18**.

| compound | solvent | absorption | | emission | | | | |
| | | 298 K | | 298 K | | | 77 K[b] | |
		λ_{max} / nm	ε / 10^4 M^{-1} cm^{-1}	λ_{max} / nm	τ / ns	Φ_{em}[a]	λ_{max} / nm	τ / ns
7	DCM	327	8.4	380	< 0.8	0.053	420	1.0, 6.2
	MeOH:DCM 9:1	330	-	470	3.6	-	420	

15	DCM	326	16.2	380	< 0.8	0.080	380 420	1.95, 7.1 3.5, 9.3
	MeOH:DCM 9:1	330	-	455	4.1	0.082	-	-
17	DCM	328	7.1	380	< 0.8	0.052	380 420	0.55, 3.7 3.8, 9.7
16	DCM	326 450	16.5	380 704	< 0.8 1.5	0.005 3.5×10^{-4}	382	-
18	DCM	328 450	7.8	380 704	< 0.8 1.6	0.003 3.3×10^{-4}	380	-

[a]Emission quantum yields were measured in dichloromethane using anthracene in EtOH as the standard. [b]Emission measurements at 77K were performed in CH_2Cl_2:$CHCl_3$ 1:1 (v/v) rigid matrix.

II. 2. 4) Photophysical features of OPE-$Y_3N@C_{80}$ dyad

Most of the photophysical properties of dyad **20** were studied in toluene in order to be comparable with the pristine $Y_3N@C_{80}$, which is practically insoluble in DCM. Furthermore, its properties were also compared to the C_{60} counterpart **16** to estimate the effect of the TNT EMF.

The absorption spectrum of **20** and **16** in both DCM and toluene solutions clearly show the contribution of the two constituent chromophores: the band around 325 nm is mainly due to the OPE units, while the absorption at λ>380 nm is characteristic of the fullerene core (Figure 65a and Figure 66a). The band at 326 nm in **20** is broader and lower in intensity compared to that of **15**, indicating a ground-state interaction between the OPE units and the endohedral fullerene core. It is worth noting that the molar absorption coefficient of **20** in the visible region is much higher than that of **16** and extends up to 750 nm due to the presence of the endohedral fullerene core. The UV-Vis spectroscopy is an adequate method to determine the addition pattern of TNT EMF derivatives, as discussed in Chapter I. The spectrum of OPE-$Y_3N@C_{80}$ derivative **20** closely resembles that of the clusterfullerene precursor, indicating that they have the same number of p orbitals. These results also suggest that the derivative is an open cage fulleroid[66] that provides high stability to the compound. Indeed, the compound was found to be stable in contrast to all the other $Y_3N@C_{80}$ based D-A dyads that were synthesized to date[44]. This may be the consequence of

the different donating strength of the grafted donor moieties. The OPE unit appeared to be a weaker electron donor than the ones used by other research groups (ie. exTTF, phthalocyanine or ferrocene) and instead of electron transfer it promoted energy transfer towards the fullerene (vide infra).
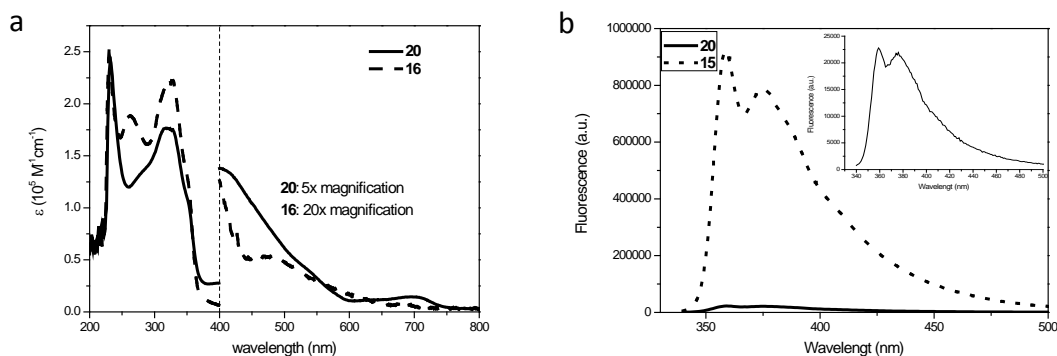

Figure 65, a) The comparison of the UV-Vis spectra of compounds **20** (solid line) and **16** (dashed line). b) The emission spectra of malonate **15** and OPE-$Y_3N@C_{80}$ D-A dyad **20** in dichloromethane at λ_{ex} = 330 nm. Inset: Magnified emission spectra of dyad **20**. (The obtained results for **15** and **16** slightly differ from the one in the previous section due to different experimental set-up.)
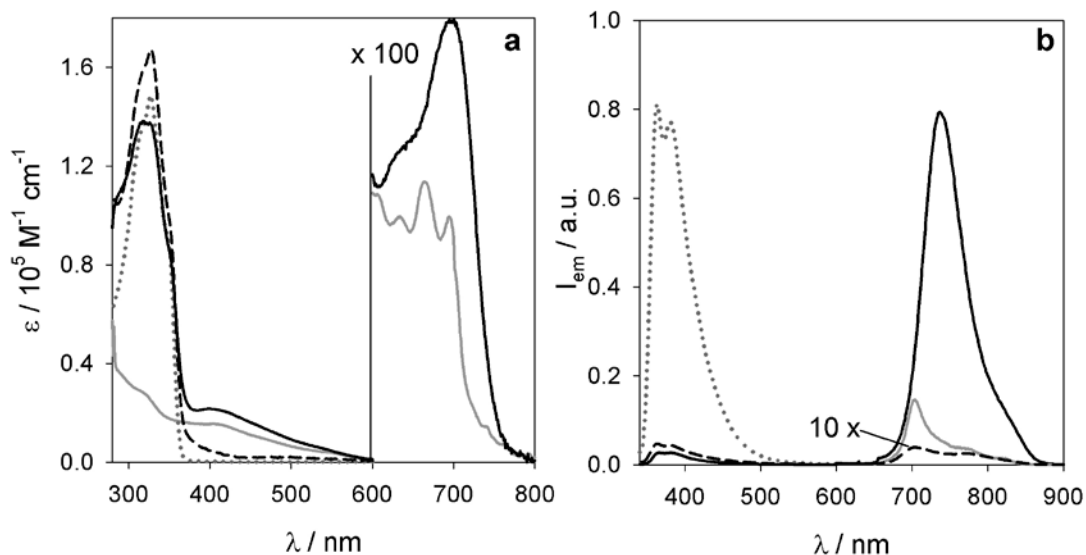

Figure 66, Absorption (a) and emission (b) spectra of **20** (solid black line), **16** (dashed black line), **15** (dotted gray line), and $Y_3N@C_{80}$ (solid gray line) in deaerated toluene solution at 298 K at λ_{ex}= 325 nm.

The emission spectra of **20** and **16** in deaerated toluene solution (Figure 66b) show two bands: one at ca. 365 nm which is centered on the OPE moiety and is strongly quenched (>20 times) compared to model compound **15**, the second one in the region between 680 and 900 nm can be attributed to the fullerene core (Table 5). Only the former band was recorded in air-equilibrated DCM and the quenching of the OPE emission was found to be similar to that in deaerated toluene solution (Figure 65b). The quenching of the OPE fluorescence can be attributed to a 100% efficient energy transfer, not only for OPE-C_{60} dyad but also for OPE-$Y_3N@C_{80}$. Indeed, the same fullerene emission intensity was recorded upon excitation of two isoabsorbing solutions of **20** at 320 nm, where most of the light is absorbed by the OPE unit, and 405 nm, where only the fullerene absorbs light (Scheme 8). Therefore, the two OPE units act as extremely efficient light harvesting antennae for the sensitization of the fullerene emission.

The most striking difference between the two liquid crystalline fullerene derivatives concerns the fullerene core emission: in the case of **16** a very weak fluorescence ($\Phi_{em} = 3 \times 10^{-4}$) with a lifetime of 1.5 ns is observed, as expected for C_{60} derivatives. On the other hand, compound **20** exhibits outstanding luminescence properties in the near-IR region, even better than the pristine $Y_3N@C_{80}$. As reported in Table 5, the emitting excited state of **20** is: (i) slightly lower in energy compared to the unsubstituted endohedral fullerene, (ii) quite highly emitting (0.08 in deaerated solution), (iii) extremely long-lived (16 μs at 298 K, 20 times higher than $Y_3N@C_{80}$ and 13 ms at 77 K), and thus (iv) highly sensitive to the presence of dioxygen in fluid solution (vide infra). Moreover, the emission band is partly overlapping with the lowest absorption band with maximum at 700 nm (Figure 66a and b). The small energy gap indicates a slight geometrical distortion between ground and emitting excited state, while the long-lived emission would point to a forbidden deactivation process.
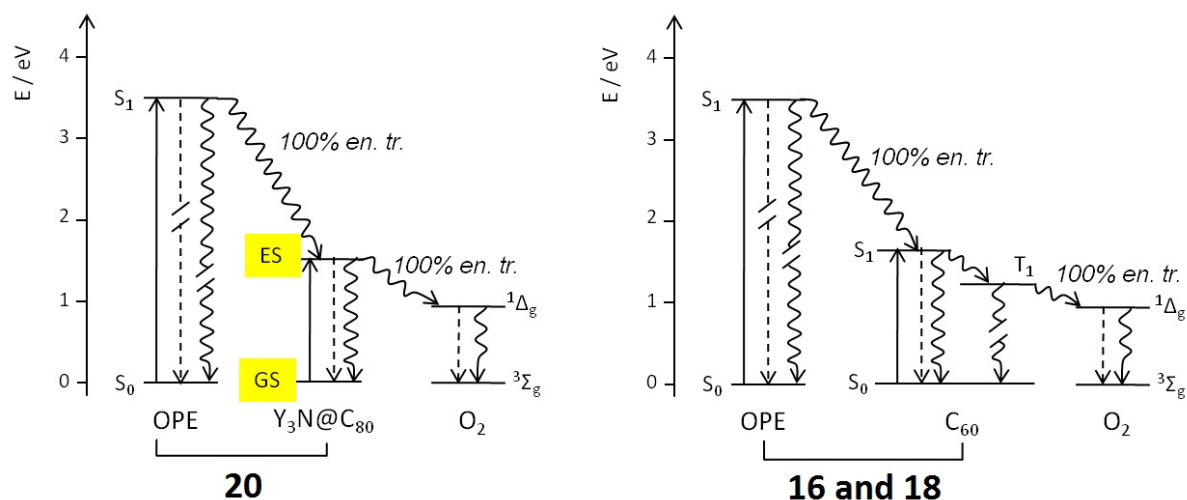
Scheme 8, Energy level diagram of compounds **16**, **18** and **20** showing the most relevant radiative (straight lines) and non-radiative (wavy lines) processes. The excited states not relevant to the present discussion have been omitted for clarity reasons.

To further explore the nature of the excited state, computational studies will be performed.

Quenching and sensitization properties of 20 with acceptor species.

The OPE-$Y_3N@C_{80}$ dyad **20** is an ideal candidate to be involved in energy and electron transfer processes because of its bright luminescence, which offers a convenient signal to monitor the quenching, and long lifetime, which allows dynamic quenching processes to take place at low concentration of the quencher. For example, dioxygen quenches efficiently this emission with a rate constant $k_q = 8 \times 10^8$ M^{-1} s^{-1}. This value is slightly lower than that of the pristine $Y_3N@C_{80}$ ($k_q = 2 \times 10^9$ M^{-1} s^{-1}), consistent with an encapsulation of the fullerene core by the OPE units of **20**. Quenching by dioxygen leads to sensitization of $^1O_2$ emission at 1270 nm with a quantum yield of 1.0 and 0.7 for **20** and $Y_3N@C_{80}$, respectively (Scheme 8). The fluorescence of compound **16** is not quenched by dioxygen because of the very short lifetime, which prevents dynamic quenching. However, **16** can sensitize $^1O_2$ by its lowest lying triplet excited state (Scheme 8) with an efficiency close to 1, as expected for C_{60} derivatives.

Quenching of the luminescence of **20** has been observed upon addition of ferrocene with $k_q = 6 \times 10^9$ M^{-1} s^{-1}, a value lower than that of $Y_3N@C_{80}$ ($k_q = 1 \times 10^{10}$ M^{-1} s^{-1}) due to the shell of OPE mesogens formed around the fullerenes of **20**. The quenching occurs by

photoinduced electron transfer from the ferrocene to **20** since the ferrocene is easy to reduce and not to oxidize and it has no excited state lower than that of **20**. Quenching of the luminescence of **20** is observed also upon addition of the electron donor poly(3-hexylthiophene) (P3HT), although a quenching constant cannot be estimated since the concentration is not known. This result is important in view of a possible application of **20** in bulk-heterojunction solar cells.

Table 6, Emission properties of **15, 16, 20** and $Y_3N@C_{80}$ in air-equilibrated or deaerated (values in brackets) toluene solution, unless otherwise noted.

T / K	298				77[a]	
	λ / nm	Φ_{em}	τ / ns	$\Phi(^1O_2)$	λ / nm	τ / ms
20	366	0.0026 (0.0026)	< 0.8 (<0.8)	-	375	-[b]
	743	0.0041 (0.080)	640 (16×10^3)	1.0	760	13
$Y_3N@C_{80}$	704	0.0025 (0.011)	200 (780)	0.7	690	12×10^{-3}
15	363	0.08	< 0.8 (< 0.8)	-	380 420	-[c]
16	363 704	0.0035 3×10^{-4}	< 0.8 1.5	1.0	382 -[b]	-[b] -

[a] In toluene:ethanol 1:1 (v/v) rigid matrix. [b] The emission intensity was too low. [c] Multiexponential decay.

II. 2. 5) Aggregation Caused Emission Shift

The emission spectra of the compounds were analysed at 77K in $CH_2Cl_2/CHCl_3$ 1:1 (v/v) matrix. The spectrum of **7** at 77K demonstrated a broad emission band at 470 nm approximately, shifted by approximately 100 nm compared to the emission spectrum recorded at 298 K in the same solvent mixture (Figure 67a). The emission intensity decay is biexponential in the nanosecond time range, suggesting the presence of more than one species (Table 5). Very similar properties are observed for **15** with a broad band at 450 nm (Figure 67b, red line). On the other hand, compound **17** shows a similar emission spectrum at 298 and 77K with a tail at lower energy in the low temperature spectrum (Figure 68).
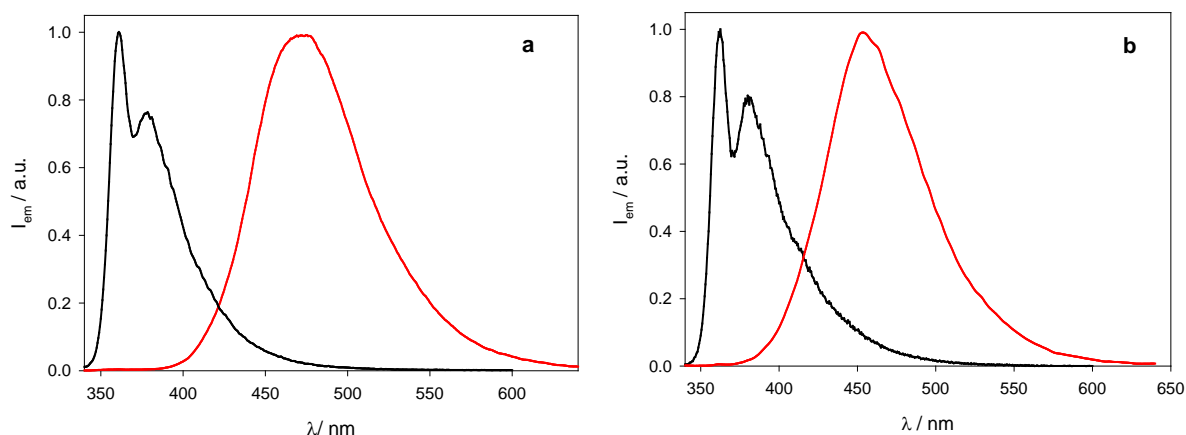
Figure 67, Normalised emission of a) **7** and b) **15** conc. approx 1 x 10^{-6} M, solvent CH$_2$Cl$_2$/CHCl$_3$ 1:1 (v/v) mixture at 298 K (black line) and 77 K (red line).

The similar behaviour observed for **7** and **15** and not for **17** suggest that the emission observed in the visible region could be due to aggregate formation via the π-π interactions of the phenyleneethynylene moieties, which is partially prevented in **17** because of the oligo(ethylene oxide) chains appended to the chromophore in a dendritic fashion and the amphiphilic nature of the molecule.
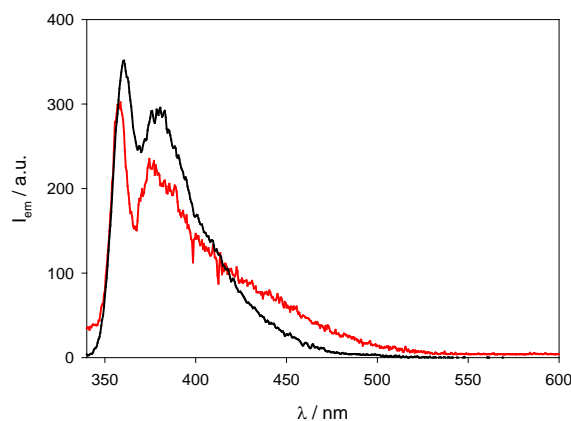

Figure 68, Normalised emission of **17** (conc. approx 1 x 10^{-6} M), solvent CH$_2$Cl$_2$/CHCl$_3$ 1:1 (v/v) mixture at 298 K (black line) and 77 K (red line).

In the case of the fullerene containing compounds, the emission intensity is too low to derive quantitative information, but the emission band has the same position and similar shape at 298 and 77 K.

In order to understand the nature of the emission obtained at 77 K, we investigated the photophysical properties of compounds **7** and **15** in different solvents and at increasing concentration to detect polarity and aggregation effects.

The investigated compounds did not demonstrate any phosphorescence during these measurements.

Effect of the concentration variations

Tests were carried out by varying the concentration in order to determine the formation of aggregates. Both the absorption and the emission spectra did not show any broadening at higher concentration in dichloromethane solution. As an example, the spectra of OPE building block **7** is depicted on Figure 69. The absorbance is proportional to the concentration, as expected by the Lambert-Beer law, in the range of $1.7 \times 10^{-7} - 8.6 \times 10^{-6}$ M.
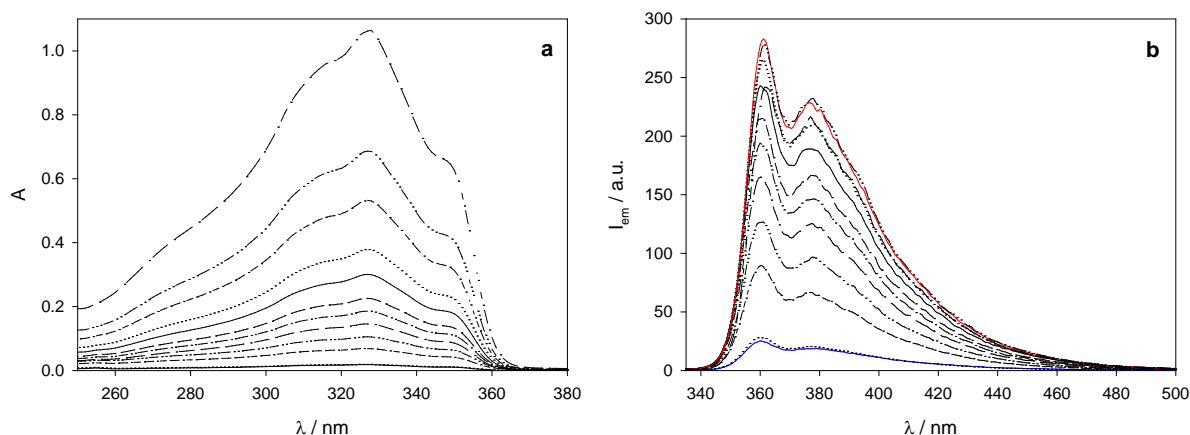

Figure 69, Absorption (a) and emission spectra (b) of **7** at different concentrations in dichloromethane solution.

Solvent dependence

Strong difference in the photophysical properties were observed in different solvents. For example, comparing dichloromethane and methanol solutions of **7** and **15**, the absorption spectra demonstrate a slight shift in the maximum and a tail due to light scattering presumably because of low solubility. Filtration of the methanol solution through a microfilter (450 nm) did not yield better results in the absorption spectrum suggesting the

presence of small aggregates. By Dynamic Light Scattering experiments, we obtained a very broad distribution of species in MeOH solution.
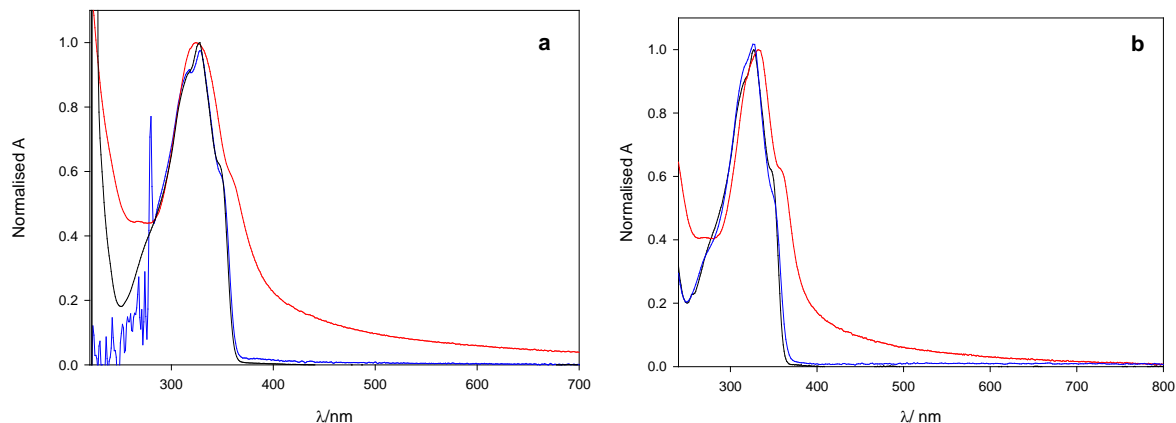

Figure 70, Normalized absorption spectra of **7** (a) and **15** (b) in methanol/dichloromethane 9:1 (v/v) (red line) dichloromethane (black line) and cyclohexane solution (blue line).

Overlapping the normalized spectra of each of the compounds demonstrates the difference in the emission properties going from apolar to polar solvents. In dichloromethane, toluene and cyclohexane the maximum emission wavelength appears at approximately 360 nm with a dramatic shift in the emission maxima in more polar solvent (eg. MeOH) to 500 nm (Figure 71). Also the fluorescence intensity decay is different from that recorded in dichloromethane solution: τ = 3.6 and 4.1 ns for **7** and **15**, respectively (Table 5).

This behaviour suggests the presence of aggregates in polar solvents and, perhaps also in cyclohexane for **15**, although to a lower extent. The emission spectrum in methanol is quite similar to that observed at 77 K (Figure 67), suggesting that also in rigid matrix aggregation occurs.
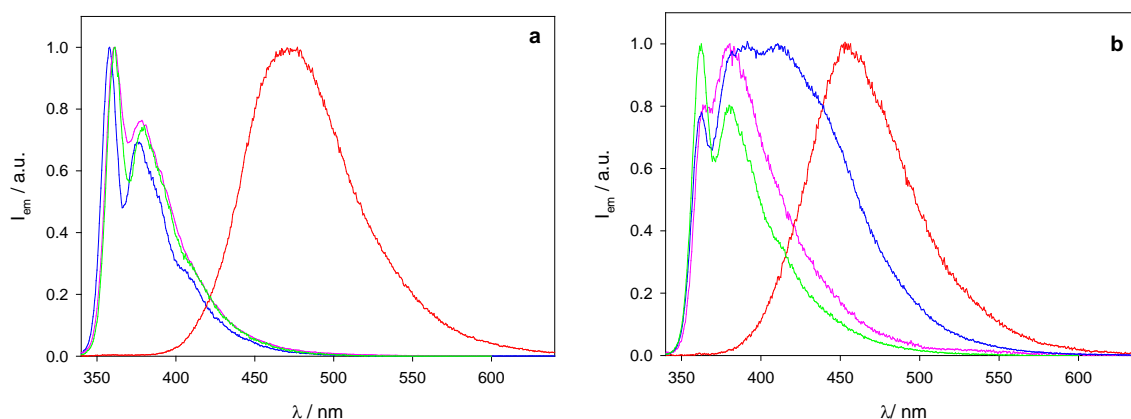
Figure 71, Normalised emission spectra of **7** (a) and **15** (b) in methanol dichloromethane 9:1 (v/v) (red line), cyclohexane (blue line), dichloromethane (pink line) and toluene (green line).

The fluorescence images of both solution and suspension of **15** were compared (Figure 72): aggregation formation and emission shift (color change) are evidenced.
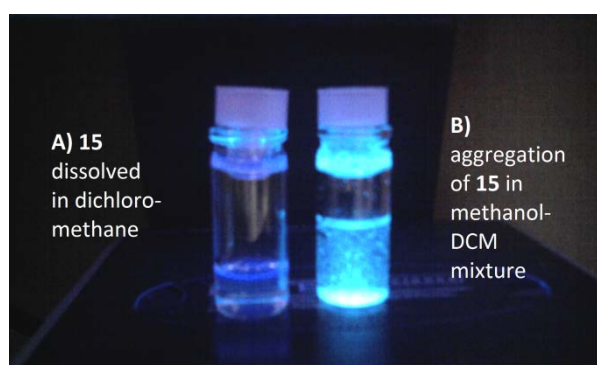

Figure 72, Solutions of **15** in dichloromethane (A), and aggregates in methanol-dichloromethane mixture (B) under 254 nm UV irradiation.

The steady-state fluorescence spectra of films made of OPE derivatives **7** and **15** is depicted on Figure 73. The solid films show further shift to lower energies relative to their aggregates in polar solvents and ca. 150 nm relative to their solutions in DCM. At high temperature the emission of the OPE chromophores is weakened. After two hours of annealing and allowing the samples to cool down to room temperature, the samples display similar luminescence intensity than before heat treatment. On the other hand, the supramolecular organization, induced by thermal annealing, causes a slight blue shift (ca. 20 and 35 nm for **7** and **15**, respectively) for both of the OPE based chromophores. The photoluminescence of the annealed films is very similar to that Lof the aggregated solutions

in DCM/MeOH 9/1 and to the results obtained at 77K, suggesting that they originate from the same emitting species with similar molecular interactions.
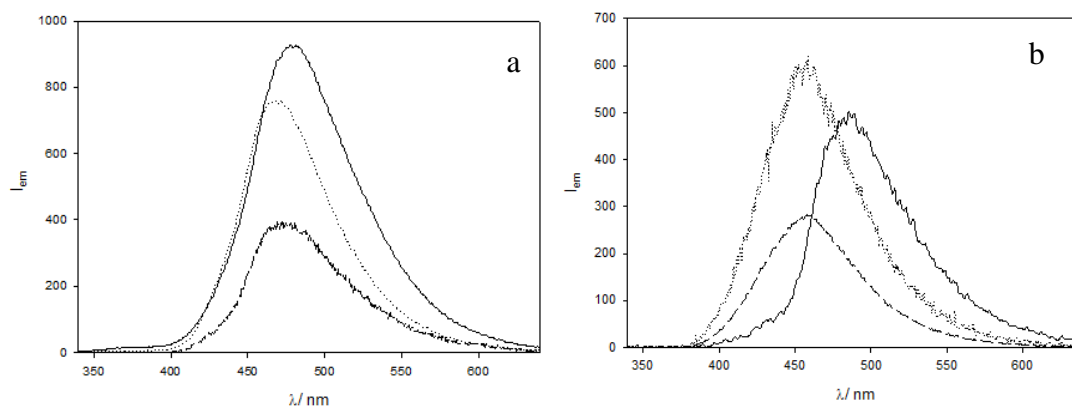

Figure 73, (a) Emission spectra of **7** on films. Solid line: at RT; dashed line: at 85 °C; dotted line: after annealing for two hours at 85 °C. (b) Emission spectra of **15** on films. Solid line: at RT; dashed line: at 100 °C; dotted line: after annealing for two hours at 100 °C.

## II. 2. 6)   Transistor fabrication and charge transfer properties

The transistors were prepared and tested in collaboration with the laboratory of Pr. Thomas Heiser, at InESS ("Institut d'Électronique du Solide et des Systèmes") in Strasbourg, France .

To understand the charge transfer properties of the materials bottom contact test transistors have been prepared. The I-V characteristics of the samples did not show the general features of conductive materials which can be the consequence of the poor quality of the films we were able to form (the results are presented in Annex III).

II. 3)   Results and discussion of OPV derivatives

II. 3. 1)   Synthesis of OPV derivatives

OPV-3 (**28**) and OPV-4 (**32**) conjugated arrays were synthesized via consecutive Wittig and Heck coupling reactions, similar to literature procedure[67]. The summary of the reaction steps leading to **28** and **32** are depicted on Scheme 9 and Scheme 10, respectively.
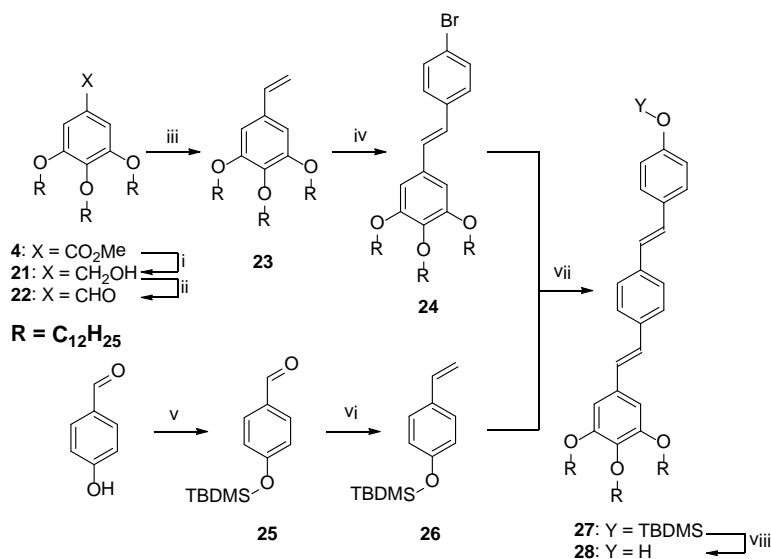
Scheme 9, Synthetic strategy of OPV3 derivative **28**. Reagents and conditions: (i) LiAlH$_4$, THF, 0°C to RT, 3h (80%); (ii) MnO$_2$, DCM, RT, 5h (87%); (iii) PPh$_3$CH$_3$Br, tBuOK, THF, 0°C to RT, 3h (98%); (iv) p-bromoiodobenzene, ToP, Pd(OAc)$_2$, Et$_3$N, 80°C, 2days (87%); (v) TBDMSCl, imidazole, DCM, RT, 2.5days (88%); (vi) PPh$_3$CH$_3$Br, tBuOK, THF, 0°C to RT, 1day (45%); (vii) ToP, Pd(OAc)$_2$, Et$_3$N, 100°C, 22h (66%); (vii) TBAF, THF, 0°C, 2.5h (89%).
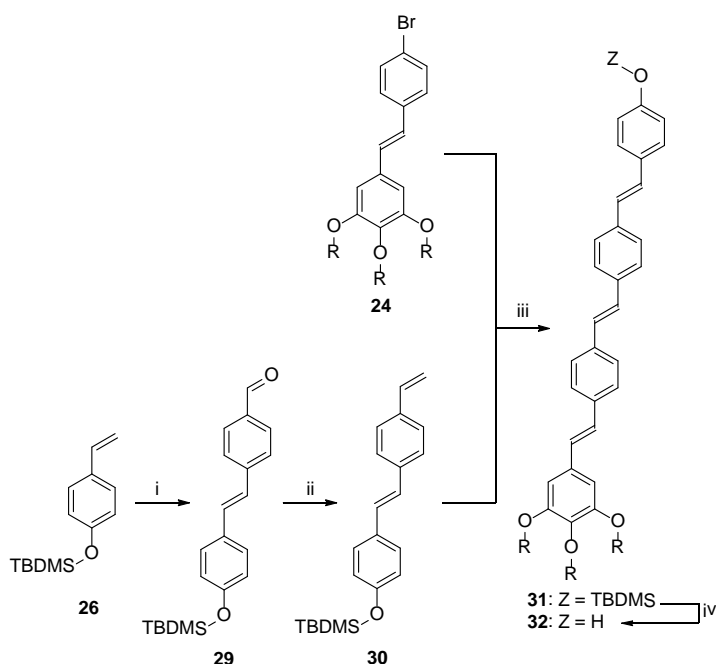
Scheme 10, Synthetic strategy of OPV4 derivative **32**. (i) p-bromobenzaldehide, ToP, Pd(OAc)$_2$, Et$_3$N 80 ^{o}C, 2days (55%); (ii) PPh$_3$CH$_3$Br, tBuOK, THF, 0°C to RT, 1day (77%); (iii) ToP, Pd(OAc)$_2$, Et$_3$N, 100°C, 15h (95%); (iv) TBAF, 0°C to RT, 4h (72%).

Methyl 3,5-dimethylbenzoate was brominated with an excess of *N*-bromosuccinimide (NBS) in CCl$_4$ to the corresponding mono- and gem-dibrominated mixtures which were then reduced with diethyl phosphite and *N,N*-diisopropylethylamine[68]

to afford the desired monobromide (**33**) in satisfactory yield and high purity. Subsequent Williamson etherification with **28** and **32** gave methyl ester **34** and **36** which were then deprotected by LiAlH$_4$ to yield the corresponding alcohols, **35** and **37**, respectively. The reaction of these alcohols with malonyl dichloride led to the malonate precursors (**38** and **40**) which were subjected to the Bingel-reaction[52] in the presence of C$_{60}$ to obtain the desired D-A dyads **40** and **41**, respectively. In the latter case, an isomeric mixture of bisadducts (**41bis**) was also obtained which was separated from the monoadduct and analysed.
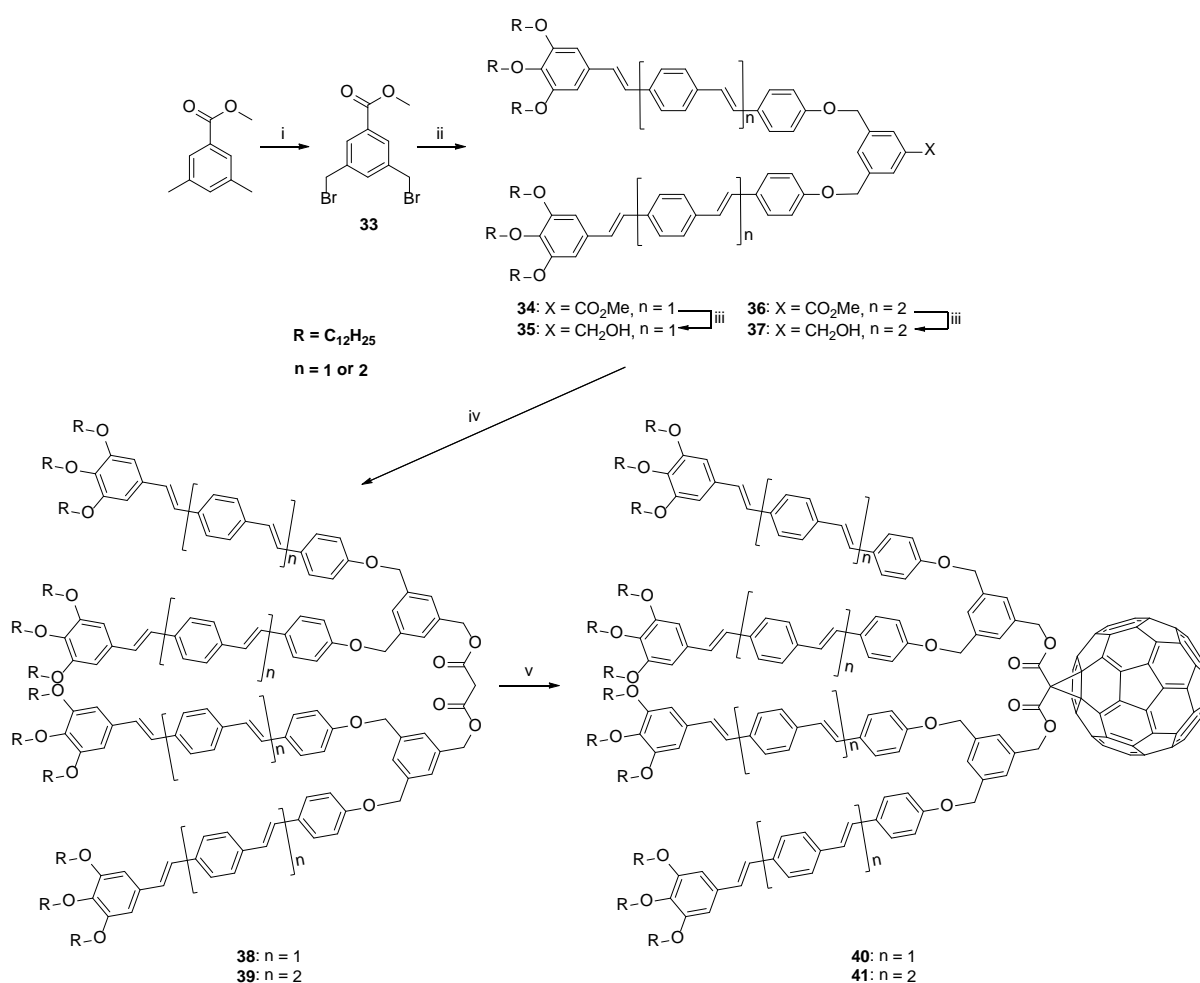
Scheme 11, OPV3 and OPV4 D-A methanofullerenes. (i) NBS, AIBN, CCl$_4$, 80 °C, 48h (39%); (ii) 26 or 30, K$_2$CO$_3$, KI, 18-crown-6, acetone, 14.5-20h (73-85%); (iii) LiAlH$_4$, THF, RT, 2.5-3h (87-91%); (iv) malonyl dichloride, DIPEA, DMAP, CH$_2$Cl$_2$, RT, 20-18.5h (75-83%);(v) C$_{60}$, DBU, I$_2$, toluene, RT, 22h (38-27%).

Although, the main products of Heck-coupling reactions are trans (E) isotropic forms of stilbene derivatives we always obtained small amount of cis (Z) isomers. It was more

significant in the case of OPV-4 derivatives, possibly due to the increasing number of available isomers. It has been already reported that cis isomers of some OPV derivatives can be turned to all-trans form by simply refluxing the compound in toluene in the presence of catalytic amount of iodine[36c]. Indeed, this process can reduce the amount of cis isomers, but we found that prolonged refluxing periods (ie. 14h) cause deterioration of the malonate related methylene protons **40**.

II. 3. 2)   NMR spectroscopic features of OPV based compounds
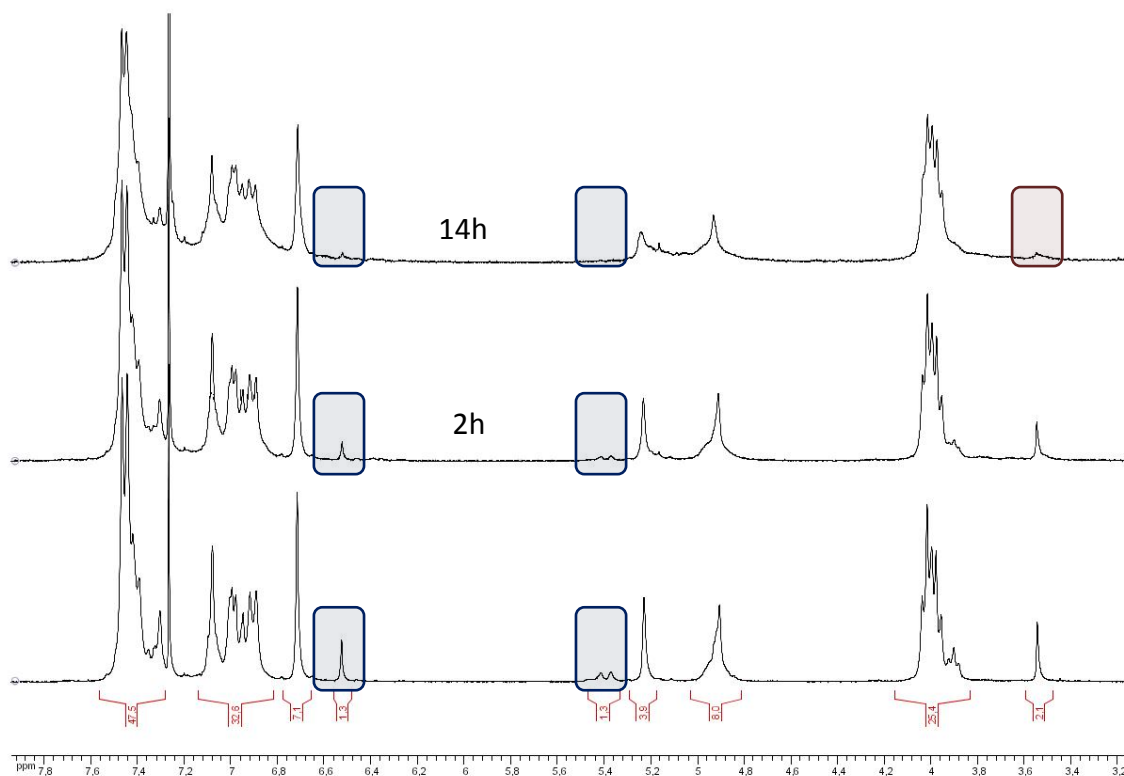
Figure 74, 1H-NMR spectra of OPV-4 based malonate **38**. Effect of refluxing time in the presence of catalytic amount of iodine on Z to E isomeric ratio.

One of the main advantages of Heck coupling reaction is its stereoselectivity with a propensity for all-E isomer formation. Despite this fact we mainly obtained isomeric mixtures, where the ratio of Z isomers increased with increasing oligomeric length. While OPV-3 oligomer and its derivatives contained only negligible amount of cis (Z) isomers their ratio in OPV-4 based compounds reached up to 18%.

136

The ¹H-NMR spectra of malonate with four OPV-4 arms **39** above 3ppm is depicted on Figure 74. Generally, the AB type coupling of vinylic protons around 7 ppm is the best indication of trans isomer formation, as we observed it for compound **24** an even for **28** with a coupling constant of 16.4 Hz. But these signals are interfered with other vinylic and aromatic protons when the number of monomer units or the complexity of the molecule increases. For that reason, the vinylic signals of **39** appear as a multiplet. On the other hand, there are two additional signals associated to cis isomers: a doublet at 5.39 ppm with a coupling constant of 12.5 Hz, characteristic of cis isomers and a singlet at 6.53 ppm (marked with blue rectangles on Figure 74). Malonate protons appear as singlets at 3.55 and 5.23 ppm, which is in good accordance with other malonate precursors.

If the compound **39** is an all-E regioisomer then the chain-end aromatic protons give only one singlet at 6.72ppm. As it was mentioned earlier, this compound was refluxed in the presence of catalytic amount of iodine for various time periods to reduce the amount of cis isomers in the mixture. The ratio of Z to E isomers was estimated by the integral ratio of the singlets at 6.53 and 6.72 ppm, those two signals represent all "chain-end" aromatic protons, therefore the one at 6.53 ppm should represent all the cis isomers. The original mixture contained approximately 18% of Z isomers, after 2h refluxing the amount of Z isomers was reduced to the half of the initial value. Further refluxing (14h) minimized the presence of Z isomers, but caused deterioration of some other signals (ie. broadened malonate peak at 3.8ppm and less sharp peaks in general were observed) as well, whose origin was uncertain. The final compound carries around the same amount of Z isomers.

II. 3. 3)   LC properties of OPV based D-A ensembles and their main building blocks

OPV derivatives (**38-41**) were studied similarly to OPE derivatives. POM observations on cooling revealed that the malonate precursors (**38, 39**) are clearly birefringent even at room temperature (Figure 75 and Figure 76). In case of **38** the optical texture changes upon cooling suggesting the occurrence of two different mesophases.
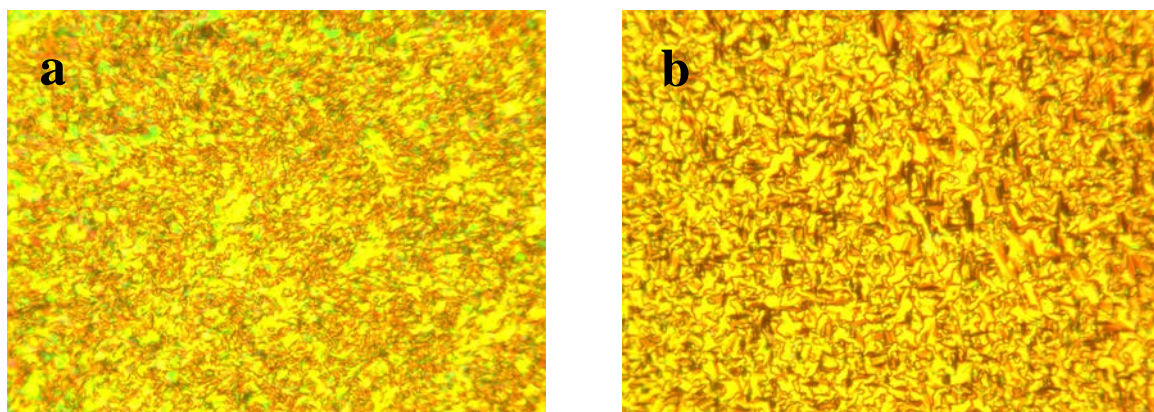
Figure 75, Polarized optical micrograph of **38**, observed on cooling from high temperature. a) At room temperature, b) at 150 °C.
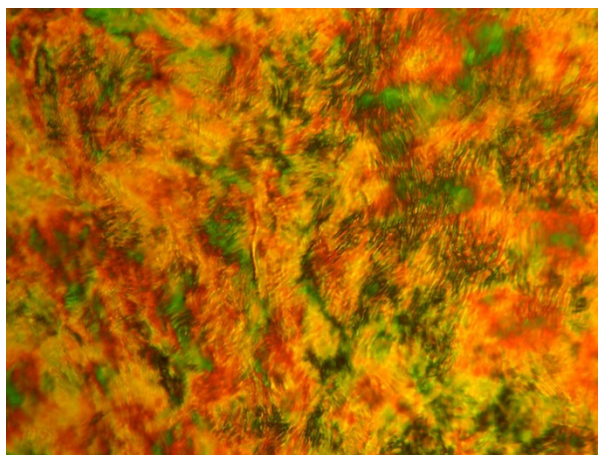

Figure 76, Polarized optical micrograph of **39**, observed on cooling from high temperature. Picture taken at room temperature.

The heating was stopped around 200-220 °C to avoid decomposition of the samples but the clearing temperature was not reached in any case. Birefringence was observed for OPV-4 based D-A system **41** (Figure 77), but its OPV-3 variation **40** did not show any characteristics of a mesophase under POM.

Figure 77, Polarized optical micrograph of **41**, observed on cooling from ca. 200 °C. Picture taken at 35 °C.

Preliminary DSC and SAXS analyses suggest that the malonate precursors (**38, 39**) organize into regular Col$_H$ phases. On the other hand the D-A dyads (**40, 41** and **41bis**) exhibited only short range columnar organization.

II. 3. 4)   Photophysical studies of OPV derivatives

II. 3. 4. 1)Steady state UV-Vis absorption spectroscopy of OPV derivatives

The absorption spectra of OPV3 and OPV4 derivatives were recorded in $1*10^{-5}$ M and $5*10^{-6}$ M dichloromethane solution, respectively. As illustrated in Figure 78 andFigure 79, the spectra of **38** and **39** contain a broad band with maxima at 371 nm and 393 nm, which are attributed to the OPV3 and OPV4 chromophores respectively, and also observed in the spectrum of their fullerene counterparts. The small shift to lower energies when moving from OPV3 to OPV4 is a general feature of π-conjugated oligomers and attributed to the increasing number of repeat units (Figure 80). The molar extinction coefficient of **39** is also

~13% higher than that of **38**. The influence of C_{60} on the spectra of D-A dyad is small, partly because it is connected to four, highly absorbing OPE chromophores. The fullerene addition does not affect significantly the shape of the spectra in the UV region. The sharp, characteristic methanofullerene monoadduct band around 425 nm is hidden in case of both of the OPV based D-A arrays by the very intense OPV centred absorption bands. Apart from that, the spectrum of **40** contains a broad band with maximum around 470 nm in the visible region, which is related to the forbidden transitions of C_{60} and characteristic feature of monoadducts, while the spectrum of **41** has a very smooth, even less structured band in the visible region (above ~450 nm). There is one more additional band in the spectrum of **41** around 280 nm which is probably related to presence of significant amount of (Z) isomers (around 18%, calculated from ^{1}H-NMR results).
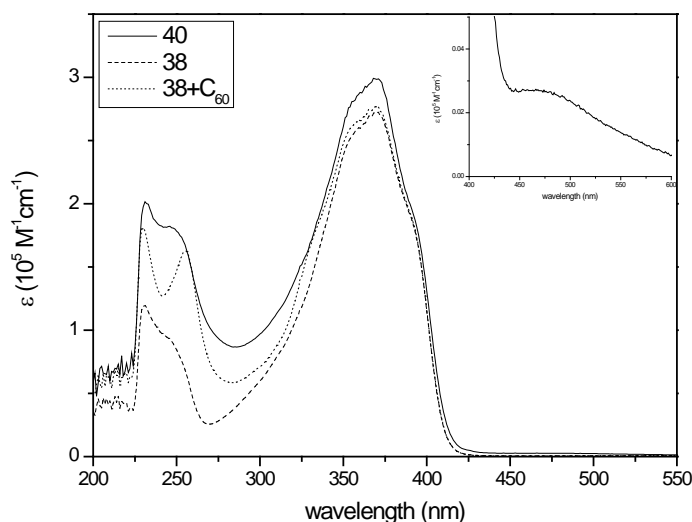

Figure 78, Absorption spectra of compound **38** and **40** and the sum of building blocks: **38** and C_{60} in dichloromethane solution. Inset: Magnification of the UV-Vis absorption spectrum of **40** above 400 nm.

A comparison with the profiles obtained upon addition of the spectra of the individual component units shows slight alterations, as depicted on Figure 78 and Figure 79. There are significant differences in the UV region, between 300 and 450 nm, with the spectrum of **40** being 10% more and **41** being 10% less intense than the sum of their components. Although, these results are within the limits of experimental error, no C_{60}

related shoulder appears around 330 nm and the UV region below 300 nm also shows less structured bands, than it would be expected from the superimposing feature of their building blocks. At first sight, these results predict ground state interaction between OPV and fullerene units. Neither cyclic voltammetry studies nor the structure of the compound (ie. several single bonds between donor and acceptor moieties should provide complete electronic isolation of those units) support this view. It has been already suggested, that rotameric equilibrium[69] within the OPV moieties, induced by the addition to the bulky fullerene moiety, is more likely to be the explanation of these differences[36c].
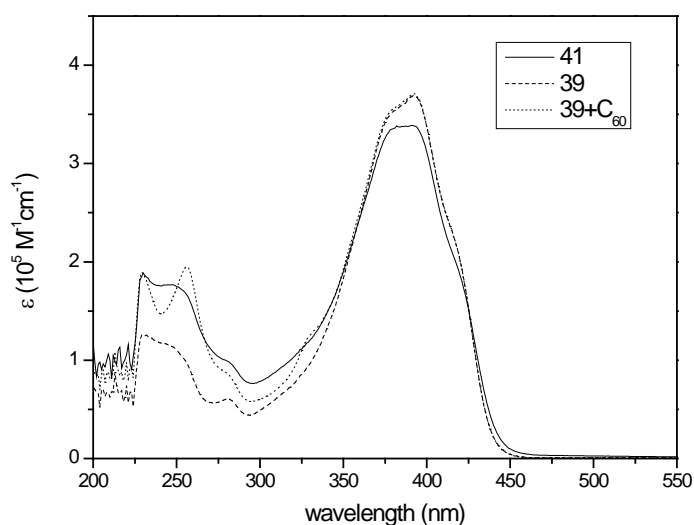

Figure 79, Absorption spectra of compound **39**, **41** and the sum of building blocks: **39** and C_{60} in dichloromethane solution.
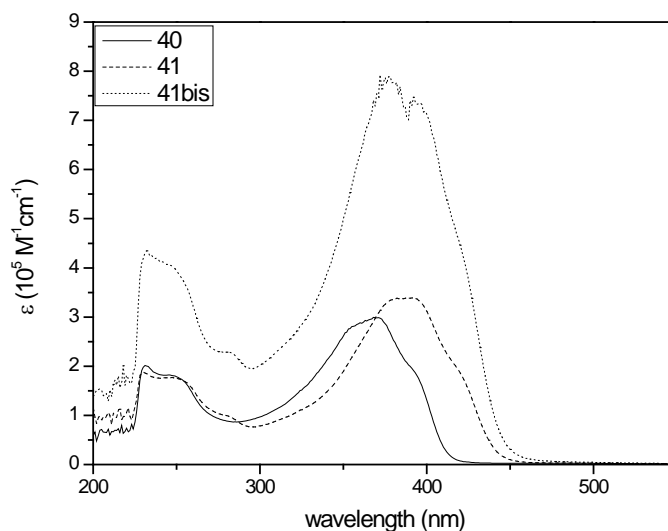
Figure 80, UV-Vis comparison of all OPV based D-A dyads: **40**, **41** and **41bis** (OPV-4 derivatives: extrapolated to $1*10^{-5}$M).

II. 3. 4. 2)Steady state fluorescence spectroscopy of OPV derivatives

The excitation of OPV-3 derivatives **38** and **40** at 370 nm and OPV-4 derivatives **39** and **41** at 390 nm, at the absorption maximum of the oligo(phenylenevinylene) unit yielded the fluorescence spectra reported in Figure 81. Each compound, demonstrated a vibrationally structured band with maximum at 432 and 462 nm. The spectra were recorded for solutions having the same absorbance at the excitation wavelength, so that they are proportional to the relative emission quantum yields.

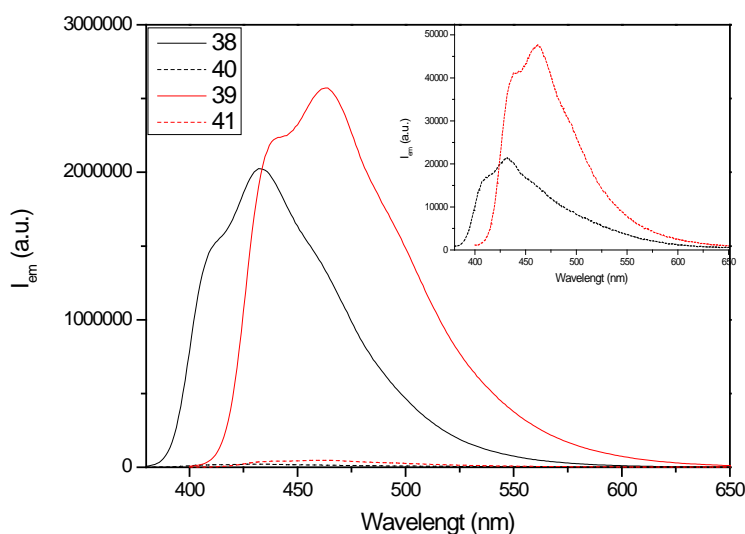**Figure 81**, Fluorescence spectra of **38**-**41** in dichloromethane. The investigated solutions have the same absorbance (0.2) (at λ_{ex} = 370 nm and 390 nm for OPV-3 and OPV-4 compounds) for the comparison of relative quantum yields. Inset: Magnified spectra of the quenched D-A dyads **39** and **41**.

II. 4)   Conclusion

In conclusion, we have synthesized different OPE-fullerene and OPV-C$_{60}$ self-assembling D-A dyads for photovoltaic applications. In the case of OPE derivatives, the effect of the chemical nature of the donor moiety (ie. lyophilic or amphiphilic) and the characteristics of the fullerene acceptor (ie. C$_{60}$ or Y$_3$N@C$_{80}$) on the properties of the dyad was investigated. All OPE-fullerene D-A ensembles were successfully synthesized, although the amphiphilic derivative decomposed within a few months. The OPE-Y$_3$N@C$_{80}$ dyad is the first synthesized TNT EMF derivative with mesomorphic properties. The NMR and UV-Vis results revealed that the compound is a [6,6] open adduct (fulleroid) which also suggests a high stability for the compound in contrast to all the other Y$_3$N@C$_{80}$ based D-A dyads that were synthesized to date.

The design of the OPE moiety followed the architecture of the typical hexacatenar (phasmidic) mesogens with a lateral carbinol group attached to the middle benzene ring. This small lateral group has a significant influence on the molecular self-assembly. It is

known that typical phasmidic compounds organize into columnar mesophases in contrast to OPE derivative **7** that gave rise to complex 2D and 3D structures. The self-organization of precursor malonate **15** led to similar 2D and 3D networks to that of **7**, although a columnar sublattice was usually preserved in both cases. These findings can help the understanding of the supramolecular organization of more complex polycatenar-like systems. All of the OPE-based D-A ensembles (**16, 18, 20**) showed liquid crystalline behavior: amphiphilic dyad **16** develops a lamellar structure typical of SmA phase, while lyophilic dyads **16** and **20** gave rise to columnar phases with core-shell cylinders. The GISAXS results of compound **16** also confirmed that molecular self-assembly can be induced in thin films. These preliminary results are very promising for the construction of electronic devices with separated donor and acceptor channels thus obtaining a nanoseparated bicontinuous network with ambipolar charge transfer properties even though the test transistors displayed poor performance.

The photophysical studies revealed that there is only minor ground state interaction between OPE donor and fullerene acceptor moieties. On the other hand, the excited state luminescence of the oligomers has been significantly quenched. The electron transfer from the OPE unit to the fullerene moiety was thermodynamically allowed, but the dominant pathway for quenching the S_1 excited state of the phenyleneethynylene and sensitization of the fullerene emission occurred via energy transfer. These materials seem promising as energy funnelling electron acceptor components or additives for polymer excitons (with morphology controlling properties) in BHJ solar cells, because the OPE units act as nearly 100% efficient light harvesting antennae to sensitize the fullerene core emission.

Not only the D-A dyads, but also their intermediates exhibited exciting photophysical features: the basic electron donating building block **7** and dyad precursor **15** formed aggregates in certain solvents and solvent mixtures which resulted in a significantly red-shifted (ca. 100 nm) photoluminescence spectrum. The compounds behavior was the same in a rigid matrix at 77K and the spin-coated thin-films presented similar shift towards lower energies which represents a useful characteristics for their application in organic optoelectronic devices.

The OPE-based liquid crystalline derivative of $Y_3N@C_{80}$ shows additional remarkable photophysical properties that are a bright (with a fluorescence quantum yield close to that of the OPE chromophore **15** in deareated toluene!) and have a long-lived OPE sensitized fullerene core emission. These luminescence properties open up numerous new applications, including near-IR luminescent sensors with time-gated detection to shut down fluorescence of the matrix or competing species.

In case of the OPV-based dyads the oligomeric length of the grafted π-conjugated oligomer donors were varied while keeping the donor to acceptor ratio constant (4 : 1). The designed dyads were successfully synthesized. Furthermore the regioisomeric mixture of OPV4 based bisadducts was also obtained and separated from the monoadduct. The birefringent POM textures and preliminary X-Ray results suggest the occurrence of mesophase for the dyads. While the quenching of the singlet excited state of the OPV moieties implies exited state communication between the donor and acceptor moieties. The detailed analysis of the SAXS results is necessary for the identification of the mesophases and to understand the supramolecular organization. Further photophysical investigation will decide between the energy and electron transfer processes. Finally, the effect of the oligomeric length (and the multiaddition in case of OPV4-C_{60} conjugate) on the photophysical and mesomorphic properties can be deduced. It is expected that these materials can find applications in photovoltaic devices either as the active layer, or as the acceptor component of a BHJ solar cell blended with an appropriate donor polymer, and similarly to the OPE-fullerene dyads, they can improve efficiencies via controlled nanomorphology.

[1] (a) M. Kimura, Y. Saito, K. Ohta, K. Hanabusa, H. Shirai and N. Kobayashi, *J. Am. Chem. Soc.*, **2002**, *124*, 5274-5275; (b) D. Felder, B. Heinrich, D. Guillon, J.-F. Nicoud and J.-F. Nierengarten, Chem.–Eur. J., **2000**, *6,* 3501-3507; (c) R. J. Bushby, I. W. Hamley, Q. Liu, O. R. Lozman and J. E. Lydon, *J. Mater. Chem.*, **2005**, *15*, 4429-4434.

[2] (a) S. Campidelli, E. Vasquez, D. Milic, M. Prato, J. Barbera, D. M. Guldi, M. Marcaccio, D. Paolucci, F. Paolucci and R. Deschenaux, *J. Mater. Chem.*, **2004**, *14*, 1266-1272; (b) E. Allard, F. Oswald, B. Donnio, D. Guillon, J. L. Delgado, F. Langa and R. Deschenaux, *Org. Lett.*, **2005**, *7*, 383-386; (c) S. Campidelli, J. Lenoble, J. Barbera, F. Paolucci, M. Marcaccio, D. Paolucci and R. Deschenaux, *Macromolecules*, **2005**, *38*, 7915-7925; (d) M. Even, B. Heinrich, D. Guillon, D. M. Guldi, M. Prato and R. Deschenaux, *Chem.–Eur. J.*, **2001**, *7*, 2595-2604; (e) Campidelli, S., Pérez, L., Rodríguez-López, J., Barberá, J., Langa, F., Deschenaux, R., *Tetrahedron*, **2006**, *62*, 2115-2122 (f) B. Dardel, D. Guillon, B. Heinrich and R. Deschenaux, *J. Mater. Chem*., **2001**, *11*, 2814-2831.

[3] (a) J. Lenoble, N. Maringa, S. Campidelli, B. Donnio, D. Guillon and R. Deschenaux, *Org. Lett.*, **2006**, *8*, 1851-1854 ; (b) Lenoble, J.; Campidelli, S.; Maringa, N.; Donnio, B.; Guillon, D.; Yevlampieva, N.; Deschenaux, R., *J. Am. Chem. Soc,.* **2007**, *129*, 9941-9952 ; (c) De la Escosura, A.; Martınez-Dıaz, M. V.; Barbera, J.; Torres, T. *J. Org. Chem.* **2008**, *73*, 1475-1480; (d) M. Ince, M. V. Martinez-Diaz, J. Barbera and T. Torres, *J. Mater. Chem.*, **2011**, *21*, 1531– 1536. (e) N. Maringa, J. Lenoble, B. Donnio, D. Guillon and R. Deschenaux, *J. Mater. Chem.*, **2008**, *18*, 1524-1534; (f) Hoang, T. N. Y.; Pociecha, D.; Salamonczyk, M.; Gorecka, E.; Deschenaux, R., *Soft Matter*, **2011**, *7*, 4948-4953.

[4] (a) H. Mamlouk, B. Heinrich, C. Bourgogne, B. Donnio, D. Guillon and D. Felder-Flesch, *J. Mater. Chem*., **2007**, *17*, 2199-2205 (b) N. Tirelli, F. Cardullo, T. Habicher, U. W. Suter and F. Diederich, *J. Chem. Soc., Perkin Trans. 2*, **2000**, 193-198; (c) Mamlouk-Chaouachi, H.; Heinrich, B.; Bourgogne, C.; Guillon, D.; Donnio, B.; Felder-Flesch, D., *J. Mater. Chem*., **2011**, *21*, 9121– 9129.

[5] (a) S. Campidelli, C. Eng, I. M. Saez, J. W. Goodby and R. Deschenaux, *Chem. Commun*., **2003**, 1520-1521; (b) S. Campidelli, T. Brandm€uller, A. Hirsch, I. M. Saez, J. W. Goodby and R. Deschenaux, *Chem. Commun*., **2006**, 4282-4284.

[6] R. Deschenaux, B. Donnio and D. Guillon, *New J. Chem.*, **2007**, *31*, 1064–1073.

[7] Chuard T. and Deschenaux R., *Helv. Chim. Acta,* **1996**, *79*, 736-741.

[8] T. Chuard, R. Deschenaux, A. Hirsch, H. Schönberger, *Chem. Commun.*, **1999**, 2103-2104.

[9] Campidelli, S.; Vazquez, E.; Milic, D.; Lenoble, J.; Atienza Castellanos, C.; Sarova, G.; Guldi, D. M.; Deschenaux, R.; Prato, M., *J. Org. Chem.,* **2006**, *71*, 7603-7610.

[10] Becquerel, E., *C. R. Acad. Sci.*, **1839**, *9*, 145-149.

[11] Steim, R., Ameri, T., Schilinsky, P., Waldauf, C., Dennler, G., Scharber, M., Brabec, C. J., *Sol. En. Mat. Sol. Cells*, **2011**, *95*, 3256-3261.

[12] C. W. Tang, *Appl. Phys. Lett.*, **1986**, *48*, 183-185.

[13] G. Yu, J. Gao, J.C. Hummelen, F. Wudl and A.J. Heeger, *Science*, **1995**, *270*, 1789-1791.

[14] B. C. Thompson, J. M. J. Fréchet, Angew. Chem. Int. Ed., 2008, 47, 58-77.

[15] B. Schmidt-Hansberg, H. Do, A. Colsmann, U. Lemmer and W. Schabel, *Eur. Phys. J. Spec. Top.*, **2009**, *166*, 49-53.

[16] Langa, F., Nierengarten, J-F. (editors), **2012**, *Fullerenes: Principles and Applications* (2nd ed.), RSC, Cambridge, Hudhomme, P, Cousseau, J., *Chapter12: Fullerene derivatives for Organic Photovoltaics*.

[17] (a) H. Hoppe and N. S. Sariciftci, *J. Mater. Chem.*, **2006**, *16*, 45-61; (b) Yang, X., Loos, J., *Macromol.*, **2007**, *40*, 1353-1361.

[18] For a review see: A. J. Heeger, *Chem. Soc. Rev.*, **2010**, *39*, 2354-2371.

[19] R. B. Ross, C. M. Cardona, D. M. Guldi, S. G. Sankaranarayanan, M. O. Reese, N. Kopidakis, J. Peet, B. Walker, G. C. Bazan, E. Van Keuren, B. C. Holloway and M. Drees, *Nat. Mater.*, **2009**, *8*, 208–212.

[20] Hummelen, J.C., B.W. Knight, F. Lepeq, F. Wudl, J. Yao, and C.L. Wilkins, *J. Org. Chem.*, **1995**, *60*, 532-538.

[21] M. Lenes , G.-J. A. H. Wetzelaer , F. B. Kooistra , S. C. Veenstra , J. C. Hummelen , P. W. M. Blom , *Adv. Mater.*, **2008**, *20*, 2116-2119.

[22] M. Lenes, S. W. Shelton, A. B. Sieval, D. F. Kronholm, J. C. Hummelen, P. W. M. Blom, *Adv. Funct. Mater.*, **2009**, *19*, 3002-3007.

[23] Honda, S.; Nogami, T.; Ohkita, H.; Benten, H.; Ito, S., *ACS Appl. Mater. Interfaces*, **2009**, *1*, 804–810.

[24] (a) Loi, M. A.; Denk, P.; Hoppe, H.; Neugebauer, H.; Winder, C.; Meissner, D.; Brabec, C.; Sariciftci, N. S.; Gouloumis, A.; Vazquez, P.; Torres, T., *J. Mater. Chem.*, **2003**, *13*, 700-704; (b) Loi, M. A., Denk, P., Hoppe, H., Neugebauer, H., Meissner, D., Winder, C., Brabec, C. J., Sariciftci, N. S., Gouloumis, A., Vazquez, P., Torres, T., *Synth. Met.*, **2003**, *137*, 1491-1492.

[25] Neugebauer, H.; Loi, M. A.; Winder, C.; Sariciftci, N. S.; Cerullo, G.; Gouloumis, A.; Vazquez, P.; Torres, T., *Sol. Energy Mater. Sol. Cells*, **2004**, *83*, 201-209.

[26] Baffeau, J.; Leroy-Lhez, S.; Anh, N.; Williams, R. M.; Hudhomme, P., *Chem.- Eur. J.*, **2008**, *14*, 4974-4992.

[27] For examples see: (a) G. Bottari, G. de La Torre, D. M. Guldi, T. Torres, *Chem. Rev.*, **2010**, *110*, 6768 – 6816; (b) Segura, J. L.; Martin, N.; Guldi, D. M., *Chem. Soc. Rev.*, **2005**, *34*, 31-47.

[28] Iwaki, M., Kumazaki, S., Yoshihara, K., Erabi, T. and Itoh, S., *J. Phys. Chem.*, **1996**, *100*, 10802-10809.

[29] Oviedo, J. J.; de la Cruz, P.; Garin, J.; Orduna, J.; Langa, F., *Tetrahedron Lett.*, **2005**, *46*, 4781-4784.

[30] (a) M. Prato, M. Maggini, C. Giacometti, G. Scorrano, G. Sandona, G. Farnia, *Tetrahedron*, **1996**, *52*, 5221 – 5234 (b) L. Perez, J. C. Garcia-Martinez, E. Diez-Barra, P. Atienzar, H. Garcia, J. Rodriguez-Lopez and F. Langa, *Chem.– Eur. J.*, **2006**, *12*, 5149-5157 (c) D.M. Guldi, C.P. Luo, T. Da Ros, S. Bosi, M. Prato, *Chem. Commun.*, **2002**, 2320 (c) D. M. Lyons , J. Mohanraj , G. Accorsi , N. Armaroli and P. D. W. Boyd, *New J. Chem.*, **2011**, *35*, 632-639.

[31] (a) K. Ohkubo, H. Kotani, J. Shao, Z. Ou, K. M. Kadish, G. Li, R. K. Pandey, M. Fujitsuka, O. Ito, H. Imahori and S. Fukuzumi, *Angew. Chem., Int. Ed.*, **2004**, *43*, 853-856 (b) S. Fukuzumi, K. Saito, K. Ohkubo, T. Khoury, Y. Kashiwagi, M. A. Absalom, S. Gadde, F. D'Souza, Y. Araki, O. Ito and M. J. Crossley, *Chem. Commun.*, **2011**, *47*, 7980-7982 (c) H. Hayashi, W. Nihashi, T. Umeyama, Y. Matano, S. Seki, Y. Shimizu and H. Imahori, *J. Am. Chem. Soc.*, **2011**, *133*, 10736–10739 (d) Imahori, H.; Umeyama, T.; Kei, K.; Yuta, T. *Chem. Commun.* **2012**, *48*, 4032-4045.

[32] Fujitsuka, M.; Ito, O.; Yamashiro, T.; Aso, Y.; Otsubo, T., *J. Phys. Chem. A,* **2000**, *104*, 4876-4881.

[33] (a) T. Gu and J. F. Nierengarten, *Tetrahedron Lett.*, **2001**, *42*, 3175–3178 (b) J. F. Nierengarten, T. Gu, G. Hadziioannou, D. Tsamouras and V. Krasnikov, *Helv. Chim. Acta*,

2004, *87*, 2948–2966 (c) J. N. Clifford, T. Gu, J.-F. Nierengarten, N. Armaroli, *Photochem. Photobiol. Sci.*, **2006**, *5*, 1165–1172 (d) T. Gu, D. Tsamouras, C. Melzer, V. Krasnikov, J.-P. Gisselbrecht, M. Gross, G. Hadziioannou and J.-F. Nierengarten, *ChemPhysChem*, **2002**, *3*, 124-127 (e) Nierengarten, J.-F.; Gu, T.; Aernouts, T.; Geens, W.; Poortmans, J.; Hadziioannou, G.; Tsamouras, D., *Appl. Phys. A: Mater. Sci. Process.*, **2004**, *79*, 47-49 (f) J. N. Clifford, A. Gegout, S. Zhang, R. Pereira de Freitas, M. Urbani, M. Holler, P. Ceroni, J.-F. Nierengarten and N. Armaroli, *Eur. J. Org. Chem.*, **2007**, 5899-5908 (g) T. M. Figueira-Duarte, Y. Rio, A. Listorti, B. Delavaux-Nicot, M. Holler, F. Marchioni, P. Ceroni, N. Armaroli and J.-F. Nierengarten, *New J. Chem.*, **2008**, *32*, 54-64.

[34] (a) A. Atienza, B. Insuasty, C. Seoane, N. Martın, J. Ramey and D. M. Guldi, *J. Mater. Chem.*, **2005**, *15*, 124-132 (b) Lembo, A.; Tagliatesta, P.; Guldi, D. M.; Wielopolski, M.; Nuccetelli, M., *J. Phys. Chem. A*, **2009**, *113*, 1779–1793 (c) Atienza, C.; Martin, N.; Wielopolski, M.; Haworth, N.; Clark, T.; Guldi, D. M., *Chem. Commun.* **2006**, 3202–3204

[35] For review see: D. M. Guldi, B. M. Illescas, C. M. Atienza, M. Wielopolski and N. Martin, *Chem. Soc. Rev.*, **2009**, *38*, 1587–1597

[36] (a) J.-F. Nierengarten, J.-F. Eckert, J.-F. Nicoud, L. Ouali, V. Krasnikov and G. Hadziioannou, *Chem. Commun.*, **1999**, 617-618. (b) N. Armaroli, F. Barigelletti, P. Ceroni, J.-F. Eckert, J.-F. Nicoud and J.-F. Nierengarten, *Chem. Commun.*, **2000**, 599-600. (c) J.-F. Eckert, J.-F. Nicoud, J.-F. Nierengarten, S.-G. Liu, L. Echegoyen, F. Barigelletti, N. Armaroli, L. Ouali, V. Krasnikov and G. Hadziioannou, *J. Am. Chem. Soc.*, **2000**, *122*, 7467-7479.

[37] (a) E. Peeters, P. A. van Hal, J. Knol, C. J. Brabec, N. S. Sariciftci, J. C. Hummelen and R. A. J. Janssen, *J. Phys. Chem. B*, **2000**, *104*, 10174-10190; (b) N. Armaroli, G. Accorsi, J.-P. Gisselbrecht, M. Gross, V. Krasnikov, D. Tsamouras, G. Hadziioannou, M. J. Gomez-Escalonilla, F. Langa, J.-F. Eckert and J.-F. Nierengarten, *J. Mater. Chem.*, **2002**, *12*, 2077-2087.

[38] (a) A. Gegout, J. L. Delgado, J.-F. Nierengarten, B. Delavaux-Nicot, A. Listorti, C. Chiorboli, A. Belbakra and N. Armaroli, *New J. Chem.*, **2009**, *33*, 2174-2182; (b) A. Gegout, J.-F. Nierengarten, B. Delavaux-Nicot, C. Duhayon, A. Saquet, A. Listorti, A. Belbakra, C. Chiorboli, N. Armaroli, *Chem. Eur. J.*, **2009**, *15*, 8825-8833.

[39] (a) G. Accorsi, N. Armaroli, J.-F. Eckert and J.-F. Nierengarten, *Tetrahedron Lett.*, **2002**, *43*, 65-68; (b) N. Armaroli, G. Accorsi, J. N. Clifford, J.-F. Eckert and J.-F. Nierengarten, *Chem. Asian J.*, **2006**, *1*, 564-574.

[40] T. M. Figueira-Duarte, A. Gegout and J.-F. Nierengarten, *Chem. Commun.*, **2007**, 109-119.

[41] L. Dunsch, S. Yang, *Small*, **2007**, *3*, 1298 –1320.

[42] J. R. Pinzon, M. E. Plonska-Brzezinska, C. M. Cardona, A. J. Athans, S. S. Gayathri, D. M. Guldi, M. A. Herranz, N. Martin, T. Torres, L. Echegoyen, *Angew. Chem. Int. Ed*., **2008**, *41*, 4173 − 4176.

[43] Feng, L.; Radhakrishnan, S. G.; Mizorogi, N.; Slanina, Z.; Nikawa, H.; Tsuchiya, T.; Akasaka, T.; Nagase, S.; Martín, N.; Guldi, D. M., *J. Am. Chem. Soc.*, **2011**, *133*, 7608-7618.

[44] Pinzón, J. R.; Gasca, D. C.; Sankaranarayanan, S. G.; Bottari, G.; Torres, T.; Guldi, D. M.; Echegoyen, L., *J. Am. Chem. Soc.*, **2009**, *131*, 7727-7734.

[45] J. R. Pinzon, C. M. Cardona, M. A. Herranz, M. E. Plonska- Brzezinska, A. Palkar, A. J. Athans, N. Martin, A. Rodriguez- Fortea, J. M. Poblet, G. Bottari, T. Torres, S. S. Gayathri, D. M. Guldi, L. Echegoyen, *Chem. Eur. J.*, **2009**, *15*, 864 − 877.

[46] Y. Hizume, K. Tashiro, R. Charvet, Y. Yamamoto, A. Saeki, S. Seki and T. Aida, *J. Am. Chem. Soc.*, **2010**, *132*, 6628–6629.

[47] C.-L. Wang, W.-B. Zhang, R. M. Van Horn, Y. Tu, X. Gong, S. Z. D. Cheng, Y. Sun, M. Tong, J. Seo, B. B. Y. Hsu and A. J. Heeger, *Adv. Mater.*, **2011**, *23*, 2951–2956.

[48] W.-S. Li, Y. Yamamoto, T. Fukushima, A. Saeki, S. Seki, S. Tagawa, H. Masunaga, S. Sasaki, M. Takata and T. Aida, *J. Am. Chem. Soc.*, **2008**, *130*, 8886-8887.

[49] S. Laschat, A. Baro, N. Steinke, F. Giesselmann, C. Hagele, G. Scalia, R. Judele, E. Kapatsina, S. Sauer, A. Schreivogel and M. Tosoni, *Angew. Chem. Int. Ed*., **2007**, *46*, 4832-4887.

[50] I. Bury, B. Heinrich, C. Bourgogne, D. Guillon, B. Donnio, *Chem. Eur. J.*, **2006**, *12*, 8396–8413.

[51] (a) Snow A. W., Foos, E. E., *Synthesis,* **2003**, *4*, 509-512. (b) Lamanna, G., L.; Kueny-Stotz, M.; Mamlouk-Chaouachi, H.; Ghobril, C.; Basly, B.; Bertin, A.; Miladi, I.; Billotey, C.; Pourroy, G.; Begin-Colin, S.; Felder-Flesch, D.; *Biomaterials*, **2011**, 32, 8562-8573.

[52] Bingel, C.; *Chem. Ber.*, **1993**, *126*, 1957 − 1959.

[53] B. Donnio, B. Heinrich, H. Allouchi, J. Kain, S. Diele, D. Guillon, D. W. Bruce, *J. Am. Chem. Soc.*, **2004**, *126*, 15258-15268.

[54] A. C. Ribeiro, B. Heinrich, C. Cruz, H. T. Nguyen, S. Diele, M. W. Schröder, D. Guillon, *Eur. Phys. J. E*, **2003**, *10*, 143-151.

[55] J. Grolik, L. Dudek, J. Eilmes, A. Eilmes, M. Gorecki, J. Frelek, B. Heinrich, B. Donnio, *Tetrahedron*, **2012**, *68*, 3875-3884.

[56] (a) H.T. Nguyen, C. Destrade, J. Malthête, *Adv. Mater.*, **1997**, *9*, 375-388. (b) D. Guillon, B. Heinrich, A. C. Ribeiro, C. Cruz, H. T. Nguyen, *Mol. Cryst. Liq. Cryst.*, **1998**, *317*, 51-64.

[57] Dubois, D.; Kadish, K. M.; Flanagan, S.; Haufler, R. E.; Chibante, L. P. F.; Wilson, L. J., *J. Am. Chem. Soc.*, **1991**, *113*, 4364-4366.

[58] Levitus, M.; Schmieder, K.; Ricks, H.; Schimizu, K. D.; Bunz, U. H. F.; Garcia-Garibay, M. A., *J. Am. Chem. Soc.*, **2001**, *123*, 4259-4265.

[59] Beeby, A.; Findlay, K.; Low, P. J.; Marder, T. B., *J. Am. Chem. Soc.*, **2002**, *124*, 8280-8284.

[60] Cardullo, F.; Seiler, P.; Isaac, L.; Nierengarten, J.-F.; Haldiman, R.-F.; Diederich, F., *Helv. Chim. Acta,* **1997**, *80*, 343-371.

[61] P. V. James, P. K. Sudeep, C. H. Suresh and K. G. Thomas, *J. Phys. Chem. A*, **2006**, *110*, 4329–4337.

[62] Sluch, M. I.; Godt, G.; Bunz, U. H. F.; Berg, M. A. *J. Am. Chem. Soc.,* **2001**, *123*, 6447-6448.

[63] A. Beeby, K. S. Findlay, P. J. Low, T. B. Marder, P. Matousek, A. W. Parker, S. R. Rutter and M. Towrie, *Chem. Commun.*, **2003**, 2406-2407.

[64] Armaroli, N.; Accorsi, G: Rio, Y.; Ceroni, P.; Vincinelli, V.; Welter, R.; Gu, T.; Saddick, M.; Holler, M.; Nierengarten, J.-F. *New J. Chem.* **2004**, *28*, 1627-1637.

[65] Ma, B.; Sun, Y.-P.   *J. Chem. Soc., Perkin Trans. 2*, **1996**, 2157-2162.

[66] Lukoyanova, O.; Cardona, C. M.; Rivera, J.; Lugo-Morales, L. Z.; Chancellor, C. J.; Olmstead, M. M.; Rodriguez-Fortea, A.; Poblet, J. M.; Balch, A. L.; Echegoyen, L., *J. Am. Chem. Soc*. **2007**, *129*, 10423-10430.

[67] (a) Buathong, S., Gehringer, L., Donnio, B., Guillon, D., *Comptes Rendus Chimie*, **2009**, *12*, 138-162; (b) Buathong, S.; Ung, D.; Daou, J.; Ulhaq-Bouillet, C.; Pourroy, G.; Guillon, D.; Ivanova, L.; Bernhardt, I.; Begin-Colin, S.; Donnio, B., *J. Phys. Chem. C*, **2009**, *113*,

12201–12212; (c) Buathong, S., *PhD Thesis*, **2007**, CNRS, IPCMS-DMO, Strasbourg; (d) Eckert, J-F., *PhD Thesis*, **2002**, CNRS, IPCMS-DMO, Strasbourg.

[68] (a) Liu, P; Chen, Y.; Deng, J.; Tu, Y., *Synthesis*, **2001**, *14*, 2078-2080; (b) Hirao, T.; Masunaga, T.; Ohshiro, Y.; Agawa, T., *J. Org. Chem.*, **1981**, *46*, 3745-3747.

[69] (a) Mazzuccato, U.; Momicchioli, F., *Chem. Rev.* **1991**, *91*, 1679-1719.

Chapter III

Fullerene-containing dendrimers: towards MRI contrast agents

This chapter summarizes our efforts to create a new generation of safe Magnetic Resonance Imaging (MRI) biomaterials based on $Gd_3N@C_{80}$. It gives a small overview of today's commercially available and next generation MRI contrast agents. While all the C_{60} based tetraethylene glycol (TEG) dendron functionalized model compounds could be easily prepared by the Bingel-Hirsch reaction, their $Gd_3N@C_{80}$ analogues showed tremendous reactivity difference towards cyclopropanation. It appeared that the malonate structure and reaction conditions play an important role in the reaction.

III. 1.   Introduction

Magnetic resonance imaging (MRI) is one of the most powerful and most studied methods in modern diagnostic medicine, because of the high quality, three dimensional images of soft tissues that can be obtained in a noninvasive manner[1]. The high resolution and great anatomical details provided by MRI are necessary for early diagnosis of many diseases and especially in oncology[2].

Paramagnetic contrast agents improve the contrast in MRI by increasing the relaxation rates of *in vivo* water protons in response to an external magnetic field. Contrast agents are evaluated on their ability to enhance the relaxation rate of the nearby water proton spins at low doses. The general theory of solvent nuclear relaxation in the presence of magnetic entities was developed by Bloembergen, Solomon and their collaborators[3]. It has been found that a number of key factors influence the proton relaxivity (Figure 1), including number of bounded solvent molecules, water exchange rate between inner (ie. solvent molecule directly coordinated to the paramagnetic ion) and outer coordination spheres (ie. second coordination sphere and bulk solvent), molecular tumbling motion on the local magnetic field disturbance and so on.
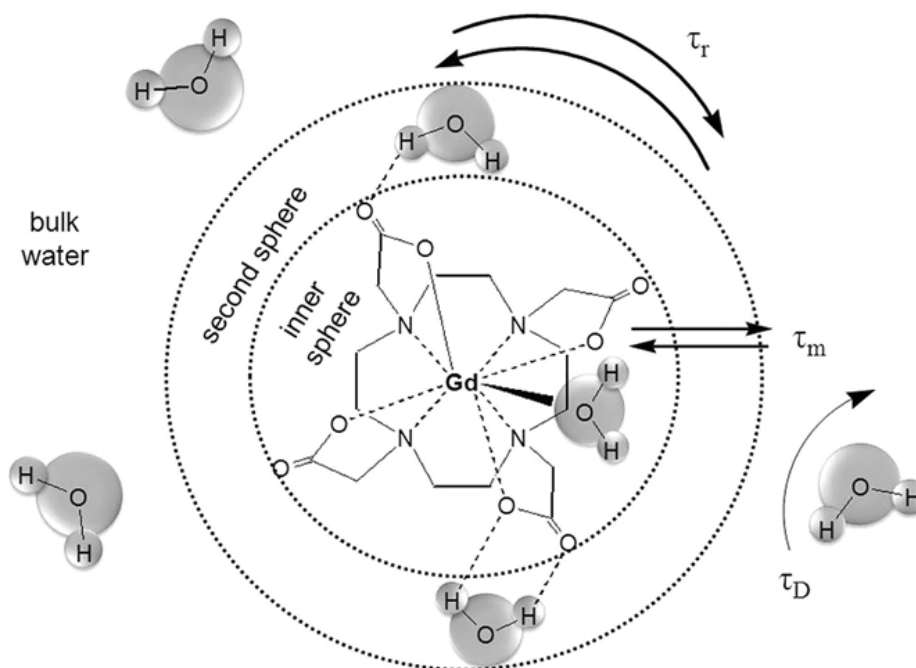
Figure 1, Different possible interactions between water molecules and a paramagnetic center.

The most commonly used MRI contrast agents are gadolinium based chelate complexes. The paramagnetic Gd (III) ion has seven unpaired electrons on the outer shell, which is the highest value observed for any atom or metal ion. Its high electron spin quantum number (s = 7/2) and large magnetic moment (m = 63μ_B^2) are directly proportional to the proton relaxation rate and the square root of the proton relaxation rate, respectively, resulting in enhancement of both longitudinal and transverse relaxation rates (Figure 2). These advantages combined with the slow electron relaxation rate, due to its high symmetry ground state, made gadolinium the primary candidate for MRI contrast agents (Figure 3)[1b,2,4].
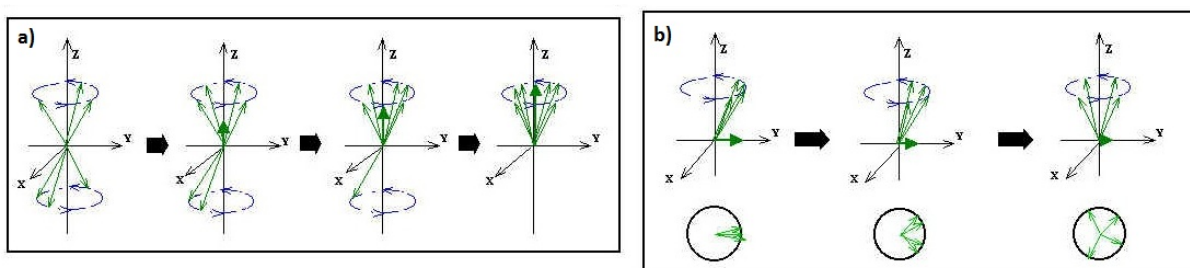
Figure 2, a) longitudinal relaxation: the z component of the magnetization return to its equilibrium position b) transverse relaxation: the xy component of the magnetization decays to zero (equilibrium).

Omniscan   Gadovist
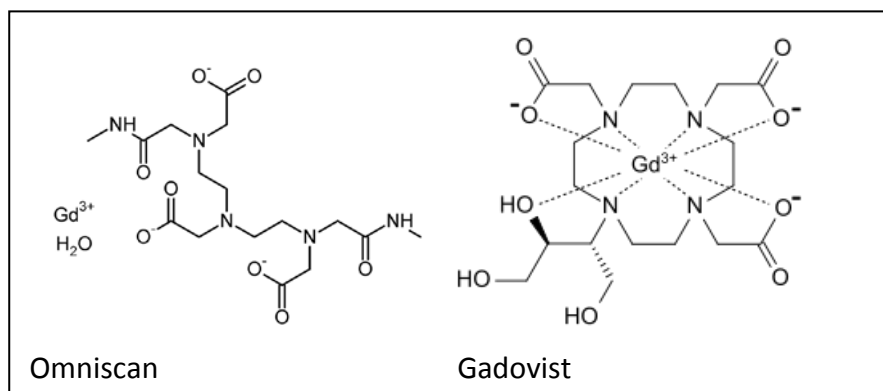
Figure 3, Two examples of the most commonly used commercial MRI contrast agents.

The main drawback of the usage of gadolinium is its toxicity. The size of Gd^{3+} is similar to Ca^{2+}, thus free gadolinium results in calcium channel blockage, inhibition of physiological processes and deactivation of metabolic enzymes together with other consequences. Moreover, life threatening diseases for patients with kidney disorders - nephrogenic system fibrosis (NSF)[5] - causing an idiopathic skin condition, fibrosis in various tissues and organs (lung, liver, muscles, heart and kidney) has been associated with the use of gadolinium

based contrast agents. Even the most stable complexes show a certain degree of dissociation that is generally denoted as the value of the stability constant, thus the exchange of Gd^{3+} ion with other body metal ions is inevitable[4a,5b,6]. For that reason, researchers started to explore alternative forms of MRI contrast agents. Another paramagnetic species, the manganese ion (Mn^{2+}) was extensively tested[7], which behaves similarly to Ca^{2+} ions and can penetrate cells via calcium channels[8]. Systems based on stabilized superparamagnetic iron oxide nanoparticles were also investigated[9]. But the replacement of gadolinium is not always required; gadofullerenes, fullerenes with Gd^{3+} ions or gadolinium cluster filled internal space, preserve all the advantages of gadolinium and while preventing any contact with the human body at the same time by encapsulating the toxic species in a carbon cage. In this way these molecules can hinder transmetallation in the body while enhancing the detection sensitivity. The exohedral derivatization of all kinds of gadonanostructures (ie. gadofullerenes and gadonanotubes (Figure 4)) can lead to controlled toxicity, enhanced biocompatibility and it can produce a biotargeting ability using antibodies and/or peptides[10].
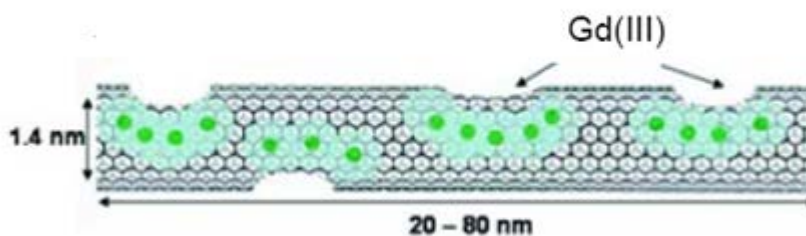

Figure 4, Schematic view of gadonanotube. The Gd^{3+} loading occurs through the side-wall defects.

III. 1. 1.   Biomedical applications of endofullerenes

Biodistribution studies of endohedral fullerenes (EMFs) were performed by *in vivo* and *in vitro* monitoring of water-soluble radioactive metallofullerene compounds. It has been found that[166] $Ho_x@C_{82}(OH)_y$ tracer - which was the first radiolabeled material - is selectively localized in the liver with slow clearance, as well as being taken up by bone without clearance[11] (Figure 5). The use of endofullerenes, as chemotherapeutics, was also

investigated. $Gd@C_{82}(OH)_{22}$ particles efficiently inhibit tumor growth and can reverse tumor resistance by enhancing the endocytosis of cisplatin via nanoparticle-mediated penetration[12]. The same hydroxylated compound showed better potential for scavenging the superoxide radical anion ($O2^-$), hydroxyl radicals ($HO^.$) and singlet oxygen than its C_{60} counterpart, presumably as a consequence of the higher electron affinity of $Gd@C_{82}$ relative to C_{60}[13].
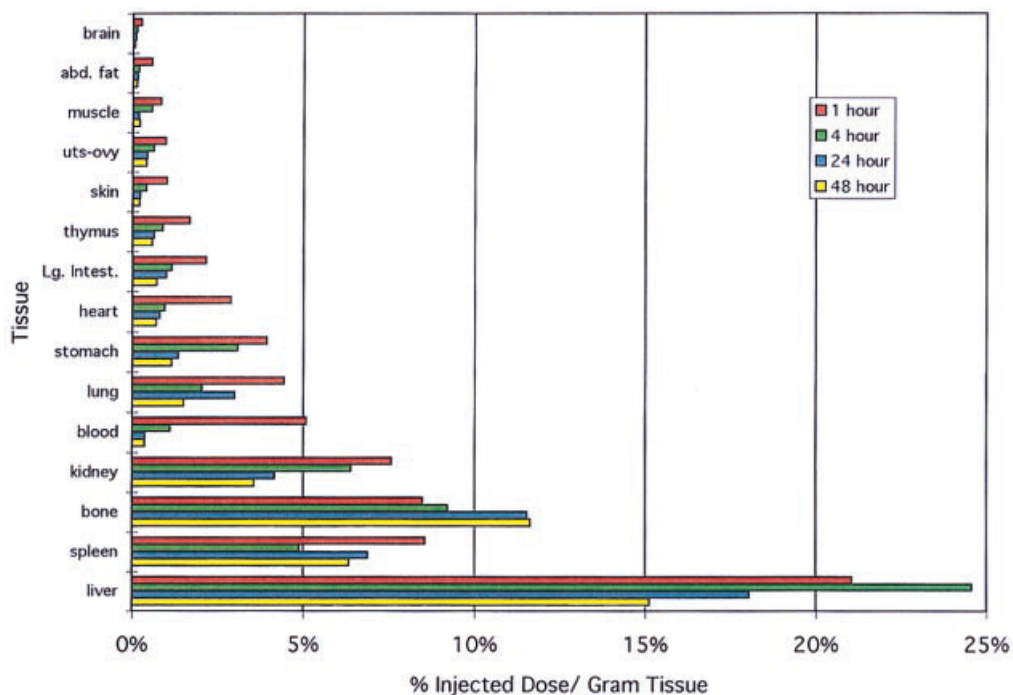

Figure 5, Biodistribution of $^{166}Ho_x@C_{82}(OH)_y$ in BALB/c mice at 1, 4, 24, and 48 h after injection. [s range: 0.32–5.69% ID per g (liver and spleen) and 0.03–1.23% ID per g (other tissue)][11].

What mostly attracted researchers' interest is undoubtedly the use of EMFs in MRI. Gadofullerenes are even less soluble in common solvents than the sparingly soluble pristine C_{60}. For MRI applications, the contrast agent has to be soluble in water thus their derivatization via chemical reaction is necessary. Numerous successful results have been already reported on $Gd@C_{60}$[14], $Gd@C_{82}$[15], $Gd_3N@C_{80}$[16] and also $Sc_xGd_{3-x}N@C_{80}$[17] (x = 1,2) derivatives. The longitudinal proton relaxivity results, together with the hydrodynamic radii of the aggregates of some of the gadonanostructures used for MRI contrast applications are summarized in Table 1. Apart from avoiding the release of gadolinium ions *in vivo*, some of those contrast agents show two orders of magnitude higher proton relaxivities than commercially-available MRI contrast agents which makes them particularly interesting

alternatives (Figure 6). It has been also speculated, that the relaxivity enhancement is related to the electronic structure of the paramagnetic metallofullerene cage and not directly to the f-orbitals of the Gd^{3+} ion, as in the case of chelated contrast agents. Simultaneous relaxation of many hydrogen bonded water molecules on the gadofullerene surface can thus take place and contribute to the contrast enhancement.

Table 1, Longitudinal proton relaxivity (r_1/mM^{-1} s^{-1}) and hydrodynamic radius (R_{hyd}/nm) of some Gd-containing MRI contrast agents[18].

Compound	r_1	R_{hyd}	Ref.
Gd–DTPA	3.9	92.8	4a
Gd@C$_{60}$[C(CO$_2$H)$_2$]$_{10}$	6.8–24.0	30–700	14
Gd@C$_{60}$(OH)$_{27}$	14.1–83.2	50–1200	14
Gd@C$_{82}$(OH)$_{40}$	81 — 92	-	15a
Gd@C$_{82}$(OH)$_{22}$	37.7–61	65–95	15e
Gd@C$_{82}$O$_6$(OH)$_{16}$(NHC$_2$H$_4$CO$_2$H)$_8$	9.1	30	15b
Gd$_3$N@C$_{80}$-Hydrochalarone	205	10–15	16c
Gd$_3$N@C$_{80}$[DiPEG(OH)$_x$]	232–460	37–96	16a,b
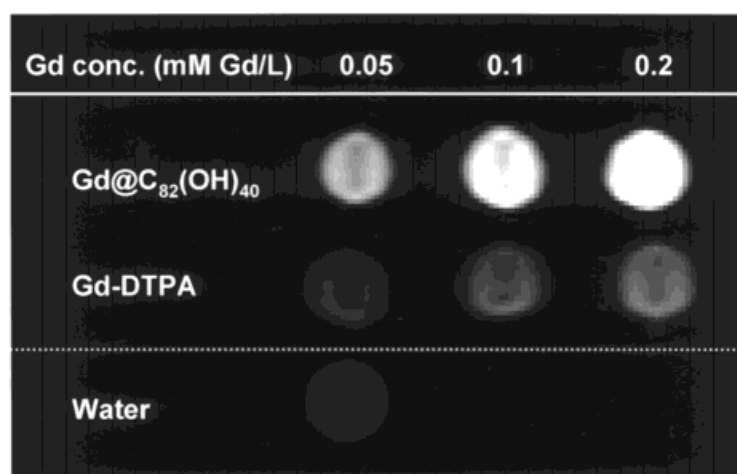
Figure 6, T1-weighted MRI of signals of Gd@C$_{82}$(OH)$_{40}$ compared to Gd-DTPA and water under the same conditions[15a]. (Approximately 20 fold higher proton relaxivity than Gd–DTPA.)

Polyhydroxylation is the easiest and most commonly applied process to transform gadofullerenes into their water-soluble forms[11,19]. It is generally performed with NaOH and hydrogen peroxide or other peroxides in the presence of a phase transfer agent (eg. tetrabutylammonium hydroxide) in an organic/inorganic solvent mixture.

Classical gadofullerenes ($Gd@C_{60}$, $Gd@C_{82}$) emerged as possible MRI contrast agents at the beginning of the last decade and showed excellent performance. In 2004 Stevenson and co-workers reported the synthesis and isolation of I_h $Gd_3N@C_{80}$, the first trimetallic nitride template (TNT) EMF with a cluster of three Gd^{3+} ions[20]. Since then, a few derivatives of these new compounds were also studied and showed even better contrast enhancement that can be only partially attributed to the higher number of gadolinium atoms inside the fullerene cage. Pegylated (ie. polyethylene glycol functionalized) and hydroxylated trimetallic nitride template (TNT) EMFs, with a general formula of $Gd_3N@C_{80}[DiPEG(OH)x]$, have been synthesized by Dorn and co-workers[16a,b] with varying the PEG chain length. Those compounds show some of the highest reported proton relaxivities to date. The authors suggested, that the high relaxivity of the TNT EMF derivatives arise from the large number of protons simultaneously relaxing in exchangeable water molecules coordinated to the hydroxyl groups which are attached to the carbon cage (Figure 7). The slow rotational correlation time and consequent enhancement of the MRI signals is caused by the long PEG chains and aggregation effects.
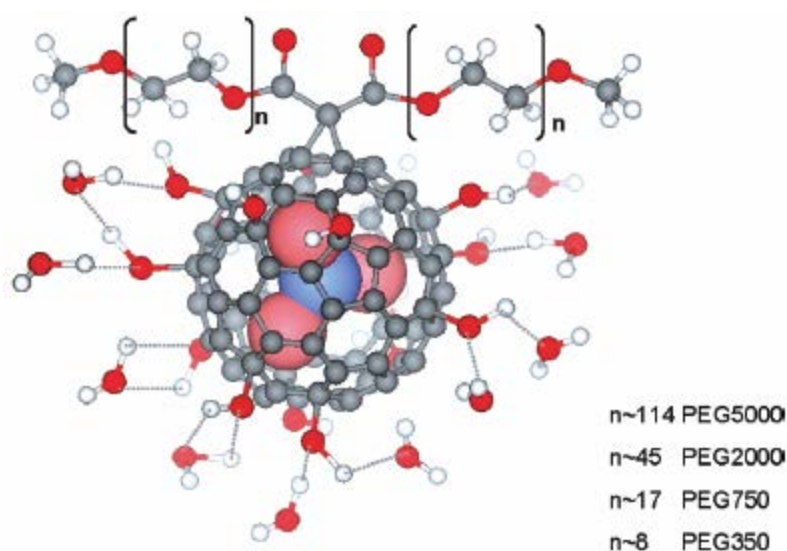

n~114 PEG5000
n~45 PEG2000
n~17 PEG750
n~8   PEG350

Figure 7, The $Gd_3N@C_{80}[DiPEG(OH)_x]$ nanoparticle with several hydrogen-bonded water molecules[16b].

Highly hydroxylated TNT fullerene derivatives aggregate in solution, a behavior partially responsible for the high proton relaxivities they induce. However, large particles may coagulate in the blood vessels causing thrombosis in patients so that several studies on their aggregation behaviours were conducted[14,21]. Results showed that the aggregation is largely environment dependent. pH and the salt concentration were found to be particularly important. Thus, varying pH values and adding salts are effective solutions to destroy the aggregations[14b,c].

On the other hand, $Gd_3N@C_{80}$ has the lowest abundance amongst TNT EMF family due to the size of the metallic nitride cluster that does not fit easily into the C_{80} carbon cage, leading to pyramidalization of the cluster[20] and an increased formation energy. Therefore, the very low production yield limits its commercial application. Due to their higher abundance, mixed metallic nitride EMFs $Sc_xGd_{3-x}N@C_{80}$ could be potential alternatives[17] even though their relaxivities are lower than that of $Gd_3N@C_{80}$. Multifunctional contrast agents for X-Ray, MRI and radiopharmaceuticals can be created when the appropriate lanthanides (eg. Lu and Gd) form a mixed cluster[22].

Our approach to functionalize $Gd_3N@C_{80}$ with the discrete but bulky water-soluble tetraethylene glycol (TEG)-based dendron could lead to aggregation-free MRI contrast agents with high proton relaxivites. The dendrons retain water in their cavities and are thus able to positively influence the water exchange rate while the simultaneous relaxation of water molecules is established by the encapsulated paramagnetic metallofullerene. Unfortunately, the structural characterization of these compounds is burdensome since paramagnetic Gd atoms preclude using standard NMR techniques. Thus, first the C_{60} based model compounds were synthesized with identical structures to the proposed $Gd_3N@C_{80}$ derivatives. Despite our efforts and successful synthesis of model compounds, only one of all of the derivatization attempts of $Gd_3N@C_{80}$ provided the desired product. Presumably, these results stem from the different reactivity and bulkiness of the TNT endofullerenes. Therefore, we found it inevitable to investigate both the role of the reaction conditions and the structure of the malonate precursor in the cyclopropanation reaction of $Gd_3N@C_{80}$ with a dendritic ligand. Proton relaxivity measurements, *in vivo* and *in vitro* relaxation studies will follow the HPLC purification of the dendritic gadofullerene **53** (Figure 8).
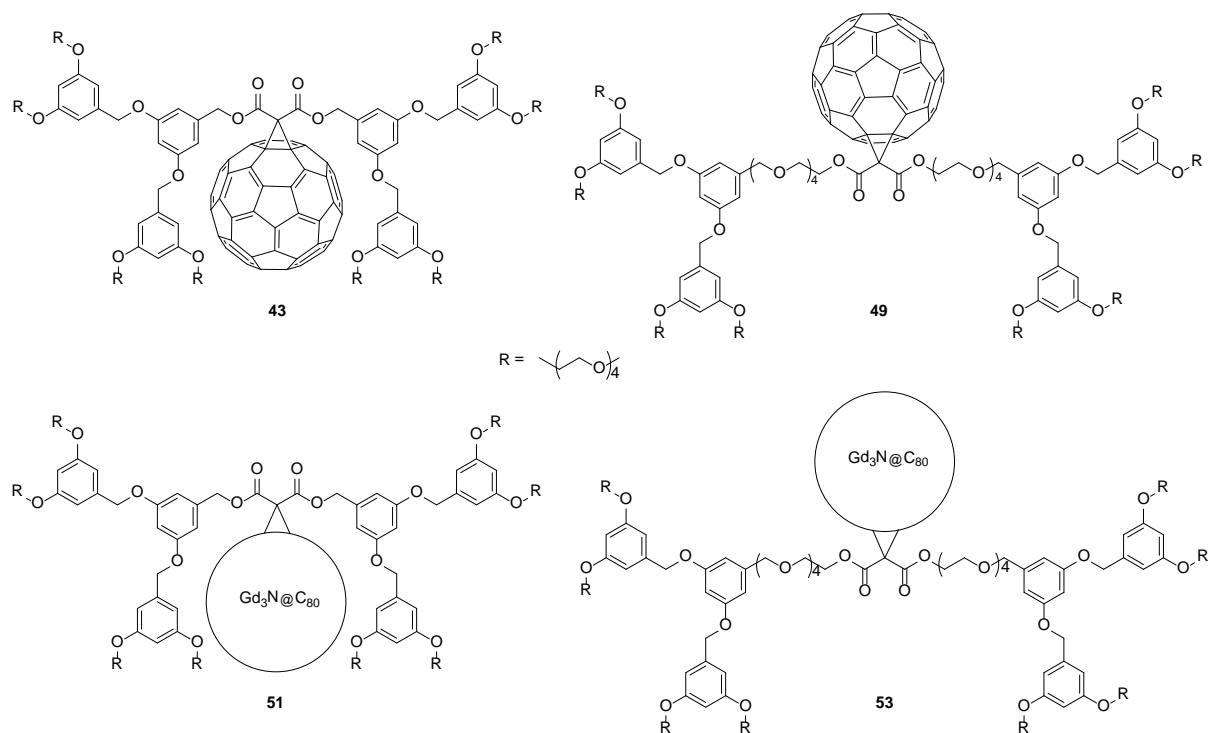
Figure 8, C_{60} based model compounds (top) and the targeted $Gd_3N@C_{80}$ containing MRI contrast enhancement agents (bottom).

## III. 2.   Results and discussion

III. 2. 1.   Synthesis

In the previous chapter we introduced second generation dendrons with tetraethylene glycol moieties **14** to induce amphiphilicity to the final D-A dyad **18**. Herein, we use the same second generation dendron to synthesize symmetric, dendritic malonates **42** by reacting the dendron with malonyl dichloride. A consecutive cyclopropanation reaction yielded a water-soluble fullerodendrimer **43**, which was the model compound for the MRI active compound **51**. The synthetic procedure is summarized in Scheme 1.
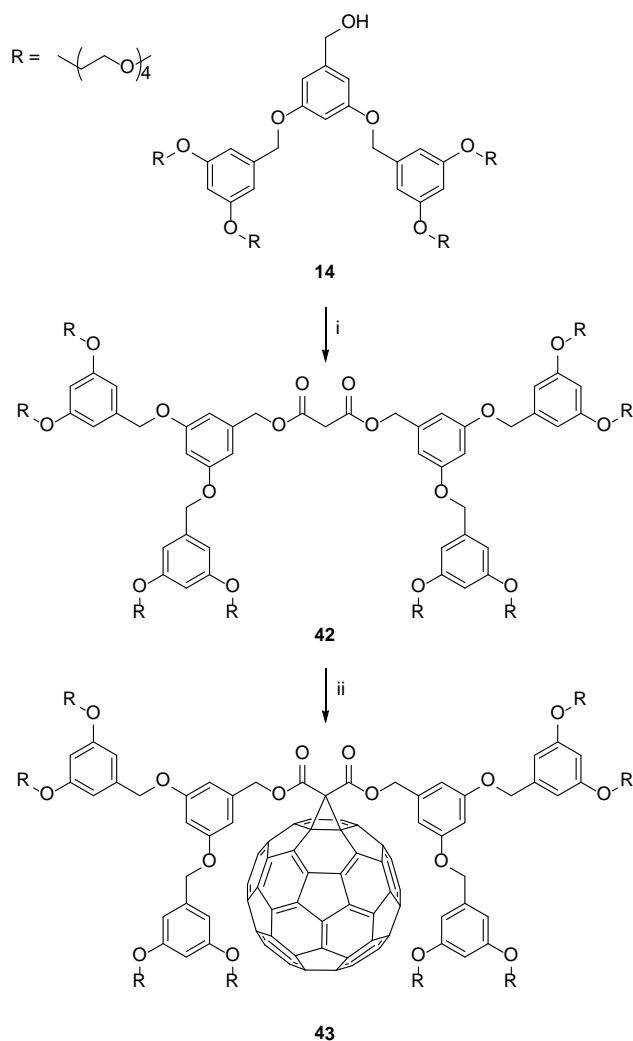
Scheme 1, Synthetic routes to methanofullerene functionalized with TEG-based dendrons. Reagents and conditions : (i) malonyl dichloride, pyridine, CH$_2$Cl$_2$, 0 °C to RT, 5.5h, 51%; (ii) C$_{60}$, 1,8-Diazabicycloundec-7-ene, I$_2$, toluene, RT, 43h, 40%.

Unfortunately, the endofullerene functionalization using malonate **42** has failed to give the desired product (vide infra). We supposed that this outcome stems from steric hindrance; therefore introduction of an oligoethyleneglycol spacer to increase the distance between the dendritic structure and the malonyl group seemed to be a logical step: heterobifunctionalized tetraethylene glycol **45,** with a good leaving group on one side and a protective group on the other side, was designated for dendron extension. The TBDMS monoprotected tetraethylene glycol **44** was obtained using a stoichiometric amount of reagents. After desymmetrization, the compound was subjected to tosylation to a furnish bifunctional TEG **45**; the two step synthesis procedure is depicted on Scheme 2.
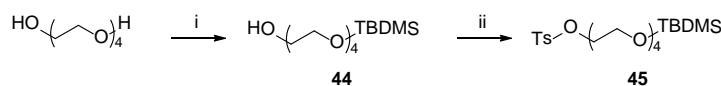
Scheme 2, Synthesis of unsymmetrical bifunctional TEG. Reagents and conditions : (i) TBDMSCl, imidazole, DMAP, CH$_2$Cl$_2$, 0 °C, 5h, 43%; (ii) Tosyl chloride, Ag$_2$O, KI, CH$_2$Cl$_2$, 40 °C, 4days, 79%.

The attachment of tosylated TEG **45** to benzyl alcohol **14** requires the use of a strong base (ie. NaH) in the presence of KI and 15-crown-5, as catalysts. Subsequent cleavage of the TBDMS group provided TEG extended dendritic alcohol **47** (Scheme 3).
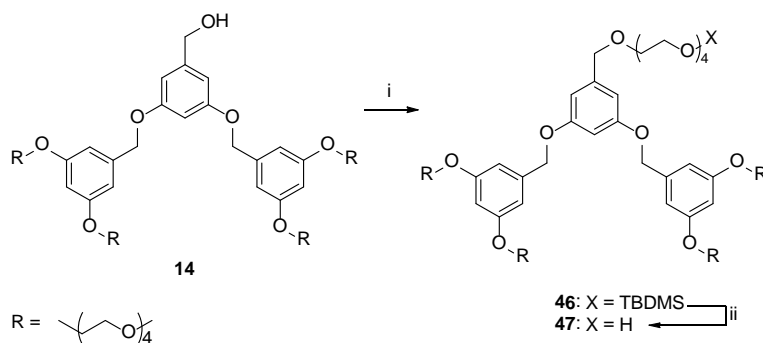
Scheme 3, Introducing TEG extension. Reagents and conditions : (i) **45**, NaH, KI, 15-crown-5, THF, RT, 9h, 75%; (ii) TBAF, THF, RT, 1.5h, 78%.

Similar to the preparation of methanofullerene **43**, malonate **48** formation was followed by a Bingel-type cyclopropanation reaction to yield a model compound **49** with elongated TEG spacers, as depicted on Scheme 4. Even in a relatively short reaction time (i.e. 5h), two compounds were obtained: a mono- and a bisadduct (or mixture of bisadduct

regioisomers), the latter being the major product. This result indicates that the monoadduct reactivity is comparable to that of pristine C_{60}.
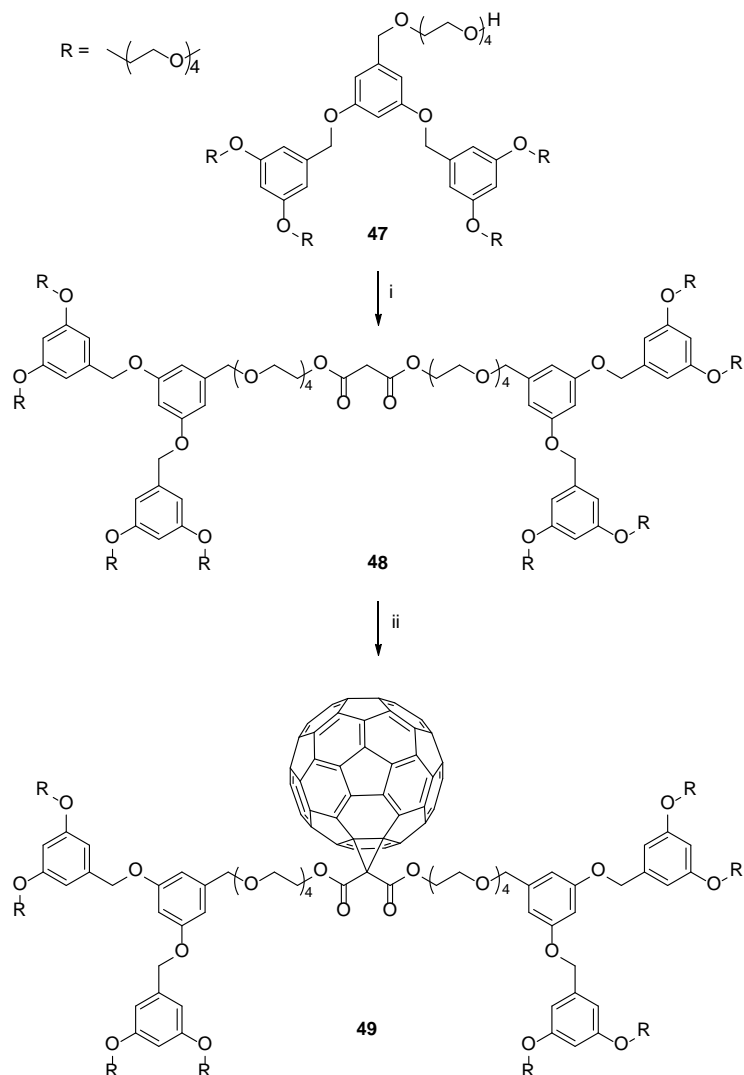
Scheme 4, Synthetic routes to methanofullerene functionalized with TEG extended TEG-based dendrons. Reagents and conditions : (i) malonyl dichloride, pyridine, CH_2Cl_2, 0 °C to RT, 6.5h, 52%; (ii) C_{60}, 1,8-Diazabicycloundec-7-ene, I_2, toluene, RT, 5h, 23%.
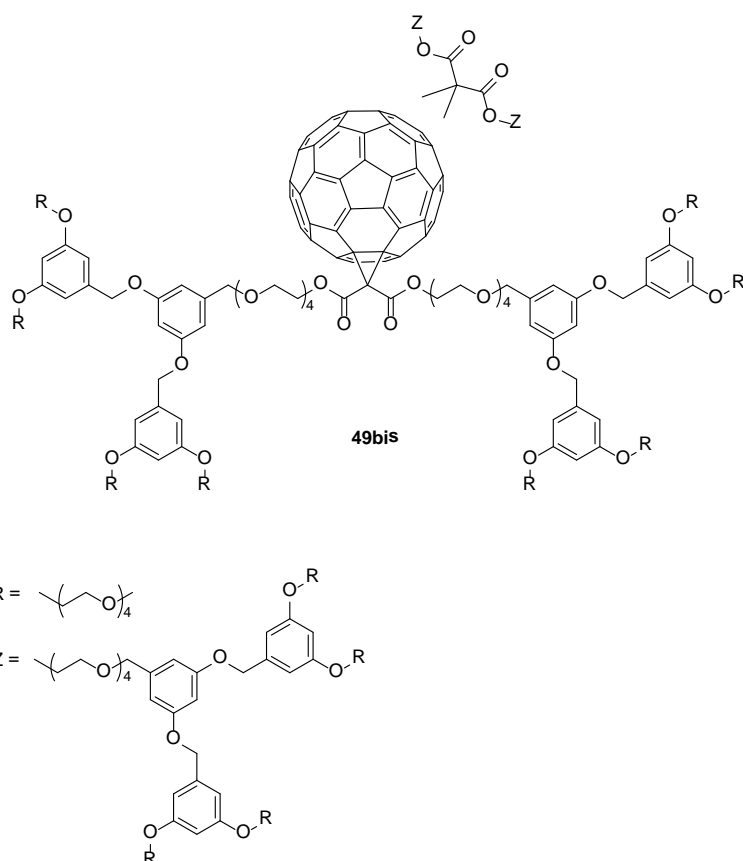
Figure 9, The structure of the bisadduct formed as major product during cyclopropanation reaction of **48** and C_{60}. (For reaction conditions, see Scheme 4)

Previously, we observed that applying the general Bingel reaction conditions for the functionalization of TNT fullerenes does not provide the desired methanofullerene (see Annex I). In one attempt, we tried to functionalize $Gd_3N@C_{80}$ using a huge excess of malonate **42**, as described by Dorn and co-workers[16a] with linear poly(ethylene glycol) malonate precursors, which are similar in nature to our malonate **48**. This method did not provide the desired TNT fullerene derivative **51**, thus we followed a two-step process. Firstly, bromomalonate **50** was prepared but the resulting mixture also contained unreacted malonate **42** and a certain amount of gem-dibrominated product, which were found to be inseparable by the employed laboratory techniques. Then, this mixture and 1,8-Diazabicyclo[5.4.0]undec-7-ene (DBU) was applied, both in large excess, for the functionalization of $Gd_3N@C_{80}$, but the required product could not be isolated at this time neither. This result was surprising, because recent studies revealed that employing a large excess (3.5-20 times higher than those used for empty cage fullerenes) of halomalonate and DBU give rise to the methano derivate of endofullerenes[23]. Hence, our conclusion was that steric hindrance between the bulky $Gd_3N@C_{80}$ and dendritic malonate **42** must be the origin

166

of unsuccessful trimetallic nitride endohedral fullerene functionalization although we cannot rule out the possibility that different reaction conditions (ie. more polar reaction media, prolonged reaction time and/or elevated temperature) favour the formation of **51** TNT dendritic gadofullerene.
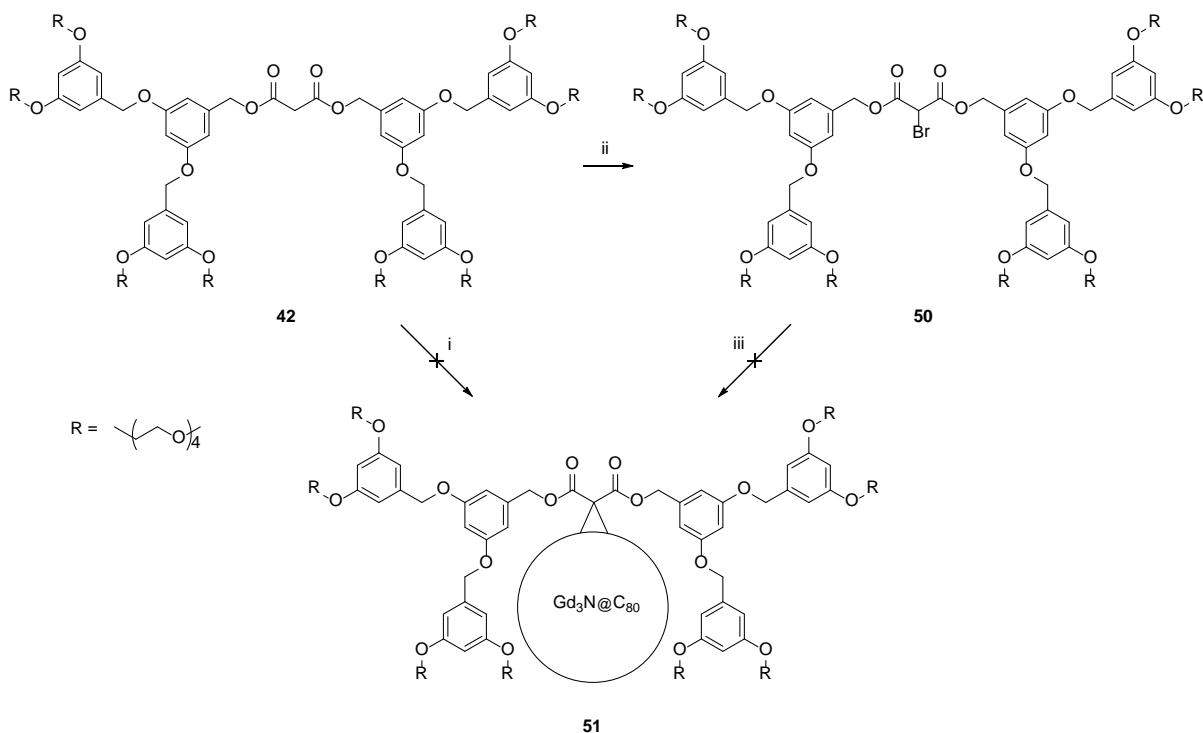
Scheme 5, Attempts to functionalize $Gd_3N@C_{80}$ with short-spacer TEG dendrons. Reagents and conditions : (i) $Gd_3N@C_{80}$, 1,8-Diazabicycloundec-7-ene, CBr_4, chlorobenzene, RT, 26.5h; (ii) N-bromosuccinimide, DMSO, RT, 2h, mixture of three different compounds; (iii) $Gd_3N@C_{80}$, 1,8-Diazabicycloundec-7-ene, chlorobenzene/DMF 12/1, RT, 1.5h.

TEG extended malonate **48** was also subjected to bromination to give bromomalonate **52**, but only the dibrominated product was obtained due to the excess of CBr_4 used for the preparation. Its conversion back to monobromomalonate or malonate **48** is possible with water in the presence of $Fe(CO)_5$[24], but we decided to use the dibrominated malonate for the cyclopropanation reaction of $Gd_3N@C_{80}$. It has been recently reported that the use of 2-bromodiethyl malonate or 2,2-dibromodiethyl malonate for the functionalization of different $M_3N@C_{80}$ (M = Sc, Lu) fullerenes in the presence of NaH produced identical results[25]. Although, the second case suggests a mechanism through a carbene intermediate which generally results in a mixture of regioisomers in contrast to the regioselective Bingel type addition-elimination mechanism.

The [2+1] cycloaddition reaction with dibromomalonate **52** yielded a water-soluble Gd$_3$N@C$_{80}$-containing dendrimer **53** (Scheme 6). The crude product was purified by preparative thin layer chromatography using CS$_2$ and acetone/methanol 95/5 mixture as eluents and gel permeation chromatography. Besides the monoadduct, a significant amount of bisadduct was also obtained. According to our knowledge, besides our compound, there was only one attempt to functionalize Gd$_3$N@C$_{80}$ with a hydrophilic dendritic ligand (polyamide in their case)[26], but the authors could not prove the successful formation of the product by means of mass spectroscopy or any other technique.
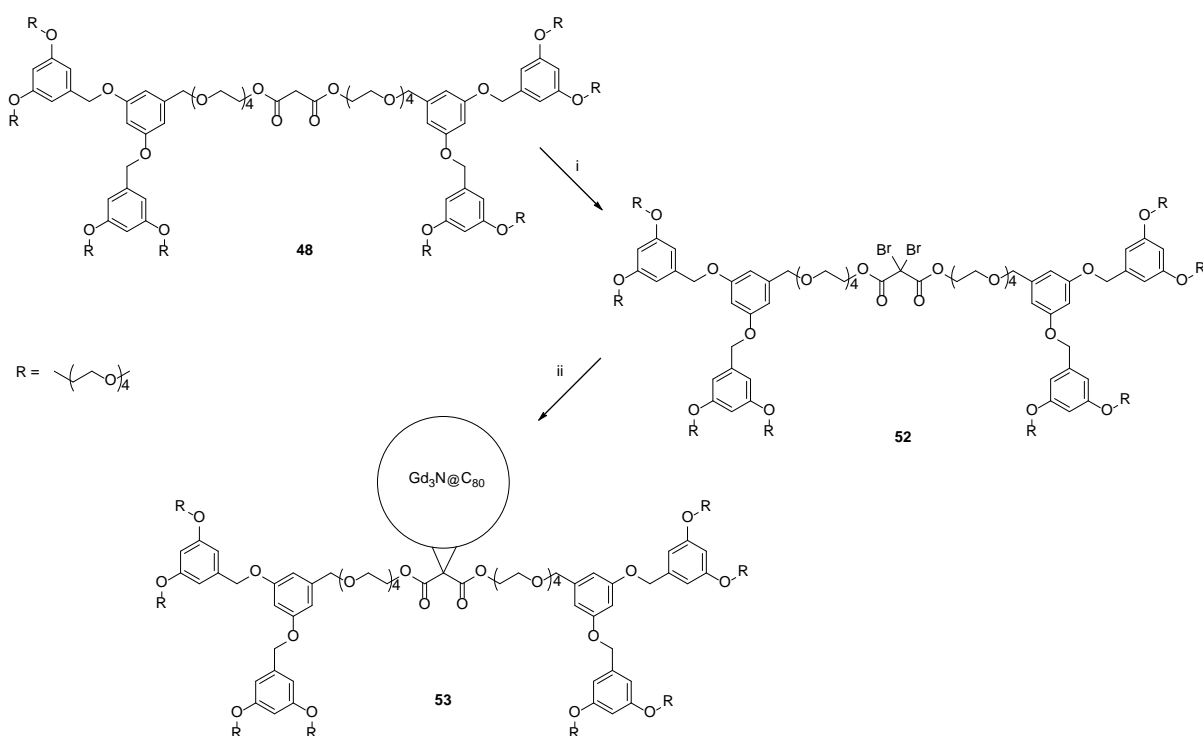
Scheme 6, Plan to functionalize Gd$_3$N@C$_{80}$ with TEG extended TEG dendrons. Reagents and conditions : (i) CBr$_4$, 1,8-Diazabicycloundec-7-ene, DCM, 0°C, 2h (ii) Gd$_3$N@C$_{80}$, DBU, chlorobenzene/CH$_3$CN 5/1, RT, 14h.

III. 2. 2. ^{13}C-NMR spectroscopic features

Surprisingly, not only mono, but bisadducts were also formed during the cyclopropanation reaction of C$_{60}$ with malonate 48, the latter being the major product. Herein, we present the ^{13}C-NMR spectra of malonate precursor **48,** model compound **49** and bismethanofullerene **49bis** (Figure 10). The spectra of the two products display two signals around 139.2 and 140.9 ppm, which are related to the aromatic protons of the Frechet type dendrons, while all the other signals, in the represented region, correlate to the sp^2 carbons of the C$_{60}$ cage

of the products (**49** and **49bis**). The most significant difference between the spectra of the products is the number of signals: **49bis** shows many more signals due to the lower symmetry caused by the second addition and the presence of different regioisomers. On the other hand, the ^{13}C-NMR spectrum of the bisadduct displays a distinct comb-like feature referring to the presence of only few regioisomers, as opposed to the broad ^{13}C-NMR signal often observed for regioisomeric mixtures of bisadducts (for example, see compound **41b** in Chapter II).
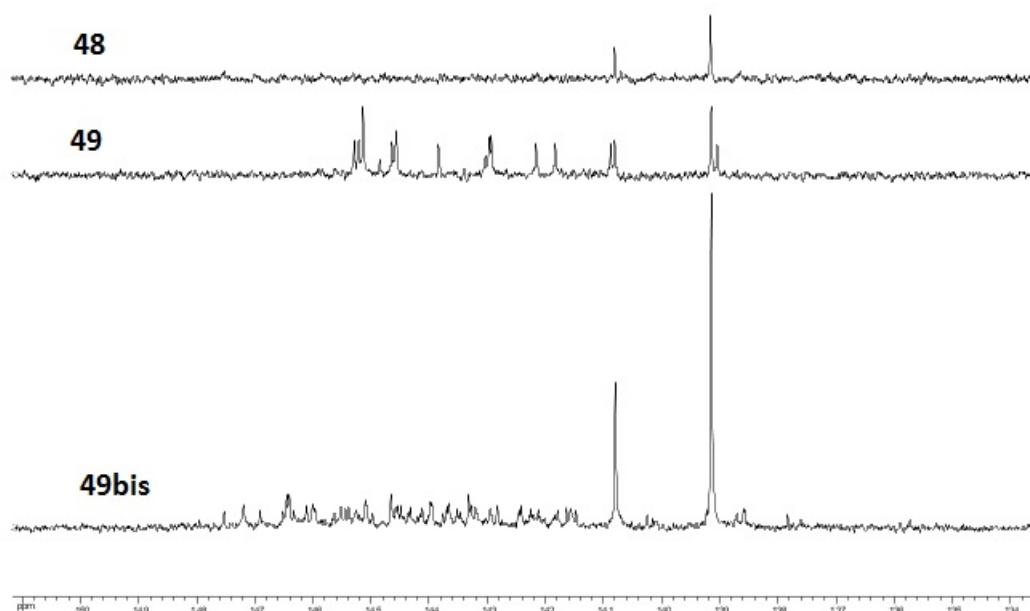
Figure 10, ^{13}C-NMR spectra of bisadduct **49bis**, model compound **49** and their precursor malonate **48** between 135 and 150 ppm. The sp2 carbons are

III. 2. 3. Mass Spectroscopy

As we mentioned earlier, the presence of paramagnetic Gd^{3+} ions excludes the analysis of $Gd_3N@C_{80}$ derivatives by NMR spectroscopy. Instead, mass spectroscopy is used for the unambiguously proof of the existence of the compound. The MALDI-ToF mass spectrum of **53** is shown in Figure 11. The peak at 4176.402 m/z corresponds to the dyad itself, while the

high intensity peaks around 1345 and 2692 m/z are fragmentations of the dendritic part and the small intensity peaks above 5000 m/z are related to multiadducts and their fragments.
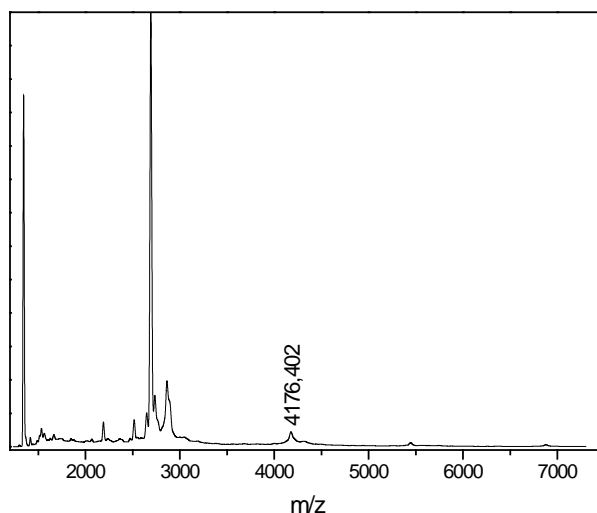

Figure 11, MALDI-ToF mass spectrum of **53**.

III. 3.   Conclusions

A TEG dendron derivatized $Gd_3N@C_{80}$ adduct was synthesized as a potentially safe, new generation MRI contrast agent. Proton relaxivitiy measurements, *in vivo* and *in vitro* relaxation studies of the water soluble compound are under investigations.

Many unsuccessful cyclopropanation attempts revealed that the type and structure of the dendritic malonates are crucial parameters to foster the reaction. The reaction of TNT gadofullerene with the bulkier dendritic malonate without an appending spacer **42,** in 20 times excess relative to the $Gd_3N@C_{80}$, failed to give the Bingel-Hirsch adduct. Moreover, the use of its bromomalonate **50,** in 10 times excess, in a more polar reaction medium did not work either. On the other hand, similar reaction conditions (with an even more polar reaction medium) employed with the brominated TEG extended dendron, which was used in 4 times excess only, resulted the exohedral derivative of $Gd_3N@C_{80}$. The reactivity of $Gd_3N@C_{80}$ towards TEG based dendritic species is dependent of the structure of the malonate. The TEG extended malonate proves to be more reactive toward the Bingel reaction than the non-extended malonate, which does not take place under any attempted

reaction conditions. Most likely, steric hindrance prevents the cycloaddition reaction if the malonate group is placed directly between two dendritic moieties making the malonate functional group inaccessible for derivatization with such a bulky species as $Gd_3N@C_{80}$.

[1] (a) R. B. Lauffer, *Chem. Rev.*, **1987**, *87*, 901-927; (b) A. E. Merbach, and E. Toth, The Chemistry of Contrast Agents in Medical Magnetic Resonance Imaging, John Wiley & Sons, **2001**.

[2] Geraldes C.F., Laurent S., *Contrast Media Mol Imaging*, **2009**, *4*, 1-23.

[3] (a) Bloembergen, N., Purcell, E.M., Pound, R.V., *Physical Review*, **1948**, *73*, 679-746; (b) N. Bloembergen, J. *Chem. Phys.,* **1957**, *27*, 572-573; (c) N. Bloembergen, *Phys. Rev.*, **1956**, *104*, 1542-1547; (d) N. Bloembergen, L. O. Morgan, *J. Chem. Phys.*, **1961**, *34*, 842-850; (e) I. Solomon, *Phys. Rev.*, **1955**, *99*, 559-565 (f) I. Solomon, N. Bloembergen, *J. Chem. Phys.*, **1956**, *25*, 261-266.

[4] (a) P. Caravan, J. Ellison, T. McMurry, R. Lauffer, *Chem. Rev.*, **1999**, *99*, 2293–2352; (b) S. Aime, M. Botta, E. Terreno, *Adv. Inorg. Chem.*, **2005**, *57*, 173–237; (c) P. Caravan, *Chem. Soc. Rev.*, **2006**, *35*, 512–523; (d) E. J. Werner, A. Datta, C. J. Jocher, K. N. Raymond, *Angew. Chem. Int. Ed,.* **2008**, *47*, 8568–8580; (e) P. Hermann, J. Kotek, V. Kubicek, I. Lukes, *Dalton Trans*., **2008**, 3027–3047.

[5] (a) Marckmann, P., Skov L., Rossen, K., Dupont, A., Damholt, M. B., Heaf, J. G., and Thomsen, H. S., *J. Am. Soc. Nephrol.*, **2006**, *17*, 2359-2362; (b) Foster, R., Rebello, R., *Clinical Rev.*, **2009**, *6*, 21-26; (c) Colletti, P.M., *Am. J. Roentgenol*, **2008**, *191*, 1-4; (d) J.-M. Idée, M. Port, C. Medina, E. Lancelot, E. Fayoux, S. Ballet, C. Corot, *Toxicology*, **2008**, *248*, 77–88; e) M. A. Sieber, T. Steger-Hartmann, P. Lengsfeld, H. Pietsch, *J. Magn. Reson. Imag.*, **2009**, *30*, 1268–1276.

[6] Rofsky N.M., Sherry A. D., Lenkinski R. E., *Radiology*, **2008**; *247*, 608–612.

[7] Kueny-Stotz, M., Garofalo, A., Felder-Flesch, D., *Eur. J. Inorg. Chem*., **2012**, 1987-2005.

[8] I. Aoki, C. Tanaka, T. Takegami, T. Ebisu, M. Umeda, M. Fukunaga, K. Fukuda, A. C. Silva, A. P. Koretsky, S. Naruse, *Magn. Reson. Med*., **2002,** *48*, 927–933.

[9] (a) Wang Y. X., *Quant. Imaging. Med. Surg.*, **2011**, *1*, 35-40 (b) B. Basly, D. Felder-Flesch, P. Perriat, C. Billotey, J. Taleb, G. Pourroy and S. Begin-Colin, *Chem. Commun.*, **2010**, *46*, 985-987.

[10] (a) Y. Mackeyev, K. B. Hartman, J. S. Ananta, A. V. Lee, L. J. Wilson, *J. Am. Chem. Soc.*, **2009**, *131*, 8342–8343; (b) Z. Ou, B. Wu, D. Xing, F. Zhou, H. Wang, Y. Tang, *Nanotechnology*, **2009**, *20*, 105102/1–105102/7; (c) A. A. Bhirde, V. Patel, J. Gavard, G. Zhang, A. A. Sousa, A.

Masedunskas, R.D. Leapman, R. Weigert, J.S. Gutkind, J.F. Rusling, *ACS Nano*, **2009**, *3*, 307–316.

[11] D. W. Cagle, S. J. Kennel, S. Mirzadeh, J. M. Alford, and L. J. Wilson, *Proc. Nat. Ac. Sci. USA*, **1999**, *96*, 5182-5187.

[12] X. J. Liang, H. Meng, Y. Z. Wang, H. Y. He, J. Meng, J. Lu, P. C. Wang, Y. L. Zhao, X. Y. Gao, B. Y. Sun, C. Y. Chen, G. M. Xing, D. W. Shen, M. M. Gottesman, Y. Wu, J. J. Yin and L. Jia, *Proc. Natl. Acad. Sci. U.S.A.*, **2010**, *107*, 7449–7454.

[13] J.-J. Yin, F. Lao, P. P. Fu, W. G. Wamer, Y. Zhao, P. C. Wang, Y. Qiu, B. Sun, G. Xing, J. Dong, X.-J. Liang, C. Chen, *Biomaterials*, **2009**, *30*, 611 – 621.

[14] (a) R. D. Bolskar, A. F. Benedetto, L. O. Husebo, R. E. Price, E. F. Jackson, S. Wallace, L. J. Wilson and J. M. Alford, *J. Am. Chem. Soc.*, **2003**, *125*, 5471–5478; (b) S. Laus, B. Sitharaman, V. Toth, R. D. Bolskar, L. Helm, S. Asokan, M. S. Wong, L. J. Wilson and A. E. Merbach, *J. Am. Chem. Soc.*, **2005**, *127*, 9368–9369; (c) S. Laus, B. Sitharaman, E. Toth, R. D. Bolskar, L. Helm, L. J. Wilson and A. E. Merbach, *J. Phys. Chem. C*, **2007**, *111*, 5633–5639.

[15] (a) M. Mikawa, H. Kato, M. Okumura, M. Narazaki, Y. Kanazawa, N. Miwa and H. Shinohara, *Bioconjugate Chem*., **2001**, *12*, 510-514; (b) C. Y. Shu, L. H. Gan, C. R. Wang, X. L. Pei and H. B. Han, *Carbon*, **2006**, *44*, 496–500; (c) H. Kato, Y. Kanazawa, M. Okumura, A. Taninaka, T. Yokawa and H. Shinohara, *J. Am. Chem. Soc.*, **2003**, *125*, 4391-4397; (d) C. Y. Shu, C. R. Wang, J. F. Zhang, H. W. Gibson, H. C. Dorn, F. D. Corwin, P. P. Fatouros and T. J. S. Dennis, *Chem. Mater*., **2008**, *20*, 2106–2109; (e) G. M. Xing, H. Yuan, R. He, X. Y. Gao, L. Jing, F. Zhao, Z. F. Chai and Y. L. Zhao, *J. Phys. Chem. B*, **2008**, *112*, 6288–6291.

[16] (a) P. P. Fatouros, F. D. Corwin, Z. J. Chen, W. C. Broaddus, J. L. Tatum, B. Kettenmann, Z. Ge, H. W. Gibson, J. L. Russ, A. P. Leonard, J. C. Duchamp and H. C. Dorn, *Radiology*, **2006**, *240*, 756–764; (b) J. F. Zhang, P. P. Fatouros, C. Y. Shu, J. Reid, L. S. Owens, T. Cai, H. W. Gibson, G. L. Long, F. D. Corwin, Z. J. Chen and H. C. Dorn, *Bioconjugate Chem*., **2010**, *21*, 610–615; (c) D. K. MacFarland, K. L. Walker, R. P. Lenk, S. R. Wilson, K. Kumar, C. L. Kepley and J. R. Garbow, *J. Med. Chem*., **2008**, *51*, 3681–3683; (d) Fillmore H.L., Shultz M.D., Henderson S.C., et.al., *Nanomedicine*. **2011**, *6*, 449-458.

[17] Zhang, E.-Y.; Shu, C.-Y.; Feng, L.; Wang, C.-R., *J. Phys. Chem. B*, **2007**, *11*, 14223-14226.

[18] X. Lu, T. Akasaka and S. Nagase, *Chem. Commun.*, **2011**, *47*, 5942–5957.

[19] For examples see : (a) S. Zhang, D. Sun, X. Li, F. Pei, S. Liu, *Fullerene Sci. Technol.*, **1997**, *5*, 1635–1643; (b) L. J. Wilson, D.W. Cagle, T. P. Thrash, S. J. Kennel, S. Mirzadeh, J. M. Alford, G. J. Ehrhardt, *Coord. Chem. Rev.*, **1999**, *190–192*, 199–207; (c) H. Kato, K. Suenaga, M. Mikawa, M. Okumura, N. Miwa, A. Yashiro, H. Fujimura, A. Mizuno, Y. Nishida, K. Kobayashi, H., Shinohara, *Chem. Phys. Lett.*, **2000**, *324*, 255–259; (d) E. B. Iezzi, F. Cromer, P. Stevenson, H. C. Dorn, *Synth. Met*., **2002**, *128*, 289–291.

[20] Stevenson, S., Phillips, J. P., Reid, J. E., Olmstead, M. M, Rath. S. P., Balch, A., *Chem. Commun*., **2004**, *24*, 2814-2815.

[21] Toth, E.; Bolskar, R. D.; Borel, A.; Gonzalez, G.; Helm, L.; Merbach, A. E.; Sitharaman, B.; Wilson, L. J., *J. Am. Chem. Soc.*, **2005**, *127*, 799-805.

[22] E. B. Iezzi, J. C. Duchamp, K. R. Fletcher, T. E. Glass, H. C. Dorn, *Nano Lett.*, **2002**, *2*, 1187 – 1190.

[23] (a) C. M. Cardona, B. Elliott, L. Echegoyen, *J. Am. Chem. Soc.*, **2006**, *128*, 6480–6485; (b) C. M. Cardona, A. Kitaygorodskiy, L. Echegoyen, *J. Am. Chem. Soc*., **2005**, *127*, 10448–10453; (c) Cardona, C. M., Drees, M., Holloway, B., WO/**2009**/067180; US/**2011**/0062390 A1.

[24] Terentev, A. B., Vasileva, T. T., Mysova, N. E. and Chakhovskaya O. V., *Russ. J. Org. Chem*., **2004**, *40*, 924-927.

[25] J. R. Pinzon, T. M. Zuo and L. Echegoyen, *Chem.–Eur. J.*, **2010**, *16*, 4864–4869.

[26] M. N. Chaur, PhD Thesis, **2009**, Clemson University, USA.

Chapter IV

Conclusion and outlook

The aim of this thesis was to develop fullerene derivatives for both materials science and biomedical applications and to show their detailed characterization and properties.

Materials for materials science

We have synthesized different π-conjugated system-fullerene dyads for photovoltaic applications, where the donor units were either oligophenylenevinylene (OPV) or oligophenyleneethynylene (OPE) derivatives and for the acceptor, C_{60} or $Y_3N@C_{80}$ were used. There was an additional requirement for our materials: liquid crystallinity. All the donor units contained a mesogenic promoter in order to induce mesomorphism in the D-A dyad and to control the morphology of the prepared film through supramolecular organization. Apart from that, we investigated the effect of the chemical nature of the donor moiety (ie. lyophilic or amphiphilic), the oligomeric length and multiaddition on the photophysical properties and on the self-assembly.

All of the D-A ensembles showed mesomorphic behavior: the amphiphilic dyad **16** develops a lamellar structure typical of a SmA phase, while lyophilic dyads **16** and **20** gave rise to columnar phases with core-shell cylinders; the mesophases of OPV based dyads (**40, 41** and **41bis**) still have to be identified. The GISAXS results of compound **16** also confirmed that molecular self-assembly can be induced in thin films.

The OPE derivatives were found to be too weak electron donating groups to induce electron transfer; on the other hand they demonstrated a unitary efficiency of energy transfer. In the case of the OPV-C_{60} dyads, further analysis is necessary to find unambiguous proof of the nature of the quenching processes (ie. energy or electron transfer).

All of the compounds are very soluble in most organic solvent and are thus easily processable (eg. by spin coating). The results on molecular organization are very promising for the construction of electronic devices with separated donor and acceptor channels thus obtaining a nanoseparated bicontinuous network with ambipolar charge transfer properties. The OPE-based dyads are probably the best used as energy funnelling electron acceptor components or as additives for polymer excitons in BHJ solar cells, because the OPE units act as nearly 100% efficient light harvesting antennae to sensitize the fullerene core.

The OPE-$Y_3N@C_{80}$ dyad is the first synthesized TNT EMF derivative with mesomorphic and photoactive properties. The NMR and UV-Vis results revealed that the

compound is a [6,6] open adduct (fulleroid) which also suggests a high stability for the compound. Its supramolecular organization is very similar to that of the C_{60} counterpart **16** and it shows remarkable photophysical properties. Similar to the OPE-C_{60} ensembles, OPE units act as 100% efficient light harvesting antennae to sensitize the fullerene core emission but – contrary to the OPE-C_{60} dyads - its luminescence is bright and long-lived. These properties, coupled with a quite strong absorption in the visible region extending up to 750 nm, open up a variety of applications, ranging from photovoltaics to near-IR luminescent sensors with time-gated detection to shut down fluorescence of the matrix or competing species.

It has been recognized, that besides structural properties of the active compounds the nanoscale organization determines the efficiency of organic solar cells. These D-A dyads can self-organize into well defined supramolecular structures, creating a high interface area between donor and acceptor components and separated charge transport channels (eg. via columnar mesophase formation) with ambipolar charge transfer properties. Thus, the next step should be the fabrication and optimization of test photovoltaic devices with the blend of the OPE-based dyads as acceptors and a suitable polymer donor (ie. with an appropriate LUMO level). This test could reveal how efficient devices can be prepared, although for commercial applications slight modification of the OPE-based dyads in order to increase their isotropization temperature by roughly 100°C might be necessary. The OPV based devices could be prepared and tested the same way or could be used as the single active layer if the photophysical studies reveal electron transfer between D and A moieties.

Another exciting topic can be the examination of the influence of C_{80} on the liquid crystalline properties. Although, the molecular self-organization of fullerene based dyads are usually governed by the mesogenic subunits due to their large number or size relative to the fullerene moiety. The steady increase of the volume ratio of the C_{80} moiety to the overall molecular volume (ie. grafting smaller mesomorphic malonate to the fullerene moiety) and synthesizing a complete family of compounds (including **20**) can help to the understand its role in the molecular self-organization.

178

Biomedical applications

A tetraethylene glycol (TEG) dendron derivatized $Gd_3N@C_{80}$ adduct was synthesized as a potentially safe, new generation MRI contrast agent. The synthesis of the compound was burdensome and required the optimization of: a) the reaction conditions b) the structure of the dendritic malonate precursor. The TEG extended dibromomalonate **52** (a tetraethylene glycol spacer has been introduced between the malonyl group and the dendron) proved to be more reactive toward the cyclopropanation reaction than the bromomalonate **50** without extension, which failed to give any identifiable products under any attempted reaction conditions. Most likely, steric hindrance prevents the cycloaddition reaction if the malonate group is placed directly between two dendritic moieties making the malonate functional group inaccessible for derivatization with such a bulky species as $Gd_3N@C_{80}$. Proton relaxivitiy measurements, in *in vivo* and *in vitro* relaxation studies of the water soluble compound are under investigation.

There is a great need for non-toxic MRI contrast enhancement agents with high proton relaxivity but, $Gd_3N@C_{80}$ can only play this role if:

- its mass production can be accomplished and its price goes down
- easily accessible, water soluble derivatives can be prepared, which probably requires the development of new synthetic strategies.

Chapter V

Experimental Part

This chapter summarizes the experimental details and synthetic procedures.

V. 1.   Materials and methods

Solvents: Tetrahydrofuran (THF), dichloromethane (DCM) and toluene were dried using dry solvent station GT S100; triethylamine (Et$_3$N) was refluxed over calcium hydroxide and chlorobenzene was stored over 4 Å molecular sieves under Ar atmosphere prior to use.

Reagents: 4-(Dimethylamino)pyridinium 4-toluenesulfonate (DPTS) was prepared by literature procedure[1] with small differences: the solvent was toluene instead of benzene and the recrystallyzation was assisted with EtOH. Ag$_2$O[2] was prepared and CuI[3] was purified according to literature processes. MnO$_2$ was activated in vacuum oven at 120 °C for 16-18h. Other reagents and solvents were purchased at reagent grade and used without further purification, unless otherwise noted. All reactions were performed in standard glassware under Ar atmosphere.

V. 2.   Experimental techniques

Column chromatography: silica gel 60 (230-400 mesh, 0.040-0.063 mm) from E. Merck. TLC was performed using precoated glass sheets with silica gel 60 F$_{254}$, Merck. Preparative TLC was performed using Merck PLC silica gel 60 F$_{254}$, 2mm (20 x 20 cm) preparative TLC plates. Gel permeation chromatography (GPC): S-X1 beads (Bio-Beads, 600-14000 daltons), using THF as eluent. NMR spectra were recorded on a Bruker AM 300 (300 MHz) instrument with solvent signal as reference (δ in ppm). MALDI-TOF mass spectra were measured on a Bruker Daltonics "FLEX" mass spectrometer at the Institut Pluridisciplinaire Hubert Curien (IPHC), Département des Sciences Analytiques (DSA) Laboratoire de Spectrométrie de Masse Bio-Organique (LSMBO), Strasbourg, France. The positive ion and linear mode or reflectron mode MALDI-MS spectra were registered depending on the molecular weight of the compound. In reflectron mode (~1-35 kDa) the obtained monoisotopic peak was compared to the calculated monoisotopic mass, in linear mode (~35-150 kDa) the isotopic distribution was not observed, therefore the calculated average mass was used for comparison. IR spectra were recorded on a Varian FTS 3000 FTIR spectrometer. UV-Vis spectra were recorded on a Hitachi U-3000 Spectrophotometer.

183

Elemental analyses were performed by the analytical service at the Institute Charles Chardon, Strasbourg**.** (Some final compounds were not characterized by elemental analysis due to the small quantity of the sample.)

Electrochemical measurements. The electrochemical experiments were carried out in argon-purged dichloromethane solution at 298 K. In the cyclic voltammetry (CV) the working electrode was a glassy carbon electrode (0.08 cm^2), the counter electrode was a Pt spiral, and a silver wire was employed as a quasi-reference electrode (AgQRE). The potentials reported are referred to SCE by measuring the AgQRE potential with respect to ferrocene ($E_{1/2}$ = 0.46 V vs SCE for Fc^+/Fc). The concentration of the compounds examined was of the order of 1 x 10^{-3} M; 0.1 M tetrabuthylammonium hexafluorophosphate ($[NBut_4]PF_6$) was added as supporting electrolyte. Cyclic voltammograms were obtained with scan rates in the range 0.05–20 V s^{-1}. The estimated experimental error on the $E_{1/2}$ value is ± 10 mV.

The electrochemical measurements were performed by the laboratory of Pr. Paola Ceroni, at the University of Bologna, Italy.

Photophysical measurements: The photophysical investigations were carried out in different solvents. UV-Vis absorption spectra were recorded with a Hitachi U-3000 spectrophotometer, using quartz cells with pathlength of 1.0 cm. The samples were placed in fluorimetric 1-cm or 0.2-cm path cuvettes. Emission spectra were obtained with a PTI A1010B instrument in Strasbourg.

More detailed photophysical measurements were performed in collaboration with the laboratory of Pr. Paola Ceroni, at the University of Bologna, Italy.

The experiments were carried out in air-equilibrated or deaerated CH_2Cl_2, CH_3OH: CH_2Cl_2 and toluene solutions at 298 K and in CH_2Cl_2:$CHCl_3$ or toluene:ethanol 1:1 (v/v) rigid matrix at 77 K. To deaerate the solution three freeze-pump-thaw cycles were performed. UV-Vis absorption spectra were recorded with a Perkin Elmer λ40 spectrophotometer, using quartz cells with pathlength of 1.0 cm. Emission spectra were obtained with a Perkin Elmer LS-50 spectrofluorimeter, equipped with a Hamamatsu R928 phototube, or an Edinburgh FLS920 spectrofluorimeter equipped with a Ge-detector for emission in the NIR spectral region.

Correction of the emission spectra for detector sensitivity in the 650-900 nm region was performed. Luminescence quantum yields were measured following the method of Demas and Crosby[4] (standard used: naphthalene in deaerated cyclohexane solution, $[Os(bpy)_3]^{2+}$ in deaerated acetonitrile solution).[5] Luminescent lifetime measurements in the range 1 ns - 1 µs were performed by an Edinburgh FLS920 spectrofluorimeter equipped with a TCC900 card for data acquisition in time-correlated single-photon counting experiments (0.5 ns time resolution) with a D_2 lamp and a LDH-P-C-405 pulsed diode laser. Luminescent lifetime measurements in the range 10 µs – 1 s were performed on a Perkin Elmer LS-50 spectrofluorimeter equipped with a pulsed Xe lamp.

To estimate the rate constant of quenching, the Stern-Volmer equation has been used:

$$\tau°/\tau = 1 + k_q \, \tau° \, [Q] \qquad\qquad (1)$$

To estimate the quantum yield of population of the luminescent singlet excited state of dioxygen ($\Phi(^1O_2)$), comparison of luminescence of $^1O_2$ at 1270 nm of the sample of interest (x) and a suitable standard (st) were recorded for isoabsorbing toluene solution at the excitation wavelength.[6] The unknown value of $\Phi(^1O_2)$ can be determined by means of eq. (2):

$$\Phi(^1O_2)_x = \Phi(^1O_2)_{st} \times (I_x/I_{st}) \qquad\qquad (2)$$

where I_x and I_{st} are the luminescence intensity at 1270 nm for the sample of interest (x) and the standard (st). In the present case, mesotetraphenylporphyrin in toluene ($\Phi(^1O_2)$ = 0.70) has been used as a standard.[7]

The estimated experimental errors are: 2 nm on the band maximum, 5% on the molar absorption coefficient and luminescence lifetime, 10% on the fluorescence quantum yield.

Polarized Optical Microscopy (POM): The optical textures of the mesophases were studied with a Leitz Orthoplan optical polarizing microscope equipped with a Mettler FP82 hotstage and a Mettler FP80 central processor.

Thermogravimetric analysis (TGA): The TGA measurements were carried out on a SDTQ 600 apparatus at scanning rate of 10 °C min^{-1}, under air.

Differential Scanning Calorimetry (DSC): The phase transition temperatures and enthalpies were determined by differential scanning calorimetry (DSC) with a TA Instruments DSC-Q1000 instrument operated at scanning rates in a range from 2 to 5 °C min^{-1}.

Small Angle X-ray Scattering (SAXS): The XRD patterns were obtained with two different experimental set-ups. In all cases, a linear monochromatic Cu-Kα1 beam (λ = 1.5405Å) was obtained using a sealed-tube generator (900W) equipped with a bent quartz monochromator. The crude sample was filled in Lindemann capillaries of 1 mm diameter and 10 μm wall1 thickness. An initial set of diffraction patterns was recorded with a curved Inel CPS 120 counter gas-filled detector linked to a data acquisition computer; periodicities up to 40 Å can be measured, and the sample temperature controlled to within ±0.01 °C from 20 to 200°C. Alternatively, patterns were also recorded on an image plate (scanned by STORM 820 from Molecular Dynamics with 50μm resolution); periodicities up to 70 Å can be measured. In each case, exposure times were varied from 1 to 24 h.

The thin films and transistors were prepared and tested in collaboration with the laboratory of Pr. Thomas Heiser, at InESS ("Institut d'Électronique du Solide et des Systèmes") in Strasbourg, France .

Film formation: Thin films were prepared by spin-coating 0.01 g/cm^3 material solutions for 20 s at 500 rpm followed by 180 s at 800 rpm, unless otherwise noted, using a spin processor Spin 150 manufactured by Semiconductor Production Systems. Analytic grade chloroform was used as solvent. Glass substrates were cut into 25 mm x 25 mm squares and washed successively with acetone, isopropanol and deionized water or they were stored in sulfochromic acid and washed with deionized water in a different process. Substrates were further cleaned by 15min ozone treatment and with compressed air. Some films were annealed in a glovebox between 50 and 85 °C, depending on the sample. The thickness of the created films was measured by a Veeco Dektak 150 profilometer.

Transistor preparation: bottom contact transistors were prepared with n-doped silicon (as gate), silicon oxide (as insulator), ITO with Au contact (as drain and source) and the tested compound (as semiconducting material). Firstly, hexamethyldisilazane (HMDS)

was deposited on the surface to make it hydrophobic and the semiconducting material was spin coated afterwards. Devices have been measured both in p-channel and n-channel biasing conditions.

V. 3. Synthetic procedure

2,5-diiodobenzyl alcohol (1b). BH_3-THF complex (55 ml, 55 mmol, 1M in THF) was added dropwise to a mixture of 2,5-diiodobenzoic acid (**1a**) (15.00 g, 40.12 mmol) dissolved in 300 ml of THF at 0°C. The reaction mixture was allowed to stir for 21 hours while warming up to RT. The excess hydride was destroyed with 150 ml of THF-water 1:1 v/v% mixture. The aqueous phase was saturated with K_2CO_3, washed with diethyl ether and the combined organic phases were dried over $MgSO_4$, filtered and the solvent was removed by evaporation. The crude product was recrystallized from water/EtOH mixture and dried in vacuum oven. White, needle-like crystals were obtained (13.61 g, 94%). ^{1}H NMR (CD_3OD): δ = 4.51 (s, 2H), 7.35 (dd, J = 8.3 Hz, 2.5 Hz, 1H), 7.57 (d, J = 8.3 Hz, 1H), 7.83 (m, 1H). ^{13}C NMR (CD_3OD) : δ = 67.30, 93.32, 94.91, 136.24, 137.48, 140.31, 145.62.

2,5-bis((trimethylsilyl)ethynyl)benzyl alcohol (2). Trimethylsilyl acetylene (1.219 g, 12.41 mmol) was added dropwise to a mixture of **1b** (1.998 g, 5.55 mmol), $PdCl_2(PPh_3)_2$ (0.124 g, 0.18 mmol), CuI (0.052 g, 0.27 mmol), DIPEA (2.0 ml, 12 mmol) and 20ml of toluene. The mixture was allowed to stir for 23 hours at RT. Evaporation gave a brown solid, which was dissolved in DCM and washed with water and brine. Drying and purification by column chromatography (eluent: DCM/toluene 3:2) gave a butter color solid (1.50 g, 90%). TLC R_f = 0.7 in DCM. ^{1}H NMR ($CDCl_3$) δ = 0.25 (s, 9H), 0.27 (s, 9H), 2.12 (t, J = 6.5 Hz, 1H), 4.79 (d, J = 6.5 Hz, 2H), 7.32 (dd, J = 8.0 Hz, 1.7 Hz, 1H), 7.39 (d, J = 8.0 Hz, 1H), 7.51-7.56 (m, 1H). ^{13}C NMR ($CDCl_3$) δ = -0.14, -0.12, 63.59, 96.46, 101.57, 102.08, 104.49, 121.04, 123.60, 130.46, 130.62, 132.21, 143.09. IR (KBr, cm^{-1}): ν = 3289 (O-H), 2158 (alkyne).

2,5-diethynylbenzyl alcohol (3). TBAF (8.8 ml, 8.8 mmol, 1M in THF) was added dropwise to the mixture of **2** (1.20 g, 3.99 mmol) in 20 ml of THF at 0°C. The reaction mixture was allowed to stir for 4h while warming up to RT. The reaction was quenched with the addition of 5 ml saturated NH_4Cl, the white precipitate was filtered off and the THF was

removed by evaporation. Then DCM was added, the organic phase was separated and washed with brine and H_2O. The organic phase was dried over $MgSO_4$, filtered and further purified by column chromatography (eluent: DCM/EtOAc 9/1). Rusty brown solid was obtained (0.57 g, 92%). TLC R_f = 0.7 in DCM/EtOAc 9/1. ^1H NMR (CDCl$_3$) δ = 2.04 (t, J = 6.4 Hz, 1H - OH), 3.18 (s, 1H), 3.43 (s, 1H), 4.83 (d, J = 5.8 Hz, 2H), 7.38 (dd, J = 7.8 Hz, 1.5 Hz, 1H), 7.46 (d, J = 7.9 Hz, 1H), 7.61 (s, 1H). ^{13}C NMR (CDCl$_3$) δ = 63.28, 79.14, 80.68, 83.02, 83.71, 120.50, 122.97, 130.70, 130.90, 132.70, 143.35. Calculated: C 84.59 %, H 5.16 %; Found: C 84.19 %, H 5.19 %.

Methyl 3,4,5-tris(dodecyloxy)benzoate (4). 1-bromododecane (125.6 g, 503.9 mmol) was added dropwise to a mixture of methyl 3,4,5-trihydroxybenzoate (30.06 g, 163.24 mmol), KI (13.52 g, 81.45 mmol), K_2CO_3 (112.6 g, 814.7 mmol) and 18-crown-6 (3.17 g, 12.0 mmol) in 450 ml of acetone. The mixture was refluxed at 60°C for 24h and then filtered on celite, which was washed thoroughly with DCM. The solution was washed with H_2O and twice with brine and dried over $MgSO_4$. Filtration and evaporation followed by flash chromatography with cyclohexane/DCM (8/2, v/v%) gave a white solid which was further purified by recrystallization from EtOH (and a few droplets of DCM) to remove the crown ether residues. White solid was obtained (107.87 g, 96%). TLC R_f = 0.9 in toluene/DCM 4/1. ^1H NMR (CDCl$_3$) δ = 0.89 (t, J = 6.7 Hz, 9H), 1.20-1.55 (m, 54H), 1.68-1.90 (m, 6H), 3.89 (s, 3H), 4.01 (t, J = 6.5 Hz, 4H), 4.02 (t, J = 6.5 Hz, 2H), 7.26 (s, 2H).

3,4,5-tris(dodecyloxy)benzoic acid (5). A solution of KOH (49.91 g, 871.7 mmol) in 55 ml of H_2O was added slowly to a stirring solution of **4** (80.0 g, 116 mmol) in 430 ml of methanol and 75 ml of THF. The mixture was refluxed at 95 ^{o}C for 24h. Then the MeOH was removed under reduced pressure, the remaining mixture was cooled down to 0°C and acidified with cc. HCl (until pH 1, appr. 160 ml 6M HCl was used). Then the white precipitate was filtered off, washed with H_2O and dried at 70 ^{o}C to yield a white solid (76.8 g, 98%). ^1H NMR (CDCl$_3$) δ = 0.89 (t, J = 6.7 Hz, 9H), 1.18-1.56 (m, 54H), 1.68-1.90 (m, 6H), 4.02 (t, J = 6.3 Hz, 4H), 4.04 (t, J = 6.3 Hz, 2H), 7.31 (s, 2H)

4-iodophenyl 3,4,5-tris(dodecyloxy)benzoate (6). **5** (500 mg, 0.74 mmol), 4-iodophenol (172 mg, 0.782 mmol), DCC (460 mg, 2.23 mmol), DPTS (222 mg, 0.754 mmol) and 4-ppy(10 mg, 0.067 mmol) were mixed in 10 ml of DCM. The mixture was allowed to

stir for 24h at RT. Then the solvent was evaporated, the crude product was dissolved in toluene and cooled down in order to precipitate DCU. The precipitate was filtered off and washed with cold toluene. The product was further purified by column chromatography (SiO$_2$, toluene/cyclohexane 4/1). White solid was obtained (614 mg, 94%). TLC R$_f$ = 0.8 in toluene/cyclohexane 4/1. ^{1}H NMR (CDCl$_3$) δ = 0.89 (t, J = 6.5 Hz, 9H), 1.18-1.56 (m, 54H), 1.69-1.91 (m, 6H), 4.05 (t, J = 6.6 Hz, 4H), 4.07 (t, J = 6.5 Hz, 2H), 6.98 (AA' part of an AA'BB' system, J = 8.7 Hz, 2H), 7.39 (s, 2H), 7.74 (BB' part of an AA'BB' system, J = 8.6 Hz, 2H). ^{13}C NMR (CDCl$_3$) δ = 14.11, 22.70, 26.09, 29.31, 29.37, 29.40, 29.58, 29.64, 29.66, 29.71, 29.74, 30.36, 31.93, 69.32, 73.60, 89.79, 108.66, 123.49, 124.01, 138.50, 143.27, 150.95, 153.00, 164.65. IR (KBr, cm^{-1}): ν = 1736 (C=O).

7. A solution of **3** (0.039 g, 0.25 mmol) in 2 ml of toluene was added dropwise to a mixture of **6** (469 mg, 0.53 mmol), PdCl$_2$(PPh$_3$)$_2$ (0.01 g, 0.01 mmol), CuI (catalytic amount), DIPEA (0.1 ml, 0.6 mmol) and 1.5 ml of toluene. The mixture was allowed to stir for 24 hours at RT. Evaporation of the solvent gave a dark brown solid, which was dissolved in DCM and washed twice with water and brine. Drying and purification by column chromatography (SiO$_2$, toluene to DCM/EtOAc 9/1) gave a rusty brown solid (0.27 g, 65%). TLC R$_f$ = 0.1-0.3 in DCM. ^{1}H NMR (CDCl$_3$) δ = 0.89 (t, J = 6.6 Hz, 18H), 1.18-1.59 (m, 108H), 1.71-1.92 (m, 12H), 2.05 (t, J = 6.5 Hz, 1H), 3.95-4.15 (m, 12H), 4.95 (d, J = 6.7 Hz, 2H), 7.23 (AA' part of an AA'BB' system, J = 8.8 Hz, 3.7 Hz, 4H), 7.41 (s, 4H), 7.46 (BB' part of an AA'BB' system, J = 8.1 Hz, 1.7 Hz, 1H), 7.54 (d, J = 7.9 Hz, 1H), 7.61 (d, J = 8.4 Hz, 4H), 7.70 (s, 1H). ^{13}C NMR (CDCl$_3$) δ = 14.11, 22.71, 26.12, 29.35, 29.39, 29.42, 29.60, 29.66, 29.69, 29.73, 29.76, 30.39, 31.95, 63.37, 69.32, 73.61, 86.71, 89.37, 90.59, 95.21, 108.68, 120.45, 120.71, 120.77, 121.99, 122.10, 123.49, 123.57, 123.63, 129.94, 130.26, 131.98, 132.77, 132.84, 142.92, 143.22, 143.26, 151.09, 151.27, 153.01, 164.70. IR (KBr, cm^{-1}): ν = 3400 (OH), 1734 (C=O). Mass calculated (C$_{109}$H$_{168}$O$_{11}$Na) = 1653.26; Found: 1653.223. Calculated C: 79.13%, H: 10.23%; Found C 78.90 %, H 10.49 %.

8. A mixture of Meldrum's acid (46 mg, 0.32 mmol) and **7** (497 mg, 0.30 mmol) was heated for 4h at 110 ^{o}C. Then the dark brown solid product was dried under vacuum (522 mg, 100%). ^{1}H NMR (CDCl$_3$) δ = 0.89 (t, J = 6.6 Hz, 18H), 1.18-1.57 (m, 108H), 1.70-1.91 (m, 12H), 3.53 (s, 2H), 4.05 (t, J = 6.2 Hz, 8H), 4.07 (t, J = 6.2 Hz, 4H), 5.48 (s, 2H), 7.22 (AA' part

of an AA'BB' system, J = 8.8 Hz, 4H), 7.41 (s, 4H), 7.43-7.60 (m, 3H), 7.61 (BB' part of an AA'BB' system, J = 8.4 Hz, 2.4 Hz, 4H). ^{13}C NMR (CDCl$_3$) δ = 14.09, 22.68, 26.09, 29.32, 29.36, 29.39, 29.57, 29.63, 29.66, 29.69, 29.73, 30.36, 31.92, 39.71, 65.84, 69.34, 73.62, 86.30, 88.75, 91.08, 95.69, 108.71, 120.25, 120.45, 122.05, 122.18, 122.60, 123.46, 131.59, 131.77, 132.28, 132.90, 136.46, 143.29, 143.33, 151.22, 151.36, 153.01, 164.69, 164.73, 164.89, 167.12, 167.62. IR (KBr, cm^{-1}): ν = 1734 (C=O), 2214 (alkyne). Mass calculated (C$_{112}$H$_{170}$O$_{14}$) = 1740.54; Found: 1740.276; Calculated C: 77.29%; H: 9.84%; Found: C: 77.88%; H: 10.10.

9. A solution of p-toluenesulfonyl chloride (36.867 g, 193.38 mmol) in 90 ml of THF was added dropwise to a stirred solution of tetraethylene glycol monomethyl ether (40.033 g, 192.24 mmol) and NaOH (13.45 g, 336.1 mmol) in a mixture of THF/H$_2$O (180 ml/90 ml, respectively) at 0 °C. The reaction mixture was stirred for 3h while the temperature was kept below 5 °C. Then the THF was evaporated, the remaining mixture was poured into cold brine and extracted three times with CH$_2$Cl$_2$. The combined organic phases were washed twice with H$_2$O and once with brine and dried over MgSO$_4$. Then the crude product was filtered and dried to give a pale yellow liquid (57.70 g, 83%). TLC R$_f$ = 0.5-0.7 in EtOAc. ^{1}H NMR (CDCl$_3$) δ = 2.44 (s, 3H), 3.37 (s, 3H), 3.50-3.72 (m, 14H), 4.15 (t, J = 5.0 Hz, 3H), 7.34 (AA' part of an AA'BB' system, J = 8.4 Hz, 2H), 7.79 (BB' part of an AA'BB' system, J = 8.4 Hz, 2H).

10. A solution of 9 (66.28 g, 182.9 mmol) in 250ml of acetone was added dropwise to a mixture of methyl 3,5-dihydroxybenzoate (15.01 g, 89.27 mmol), K$_2$CO$_3$ (61.65 g, 446.1 mmol), KI (4.49 g, 27.1 mmol), 18-crown-6 (1.18 g, 4.47 mmol) in 500 ml of acetone. The pink heterogeneous mixture was refluxed at 65°C for 4 days. The precipitated byproducts were filtered on celite and the solvent was evaporated. The product was dissolved in CH$_2$Cl$_2$ and washed twice with saturated NaHCO$_3$ solution, H$_2$O and brine, dried over MgSO$_4$, filtered and the solvent was removed by rotary evaporator. The brown liquid was further purified by column chromatography (SiO$_2$, EtOAc/Ac 9/1 to 1/1) to obtain a transparent, yellow oil (48.3 g, 99%). TLC R$_f$ = 0.7 in EtOAc/Ac 4/1. ^{1}H NMR (CDCl$_3$) δ = 3.37 (s, 6H), 3.49-3.74 (m, 24H), 3.85 (t, J = 4.7Hz, 4H), 3.88 (s, 3H), 4.13 (t, J = 4.8 Hz, 4H), 6.69 (t, J = 2.3 Hz, 1H), 7.18 (d, J = 2.4 Hz, 2H). ^{13}C NMR (CDCl$_3$) δ = 52.16, 58.98, 67.77, 69.57, 70.51, 70.61, 70.63, 70.83, 71.94, 106.91, 108.05, 131.90, 159.78, 166.71.

11. A solution of **10** (25.006 g, 45.58 mmol) in THF (75 mL) was added slowly to a stirred suspension of $LiAlH_4$ (2.42 g, 63.8 mmol) in 160 ml of THF. The reaction was stirred at RT for 3h. Then the mixture was acidified by the addition of 1M HCl, and the THF was removed under vacuum. The resulting solution was filtered on celite, the solvent was evaporated and the resulting aqueous mixture was extracted several times with DCM. The combined organic layers were washed with water and brine and dried over $MgSO_4$. Filtration and evaporation of the solvent gave a slightly yellow oil (21.83 g, 92%). TLC R_f = 0.5-0.7 in EtOAc/Ac 1/1. ^1H NMR ($CDCl_3$) δ = 2.49 (t, J = 5.6Hz, 1H), 3.33 (s, 6H), 3.47-3.52 (m, 4H), 3.55-3.71 (m, 20H), 3.79 (t, J = 4.7Hz, 4H), 4.06 (t, J = 4.7Hz, 4H), 4.55 (d, J = 5.7Hz, 2H), 6.36 (t, J=2.2Hz, 1H), 6.49 (d, J=2.3Hz, 2H). ^{13}C NMR ($CDCl_3$) δ 58.96, 64.98, 67.47, 69.68, 70.46, 70.57, 70.61, 70.77, 71.90, 100.78, 105.40, 143.64, 106.02.

12. Trimethylsilyl bromide (6.74 g, 42.0 mmol) was added dropwise to a stirred solution of **11** (18.506 g, 35.55 mmol) in 42 mL of anhydrous $CHCl_3$ at 0℃. After 48 h stirring at room temperature, the reaction mixture was evaporated to dryness. An orange liquid was obtained, which was further purified by column chromatography (SiO_2, EtOAc/Ac 1/1) to give a colorless oil (14.82 g, 71%). TLC R_f = 0.6-0.7 in EtOAc/Ac 1/1. ^1H NMR ($CDCl_3$) δ = 3.35 (s, 6H), 3.49-3.55 (m, 4H), 3.59-3.72 (m, 20H), 3.81 (t, J=4.8 Hz, 4H), 4.07 (t, J=4.9 Hz, 4H), 4.37 (s, 2H), 6.40 (t, J=2.3 Hz, 1H), 6.52 (t, J=2.3 Hz, 2H). ^{13}C NMR ($CDCl_3$) δ 33.53, 59.00, 67.56, 69.61, 70.51, 70.62, 70.82, 71.93, 101.74, 101.87, 139.60, 160.00.

13. A solution of **12** (14.014 g, 24.017 mmol) in 20ml of acetone was added dropwise to a mixture of methyl 3,5-dihydroxybenzoate (2.001 g, 11.90 mmol), K_2CO_3 (8.233 g, 59.57 mmol), KI (622 mg, 3.75 mmol), 18-crown-6 (222 mg, 0.841 mmol) in 60 ml of acetone. The mixture was refluxed at 65°C for 24h. The precipitated byproducts were filtered on celite and the solvent was evaporated. The product was dissolved in CH_2Cl_2 and washed twice with saturated $NaHCO_3$ solution, H_2O and brine and dried over $MgSO_4$, filtered and the solvent was removed by rotary evaporator. The yellow liquid was further purified by column chromatography (SiO_2, EtOAc to EtOAc/Ac 1/3) to obtain a transparent, yellow oil (12.1 g, 87%). TLC R_f = 0.2-0.5 in EtOAc/Ac 1/1. ^1H NMR ($CDCl_3$) δ = 3.33 (s, 12H), 3.47-3.53 (m, 8H), 3.58-3.72 (m, 40H), 3.81 (t, J = 4.8Hz, 8H), 3.87 (s, 3H), 4.08 (t, J = 4.9 Hz, 8H), 4.96 (s, 4H), 6.42 (t, J = 2.3 Hz, 2H), 6.56 (d, J = 2.3 Hz, 4H), 6.74 (t, J = 2.4 Hz, 1H), 7.23 (d, J = 2.3 Hz,

2H). ^{13}C NMR (CDCl$_3$) δ = 52.20, 58.96, 67.52, 69.63, 70.12, 70.49, 70.61, 70.78, 71.92, 101.25, 106.08, 107.15, 108.36, 132.04, 138.41, 159.69, 160.12, 166.64.

14. A solution of **13** (5.006 g, 4.226 mmol) in 10 ml of THF was injected slowly into a stirred suspension of LiAlH$_4$ (0.23 g, 6.0 mmol) in 15 ml of THF at 0°C. The reaction mixture was allowed to warm up to RT and stirred for 4h. The mixture was acidified with the addition of 1N HCl, and the THF was removed under vacuum. The resulting solution was extracted multiple times with ethyl acetate, washed with NaHCO$_3$, water and brine. The organic phase was dried over MgSO$_4$ and filtered. Evaporation of the solvent gave a colorless oil (4.67 g, 96%). TLC R$_f$ = 0.7 in Ac. ^{1}H NMR (CDCl$_3$) δ = 2.05 (t, J = 6.2Hz, 1H), 3.37 (s, 12H), 3.50-3.56 (m, 8H), 3.60-3.75 (m, 40H), 3.84 (t, J = 5.0Hz, 8H), 4.11 (t, J = 5.0Hz, 8H), 4.61 (d, J = 5.9Hz, 2H), 4.96 (s, 4H), 6.44 (t, J = 2.2 Hz, 2H), 6.50 (t, J = 2.2 Hz, 1H), 6.55-6.61 (m, 6H). ^{13}C NMR (CDCl$_3$) δ 59.01, 65.17, 67.53, 69.67, 69.95, 70.52, 70.64, 70.82, 71.95, 101.16, 101.34, 105.73, 106.07, 139.20, 143.62, 160.06, 160.10.

15 (dOPE). Malonyl dichloride (25 mg, 0.18 mmol) was added dropwise to a stirred and degassed solution of **7** (495 mg, 0.299 mmol), DIPEA (82 mg, 630 mmol) and DMAP (6 mg, 0.05 mmol) in 5 ml of DCM at 0°C. This mixture was allowed to stir for 20h at RT. The resulting CH$_2$Cl$_2$ solution was washed with water and brine, dried over MgSO$_4$, paperfiltered and the solvent was removed by rotary evaporator. Further purification by column chromatography (SiO$_2$, DCM/cyclohexane 4/1 to DCM) gave a yellow glassy solid (385 mg, 76%). TLC R$_f$ = 0.2-0.4 in DCM. ^{1}H NMR (CDCl$_3$) δ = 0.88 (t, J = 6.6 Hz, 36H), 1.18-1.59 (m, 216H), 1.70-1.90 (m, 24H), 3.61 (s, 2H), 3.96-4.11 (m, 24H), 5.46 (s, 4H), 7.19 (d, J = 8.7 Hz, 8H), 7.40 (s, 8H), 7.46 (AA' part of an AA'BB' system, J= 8.0 Hz, J = 1.7 Hz, 2H), 7.49-7-60 (m, 4H), 7.58 (BB' part of an AA'BB' system, J = 8.8 Hz, J = 2.6 Hz, 8H). ^{13}C NMR (CDCl$_3$) δ = 14.09, 22.69, 26.11, 29.36, 29.39, 29.41, 29.58, 29.64, 29.66, 29.70, 29.74, 30.38, 31.92, 41.52, 65.28, 69.33, 73.60, 86.34, 88.96, 90.94, 95.61, 108.69, 120.26, 120.53, 122.00, 122.07, 122.32, 123.42, 123.59, 131.30, 131.83, 132.21, 132.87, 136.92, 143.26, 151.16, 151.32, 153.00, 164.63, 164.68, 166.04. IR (KBr, cm^{-1}): ν = 1735 (C=O), 2215 (alkyne). Mass calculated (C$_{221}$H$_{336}$O$_{24}$) = 3374.51; Found (M+H): 3375.981. Calculated C: 78.60%; H: 10.03%; Found C: 78.67%; H: 10.02%.

16 (dOPE-C₆₀). A solution of **15** (552 mg, 0.163 mmol), C_{60} (115 mg, 0.160 mmol), DBU (130 mg, 0.854 mmol), I_2 (107 mg, 0.442 mmol) in 170 ml of toluene were stirred at RT for 72h. Then the product was filtered on a short silica plug, washed with toluene and later with DCM in order to separate starting material, product and byproducts. Then it was further purified by column chromatography (SiO_2, cyclohexane to cyclohexane/EtOAc 9/1). 630 mg (84%) dark brown solid was obtained. TLC R_f = 0.6-0.7 in cyclohexane/EtOAc 9/1. ^{1}H NMR ($CDCl_3$) δ = 0.81-0.96 (m, 36H), 1.18-1.55 (m, 216H), 1.68-1.92 (m, 24H), 3.93-4.12 (m, 24H), 5.48-5.95 (m, 4H), 7.05-7.24 (m, 8H), 7.34-7.42 (m, 8H), 7.45-7.78 (m, 14H). ^{13}C NMR ($CDCl_3$) δ = 14.09, 22.68, 26.08, 26.12, 29.36, 29.42, 29.58, 29.65, 29.70, 29.74, 30.38, 31.92, 51.76, 66.91, 69.34, 71.39, 73.60, 86.50, 88.97, 91.28, 95.97, 108.70, 120.21, 120.47, 122.02, 122.13, 122.85, 123.51, 123.59, 131.77, 132.31, 132.89, 133.04, 136.25, 139.11, 140.85, 141.86, 142.18, 142.86, 142.90, 142.93, 143.27, 143.29, 143.80, 144.51, 144.63, 144.84, 144.92, 145.08, 145.09, 145.17, 151.21, 151.42, 153.00, 163.24, 164.57, 164.64. IR (KBr, cm^{-1}) 1735 (C=O), 2214 (alkyne). Mass calculated ($C_{281}H_{334}O_{24}$) = 4095.64 (average mass), Found: 4096.588. Calculated C: 82.40%; H: 8.23%; Found C: 81.81%; H: 8.32%.

17 (OPE-TEGd2). A mixture of **8** (1.600 g, 0.919 mmol), **14** (1.051 g, 0.918 mmol), DCC (623 mg, 3.02 mmol), DPTS (273 mg, 0.927 mmol) and 4-ppy(20 mg, 0.14 mmol) in 40 ml of DCM was stirred for 48h at RT. The solvent was evaporated; the crude product was dissolved in toluene and cooled down to precipitate DCU. The precipitate was filtered off and washed with cold toluene. Then the solvent was evaporated, the residue was dissolved in DCM washed with water and brine and dried over $MgSO_4$. The crude product was further purified by column chromatography (SiO_2, DCM to EtOAc). Yellow amorphous compound was obtained (520 mg, 32%; 60% based on unreacted **8**). In this reaction significant amount of **15** (**dOPE**) byproduct was also isolated as yellow solid (563 mg, 36%). TLC R_f = 0.4 in EtOAc/Ac 4/1. ^{1}H NMR ($CDCl_3$) δ = 0.87 (t, J = 6.8 Hz, 18H), 1.16-1.56 (m, 108H), 1.70-1.90 (m, 12H), 3.35 (s, 12H), 3.48-3.57 (m, 10H), 3.59-3.73 (m, 40H), 3.81 (t, J = 5.0 Hz, 8H), 3.99-4.12 (m, 20H), 4.91 (s, 4H), 5.11 (s, 2H), 5.45 (s, 2H), 6.43 (t, J = 2.4 Hz, 2H), 6.51 (t, J = 2.2 Hz, 1H), 6.6.56 (d, J = 2.2 Hz, 6H) 7.20 (AA' part of an AA'BB' system, J = 8.5 Hz, 4H), 7.40 (s, 4H), 7.47 (dd, J = 8.2 Hz, 1.3 Hz, 1H), 7.53 (d, J = 8.0 Hz, 1H), 7.54 (BB' part of an AA'BB' system, J = 8.5 Hz, 4H), 7.63 (br s, 1H).. ^{13}C NMR ($CDCl_3$) δ = 14.10, 22.68, 26.07, 26.11,

29.35, 29.40, 29.57, 29.63, 29.65, 29.69, 29.72, 30.37, 31.92, 41.45, 58.98, 65.18, 67.09, 67.51, 69.32, 69.65, 69.98, 70.51, 70.63, 70.80, 71.95, 73.59, 86.32, 88.93, 90.96, 95.62, 101.17, 102.07, 106.10, 107.03, 108.67, 120.23, 120.47, 122.03, 122.11, 122.29, 123.41, 123.58, 131.33, 132.24, 132.87, 132.90, 136.96, 137.49, 139.00, 143.26, 151.18, 151.35, 153.00, 160.02, 160.10, 164.63, 164.65, 166.08, 166.15. IR (KBr, cm^{-1}): ν = 1736 (C=O). Mass calculated ($C_{169}H_{260}O_{36}Na$) = 2888.84, Found: 2888.677. Calculated C: 70.78%; H: 9.14%; Found C: 70.83%; H, 9.29%.

18 (OPE-TEGd2-C$_{60}$). A solution of **17 (OPE-TEGd2)** (497 mg, 0.173 mmol), C_{60} (124 mg, 0.172 mmol), DBU (138 mg, 0.906 mmol) and I_2 (105 mg, 0.414 mmol) in 180 ml of toluene was stirred at RT for three days. Then the product was filtered on a short silica plug, washed with toluene in order to remove the unreacted C_{60} and with acetone afterwards to separate the product. No further purification was necessary. Dark brown solid was obtained (535 mg, 87%). TLC R_f = 0.8 in EtOAc/Ac 4/1. ^{1}H NMR (CDCl$_3$) δ = 0.76-0.98 (m, 18H), 1.14-1.57 (m, 108H), 1.68-1.91 (m, 12H), 3.20-3.35 (m, 12H), 3.45-3.88 (m, 56H), 3.94-4.16 (m, 20H), 4.70-5.03 (m, 4H), 5.11-5.98 (m, 4H), 6.35-6.71 (m, 9H) 7.03-7.24 (m, 4H), 7.29-7.80 (m, 11H). ^{13}C NMR (CDCl$_3$) δ = 14.10, 22.68, 26.07, 26.11, 29.35, 29.40, 29.57, 29.63, 29.65, 29.69, 29.72, 30.37, 31.92, 41.45, 58.98, 65.18, 67.09, 67.51, 69.32, 69.65, 69.98, 70.51, 70.63, 70.80, 71.95, 73.59, 86.32, 88.93, 90.96, 95.62, 101.17, 102.07, 106.10, 107.03, 108.67, 120.23, 120.47, 122.03, 122.11, 122.29, 123.41, 123.58, 131.33, 132.24, 132.87, 132.90, 136.96, 137.49, 139.00, 143.26, 151.18, 151.35, 153.00, 160.02, 160.10, 164.63, 164.65, 166.08, 166.15. IR (KBr, cm^{-1}): ν =1736 (C=O), 2214 (alkyne). Mass calculated ($C_{229}H_{258}O_{36}Na$) = 3606.83, Found: 3606.599. Calculated C: 76.69 %; H: 7.27%; Found C: 72.86%; H, 7.87%.

19. A solution of DBU (23 mg, 0.15 mmol) in 3.2 ml of DCM was added dropwise to a stirred and degassed solution of **15** (502 mg, 0.149 mmol) and CBr$_4$ (200 mg, 0.603 mmol) in 15 ml of CH$_2$Cl$_2$ at 0 °C. The solution was allowed to stir for 2 hours while warming up to RT. Further purification with column chromatography (SiO$_2$, DCM/cyclohexane 4/1) gave a yellow amorphous solid (164 mg, 32%). TLC R_f = 0.3 in DCM/cyclohexane 4/1. ^{1}H NMR (CDCl$_3$) δ = 0.83-0.96 (m, 36H), 1.18-1.60 (m, 216H), 1.70-1.93 (m, 24H), 3.95-4.16 (m, 24H), 5.07 (s, 1H), 5.46, 5.53 (ABq, 4H, J = 12.7 Hz), 7.21 (d, J = 8.7 Hz, 8H), 7.42 (s, 8H), 7.46 (d, J=

8.5 Hz, 2H), 7.52 (d, J= 8.0 Hz, 2H), 7.54-7-64 (m, 10H). ^{13}C NMR (CDCl$_3$) δ = 14.11, 22.71, 26.14, 29.39, 29.42, 29.44, 29.61, 29.67, 29.69, 29.73, 29.77, 30.41, 31.95, 42.17, 66.77, 69.31, 73.58, 86.22, 88.89, 91.09, 95.80, 108.68, 120.16, 120.49, 122.02, 122.07, 122.48, 123.46, 123.61, 131.57, 132.23, 132.87, 132.94, 136.13, 143.27, 151.20, 151.38, 153.02, 164.13, 164.59, 164.64. Mass calculated (C$_{221}$H$_{335}$BrO$_{24}$) = 3452.42; Found (M+H): 3454.193.

20 dOPE-Y3N@C80. DBU (6 mg, 0.04 mmol – in 0.6 ml of chlorobenzene) was added dropwise to a mixture of Y$_3$N@C$_{80}$ (10 mg, 0.008 mmol) and **19** (84 mg, 0.024 mmol) in 15 ml of chlorobenzene. After 2h stirring at RT the solvent was removed by rotary evaporator, the dark brown crude product was dissolved in DCM and purified by preparative TLC. First the plate was eluted with CS$_2$ to remove unreacted Y$_3$N@C80 which elutes with the solvent front, then with DCM/cyclohexane 3/2 (R$_f$ = 0.2) to separate the product. The product was scraped off, stirred in DCM for 15min and paperfiltered. Brown solid was obtained (7.5 mg, 20%). ^{1}H NMR (CDCl$_3$) δ = 0.88 (t, J = 6.5 Hz, 36H), 1.15-1.58 (m, 216H), 1.70-1.90 (m, 24H), 5.77 (s, 4H), 7.14-7.23 (m, 8H), 7.39 (d, J = 6.3 Hz, 8H), 7.48 (dd, J= 7.9 Hz, J = 1.3 Hz, 2H), 7.52-7-59 (m, 6H), 7.62 (d, J = 8.5 Hz, 8H), 7.68 (s, 1H). ^{13}C NMR (CDCl$_3$) δ = 14.10, 22.69, 26.08, 26.12, 26.14, 29.37, 29.42, 29.58, 29.66, 29.69, 29.72, 30.38, 31.93, 51.11, 67.50, 69.34, 73.60, 86.45, 88.89, 91.41, 96.02, 108.69, 120.18, 120.42, 122.04, 122.18, 122.88, 123.57, 123.59, 126.77, 127.06, 128.18, 129.27, 131.91, 132.40, 132.94, 133.04, 134.63, 135.14, 135.88, 135.93, 136.58, 137.78, 139.23, 139.33, 139.46, 139.48, 139.65, 139.99, 140.02, 141.71, 142.01, 142.70, 142.86, 143.27, 143.43, 143.72, 143.77, 144.34, 144.82, 145.48, 146.19, 146.37, 146.44, 147.14, 147.21, 147.38, 147.45, 148.47, 149.03, 149.16, 151.24, 151.48, 153.00, 164.60. Mass calculated (C$_{301}$H$_{334}$O$_{24}$Y$_3$N) = 4613.21; Found (M+H): 4614.463.

3,4,5-tris(dodecyloxy)benzyl alcohol (21). A solution of **4** (25.103 g, 36.43 mmol) in 125 ml of dry THF was added slowly to a stirred suspension of LiAlH$_4$ (2.755 g, 72.60 mmol) in 75 ml of THF at 0°C. The reaction was allowed to warm up to RT and stirred 3h. The mixture was quenched with the addition of 5 ml of methanol and 50 ml of H$_2$O, and THF was removed under vacuum. The resulting solution was extracted with DCM, washed with NH$_4$Cl, H$_2$O and brine and dried over anhydrous MgSO$_4$. Filtration and evaporation of the solvent gave a white solid (19.18 g, 80%). TLC R$_f$ = 0.2 in EtOAc. ^{1}H NMR (CDCl$_3$) δ = 0.89 (t, J

= 6.7Hz, 9H), 1.20-1.53 (m, 54H), 1.60 (t, J = 6.3Hz, 1H), 1.68-1.86 (m, 6H), 3.94 (t, J = 6.5Hz, 2H), 3.96 (t, J = 6.5Hz, 4H), 4.60 (d, J = 6.0Hz, 2H), 6.56 (s, 2H).

3,4,5-tris(dodecyloxy)benzaldehyde (22). Activated MnO_2 (71.90 g 0.83 mol) and **21** (17.740 g 26.834 mmol) were stirred in 270 ml of CH_2Cl_2 at room temperature for 5 h. The mixture was filtered through a silica pad and the solvent was removing by rotary evaporator to yield a white solid (15.40 g 87%). TLC R_f = 0.8 in EtOAc. ^{1}H NMR ($CDCl_3$) δ = 0.88 (t, J = 6.8Hz, 9H), 1.18-1.57 (m, 54H), 1.69-1.90 (m, 6H), 4.04 (t, J = 6.6Hz, 4H), 4.06 (t, J = 6.6Hz, 2H), 7.09 (s, 2H), 9.83 (s, 1H). ^{13}C NMR ($CDCl_3$) δ = 14.09, 22.69, 26.03, 26.07, 29.27, 29.38, 29.55, 29.63, 29.66, 29.69, 29.71, 30.35, 31.92, 69.27, 73.63, 107.91, 131.46, 143.92, 153.53, 191.21.

3,4,5-tris(dodecyloxy)styrene (23). A solution of tBuOK (3.32 g, 28.8 mmol) in 40 ml of THF was slowly added to a solution of PPh_3CH_3Br (9.19 g, 25.7 mmol) in 130 ml of THF at 0°C. The mixture was allowed to warm up to RT and stir for another 10min. Then **22** (15.06 g, 22.85 mmol) in 60 ml of THF was added dropwise. The reaction mixture was allowed to stir for 3h, and then quenched with 15 ml of NH_4Cl solution. The THF was removed by rotary evaporator; the residue was extracted with DCM and washed with NH_4Cl, water and brine. The organic phase was dried over $MgSO_4$ and filtered twice on a short silica plug. Evaporation of the solvent yielded a white solid (14.75 g, 98%). TLC R_f = 0.9 in DCM/cyclohexane 3/2. ^{1}H NMR ($CDCl_3$) δ = 0.90 (t, J = 6.7Hz, 9H), 1.15-1.55 (m, 54H), 1.68-1.88 (m, 6H), 3.96 (t, J = 6.6Hz, 2H), 4.00 (t, J = 6.6Hz, 4H), 5.18 (d, J = 10.8Hz, 1H), 5.63 (d, J = 17.5Hz, 1H), 6.55-6.69 (m, 3H). ^{13}C NMR ($CDCl_3$) δ = 14.10, 22.70, 26.12, 29.37, 29.39, 29.43, 29.46, 29.66, 29.71, 29.76, 30.35, 31.93, 69.20, 73.49, 105.04, 112.66, 132.78, 136.96, 138.48, 153.21.

24. A mixture of **23** (14.53 g, 22.13 mmol), p-bromoiodobenzene (6.56 g, 23.2 mmol), ToP (399 mg, 1.31 mmol), $Pd(OAc)_2$ (198 mg, 0.88 mmol) in 100 ml of Et_3N was stirred at 80 °C for 2days. Then the solvent was removed by rotary evaporator, and the crude product was dissolved in DCM, washed twice with water and brine, dried over $MgSO_4$ and filtered on a short silica plug. The crude product was further purified by recrystallization (from EtOH/Ac mixture) and column chromatography (SiO_2, cyclohexane/DCM 3/2) to give a brown solid (15.65 g, 87%). TLC R_f = 0.6 in cyclohexane/DCM 3/2. ^{1}H NMR ($CDCl_3$) δ = 0.89 (t, J = 6.9Hz,

9H), 1.18-1.55 (m, 54H), 1.69-1.89 (m, 6H), 3.94-4.07 (m, 6H), 6.70 (s, 2H), 6.89 (AB, d, J = 16.3Hz, 1H), 7.00 (AB, d, J = 16.4Hz, 1H), 7.35 (AA' part of an AA'BB' system, J = 8.6Hz, 2H), 7.47 (BB' part of an AA'BB' system, J = 8.5Hz, 2H). ^{13}C NMR (CDCl$_3$) δ = 14.09, 22.69, 26.13, 29.36, 29.39, 29.43, 29.46, 29.66, 29.71, 29.75, 30.35, 31.92, 69.27, 73.56, 105.41, 121.06, 126.40, 127.81, 129.67, 131.75, 132.15, 136.40, 138.66, 153.35.

25. A mixture of p-hydroxybenzaldehyde (508 mg, 4.16 mmol), imidazole (340 mg, 4.99 mmol), TBDMSCl (653 mg, 4.33 mmol) in 8 ml of DCM was allowed to stir at RT for 2.5 days. The organic solution was filtered on a short silica plug to afford a pale yellow oil (0.85 g, 88%). TLC R$_f$ = 0.5 in DCM. ^{1}H NMR (CDCl$_3$) δ = 0.25 (s, 6H), 1.00 (s, 9H), 6.95 (AA' part of an AA'BB' system, J = 8.5Hz, 2H), 7.79 (BB' part of an AA'BB' system, J = 8.6Hz, 2H), 9.89 (s, 1H). ^{13}C NMR (CDCl$_3$) δ = -4.36, 18.25, 25.55, 120.48, 130.43, 131.89, 161.48.

26. A solution of tBuOK (15.25 g, 135.9 mmol) in 30 ml of THF was slowly added to a solution of PPh$_3$CH$_3$Br (44.9 g, 126 mmol) in 100 ml of THF at RT. The mixture was allowed to warm up to RT and stir for another 30min. Then **25** (24.7 g, 105 mmol) in 130 ml of THF was added dropwise to the mixture. The reaction mixture was allowed to stir overnight. The THF was removed by rotary evaporator; the residue was extracted with DCM and washed with NH$_4$Cl. The organic phase was dried over MgSO$_4$, filtered and purified twice by column chromatography (eluent: cyclohexane/DCM 4/1). Evaporation of the solvent yielded a colorless oil (11 g, 45%). ^{1}H NMR (CDCl$_3$) δ = 0.21 (s, 6H), 0.99 (s, 9H), 5.13 (d, J = 10.7Hz, 1H), 5.61 (d, J = 17.4Hz, 1H), 6.66 (dd, J = 17.5 Hz, 10.8 Hz, 1H), 6.80 (AA' part of an AA'BB' system, J = 8.4 Hz, 2H), 7.29 (BB' part of an AA'BB' system, J = 8.4 Hz, 2H).

27. A mixture of **26** (924 mg, 3.94 mmol), **24** (3.000 g, 3.694 mmol), ToP (67 mg, 0.22 mmol), Pd(OAc)2 (35 mg, 0.16 mmol) in 21 ml of Et$_3$N was stirred at 100°C for 22h. Then the solvent was removed by rotary evaporator, and the crude product was dissolved in DCM, washed with water and brine, dried over MgSO$_4$ and further purified by column chromatography (SiO$_2$, cyclohexane/DCM 3/2) to yield a yellow solid (2.35g, 66%). TLC R$_f$ = 0.3 in DCM/cyclohexane 3/2. ^{1}H NMR (CDCl$_3$) δ = 0.25 (s, 6H), 0.92 (t, J = 6.6Hz, 9H), 1.03 (s, 9H), 1.20-1.60 (m, 54H), 1.70-1.94 (m, 6H), 3.90-4.12 (m, 6H), 6.75 (s, 2H), 6.87(AA' part of an AA'BB' system, J = 8.6Hz, 2H), 6.94-7.14 (m, 4H), 7.42 (BB' part of an AA'BB' system, J = 8.6Hz, 2H), 7.49 (s, 4H). ^{13}C NMR (CDCl$_3$) δ = -4.38, 14.11, 18.25, 22.70, 25.70, 26.15, 26.94,

29.37, 29.40, 29.45, 29.50, 29.67, 29.72, 29.76, 30.38, 31.94, 69.26, 73.56, 105.34, 120.36, 126.38, 126.57, 126.67, 127.38, 127.65, 128.19, 128.60, 130.74, 132.61, 136.41, 136.91, 138.47, 153.33, 155.53.

28. A solution of TBAF (3.0 ml, 3.0 mmol, 1M in THF) was added dropwise to a solution of **27** (2.612 g, 2.705 mmol) in 12 ml of dry THF at 0°C. The reaction mixture was allowed to stir for 2.5h at 0°C. The THF was removed by evaporation; the crude product was dissolved in DCM and washed with H_2O and brine. The organic phase was dried over $MgSO_4$, filtered and further purified by column chromatography (SiO_2, DCM/cyclohexane 4/1) to yield a yellow solid (2.05 g, 89%). TLC R_f = 0.5 in DCM/cyclohexane 4/1. ^{1}H NMR (CDCl$_3$) δ = 0.89 (t, J = 6.7Hz, 9H), 1.18-1.56 (m, 54H), 1.70-1.90 (m, 6H), 3.99 (t, J = 6.8Hz, 2H), 4.04 (t, J = 6.5Hz, 4H), 5.01 (s, 1H), 6.73 (s, 2H), 6.84 (AA' part of an AA'BB' system, J = 8.5Hz, 2H), 6.91-7.12 (m, 4H), 7.42 (BB' part of an AA'BB' system, J = 8.5Hz, 2H), 7.48 (s, 4H). ^{13}C NMR (CDCl$_3$) δ = 14.10, 22.69, 26.14, 29.37, 29.39, 29.44, 29.48, 29.63, 29.67, 29.71, 29.74, 29.76, 30.34, 31.93, 69.27, 73.61, 105.33, 115.67, 126.27, 126.56, 126.68, 127.40, 127.90, 128.02, 128.61, 130.37, 132.65, 136.42, 136.85, 138.36, 153.32, 155.36.

29. A mixture of **26** (8.0 g, 34 mmol), p-bromobenzaldehyde (7.6 g, 41 mmol), ToP (1.56 g, 5.13 mmol), Pd(OAc)$_2$ (0.3 g, 1 mmol) in 200 ml of Et$_3$N was stirred at 60°C for 2 hours, and at 80°C 2days. The reaction mixture was filtered through celite, the solvent was removed by rotary evaporator and the crude product was dissolved in DCM, washed with water and dried over MgSO$_4$. Filtration, evaporation and purification by column chromatography (SiO$_2$, cyclohexane/DCM 4/1 to 3/7) yielded a yellow solid (6.4 g, 55%). ^{1}H NMR (CDCl$_3$) δ = 0.23 (s, 6H), 1.00 (s, 9H), 6.86 (AA' part of an AA'BB' system, J = 8.6 Hz, 1H), 7.01 (d, J = 16.4Hz, 1H), 7.22 (d, J = 16.6 Hz, 1H), 7.44 (BB' part of an AA'BB' system, J = 8.6 Hz, 2H), 7.63 (AA' part of an AA'BB' system, J = 8.2 Hz, 2H), 7.86 (BB' part of an AA'BB' system, J = 8.4 Hz, 2H), 9.99 (s, 1H).

30. A solution of tBuOK (3.18 g, 28.3 mmol) in 20 ml of THF was slowly added to a solution of PPh$_3$CH$_3$Br (10.14 g, 28.39 mmol) in 30 ml of THF at RT. The mixture was allowed to warm up to RT and stir for another 30min. Then **29** (6.4 g, 19 mmol) in 50 ml of THF was added dropwise to the mixture, which was allowed to stir overnight. The THF was removed by rotary evaporator; the residue was extracted with DCM and washed with NH$_4$Cl. The

organic phase was dried over MgSO$_4$, filtered and purified by column chromatography (SiO$_2$, cyclohexane/DCM 4/1). Evaporation of the solvent yielded a white solid (4.9 g, 77%). ^{1}H NMR (CDCl$_3$) δ = 0.22 (s, 6H), 1.00 (s, 9H), 5.24 (d, J = 10.9 Hz, 1H), 5.76 (d, J = 17.5 Hz, 1H), 6.72 (dd, J = 17.5 Hz, J = 10.8 Hz, 1H), 6.84 (d, J = 8.3 Hz, 2H), 6.96, 7.07 (ABq, 2H, J = 16.1 Hz), 7.35-7.48 (m, 6H).

31. A mixture of **30** (2.617 g, 7.776 mmol), **24** (6.015 g, 7.407 mmol), ToP (134 mg, 0.440 mmol) and Pd(OAc)2 (66 mg, 0.29 mmol) in Et$_3$N was stirred at 100°C for 15h. Then the solvent was removed by rotary evaporator, and the crude product was dissolved in DCM, washed with water and brine, dried over MgSO$_4$ and further purified by column chromatography (cyclohexane/DCM 3/2) to yield a yellow solid (7.50 g, 95%). TLC R$_f$ = 0.5-0.6 in DCM/cyclohexane 1/1. ^{1}H NMR (CDCl$_3$) δ = 0.23 (s, 6H), 0.89 (t, J = 6.8Hz, 9H), 1.01 (s, 9H), 1.15-1.55 (m, 54H), 1.70-1.90 (m, 6H), 3.90-4.08 (m, 6H), 6.73 (s, 2H), 6.85 (AA' part of an AA'BB' system, J = 8.6Hz, 2H), 6.92-7.09 (m, 4H), 7.12 (s, 2H), 7.41 (BB' part of an AA'BB' system, J = 8.7Hz, 2H), 7.50 (s, 8H). ^{13}C NMR (CDCl$_3$) δ = -4.38, 14.10, 18.25, 22.70, 25.69, 26.14, 29.37, 29.39, 29.44, 29.48, 29.67, 29.71, 29.74, 29.76, 30.37, 31.93, 69.25, 73.56, 105.35, 120.37, 126.35, 126.61, 126.71, 126.81, 127.30, 127.67, 127.95, 128.17, 128.31, 128.82, 130.71, 132.55, 136.34, 136.60, 136.78, 137.12, 138.50, 153.34, 155.56.

32. A solution of TBAF (7.8 ml, 7.8 mmol, 1M in THF) was added dropwise to a solution of **31** (7.50 g, 7.02 mmol) in 40 ml of dry THF. The reaction mixture was allowed to stir for 4h at RT. The THF was removed by evaporation and the crude product was dissolved in DCM and washed with H$_2$O and brine. The organic phase was dried over MgSO$_4$, filtered and further purified by column chromatography (SiO$_2$, DCM/cyclohexane 4/1) to give a yellow solid was (4.85 g, 72%). TLC R$_f$ = 0.5 in DCM/cyclohexane 4/1. ^{1}H NMR (CDCl$_3$) δ = 0.90 (t, J = 6.6Hz, 9H), 1.15-1.57 (m, 54H), 1.70-1.90 (m, 6H), 3.95-4.09 (m, 6H), 5.00 (s, 1H), 6.73 (s, 2H), 6.84 (AA' part of an AA'BB' system, J = 8.6Hz, 2H), 6.92-7.09 (m, 4H), 7.12 (s, 2H), 7.42 (BB' part of an AA'BB' system, J = 8.6Hz, 2H), 7.45-7.55 (m, 8H). ^{13}C NMR (CDCl$_3$) δ = 14.11, 22.70, 26.15, 29.38, 29.40, 29.45, 29.48, 29.63, 29.68, 29.72, 29.74, 29.76, 30.35, 31.94, 69.27, 73.62, 105.34, 115.68, 126.26, 126.60, 126.72, 126.82, 127.34, 127.93, 127.97, 128.13, 128.16, 128.82, 130.35, 132.61, 136.36, 136.60, 136.78, 137.05, 138.41, 153.32, 155.37.

33. A solution of methyl 3,5-dimethylbenzoate (6.005 g, 36.6 mmol), N-bromosuccinimide (13.677 g, 76.8 mmol) and catalytic amount of AIBN in CCl_4 was stirred at 80°C. After 48 hours the mixture was cooled down to room temperature and filtered. The filtrate was washed with sat. aq. $NaHCO_3$ and sat. aq. NaCl. The organic layer was dried over anhydrous Na_2SO_4, filtrated, concentrated, suspended in petroleum ether and refrigerated. The crystallized part (mainly product) was decanted while the filtrate (containing mono- and gem-dibrominated mixture) was concentrated and dissolved in THF. Then diethyl phosphite (10.5 ml, 81.9 mmol) and DIPEA (14.3 ml, 81.9 mmol) was added to the former solution at 0 °C under Ar. The mixture was allowed to warm up to RT and stirred for 24h. Most of the THF was removed by evaporation and the mixture was poured into ice-water and extracted with Et_2O. The organic layer was washed with 1N HCl and brine, dried over $MgSO_4$, filtered and evaporated. Then the combined crude products were further purified by column chromatography (SiO_2, cyclohexane/EtOAc 9:1) to obtain white crystals (4.634 g, 39%). TLC R_f = 0.7 in cyclohexane/EtOAc 4/1. ^1H NMR ($CDCl_3$) δ = 3.94 (s, 3H), 4.51 (s, 4H), 7.62 (t, J = 1.7Hz 1H), 8.01 (d, J = 1.5Hz 2H). ^{13}C NMR ($CDCl_3$) δ = 31.79, 52.37, 130.01, 131.46, 133.81, 138.96, 165.91.

34. A mixture of **33** (367 mg, 1.14 mmol), **28** (1.957 g, 2.30 mmol), K_2CO_3 (802 mg, 5.80 mmol), KI (104 mg, 0.63 mmol) and 18-crown-6 (30 mg, 0.11 mmol) in 55 ml of acetone was stirred for 20h at 60°C. The precipitated byproducts were filtered on celite, washed and the solvent was evaporated. The crude product was dissolved in CH_2Cl_2 and washed with NH_4Cl, H_2O and brine and dried over $MgSO_4$. Then the solvent was removed by rotary evaporator and the residue was further purified by column chromatography (SiO_2, DCM/cyclohexane 4/1) to give a yellow solid (1.54 g, 73%). TLC R_f = 0.4 in DCM/cyclohexane 4/1. ^1H NMR ($CDCl_3$) δ = 0.89 (t, J = 6.5Hz, 18H), 1.15-1.58 (m, 108H), 1.70-1.90 (m, 12H), 3.90-4.08 (m, 15H), 5.15 (s, 4H), 6.72 (s, 4H), 6.91-7.14 (m, 12H), 7.40-7.52 (m, 12H), 7.75 (s, 1H), 8.10 (s, 2H). ^{13}C NMR ($CDCl_3$) δ = 14.09, 22.69, 26.15, 29.37, 29.39, 29.45, 29.50, 29.67, 29.70, 29.71, 29.74, 29.76, 30.38, 31.93, 52.27, 69.27, 69.42, 73.55, 105.37, 115.17, 126.60, 126.69, 127.35, 127.78, 127.91, 128.10, 128.68, 130.63, 130.79, 130.97, 132.58, 136.50, 136.79, 137.97, 138.51, 153.34, 158.21, 166.60. Mass calculated ($C_{126}H_{188}O_{10}$) = 1861.42, Found: 1861.317.

35. LiAlH$_4$ (1.1 ml, 1.1 mmol, 1M in THF) was added slowly to a stirred solution of **34** (1.451 g, 0.779 mmol) in 9 ml of dry THF at 0°C. The reaction was stirred for 3h while warming up to RT. The mixture was acidified by the addition of 1N HCl (1 mL), and the THF was removed under vacuum. The resulting mixture was extracted with DCM, washed with water and brine. The organic phase was dried over anhydrous MgSO$_4$, paperfiltered and further purified by column chromatography (SiO$_2$, DCM/cyclohexane 4/1 to DCM/Ac 9/1). A yellow solid was obtained (1.239 g, 87%). TLC R$_f$ = 0.4 in DCM. ^{1}H NMR (CDCl$_3$) δ = 0.9 (t, J = 6.3Hz, 18H), 1.20-1.55 (m, 108H), 1.70-1.90 (m, 12H), 3.92-4.09 (m, 12H), 4.76 (d, J = 5.7Hz, 2H), 5.11 (s, 4H), 6.72 (s, 4H), 6.91-7.12 (m, 12H), 7.40-7.51 (m, 15H). ^{13}C NMR (CDCl$_3$) δ = 14.10, 22.69, 26.15, 29.37, 29.39, 29.45, 29.50, 29.67, 29.71, 29.74, 29.76, 30.38, 31.93, 65.04, 69.27, 69.84, 73.56, 105.36, 115.14, 125.49, 125.64, 126.48, 126.59, 126.69, 127.35, 127.76, 127.97, 128.64, 130.61, 132.58, 136.47, 136.82, 137.78, 138.49, 141.86, 153.34, 158.43. Mass calculated (C$_{125}$H$_{188}$O$_9$): 1833.43, Found: 1833.346.

36. A mixture of **33** (700 mg, 2.174 mmol), **32** (4.164 g, 4.367 mmol), K$_2$CO$_3$ (1.594 g, 11.53 mmol), KI (186 mg, 1.12 mmol) and 18-crown-6 (62 mg, 0.24 mmol) in 155 ml of acetone was stirred for 14.5h at 60°C. Then the solvent was evaporated; the crude product was dissolved in CH$_2$Cl$_2$ and washed with NH$_4$Cl, H$_2$O and brine. The combined organic layers were dried over MgSO$_4$, the solvent was removed by rotary evaporator and the residue was further purified by column chromatography (SiO$_2$, DCM/cyclohexane 9/1) to give a yellow solid (3.808 g, 85%). TLC R$_f$ = 0.7 in DCM/cyclohexane 9/1. ^{1}H NMR (CDCl$_3$) δ = 0.9 (t, J = 6.6Hz, 18H), 1.05-1.58 (m, 108H), 1.67-1.92 (m, 12H), 3.75-4.13 (m, 15H), 5.14 (s, 4H), 6.73 (s, 4H), 6.85-7.15 (m, 16H), 7.30-7.57 (m, 20H), 7.74 (s, 1H), 8.09 (s, 2H). ^{13}C NMR (CDCl$_3$) δ = 14.14, 22.72, 26.19, 29.41, 29.50, 29.53, 29.71, 29.80, 30.43, 31.97, 52.25, 69.26, 69.33, 73.57, 105.37, 115.17, 126.46, 126.53, 126.55, 126.66, 126.74, 126.87, 127.30, 127.83, 128.03, 128.14, 128.63, 128.87, 130.61, 130.69, 130.93, 132.55, 136.39, 136.58, 136.80, 136.98, 137.96, 138.54, 152.82, 153.37, 158.20, 166.57. Mass calculated (C$_{142}$H$_{200}$O$_{10}$): 2065.51, Found: 2065.284.

37. LiAlH$_4$ (2.5 ml, 2.5 mmol, 1M in THF) was added slowly to a stirred solution of **38** (3.646 g, 1.764 mmol) in 30 ml of THF at RT. The reaction was stirred for 2.5h at RT. The mixture was acidified by the addition of 1N HCl (1 mL), and the THF was removed under

vacuum. The resulting solution was extracted with DCM, washed with water and brine. The organic phase was dried over anhydrous $MgSO_4$, paperfiltered and further purified by column chromatography (SiO_2, DCM). A yellow solid was obtained (2.937 g, 91%). TLC R_f = 0.1-0.3 in DCM. ^1H NMR ($CDCl_3$) δ = 0.89 (t, J = 6.6Hz, 18H), 1.10-1.58 (m, 108H), 1.70-1.90 (m, 12H), 3.87-4.10 (m, 12H), 4.75 (d, J = 5.4Hz, 2H), 5.10 (s, 4H), 6.73 (s, 4H), 6.9-7.16 (m, 16H), 7.32-7.57 (m, 23H). ^{13}C NMR ($CDCl_3$) δ = 14.11, 22.70, 26.15, 29.38, 29.40, 29.46, 29.49, 29.68, 29.72, 29.76, 30.38, 31.94, 65.04, 69.25, 69.81, 73.57, 105.34, 115.17, 125.46, 125.63, 126.44, 126.63, 126.72, 126.84, 127.30, 127.78, 127.98, 128.08, 128.15, 128.62, 128.84, 130.55, 132.54, 136.38, 136.58, 136.79, 137.02, 137.77, 138.49, 141.85, 152.79, 153.34, 158.42. Mass calculated ($C_{141}H_{200}O_9$): 2037.52; Found: 2037.349.

38. A solution of malonyl dichloride (40 mg, 0.30 mmol) in 2.1 ml of DCM was added dropwise to a stirred, degassed solution of **35** (1.103 g, 0.601 mmol), DIPEA (0.11 ml, 0.62 mmol) and DMAP (8 mg, 0.07 mmol) in 10 ml of CH_2Cl_2. The mixture was allowed to stir for 20h at RT. The resulting CH_2Cl_2 solution was washed with water and brine, dried over $MgSO_4$, paperfiltered and the solvent was removed by rotary evaporator. Further purification by column chromatography (SiO_2, DCM/cyclohexane 9/1 → DCM) yielded a yellow solid (838 mg, 75%). TLC R_f = 0.7 in DCM. ^1H NMR ($CDCl_3$) δ = 0.89 (t, J = 6.7Hz, 36H), 1.15-1.55 (m, 216H), 1.70-1.90 (m, 24H), 3.53 (s, 2H), 3.88-4.08 (m, 24H), 5.01 (s, 8H), 5.24 (s, 4H), 6.72 (s, 8H), 6.89-7.11 (m, 24H), 7.31-7.50 (m, 30H). ^{13}C NMR ($CDCl_3$) δ = 14.12, 22.72, 26.19, 29.40, 29.49, 29.70, 29.78, 30.41, 31.96, 41.64, 66.77, 69.25, 69.55, 73.55, 105.33, 115.09, 126.32, 126.42, 126.50, 126.62, 126.71, 127.32, 127.79, 127.90, 128.70, 130.63, 132.58, 136.15, 136.49, 136.76, 137.87, 138.49, 153.35, 158.31, 166.08. Mass calculated ($C_{253}H_{376}O_{20}$): 3734.84; Found (M+H): 3735.960.

39. A solution of malonyl dichloride (70 mg, 0.50 mmol) in 3.5ml of DCM was added to a stirred degassed solution of **37** (2.004 g, 0.983 mmol), DIPEA (20 mg, 0.15 mmol) and DMAP (17 mg, 0.14 mmol) in 21 ml of CH_2Cl_2. Then the mixture was allowed to stir for 18.5 h at RT. The resulting CH_2Cl_2 solution was washed with water and brine, dried over $MgSO_4$, paperfiltered and the solvent was removed by rotary evaporator. Further purification by column chromatography (SiO_2, DCM/cyclohexane 9/1) gave an orange solid (1.70 mg, 83%). ^1H NMR ($CDCl_3$) δ = 0.89 (t, J = 6.6Hz, 36H), 1.15-1.57 (m, 216H), 1.70-1.90 (m, 24H), 3.55 (s,

2H), 3.85-4.10 (m, 24H), 4.91 (br s, 8H), 5.23 (br s, 4H), 6.72 (s, 8H), 6.83-7.14 (m, 32H), 7.28-7.55 (m, 46H). ^{13}C NMR (CDCl$_3$) δ = 14.10, 22.70, 26.12, 26.16, 29.38, 29.39, 29.48, 29.51, 29.68, 29.71, 29.73, 29.77, 30.40, 31.94, 41.76, 66.70, 69.24, 69.48, 73.55, 105.34, 115.08, 126.19, 126.25, 126.45, 126.66, 126.74, 126.87, 127.26, 127.81, 127.98, 128.10, 128.87, 130.56, 132.51, 136.14, 136.36, 136.52, 136.79, 136.94, 137.83, 138.52, 152.79, 153.35, 158.29, 166.04. Mass calculated (C$_{285}$H$_{400}$O$_{20}$): 4143.03; Found (M+H) : 4143.606.

40. DBU (97 mg, 0.64 mmol) was added dropwise to a solution of **38** (432 mg, 0.116 mmol), C$_{60}$ (83 mg, 0.12 mmol), and I$_2$ (80 mg, 0.32 mmol) in 125 ml of toluene. The mixture was stirred at RT for 22h. Then the product was filtered on a short silica plug, washed with toluene and evaporated. The residue was further purified by column chromatography (SiO$_2$, cyclohexane/DCM 4/1 → 1/1). Dark brown solid was obtained (193 mg, 38%; plus another 60 mg, 11% of isomeric mixture). TLC R$_f$ = 0.2 in cyclohexane/DCM 4/1. ^{1}H NMR (CDCl$_3$) δ = 0.91 (t, J = 6.3Hz, 36H), 1.15-1.57 (m, 216H), 1.70-1.90 (m, 24H), 3.85-4.10 (m, 24H), 4.75-5.10 (m, 8H), 5.30-5.60 (m, 4H), 6.73 (d, J=1.6Hz, 8H), 6.81-7.11 (m, 24H), 7.28-7.55 (m, 30H). ^{13}C NMR (CDCl$_3$) δ = 14.12, 22.72, 26.19, 29.40, 29.50, 29.53, 29.71, 29.75, 29.79, 30.43, 31.96, 51.78, 68.35, 69.25, 69.56, 71.39, 73.56, 105.33, 115.11, 126.65, 126.72, 127.31, 127.84, 128.73, 130.69, 132.57, 135.62, 136.50, 136.74, 138.01, 138.50, 139.03, 140.94, 141.77, 142.15, 142.94, 142.98, 143.02, 143.83, 144.49, 144.59, 144.65, 144.89, 145.02, 145.15, 145.22, 153.36, 158.29, 163.27. Mass calculated (C$_{313}$H$_{374}$O$_{20}$): 4452.82; Found: 4452.545.

41. DBU (60 mg, 0.394 mmol) was added dropwise to a solution of **39** (350 mg, 0.084 mmol), C$_{60}$ (63 mg, 0.087 mmol), and I$_2$ (87 mg, 0.34 mmol) in 91 ml of toluene. The mixture was stirred at RT for 22h. Then the product was filtered on a short silica plug, washed with DCM/cyclohexane 4/1 v/v mixture. The residue was further purified by column chromatography (cyclohexane/DCM 4/1 to 1/4) and GPC. Dark brown solid was obtained (110 mg, 27%). TLC R$_f$ = 0.2 in cyclohexane/DCM 4/1. ^{1}H NMR (CDCl$_3$) δ = 0.80-0.98 (m, 36H), 1.15-1.57 (m, 216H), 1.65-1.90 (m, 24H), 3.75-4.15 (m, 24H), 4.30-5.00 (m, 8H), 5.10-5.70 (m, 4H), 6.40-7.10 (m, 40H), 7.10-7.60 (m, 46H). ^{13}C NMR (CDCl$_3$) δ = 14.11, 22.71, 26.21, 29.41, 29.55, 29.72, 30.44, 31.96, 51.76, 63.12, 69.23, 71.41, 73.55, 105.36, 115.09, 126.47, 126.78, 126.92, 127.23, 127.92, 128.64, 128.93, 130.53, 132.52, 135.62, 136.32, 136.47,

136.78, 137.90, 138.31, 138.55, 139.08, 140.94, 141.78, 142.15, 142.94, 142.98, 143.82, 144.60, 144.65, 144.87, 145.02, 145.15, 145.22, 152.80, 153.37, 158.26, 163.24. Mass calculated ($C_{345}H_{398}O_{20}$): 4861.01; Found (M+H): 4862.263.

41bis. Another dark brow solid (isomeric mixture of bisadducts) was also obtained (70 mg, 18%). Mass calculated ($C_{630}H_{796}O_{40}$) = 9009.04; Found: 9015.734 (linear mode).

42. Malonyl dichloride (130 mg, 0.922 mmol) was added to a stirred degassed solution of **14** (2.118 g, 1.849 mmol) and pyridine (0.15 ml, 1.9 mmol) in 25 ml of CH_2Cl_2 at 0 °C. The solution was allowed to warm up to room temperature and stirred for another 4.5 hours. The resulting CH_2Cl_2 solution was washed with water twice and brine, dried over $MgSO_4$, filtered and evaporated. Further purification with column chromatography (SiO_2, EtOAc to Ac) gave a yellow oil (1.11 g, 51%, 64% based on recovered **14**). TLC R_f = 0.3-0.7 in Ac. ^{1}H NMR ($CDCl_3$) δ = 3.36 (s, 24H), 3.49-3.56 (m, 18H), 3.58-3.74 (m, 80H), 3.83 (m, 16H), 4.10 (t, J = 4.8Hz, 16H), 4.92 (s, 8H), 5.12 (s, 4H), 6.44 (t, J = 2.1 Hz, 4H), 6.53 (t, J = 2.1 Hz, 2H), 6.57 (m, 12H). ^{13}C NMR ($CDCl_3$) δ = 41.38, 58.97, 67.02, 67.51, 69.64, 69.99, 70.49, 70.61, 70.78, 71.92, 101.17, 101.97, 106.11, 107.01, 137.51, 138.97, 160.02, 160.10, 166.17. FTIR (KBr, cm^{-1}) 1736 and 1751 (C=O). Mass calculated ($C_{117}H_{184}O_{48}$) = 2380.19; Found: 2379.978. Calculated C: 59.58%; H: 7.86%; Found C: 59.25%; H, 8.00%.

43. A mixture of **42** (190 mg, 0.081 mmol), C_{60} (81 mg, 0.11 mmol), DBU (71 mg, 0.47 mmol) and I_2 (54 mg, 0.21 mmol) in 87 ml of toluene was stirred at RT for 43h. Then the product was filtered on a short silica plug, washed with toluene in order to remove the unreacted C_{60} and the I_2, with DCM and with Ac + 5% MeOH afterwards to separate the product. The crude product was further purified by column chromatography (SiO_2, Ac to Ac + 5% MeOH) to give a dark brown liquid (100 mg, 40%). TLC R_f = 0.5-0.8 in Ac + 5% MeOH. ^{1}H NMR ($CDCl_3$) δ = 3.35 (s, 24H), 3.48-3.54 (m, 16H), 3.58-3.72 (m, 80H), 3.80 (t, J = 4.6Hz, 16H), 4.06 (t, J = 4.8Hz, 16H), 4.86 (s, 8H), 5.44 (s, 4H), 6.42 (t, J = 2.1 Hz, 4H), 6.53 (m, 10H), 6.68 (d, J = 2.2 Hz, 4H). ^{13}C NMR ($CDCl_3$) δ = 51.91, 58.99, 67.53, 68.82, 69.64, 70.08, 70.49, 70.60, 70.77, 71.44, 71.92, 101.29, 102.47, 106.23, 107.78, 136.86, 138.80, 138.95, 140.82, 141.78, 142.12, 142.90, 142.95, 143.77, 144.43, 144.46, 144.60, 144.82, 144.94, 145.03, 145.09, 145.14, 160.08, 160.11, 163.27. FTIR (KBr, cm^{-1}) 1748 (C=O). Mass calculated

($C_{177}H_{182}O_{48}Na$) = 3098.17; Found: 3098.212. Calculated C: 69.08%; H: 5.97%; Found C: 67.94%; H, 5.73%.

44. A solution of TBDMSCl (653 mg, 4.33 mmol) in 50ml of DCM was added dropwise to a solution of tetraethylene glycol (8.006 g, 41.22 mmol), imidazole (3.368 g, 49.47 mmol) and DMAP (0.460 mg, 4.10 mmol) in 125 ml of DCM at 0 °C. The reaction mixture was allowed to stir at 0-5°C for 5h. The reaction was quenched with 250ml of H_2O, the organic layer was separated and washed with brine. The organic solution was dried over $MgSO_4$, filtered and further purified by column chromatography (SiO_2, EtOAc) to afford a colorless oil (5.46 g, 43%). TLC R_f = 0.3-0.5 in EtOAc. ^1H NMR ($CDCl_3$) δ = 0.00 (s, 6H), 0.83 (s, 9H), 2.89 (br s, 1H), 3.45-3.74 (m, 16H). ^{13}C NMR ($CDCl_3$) δ = -5.32, 18.29, 25.87, 61.60, 62.66, 70.33, 70.59, 70.66, 72.51, 72.61.

45. A solution of TsCl (3.625 mg, 19.01 mmol) in 10 ml of DCM was added dropwise to a solution of **44** (5.261 mg, 17.05 mmol), freshly prepared Ag_2O (5.894 mg, 25.43 mmol) and KI (0.283 mg, 1.69 mmol) in 35 ml of DCM. The reaction mixture was allowed to stir at 0 °C for 20min and at 40 °C for 4days (during that time the TLC spot of **44** did not disappear totally, even if more reagents were added). The precipitated silver salts were removed by filtration through a pad of silica, which was washed first with DCM (in order to remove unreacted TsCl) and with EtOAc afterwards. The EtOAc fraction was evaporated and the crude product was purified by column chromatography (SiO_2, DCM/EtOAc 9/1 to 4/1) to afford a transparent, pale yellow oil (6.26 g, 79%; 84% based on recovered **44**). TLC R_f = 0.6-0.8 in DCM/EtOAc 9/1. ^1H NMR ($CDCl_3$) δ = 0.04 (s, 6H), 0.87 (s, 9H), 2.43 (s, 3H), 3.53 (t, J=5.5Hz, 2H), 3.55-3.65 (m, 8H), 3.67 (t, J=4.8Hz, 2H), 3.74 (t, J=5.5Hz, 2H), 4.14 (t, J=4.9Hz, 2H), 7.33 (AA' part of an AA'BB' system, J = 8.5Hz, 2H), 7.78 (BB' part of an AA'BB' system, J = 8.3Hz, 2H). ^{13}C NMR ($CDCl_3$) δ = -5.27, 18.35, 21.60, 25.92, 62.70, 68.67, 69.22, 70.54, 70.68, 70.70, 70.75, 72.67, 127.96, 129.79, 133.10, 144.73.

46. A solution of **45** (1.785 g, 3.858 mmol) in 5 ml of THF was added dropwise to a mixture of **14** (4.002 mg, 3.494 mmol), KI (120 mg, 0.723 mmol), NaH (341 mg, 8.52 mmol – 60% in mineral oil) and 15-crown-5 (769 mg, 3.49 mmol) in 12.5 ml of dry THF. The mixture was allowed to stir at RT for 9h and then the excess of NaH was quenched with MeOH (~10ml – until the mixture became transparent). The solvent was evaporated; the residue

was dissolved in DCM and washed with NaHCO$_3$ and brine. The organic solution was dried over MgSO$_4$, filtered and further purified by column chromatography (SiO$_2$, DCM to EtOAc/Ac 1/1). Evaporation of the solvent gave a yellow oil (3.77 g, 75%). TLC R$_f$ = 0.4 in EtOAc/Ac 1/1. ^{1}H NMR (CDCl$_3$) δ = -0.05 (s, 6H), 0.78 (s, 9H), 3.25 (s, 12H), 3.38-3.45 (m, 10H), 3.47-3.67 (m, 54H), 3.73 (t, J=4.8Hz, 8H), 4.00 (t, J=4.8Hz, 8H), 4.39 (s, 2H), 4.83 (s, 4H), 6.33 (t, J = 2.1Hz, 2H), 6.39 (t, J = 2.1Hz, 1H), 6.44-6.50 (m, 6H). ^{13}C NMR (CDCl$_3$) δ = -5.30, 18.26, 25.88, 58.87, 62.63, 67.42, 69.38, 69.56, 69.80, 70.40, 70.51, 70.53, 70.62, 70.71, 71.84, 72.56, 72.94, 101.01, 101.15, 105.95, 106.39, 139.13, 140.76, 159.86, 160.01.

47. TBAF (0.15 ml, 0.15 mmol, 1M in THF) was added dropwise to a solution of **46** (0.20 g, 0.14 mmol) in 1 ml of dry THF at RT. After stirring for 1.5h the THF was removed by evaporation. The crude product was dissolved in DCM and washed with brine, dried over MgSO$_4$, filtered and further purified by column chromatography (SiO$_2$, Ac + 2% MeOH → Ac + 4% MeOH). 145 mg (78%) of colorless oil was obtained. TLC R$_f$ = 0.3-0.6 in Ac + 2% MeOH. ^{1}H NMR (CDCl$_3$) δ = 2.55 (t, J=6.2Hz, 1H), 3.36 (s, 12H), 3.50-3.55 (m, 8H), 3.51-3.75 (m, 56H), 3.83 (t, J=4.9Hz, 8H), 4.10 (t, J=4.8Hz, 8H), 4.50 (s, 2H), 4.93 (s, 4H), 6.44 (t, J=2.2Hz, 2H), 6.50 (t, J=2.0Hz, 1H), 6.55-6.60 (m, 6H). ^{13}C NMR (CDCl$_3$) δ = 58.93, 61.64, 67.50, 69.42, 69.63, 69.91, 70.31, 70.46, 70.59, 70.77, 71.90, 72.48, 73.01, 101.12, 101.25, 106.08, 106.50, 139.16, 140.79, 159.93, 160.06. Mass calculated (C$_{65}$H$_{108}$O$_{27}$Na) = 1343.70; Found: 1343.957.

48. Malonyl dichloride (0.10 g, 0.71 mmol) was added to a stirred and degassed solution of **47** (1.908 g, 1.444 mmol) and pyridine (0.12 ml, 1.5 mmol) in 20 ml of CH$_2$Cl$_2$ at 0 °C. The solution was allowed to warm up slowly to room temperature (over 1 h) and stirred for another 5.5 hours at RT. The resulting CH$_2$Cl$_2$ solution was washed with NaHCO$_3$, and brine, dried over MgSO$_4$, filtered and evaporated. Further purification of the dark blue crude product by column chromatography (SiO$_2$, Ac + 2% MeOH) gave a yellow oil (1.006 g, 52%). TLC R$_f$ = 0.7 in Ac/MeOH 9/1. ^{1}H NMR (CDCl$_3$) δ = 3.36 (s, 24H), 3.42 (s, 2H), 3.49-3.56 (m, 16H), 3.60-3.74 (m, 108H), 3.83 (t, J = 4.9Hz, 16H), 4.10 (t, J = 4.9Hz, 16H), 4.27 (t, J = 5.0Hz, 4H), 4.49 (s, 4H), 4.93 (s, 8H), 6.43 (t, J = 2.2 Hz, 4H), 6.49 (t, J = 2.2 Hz, 2H), 6.54-6.60 (m, 12H). ^{13}C NMR (CDCl$_3$) δ = 41.22, 58.98, 64.52, 67.53, 68.82, 69.46, 69.66, 69.96, 70.51, 70.62, 70.80, 71.95, 73.08, 101.15, 101.25, 106.14, 106.53, 139.16, 140.82, 159.98, 160.10,

166.39. Mass calculated ($C_{133}H_{216}O_{56}Na$) = 2732.40; Found: 2732.400. Calculated C: 58.92%; H: 8.03%; Found C: 57.93%; H, 8.00%.

49. A mixture of **48** (199 mg, 0.073 mmol), C_{60} (50 mg, 0.069 mmol), DBU (62 mg, 0.41 mmol), I_2 (46 mg, 0.18 mmol) in 76 ml of toluene was stirred at RT for 5h. Then the product was filtered on a short silica plug, washed with toluene in order to remove the unreacted C_{60} and the I_2 and with Ac + 10% MeOH afterwards to separate the product. The solvent was evaporated and the residue was further purified by column chromatography (SiO_2, Ac + 5% MeOH). The fraction containing the monoadduct was further purified by GPC and a dark brown oil was obtained (55 mg, 23%). TLC R_f = 0.7 (monoadduct) in Ac/MeOH 9/1. ^{1}H NMR (CDCl$_3$) δ = 3.36 (s, 24H), 3.49-3.56 (m, 16H), 3.60-3.75 (m, 104H), 3.83 (t, J = 4.7Hz, 20H), 4.10 (t, J = 4.7Hz, 16H), 4.48 (s, 4H), 4.62 (t, J = 4.7 Hz, 4H) 4.92 (s, 8H), 6.40-6.45 (m, 4H), 6.46-6.51 (m, 2H), 6.52-6.60 (m, 12H). ^{13}C NMR (CDCl$_3$) δ = 58.99, 66.23, 67.54, 68.76, 69.47, 69.68, 69.97, 70.51, 70.64, 70.81, 71.50, 71.95, 73.09, 101.18, 101.25, 106.18, 106.54, 139.05, 139.15, 140.82, 140.88, 141.83, 142.17, 142.94, 142.98, 143.04, 143.85, 144.58, 144.65, 144.85, 145.14, 145.22, 145.30, 159.99, 160.10, 163.43. Mass calculated a) monoadduct: ($C_{193}H_{214}O_{56}Na$) = 3450.38; Found: 3450.200; ($C_{193}H_{214}O_{56}K$) = 3466.35; Found: 3466.156.

49bis. Another dark brown oil (84 mg, 20%; 37% based on the amount of initial **48**) was separated and identified as bisadduct. TLC R_f = 0.3 in Ac/MeOH 9/1. Mass calculated ($C_{326}H_{428}O_{112}Na$) = 6161.81; Found: 6160.04 (linear mode).

50. A solution of **42** (82 mg, 0.035 mmol) and N-bromosuccinimide (6 mg, 0.04 mmol) was dissolved in 2 ml of DMSO and stirred at RT for 2 h. The solution was washed with NH$_4$Cl and brine and dried over MgSO$_4$. Further purification with preparative TLC (Ac + 5% MeOH) yielded a yellow oil (58 mg, no yield was calculated, because the product is an inseparable mixture of unreacted, mono- and dibrominated compounds). Mass calculated a) unreacted: ($C_{117}H_{183}O_{48}Na$) = 2379.18; Found: 2380.377; b) monobrominated compound ($C_{117}H_{182}O_{48}NaBr$) = 2458.10; Found: 2458.282; c) dibrominated compound ($C_{117}H_{181}O_{48}Br_2$) = 2535.00; Found: 2537.207.

51. Method A: DBU (30 mg, 0.20 mmol) was injected into a mixture of **42**, Gd$_3$N@C$_{80}$ (16 mg, 0.011 mmol) and CBr$_4$ (244 mg, 0.736 mmol) in 33 ml of chlorobenzene and the mixture was allowed to stir at RT for 26.5h. Then the product was filtered on a short silica plug, washed with solvents with different polarity (toluene to Ac + 10% MeOH) in order to separate different products. Only unidentifiable products were obtained.

Method B: DBU (8 mg, 0.05 mmol) in 3 ml of DMF was injected into a mixture of **50** (254 mg, appr. 0.1 mmol) and Gd$_3$N@C$_{80}$ (16 mg, 0.011 mmol) in 30 ml of chlorobenzene and the reaction mixture was allowed to stir at RT for 1.5h. The reaction mixture was purified by preparative TLC. First the plate was eluted with CS$_2$ to remove unreacted Gd$_3$N@C$_{80}$ which elutes with the solvent front and then with more polar solvents to separate the products. The isolation of the desired product was unsuccessful.

52. DBU (0.03 g, 0.22 mmol) in 1 ml of CH$_2$Cl$_2$ was added dropwise to a stirred and degassed solution of **48** (502 mg, 0.185 mmol) and CBr$_4$ (630 mg, 1.900 mmol) in 15 ml of CH$_2$Cl$_2$ at 0 °C. The solution was allowed to stir for 2 hours at 0°C. Further purification with column chromatography (SiO$_2$, Ac +3% MeOH) gave a yellow oil (380 mg, 72%). ^{1}H NMR (CDCl$_3$) δ = 3.39 (s, 24H), 3.49-3.56 (m, 16H), 3.60-3.74 (m, 108H), 3.84 (t, J = 4.8Hz, 16H), 4.11 (t, J = 5.2Hz, 16H), 4.38-4.44(m, 4H), 4.50 (s, 4H), 4.93 (s, 8H), 6.44 (t, J = 2.3 Hz, 4H), 6.50 (t, J = 2.2 Hz, 2H), 6.54-6.61 (m, 12H). ^{13}C NMR (CDCl$_3$) δ = 49.95, 58.90, 67.45, 67.50, 68.26, 69.39, 69.57, 69.84, 70.41, 70.53, 70.67, 70.72, 71.85, 72.95, 101.04, 101.15, 106.00, 106.43, 139.13, 140.78, 159.88, 160.02, 162.96. Mass calculated (C$_{133}$H$_{214}$Br$_2$NaO$_{56}$) = 2888.22; Found: 2888.138.

53. A mixture of DBU (16 mg, 0.11 mmol) in 0.8ml of CH$_3$CN was added dropwise to a stirred degassed solution of **52** (117 g, 0.042 mmol) and Gd$_3$N@C$_{80}$ (15 mg, 0.010 mmol) in chlorobenzene (23 mL)/ CH$_3$CN (5 ml) mixture at RT. The solution was allowed to stir for 14 hours at RT and purified on preparative TLC plates. First the plate was eluted with CS$_2$ to remove unreacted Gd$_3$N@C80 which elutes with the solvent front, then with Ac + 5% MeOH to separate the product. A dark brown liquid was obtained. Mass calculated (C$_{213}$H$_{214}$Gd$_3$NNaO$_{56}$) = 4178.69; Found: 4176.402.

A1. The TBDMSCl (4.99 g, 33.29 mmol) and imidazole (4.32 g, 63.42 mmol) were added to a solution of dimethyl-5-hydroxyisophtalate (6.67 g, 31.71 mmol) in DMF (125 mL) at 0 °C. After stirring for 3 h at 0 ° C, the solvent was evaporated and the resulting residue was taken up in Et_2O. The organic phase was then washed with saturated aqueous NaCl and dried (MgSO4), filtered and evaporated. After purification by column chromatography (SiO_2, CH_2Cl_2), the pure product was obtained as a white solid with a yield of 86% (8.84 g, 27.24 mmol). ^{1}H NMR (CDCl 3, 200 MHz): δ = 0.24 (s, 6H), 1.01 (s, 9H), 3.94 (s, 6H), 7.68 (d, J = 2 Hz, 2H), 8.30 (t , J = 2 Hz, 1H). ^{13}C NMR (CDCl3, 50 MHz): δ = 18.15, 25.58, 52.36, 68.67, 70.55, 71.89, 123.63, 125.32, 131.77, 155.89, 166.08; Calculated C: 59.22, H: 7.46; Found C: 59.44, H: 7.47.

A2. $LiAlH_4$ (23 ml, 23 mmol, 1M in THF) was added dropwise to a stirred solution of **A1** (5.02 g, 15.5 mmol) in 5 ml of THF at 0 °C. The mixture was allowed to stir for 3.5 hours while warming up to RT. The access $LiAlH_4$ was neutralized with a few droplets of MeOH and 10 ml of water. After filtration on celite and evaporation the crude product was dissolved in DCM and washed twice with brine. Then the collected organic phases were dried over $MgSO_4$, filtered and evaporated. White solid material was obtained (3.05 g, 74%). ^{1}H NMR (CDCl$_3$) δ = 0.20 (s, 6H), 0.99 (s, 9H), 2.06 (br s, 2H), 4.61 (s, 4H), 6.75 (s, 2H), 6.94 (s, 1H). ^{13}C NMR (CDCl$_3$) δ = -4.38, 18.17, 25.66, 65.01, 117.66, 118.15, 142.75, 156.12.

A3. A mixture of Meldrum's acid (35 mg, 2.4 mmol) and **A2** (31 mg, 1.2 mmol) was heated for 4h at 120 °C. Then the product was dried under vacuum. ^{1}H NMR (CDCl$_3$) δ = 0.20 (s, 6H), 0.98 (s, 9H), 3.47-3.54 (m, 4H), 5.02-5.19 (m, 4H), 6.70-6.83 (m, 2H), 6.89-7.02 (m, 1H). ^{13}C NMR (CDCl$_3$) δ = -4.43, 18.17, 25.63, 41.21, 66.96, 119.38, 120.20, 136.95, 155.98, 166.10, 171.61.

A5. A mixture of **A3** (103 mg, 0.234 mmol), **A4**[8] (336 mg, 0.450 mmol), DCC (276 mg, 1.34 mmol), DPTS (127 mg, 0.431 mmol) and 4-ppy(11 mg, 0.074 mmol) in 3 ml of DCM was stirred overnight at RT. The solvent was evaporated, the crude product was dissolved in toluene and cooled down (kept in the fridge) in order to precipitate DCU. The precipitate was filtered and washed with toluene. The crude product was further purified by column chromatography (SiO_2, DCM to DCM + 2% EtOAc) to yield a white solid material (0.39g, 89%). TLC R$_f$ = 0.3 in DCM. ^{1}H NMR (CDCl$_3$) δ = 0.20 (s, 6H), 0.80-0.94 (t, J = 6.7Hz, 12H), 0.98

(s, 9H), 1.13-1.68 (m, 68H), 1.71-1.91 (m, 12H), 3.42 (br s, 4H), 3.95 (t, J= 6.5 Hz, 4H),), 4.05 (t, J= 6.6 Hz, 8H), 4.12 (t, J= 6.8 Hz, 4H), 5.11 (br s, 4H), 6.79 (s, 2H), 6.85-6.95 (m, 9H), 6.99 (d, J = 9.0 Hz, 4H), 7.11 (d, J = 9.0 Hz, 4H), 8.07 (d, J = 9.0 Hz, 2H), 8.14 (d, J = 8.8 Hz, 4H). ^{13}C NMR (CDCl$_3$) δ = -4.43, 14.08, 18.17, 22.64, 25.64, 25.74, 25.92, 25.98, 26.05, 28.43, 29.10, 29.16, 29.20, 29.23, 29.26, 29.30, 29.31, 29.36, 29.40, 31.79, 31.82, 41.50, 65.75, 66.63, 66.72, 68.40, 68.46, 69.23, 107.17, 113.41, 114.42, 115.08, 116.80, 119.66, 120.58, 121.06, 121.42, 122.47, 129.22, 132.37, 133.32, 137.11, 144.39, 155.70, 156.09, 156.78, 160.57, 163.80, 164.29, 164.39, 166.34, 166.39. IR (KBr, cm^{-1}): ν = 1734 (C=O).

A6. A mixture of **A5** (252 mg, 0.133 mmol), C$_{60}$ (94 mg, 0.13 mmol), DBU (100 mg, 0.657 mmol) and I$_2$ (92 mg, 0.36 mmol) in 136 ml of toluene was stirred at RT for 24h. Then the product was filtered on a short silica plug, washed with toluene in order to remove the unreacted C$_{60}$ and the I$_2$ and with DCM + 5% EtOAc mixture afterwards to separate the product. The crude product was further purified by column chromatography (SiO$_2$, DCM to DCM + 2% EtOAc) to give a rusty brown solid (80 mg, 24%). TLC R$_f$ = 0.8 in DCM. ^{1}H NMR (CDCl$_3$) δ = 0.25 (s, 6H), 0.84-0.95 (m, 12H), 1.01 (s, 9H), 1.13-1.56 (m, 64H), 1.63-1.91 (16H), 3.96 (t, J = 6.5 Hz, 4H), 4.06 (t, J = 6.3 Hz, 8H), 4.34 (t, J = 6.3 Hz, 4H), 5.08 (d, J = 12.6 Hz, 2H), 5.80 (d, J = 12.6 Hz, 2H), 6.74 (d, J = 1 Hz, 2H), 685-6.95 (m, 8H), 6.99 (d, J = 9.0 Hz, 4H), 7.07-7.15 (m, 5H), 8.08 (d, J = 9.0 Hz, 2H), 8.15 (d, J = 8.7 Hz, 4H). ^{13}C NMR (CDCl$_3$) δ = -4.29, 14.11, 18.19, 22.66, 25.67, 25.85, 25.91, 26.01, 26.08, 28.49, 29.11, 29.22, 29.26, 29.34, 29.38, 29.43, 31.81, 31.83, 49.52, 67.11, 67.21, 67.25, 68.43, 68.47, 69.23, 70.82, 107.18, 113.45, 114.45, 115.09, 116.32, 116.79, 118.15, 121.10, 122.49, 132.42, 133.37, 134.96, 135.87, 136.24, 137.62, 137.98, 140.03, 141.05, 141.30, 142.35, 143.16, 143.31, 143.59, 143.78, 143.99, 144.15, 144.28, 144.42, 144.59, 145.06, 145.20, 145.40, 145.63, 145.75, 145.79, 146.08, 146.26, 147.32, 147.48, 147.54, 148.82, 155.73, 156.78, 160.59, 162.84, 162.90, 163.82, 164.26, 164.35. IR (KBr, cm^{-1}): ν = 1738 (C=O). Mass calculated: (C$_{172}$H$_{152}$O$_{23}$SiNa) = 2636.04; Found: 2636.019. Calculated C: 78.94%; H: 5.93%; Found C: 78.67%; H, 5.85%.

---

[1] Moore, J. S.; Stupp, S. I., *Macromolecules,* **1990,***23*, 65.

[2] Tanabe, M., Peters R. H., *Org Synth. Coll. Vol. VII*, **1990**, 386.

[3] Kauffman, G. B.; Fang, L. Y., *Inorg. Synth.*, **1983**, 101–103.

[4] J. N. Demas and G. A. Crosby, *J. Phys. Chem.* **1971**, *75*, 991-1024.

[5] M. Montalti, A. Credi, L. Prodi, M. T. Gandolfi, in *Handbook of Photochemistry*, ed. Taylor & Francis, London, 3rd edn., **2006**, ch. 10.

[6] Y. Rio, G. Accorsi, H. Nierengarten, C. Bourgogne, J.-M. Strub, A. Van Dorsselaer, N. Armaroli, J.-F. Nierengarten *Tetrahedron* **2003**, *59*, 3833-3844.

[7] J. C. Scaiano, R. W. Redmond, B. Mehta and J. T. Arnason, *Photochem. Photobiol*. **1990**, *52*, 655.

[8] H. Mamlouk, B. Heinrich, C. Bourgogne, B. Donnio, D. Guillon and D. Felder-Flesch, *J. Mater. Chem*., **2007**, *17*, 2199-2205.

Résumé en français

Depuis la découverte des fullerènes en 1985,[1] différentes méthodes de production à l'échelle de plusieurs centaines de grammes, et notamment la méthode dite de Krätschmer-Hufmann,[2] ainsi que de nombreuses techniques de purification ont été très largement optimisées. Dans le domaine de la chimie des matériaux, la nature déficiente en électrons du [60]Fullerène permet non seulement sa fonctionnalisation par substitution nucléophile, mais également son utilisation en tant qu'accepteur d'électrons dans des dispositifs photovoltaïques. Cependant, dans ce domaine, la tendance du C_{60} à induire une séparation de phases dans des dispositifs moléculaires du type hétérojonction en volume (BHJ) reste un obstacle à l'efficacité de ces systèmes.[3] Une possibilité d'éviter cette séparation de phase est basée sur le concept de jonctions moléculaires dans lesquelles donneur et accepteur d'électrons sont reliés de façon covalente formant une diade (D-A).[4] D'autre part, étant largement admis que l'auto-organisation moléculaire améliore l'efficacité photovoltaïque, le greffage de promoteurs mésomorphes sur la sphère carbonée permettrait également de palier à la séparation de phase tout en augmentant la séparation des charges.

La découverte des fullerenes dits "endohédraux", capables d'encapsuler différents éléments sous forme ionique ou en cluster, a immédiatement suivi celle du C_{60}.[5] Dans cette famille, les métallofullerènes endohédraux dits « Nitride trimétalliques » (TNT) méritent une attention particulière, non seulement en raison de leur disponibilité ($Sc_3N@C_{80}$ est le troisième fullerène le plus abondant après le C_{60} et le C_{70}) et de leur très grande stabilité, mais également de leurs propriétés structurelle et électrochimique uniques. En effet, dans une telle molécule, les deux espèces moléculaires instables (C_{80} and Sc_3N^{6-}) se stabilisent mutuellement par transfert électronique formant un sel indissociable extrêmement stable. Par conséquent, les propriétés chimiques des fullerènes TNT diffèrent significativement de ceux de fullerènes vides. Si le métal encapsulé est paramagnétique (eg. gadolinium), de

[1] H. W. Kroto, J. R. Heath, S. C. O'Brien R. F. Curl, R. E; Smalley, *Nature,* **1985**, *318*, 162-163.
[2] W. Krätschmer, L. D. Lamb, K. Fostiropoulos, D. R. Huffman, *Nature*, **1990**, *347*, 354-358.
[3] Yu, G., Gao, J., Hummelen, J. C., Wudl, F. and Heeger, A. J., *Science*, **1995**, *270*, 1789–1791.
[4] Segura, J. L., Martin, N. and Guldi, D. M., *Chem. Soc. Rev.*, **2005**, *34*, 31–47.
[5] Heath, J. R.; O'Brien, S. C.; Zhang, Q.; Liu, Y.; Curl, R. F.; Kroto, H. W.; Tittel, F. K.; Smalley, R. E.; *J. Am. Chem. Soc.*, **1985**, *107*, 7779-7780.

telles molécules « cages » peuvent être utilisées en tant qu'agents de contraste en imagerie par résonance magnétique (IRM) car induisent une relaxivité des protons de l'eau très élevée tout en réduisant fortement la toxicité du gadolinium. En outre, les TNT fullerènes peuvent être utilisés avec succès dans des dispositifs photovoltaïques car il a été a démontré que des diades D-A à base de TNT ont des durées de vie des états à charges séparées nettement augmentées par rapport à leurs homologues contenant du C_{60}.[6]

Cette thèse aborde dans un premier temps la synthèse de diades D-A liquides-cristallines par greffage d'oligomères ð-conjugués au C_{60} ou au $Sc_3N@C_{80}$. Une attention particulière a été portée à l'ingénierie chimique des différents oligomères, ceci afin d'assurer des propriétés liquides-cristallines, amphiphiles et conductrices optimales aux produits finaux et d'examiner l'effet de telles propriétés sur l'efficacité du dispositif photovoltaïque. Dans un second temps, la fonctionnalisation de $Gd_3N@C_{80}$ par un dendron hydrophile et biocompatible est abordée pour confirmer l'intérêt de ces molécules en tant qu'agent de contraste T1 pour l'imagerie par résonance magnétique.

Matériaux cristaux-liquides pour dispositifs photovoltaïques

Synthèse. Les différents oligomères ð -conjugués (oligophénylène éthynylène (OPE), oligophénylène vinylène (OPV3 et OPV4)) utilisés pour la synthèse des diades D-A sont représentés sur la figure 1. Ces unités ont été utilisées - séparément ou combinées à d'autres structures moléculaires - pour préparer le malonate nécessaire à la fonctionnalisation dite de Bingel du C_{60}.[7] L'unité OPE peut être greffée à un dendron oligoéthylène glycol de seconde génération (**14**) par une estérification de Steglich pour former le malonate (**17**) (Figure 2). Le greffage sur le C_{60} aboutit dans ce cas à la formation d'une diade D-A amphiphile avec un rendement de 32%. Dans un second exemple, la synthèse d'un malonate non-dendritique composé uniquement d'unités oligomériques de type OPE a été entreprise (Figure 3).

---

[6] Pinzon, J. R.; Plonska-Brzezinska, M. E.; Cardona, C. M.; Athans, A. J.; Gayathri, S. S.; Guldi, D. M.; Herranz, M. A.; Martin, N.; Torres, T.; Echegoyen, L.; *Angew. Chem. Int. Ed.*, **2008**, *47*, 4173 – 4176.
[7] Bingel, C.; *Chem. Ber.*, **1993**, *126*, 1957 – 1959.
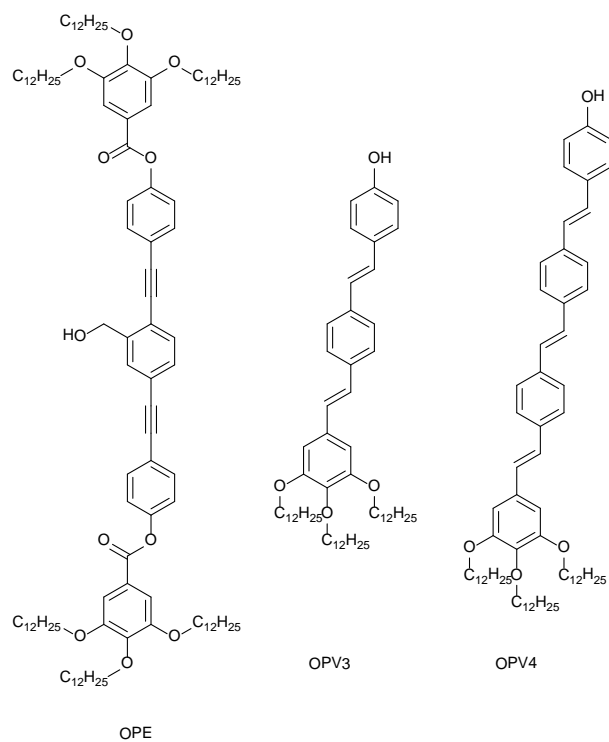
Figure 1 Oligomères π-conjugués utilisés dans les dispositifs photovoltaïques.
A) OPE B) OPV-3 C) OPV-4.
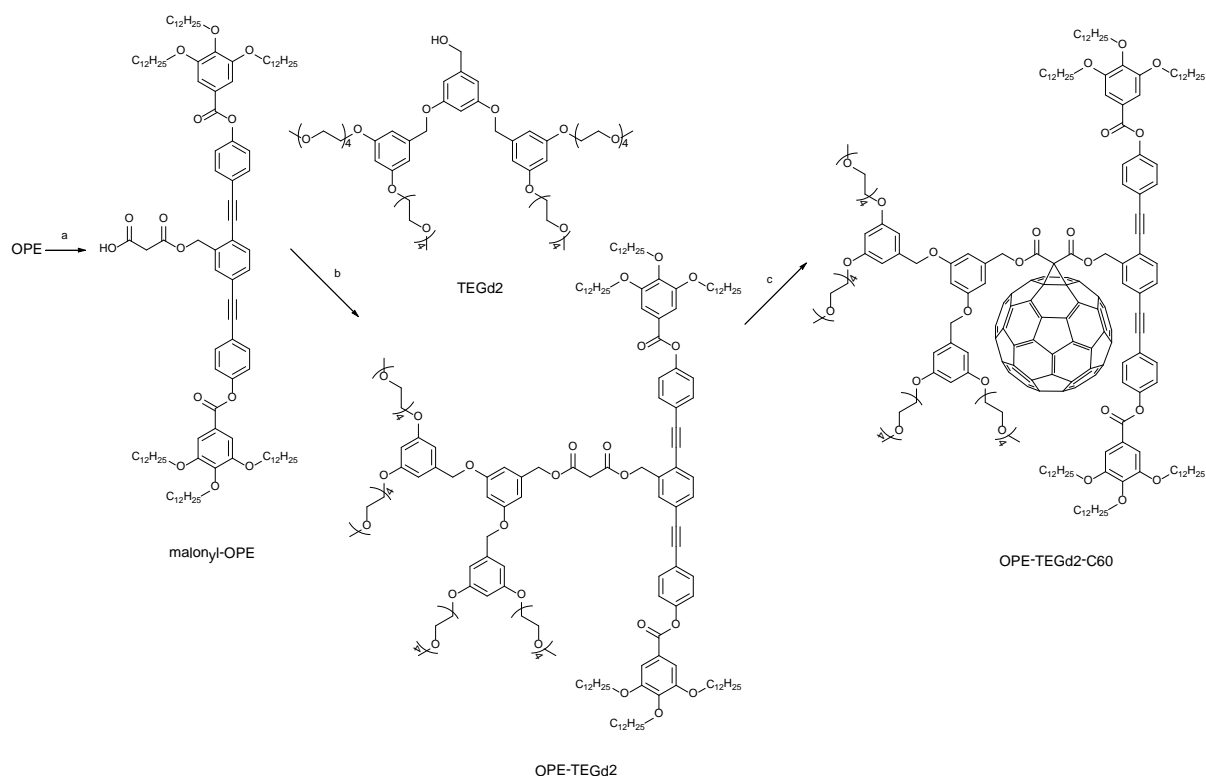
Figure 2 Schéma de synthèse de la diade **18**. Réactifs et conditions: (a) Acide de Meldrum, 110°C, 4h, 100%; (b) *N,N'*-Dicyclohexylcarbodiimide, 4-(diméthylamino)pyridinium 4-toluènesulfonate, 4-pyrrolidinopyridine, CH_2Cl_2, TA, 48h, 32%; (c) C_{60}, 1,8-Diazabicycloundéc-7-ène, I_2, toluène, TA, 3 jours, 87%.
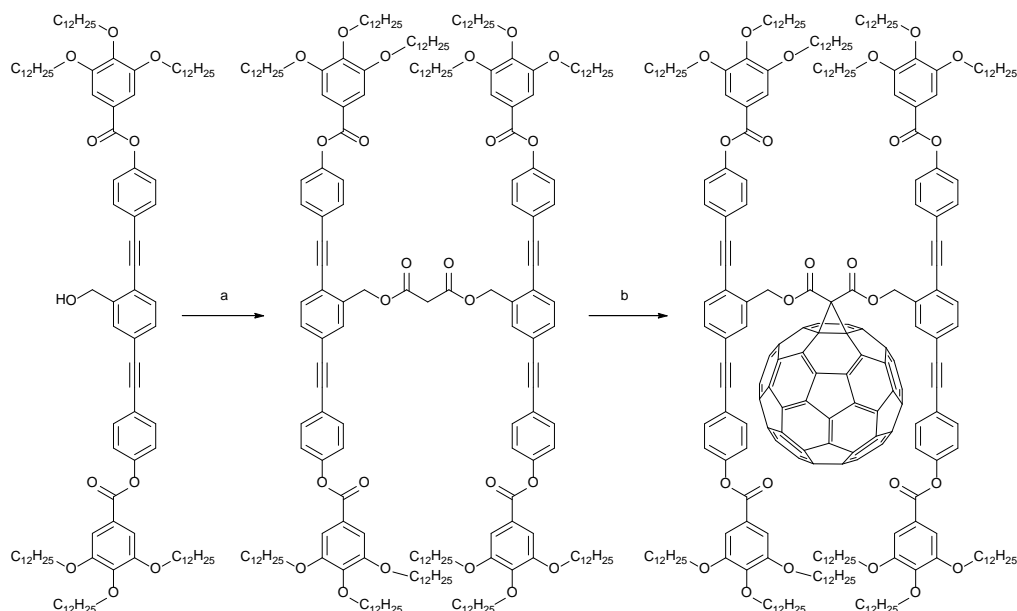
Figure 3 Schéma de synthèse de la diade **16**. Réactifs et conditions: (a) Dichlorure de malonyl, *N,N*-Diisopropyléethylamine, 4-Dimethylaminopyridine, CH_2Cl_2, TA, 20h, 76%; (b) C_{60}, 1,8-Diazabicycloundéc-7-ène, I_2, toluène, TA, 3 jours, 84%.

R = -C₁₂H₂₅
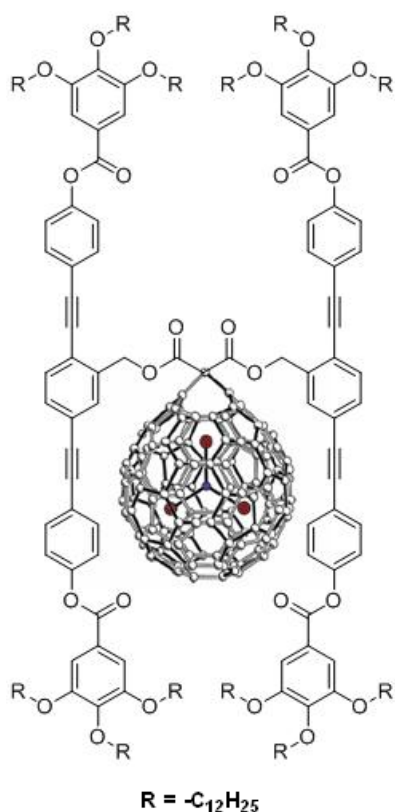
L'OPV est une brique élémentaire électroactive bien connue. Le greffage de quatre unités OPV3 ou OPV4 sur le C_{60} a été effectuée selon le schéma réactionnel décrit Figure 4.

R = OPV3 or OPV4
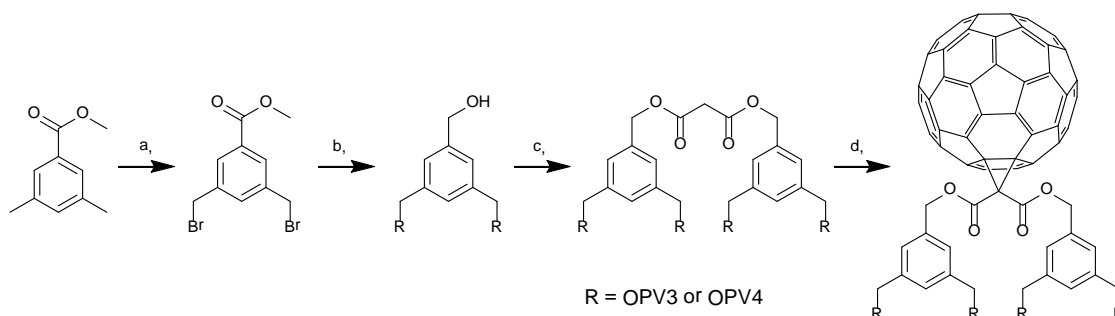
Figure 4 Schéma de synthèse des diades tOPV3-C_{60} et tOPV4-C_{60}. Réactifs et conditions: (a) NBS, AIBN, CCl₄; (b) 1) OPV3, K₂CO₃, KI, Ether couronne 18-c-6, acétone, 20h, 60°C, 79%; 2) LiAlH₄, THF, RT, 4h, 57%; (c) Dichlorure de malonyle, *N,N*-Diisopropyléthylamine, 4-Diméthylaminopyridine, CH₂Cl₂, TA, 36h, 39%; (d) C_{60}, 1,8-Diazabicycloundéc-7-ène, I₂, toluène, TA, 24h, 32%.*

* b, c et d : conditions réactionnelles pour la synthèse de la diade OPV3-C_{60}.

Propriétés mésomorphes. Les propriétés mésomorphes des matériaux mentionnés ci-dessus ont été étudiées par microscopie optique à lumière polarisée (POM) (Figure 5), calorimétrie différentielle (DSC) et diffraction des rayons x aux petits angles (SAXS). Ces études ont révélé une phase SmA de température ambiante à 100°C pour la diade **18**, et une

phase colonnaire rectangulaire avec symétrie pseudo-hexagonale pour la diade dOPE-C$_{60}$ après chauffage à 80°C. L'organisation moléculaire la plus probable de ces composés, basées sur les résultats expérimentaux et notamment les rayons x, est représentée figures 6 et 7.
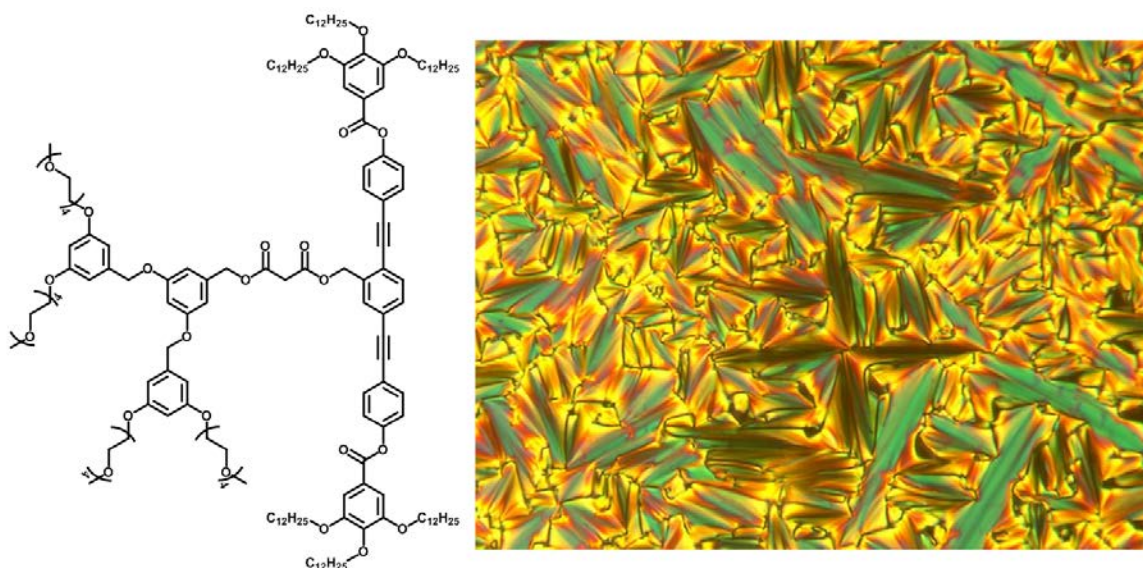
Figure 5 Image POM obtenue à 50°C pour le ligand **17**.
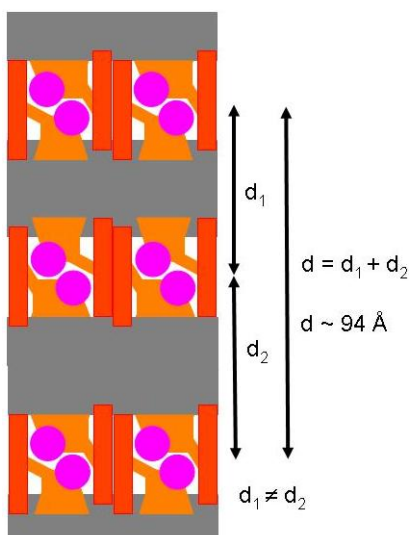
Figure 6 Représentation schématique de l'organisation moléculaire dans la phase SmA pour la diade **18** (rouge: partie calamitique; orange: partie dendritique; gris: chaînes aliphatiques, rose: fullerènes).
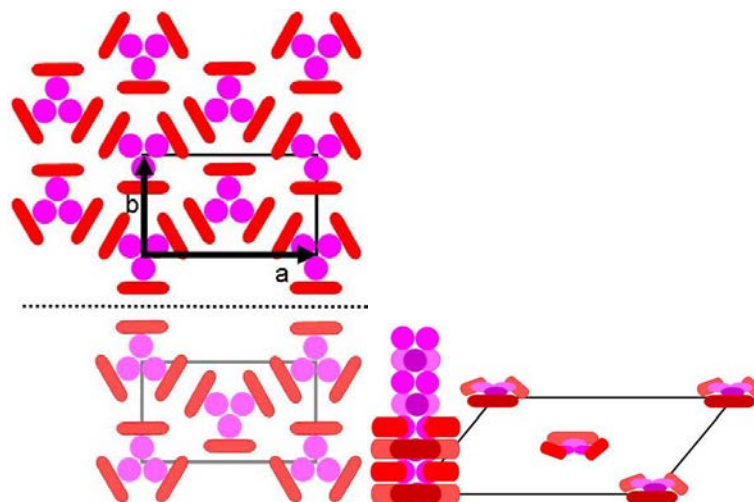
Figure 7 Représentation schématique de l'organisation moléculaire dans la phase ColRpH pour la diade **16** (rouge: partie calamitique; orange: partie dendritique; rose: fullerènes).

Des études photophysiques en solution et sur film, menées en collaboration avec le Professeur Paola Ceroni de l'université de Bologne, ont montré le piégeage significatif de la fluorescence des produits contenant le C_{60}, comparativement aux ligands (Figure 8). En se basant sur les résultats des études électrochimiques, le transfert électronique photoinduit des unités triméthoxy vers le Fullerène est thermodynamiquement autorisé (ΔG ca. -1 eV). Néanmoins, le transfert d'énergie est le processus dominant conduisant au piégeage de l'état excité singulet S_1 de l'OPE et à la sensibilisation de l'émission du Fullerène. En effet, l'intensité d'émission du fullerène à 705 nm, après excitation de deux solutions isoabsorbantes de **16** à 326 nm (plus de 90% de la lumière est absorbée par le chromophore OPE) et à 480 nm (lumière uniquement absorbée par le fullerène), est la même, ce qui démontre l'efficacité unitaire du processus de transfert énergétique. Des résultats similaires ont été obtenus pour le composé **18**.

A 298 K, le temps de vie de l'état excité du fullerène dans le dichlorométhane est de 1.5 ns pour dOPE-C_{60} et de 1.6 ns pour **18**, des valeurs similaires à celles classiquement

observées dans la littérature, de l'ordre de 1.2 - 1.6 ns, pour divers dérivés de C_{60}, suggérant l'absence de piégeage de l'émission du fullerène.

Des études de photophysique en solution dans différents solvants (dichlorométhane, cyclohexane, méthanol, toluène) et à différentes températures (298 et 77K) ont également permis de mettre en évidence une influence de l'état d'agrégation (en fonction de la polarité du solvant) sur les propriétés d'émission (déplacement du maximum d'émission et augmentation du temps de décroissance de la fluorescence) des ligands OPE et dOPE.
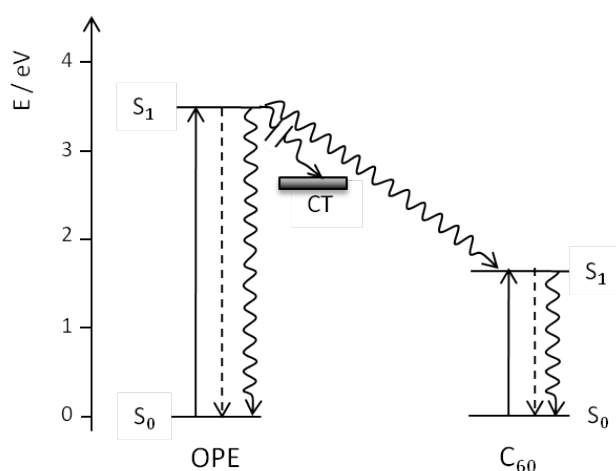
Figure 8 Diagramme des niveaux d'énergie des composés **16** et **18** montrant les processus d'absorption (ligne pleine), d'émission (ligne pointillée) et de désactivation non-radiative (vagues).
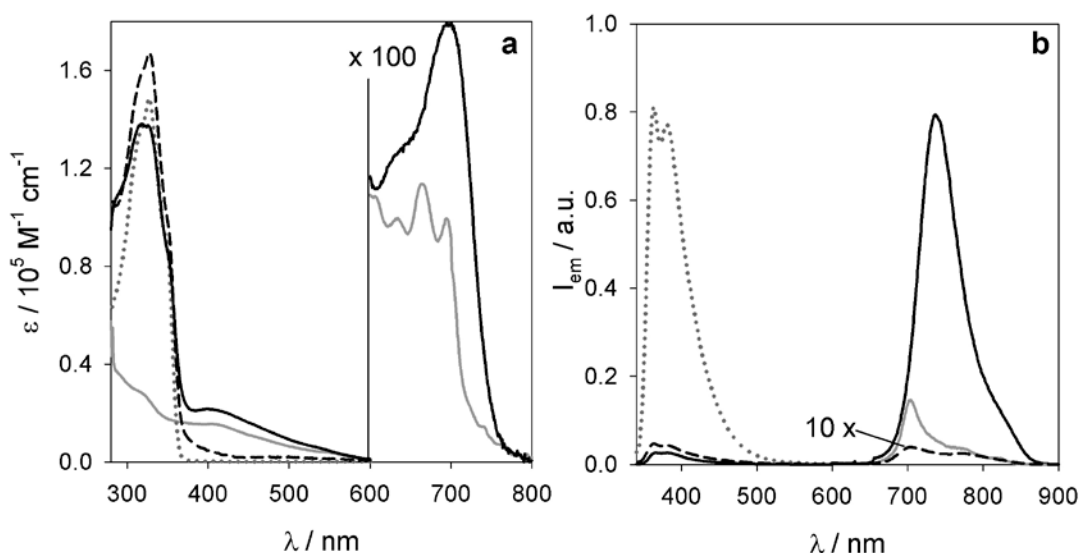
Figure 9, Spectres d'absorption (a) et d'émission (b) du composé **20** (ligne pleine noire), **16** (ligne pointillée noire), **15** (ligne pointillée grise), et $Y_3N@C_{80}$ (ligne pleine grise) dans une solution de toluène désoxygénée, à 298 K et λ_{ex}= 325 nm.
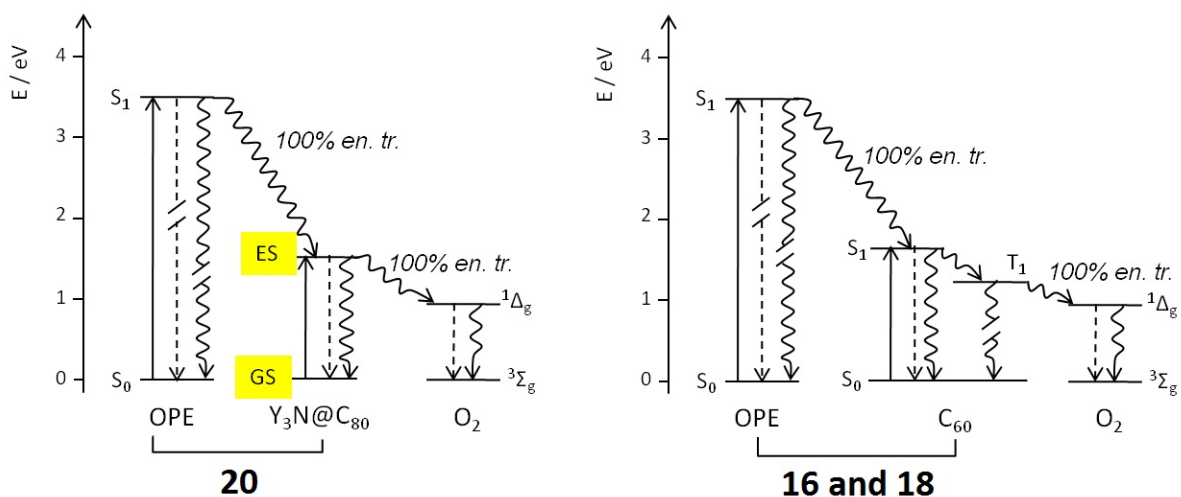
Figure 10 Diagrammes de niveaux d'énergie pour les composes **16**, **18** et **20** montrant les préocessus radiatifs (lignes droites) et non-radiatifs (lignes en vagues) les plus importants.

OPV
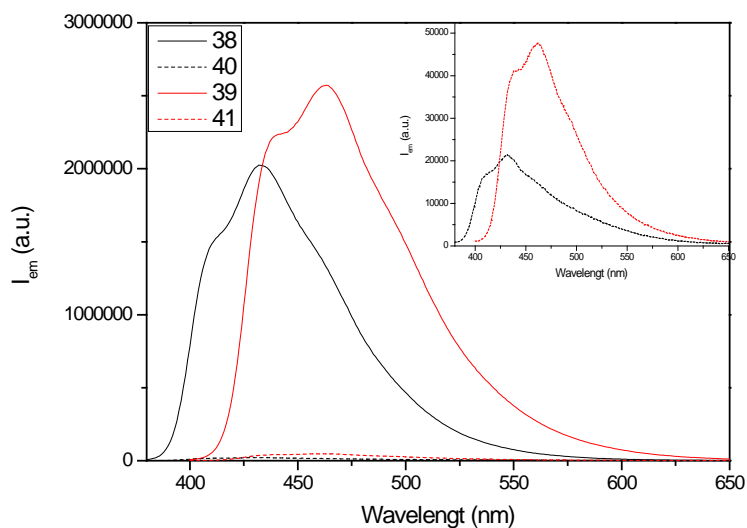
Figure 11 Spectres de fluorescence des composés **38**-**41** dans le dichloromethane (λ_{ex} = 370 nm et 390 nm pour l'OPV-3 et l'OPV-4 respectivement). Insert: amplification des spectres obtenus pour les diades **39** et **41**.

Agents de contraste en IRM

L'hydrosolubilité, la biocompatibilité et la non-toxicité sont des propriétés pré-requises à l'élaboration d'agents de contraste pouvant être administrés *in vivo*. Nous avons donc choisi de fonctionnaliser le $Gd_3N@C_{80}$ par une structure dendritique de type oligoéthylène glycol (OEG) car les OEG sont bien connus pour leur furtivité et leur non-toxicité.
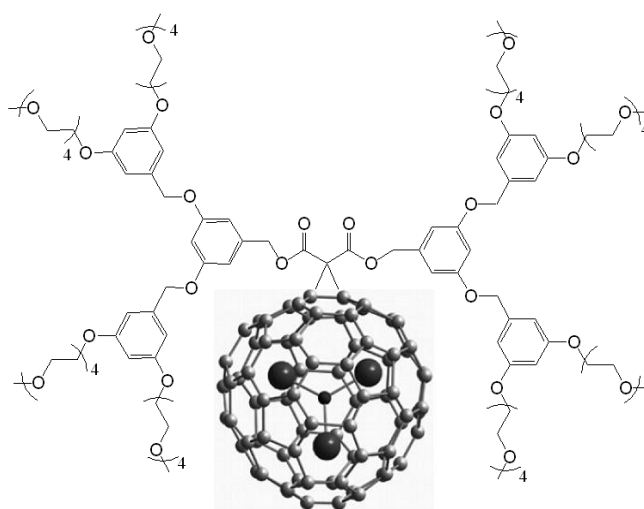
Figure 12 TNT dendritique en tant qu'agent de contraste T1 pour l'IRM
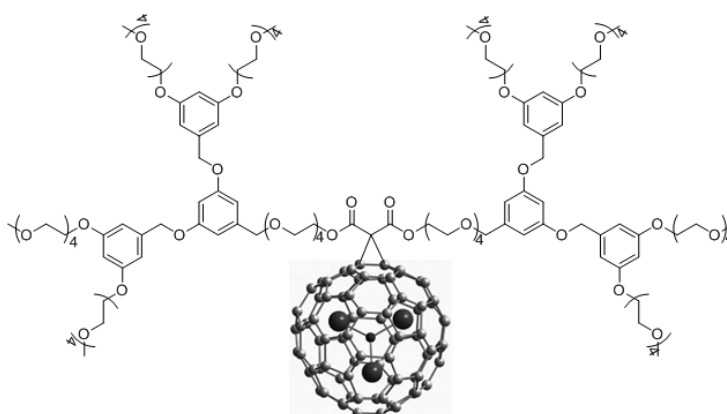
L'avantage du TNT fullerène $Gd_3N@C_{80}$ est de réduire très fortement la toxicité des ions Gd^{3+} du fait de leur encapsulation dans la sphère de carbone. Ceci est particulièrement important pour des patients souffrant d'insuffisance rénale pour lesquels l'administration de chélates macromoléculaires de gadolinium actuellement utilisés en routine dans les examens d'IRM ne peut pas être effectuée sans de fortes probabilités d'effets secondaires très sévères. Nous avons effectué plusieurs tests de synthèse et de purification du TNT-dendritique tel que décrit Figure 9. Des études IRM *in vitro* sont actuellement en cours.

Annex I

Tether-directed bisfunctionalization of C_{60}

Our group has reported earlier the hexaaddition of **A4** based malonate on C_{60}2. Surprisingly, this polyadduct showed liquid-crystalline properties and nematic texture even though no mesogenic unit was used for the synthesis. These findings inspired us to synthesize the bisudduct of C_{60} (**A6**) and $Gd_3N@C_{80}$ (**17b**) by tether-directed remote fictionalization and by using the same building blocks for the synthesis of bismalonates. We supposed that the regioselective double cyclopropanation reaction between the fullerene and non-mesomorphic, bismalonate units could also lead to liquid-crystalline product.

The hydroxyl group of dimethyl 5-hydroxyisophthalate was protected with TBDMS and its methyl ester groups were reduced with $LiAlH_4$ afterwards to give diol **A2**. The reaction of **A2** with Meldrum's acid at high temperature gave **A3**, which was esterified with **A4** (which was prepared by Hind Mamlouk-Chaouachi according to the process summarized in Scheme 2) under mild conditions, in the presence of DCC, DPTS and 4-ppy. The Bingel-type tether directed[1] cyclopropanation reaction between bismalonate **A5** and C_{60} led to the regioselective formation of bisaduuct **A6** (Scheme 1). The same conditions were used in an attempt to functionalize $Gd_3N@C_{80}$, but it failed to give any identifiable product.
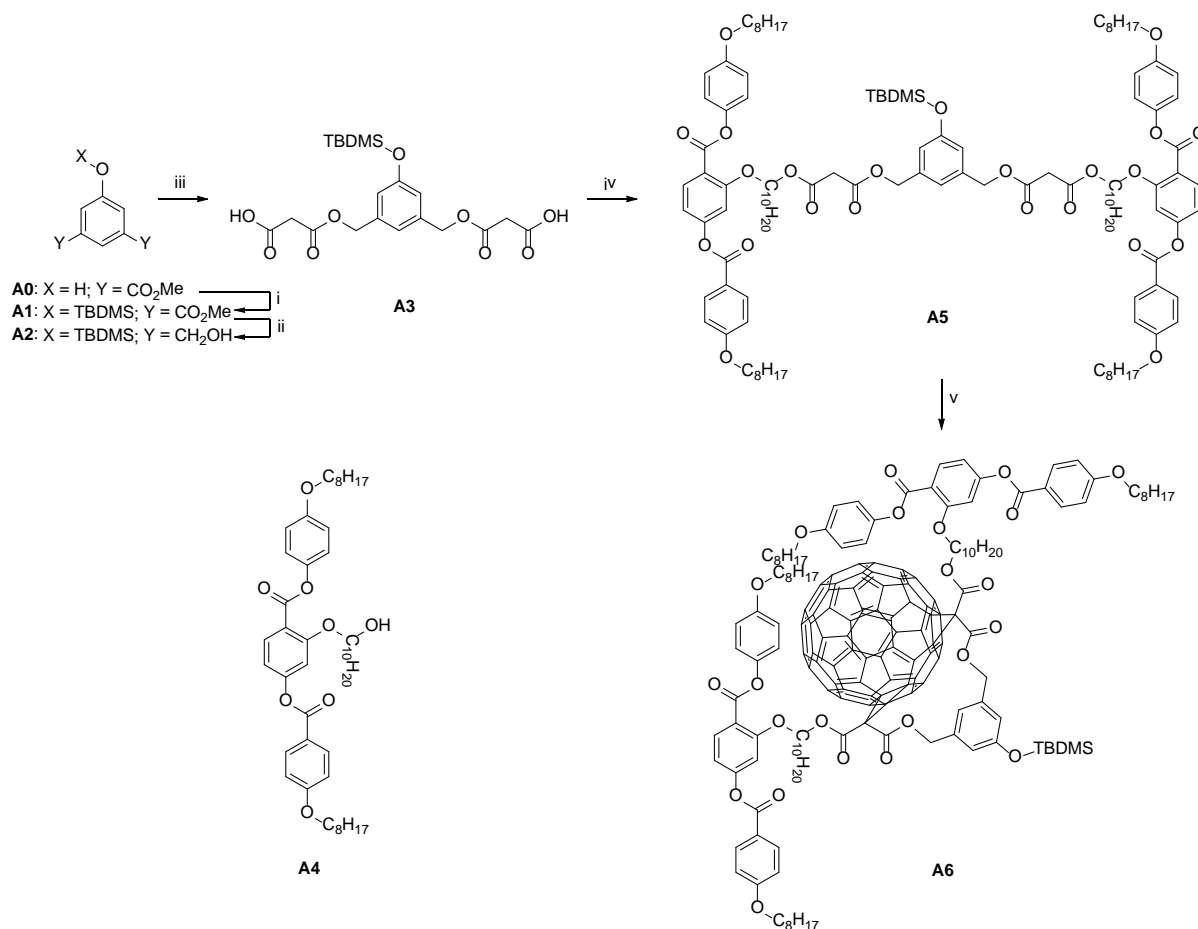
Scheme 1, Tether directed functionalization of bismethanofullerene **A6**. Reagents and conditions : (i) TBDMSCl, 0 °C, xh (89%); (ii) LiAlH$_4$, THF, 0 °C to RT, 3.5h (74%); (iii) Meldrum's acid, 120°C, 4h (100%); (iv) **A4**, DCC, DPTS, 4-ppy, DCM, RT, 24h (89%); (v) C$_{60}$, DBU, I$_2$, toluene, RT, 24h (24%); (iv) Gd$_3$N@C$_{80}$, DBU, I$_2$, o-DCB, RT, 24h (not yet purified)
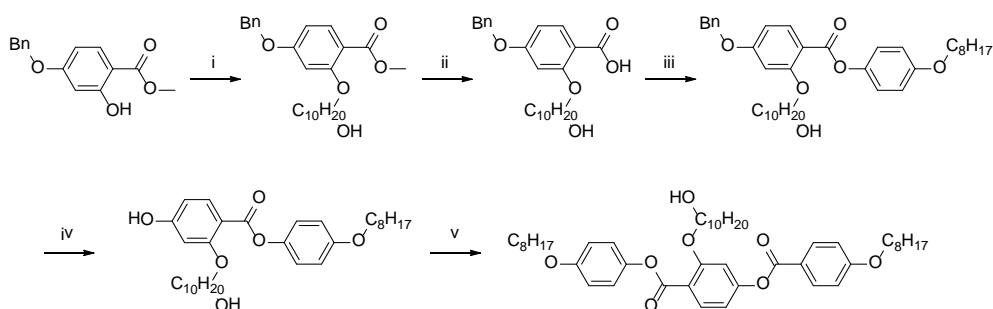
Scheme 2, Synthesis steps of compound **A4**. Prepared by Hind Mamlouk-Chaouachi[2].

The structural analysis of **A6** confirmed the regioselective bisadduct formation. But in contrast to the hexakisadduct built up from the same non-mesogenic promoters (Figure 1), it does not show supramolecular self-organization and liquid crystalline properties.
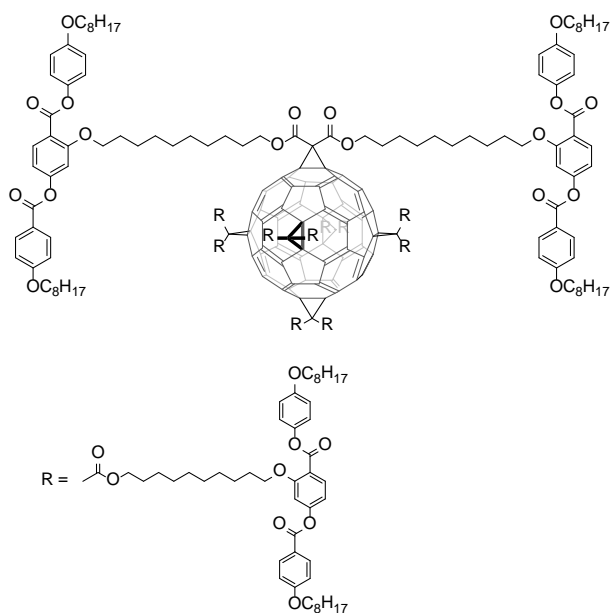
Figure 1, Structure of mesomorphic hexakisadduct built up of non-mesogenic promoters **A4**.

[1] L. Isaacs, R. F. Haldimann, F. Diederich, *Angew. Chem. Int. Ed.*, **1994**, *33*, 2339.

[2] H. Mamlouk, B. Heinrich, C. Bourgogne, B. Donnio, D. Guillon and D. Felder-Flesch, *J. Mater. Chem*., **2007**, *17*, 2199-2205.

Annex II

Cyclic voltammograms
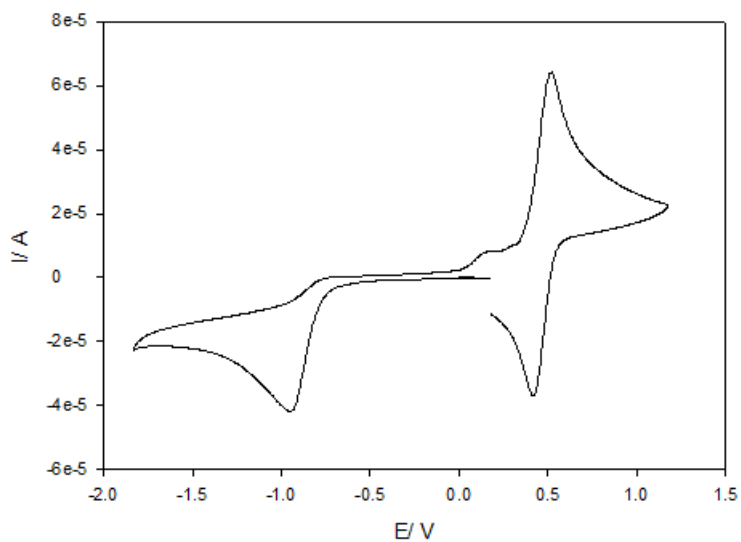
Figure 1, Cyclic voltammogram of **15**.
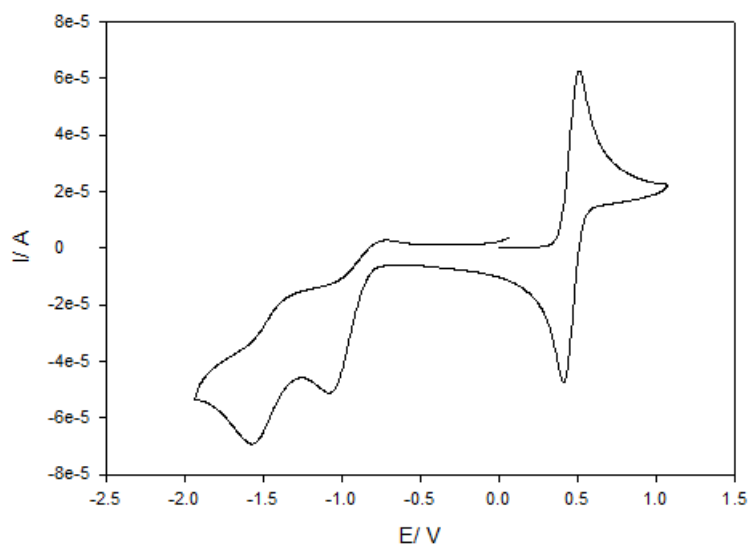
Figure 2, Cyclic voltammogram of **17**.
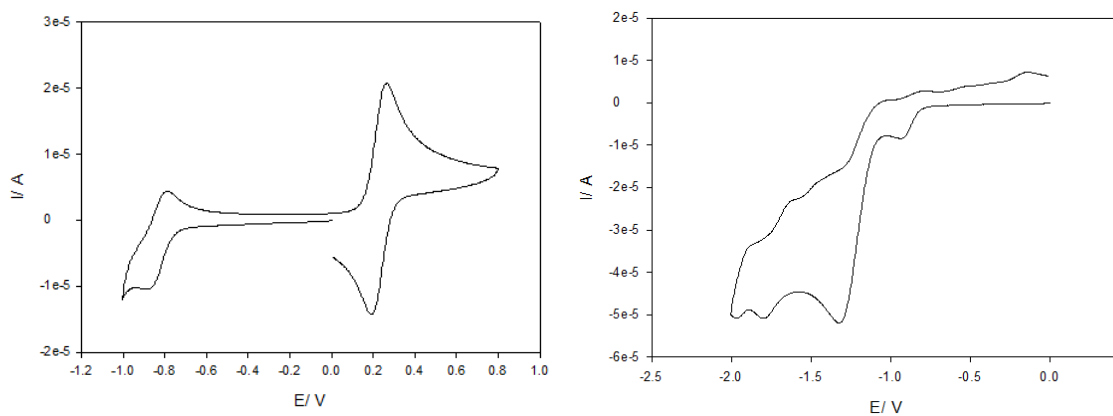
Figure 3, Cyclic voltammograms of **16**.
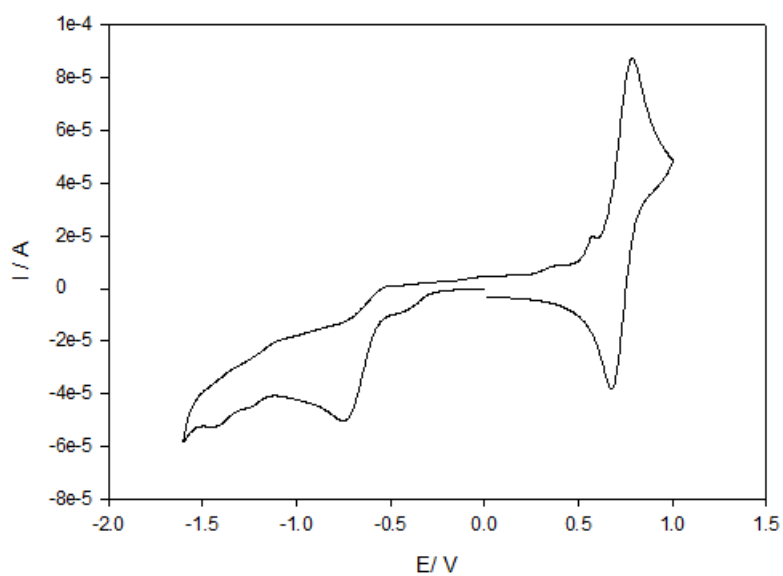
Figure 4, Cyclic voltammograms of **18**.

Annex III

I-V characteristics of the test transistors
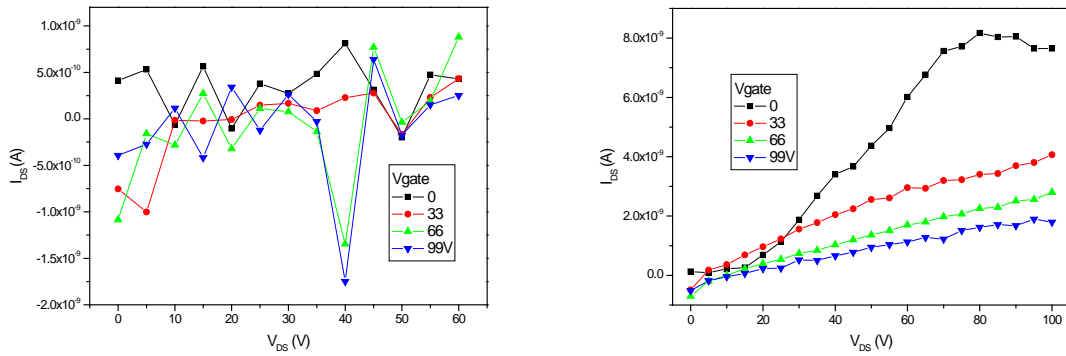
Figure 1, I-V characteristics of **18** for (left) 20µm and (right) 2.5µm channel lengths at different gate voltages before annealing.
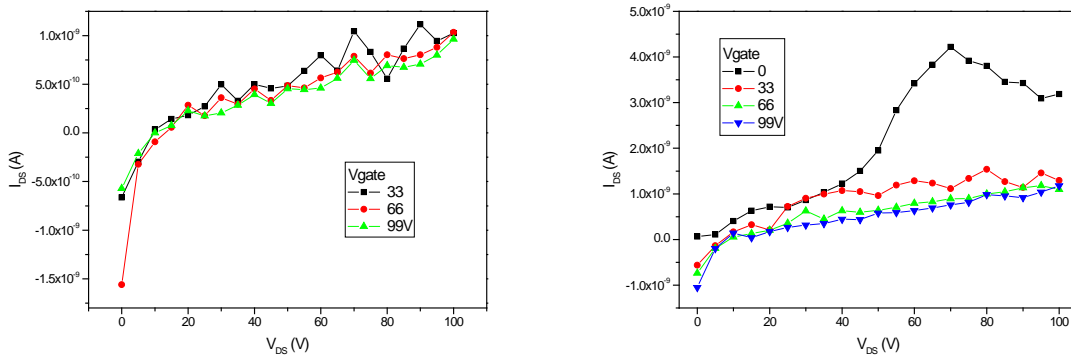
Figure 2, I-V characteristics of **18** for (left) 20µm and (right) 2.5µm channel lengths at different gate voltages after annealing.
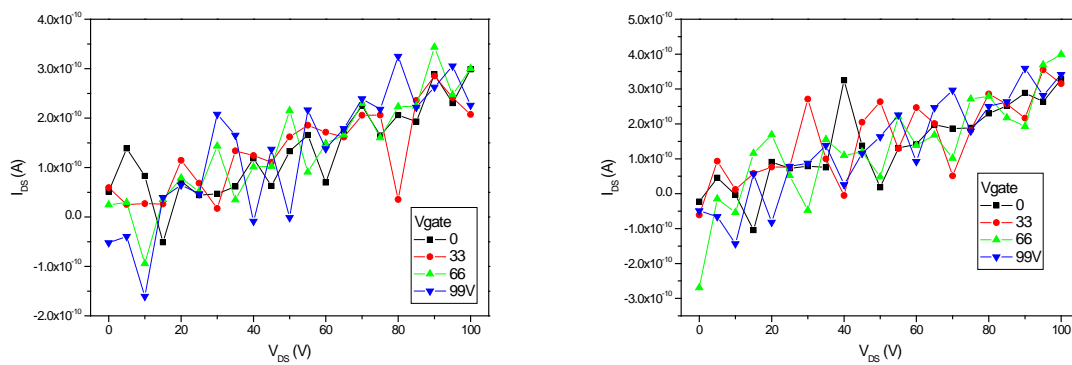
Figure 3, I-V characteristics of **16** for (left) 20µm and (right) 2.5µm channel lengths at different gate voltages before annealing.
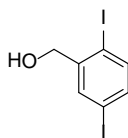
Compound 1b
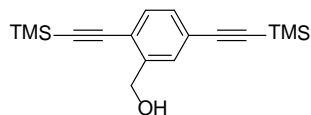
Compound 2
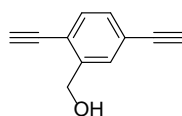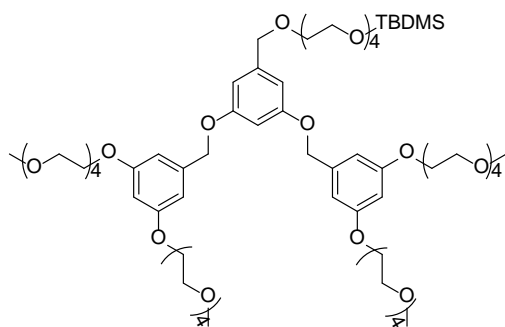
Compound 3
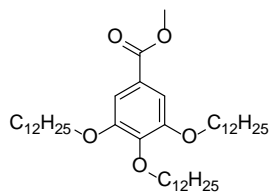
Compound 4
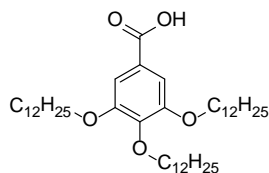
Compound 5
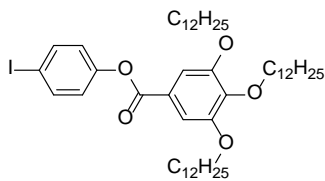
Compound 6
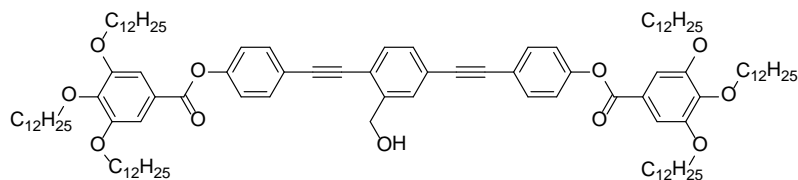
Compound 7
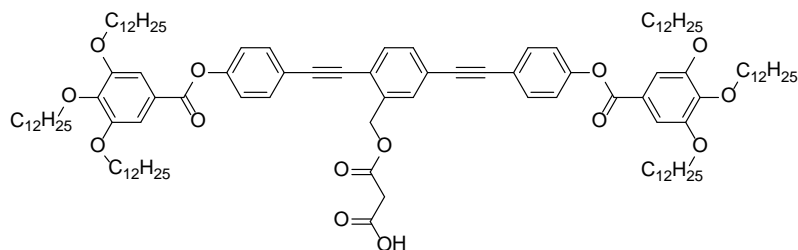
Compound 8
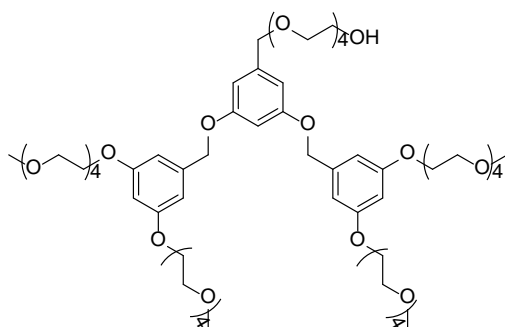

Compound 9
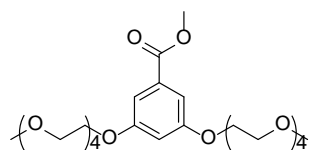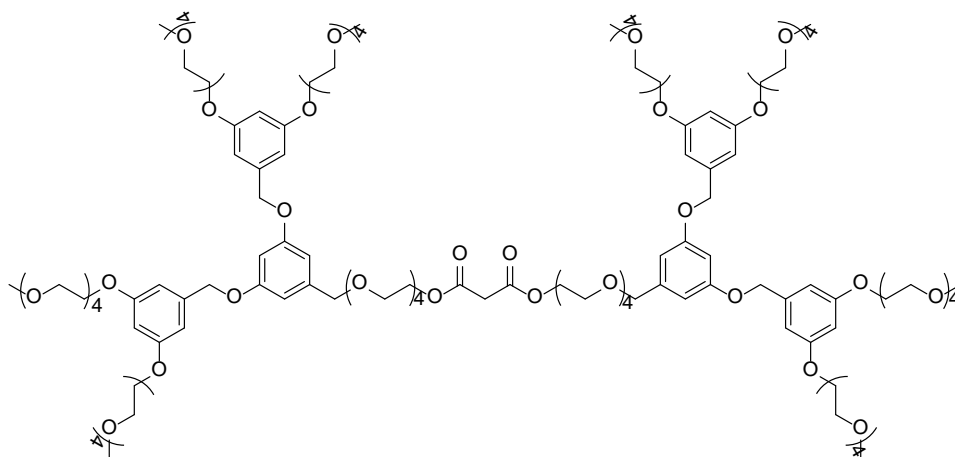

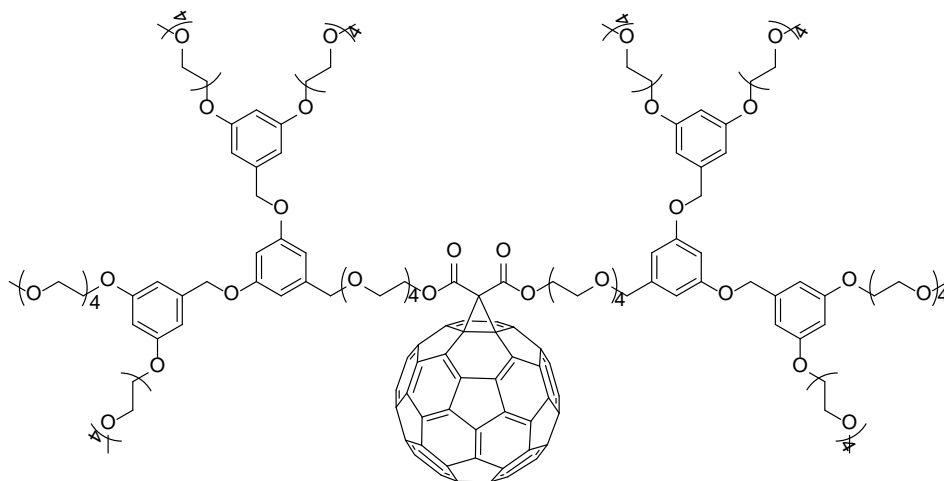**Compound 10**
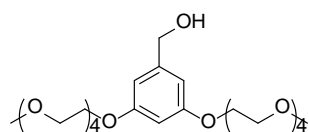
Compound 11
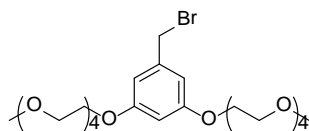
Compound 12
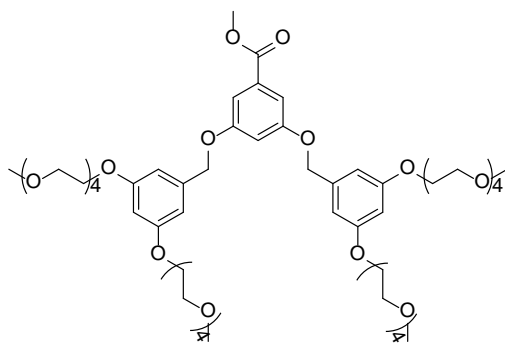
Compound 13
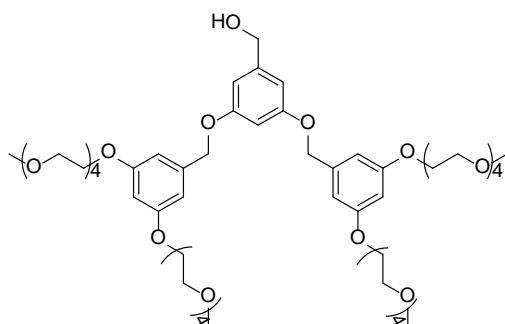
Compound 14
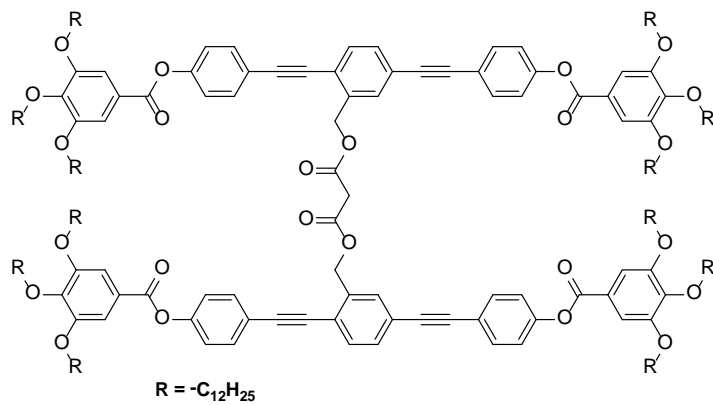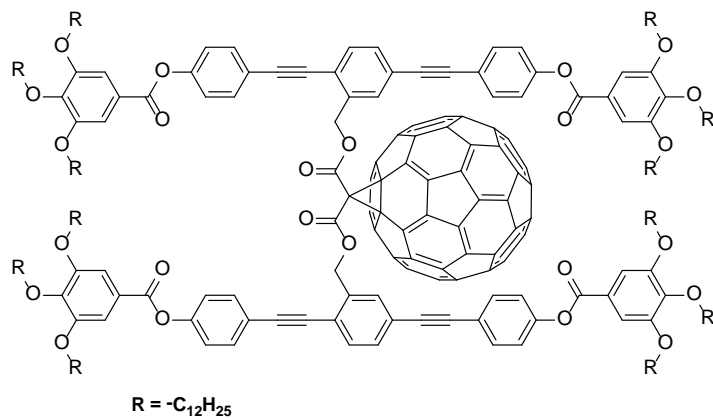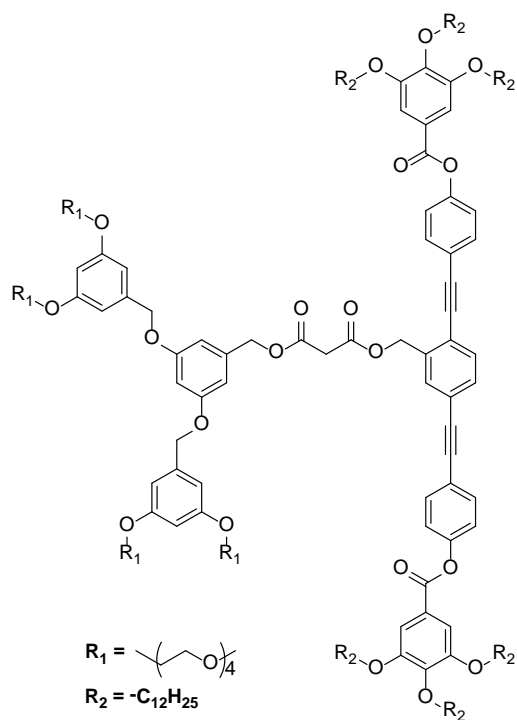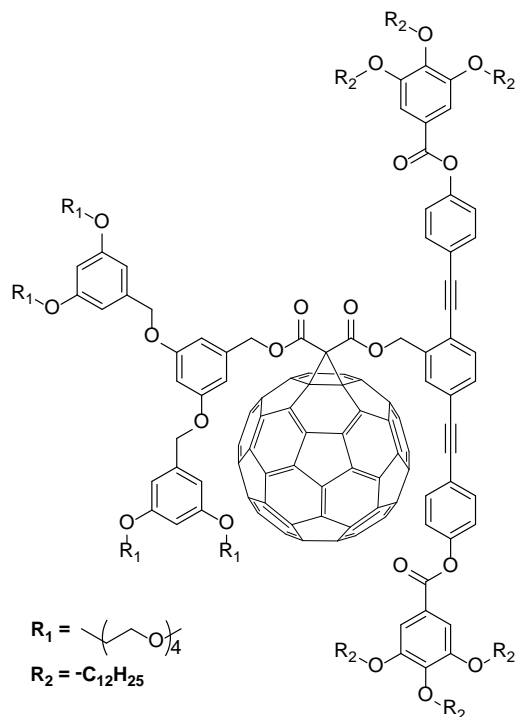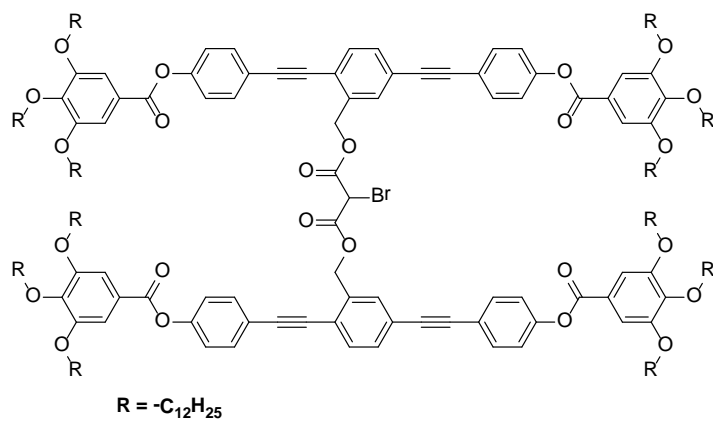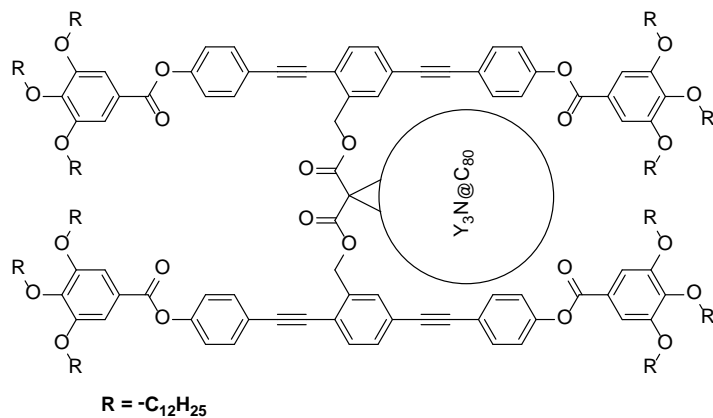
R = -C$_{12}$H$_{25}$

Compound 15

R = -C₁₂H₂₅

Compound 16

$R_1 = \left(\!\!\!\!\! \diagdown\!\!\diagup O \right)_4$

$R_2 = $ -C₁₂H₂₅

Compound 17

$R_1 =$ $\left(\diagdown\diagup O \right)_4$

$R_2 = -C_{12}H_{25}$

Compound 18

$R = -C_{12}H_{25}$

Compound 19

$Y_3N@C_{80}$

$R = -C_{12}H_{25}$

Compound 20

OH

$C_{12}H_{25}$O—⬡—O$C_{12}H_{25}$

O–$C_{12}H_{25}$

Compound 21

O

$C_{12}H_{25}$O—⬡—O$C_{12}H_{25}$

O–$C_{12}H_{25}$

Compound 22

$C_{12}H_{25}$O—⬡—O$C_{12}H_{25}$

O–$C_{12}H_{25}$

Compound 23

Br—⬡—CH=CH—⬡

O–$C_{12}H_{25}$

O–$C_{12}H_{25}$

O–$C_{12}H_{25}$

Compound 24

O

TBDMS–O

Compound 25

TBDMS–O
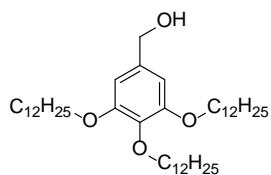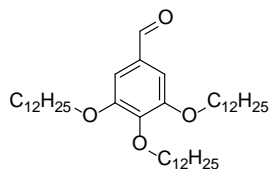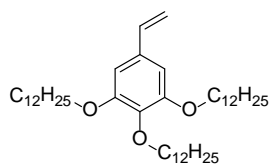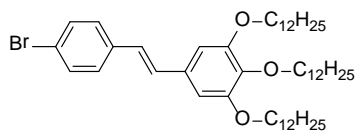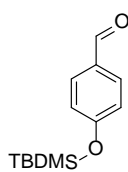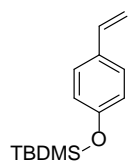
Compound 26

236
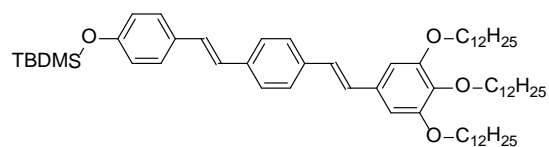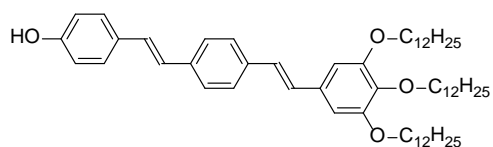
Compound 27

Compound 28
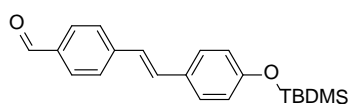
Compound 29
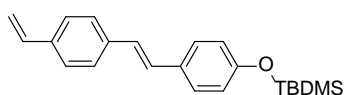
Compound 30
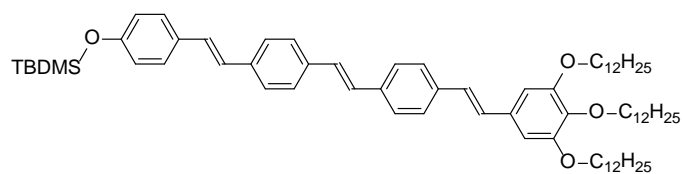
Compound 31
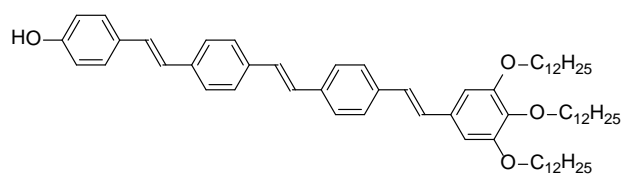
Compound 32
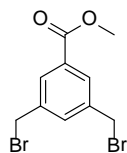
Compound 33
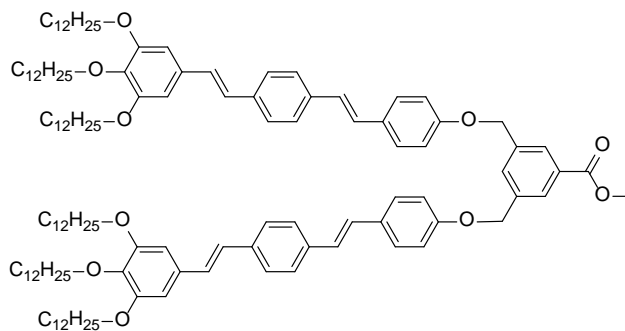
Compound 34
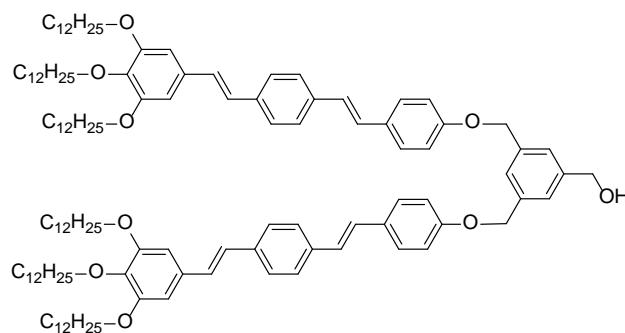
Compound 35
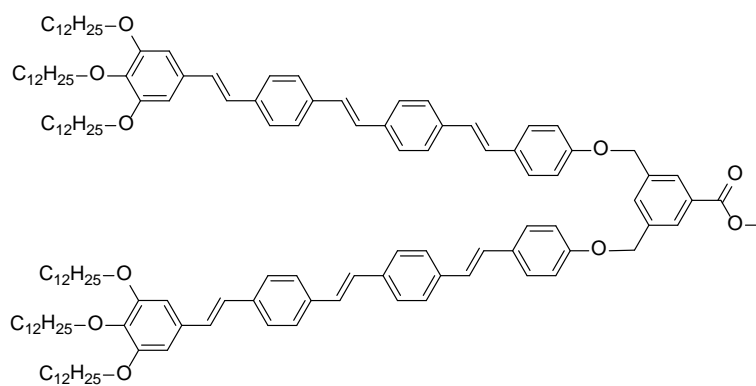
Compound 36
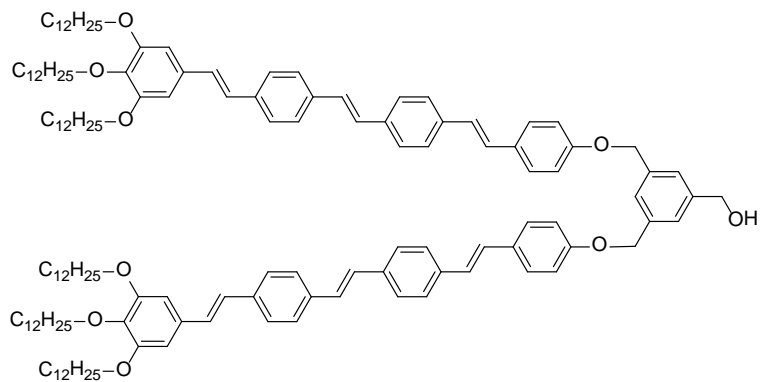
Compound 37
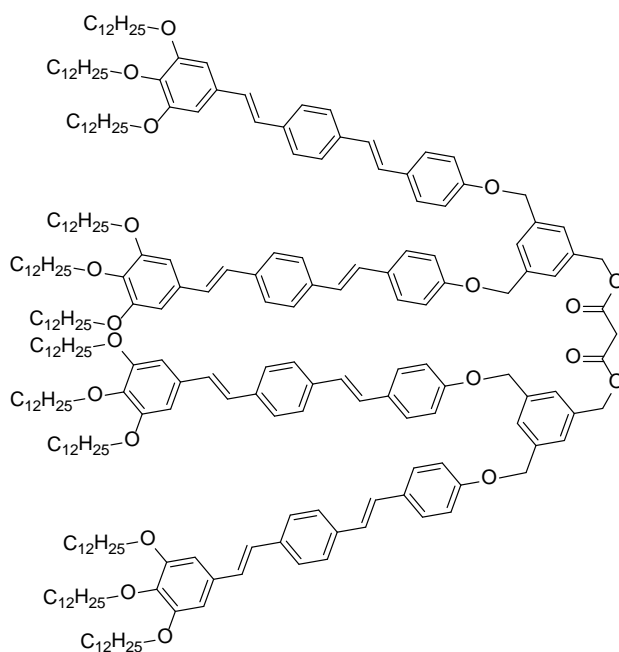
Compound 38
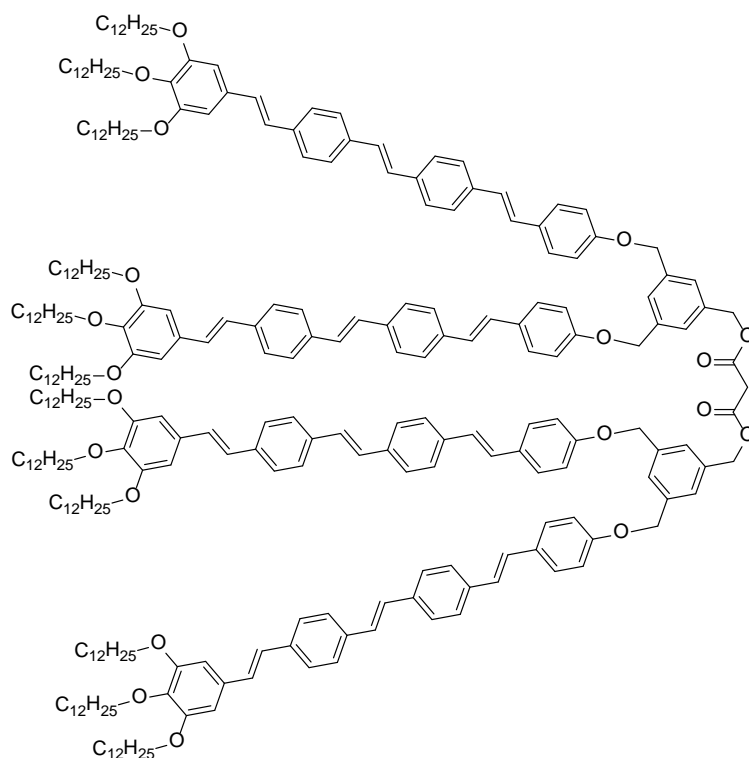
Compound 39
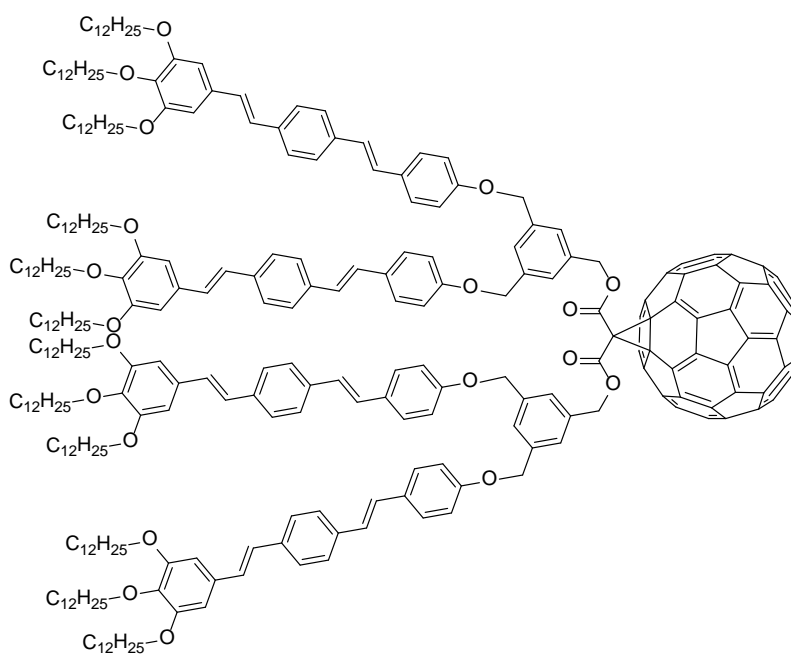
Compound 40

240
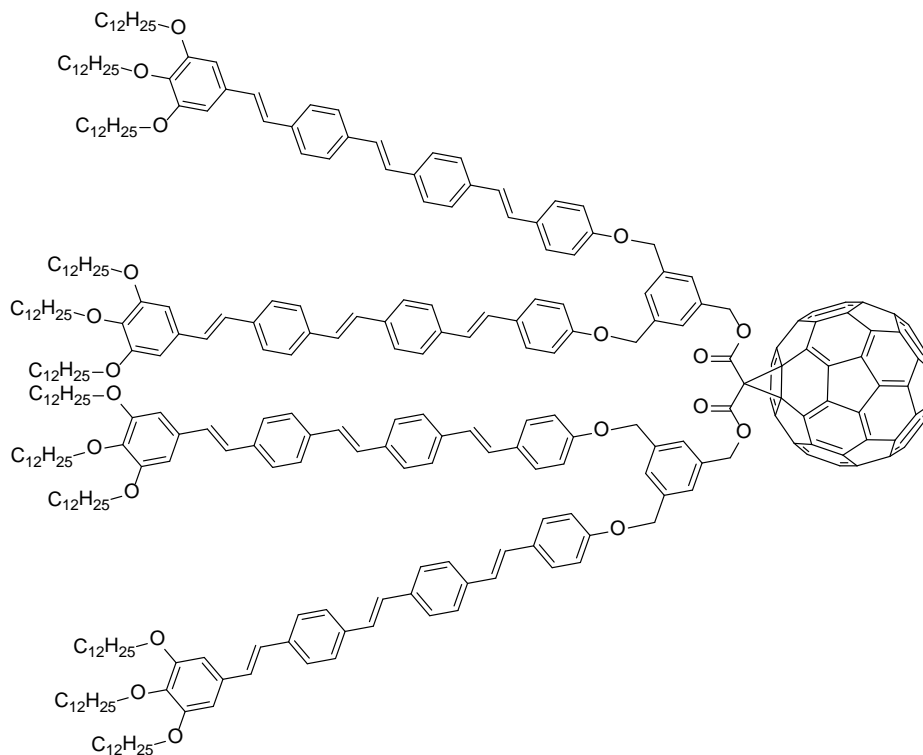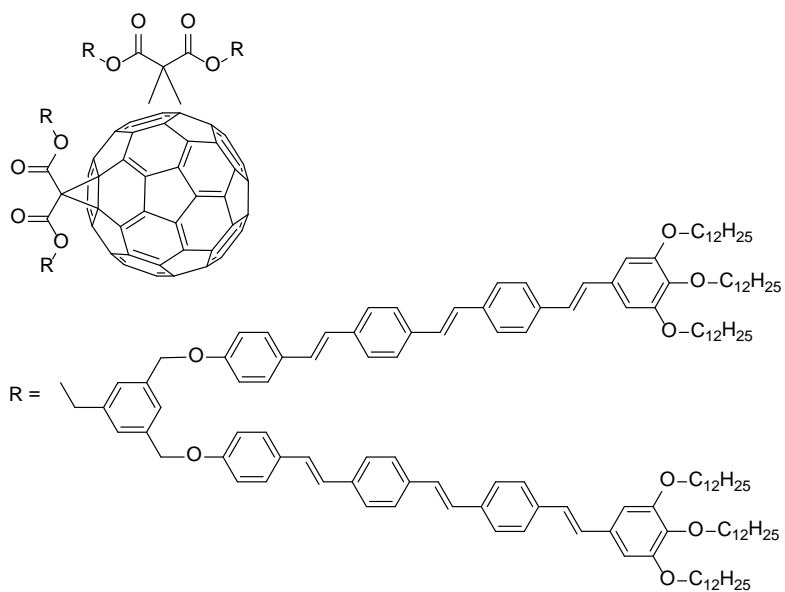
Compound 41

Compound 41bis
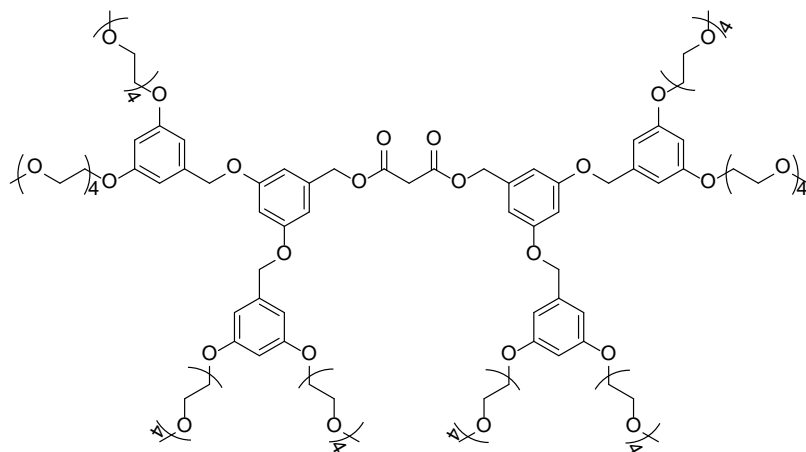
Compound 42
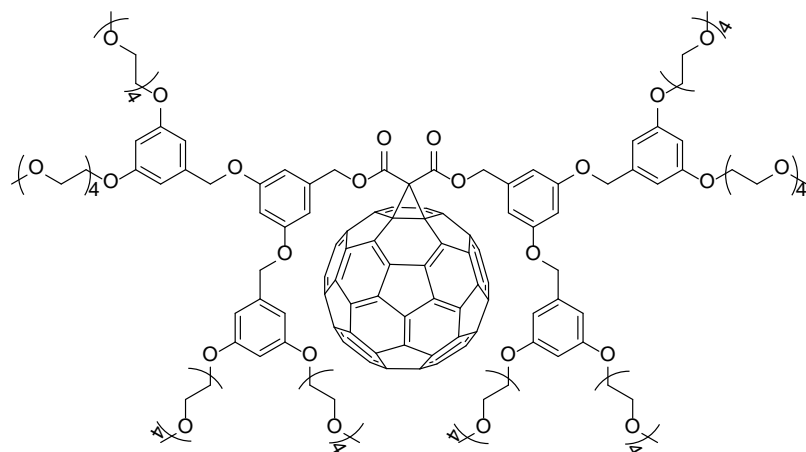
Compound 43
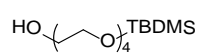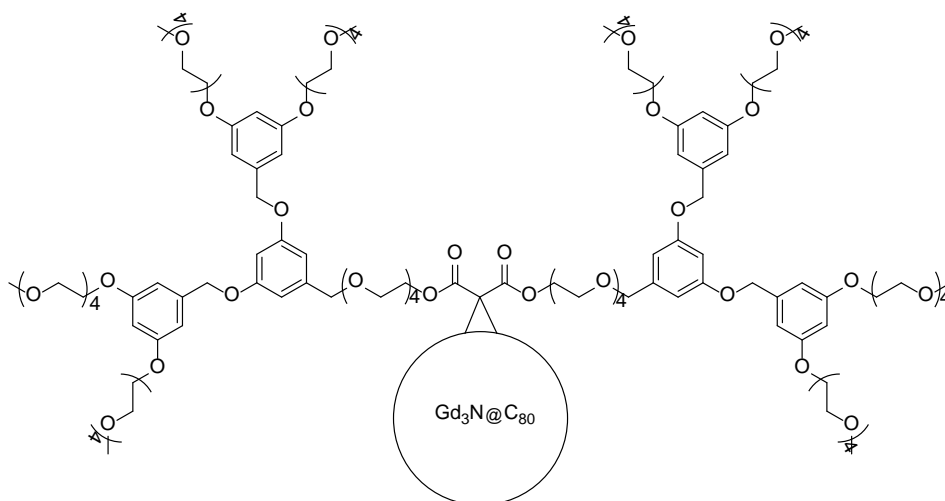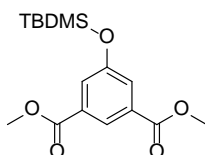

Compound 44
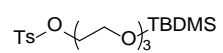
Compound 45

Compound 46

Compound 47

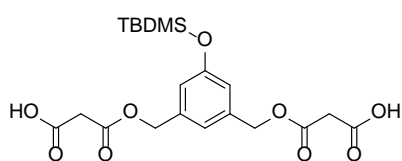**Compound 48**

243
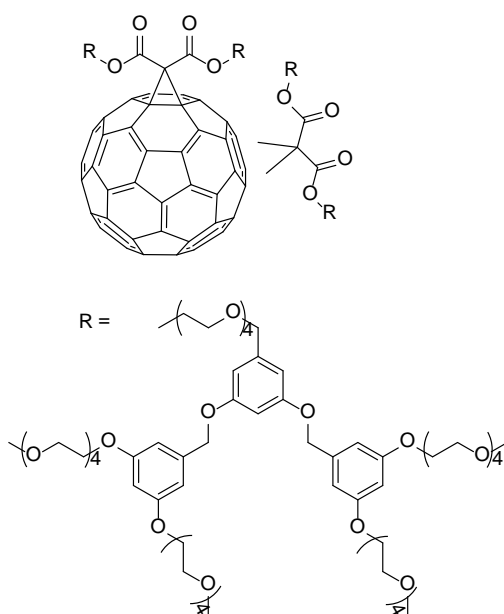
Compound 49
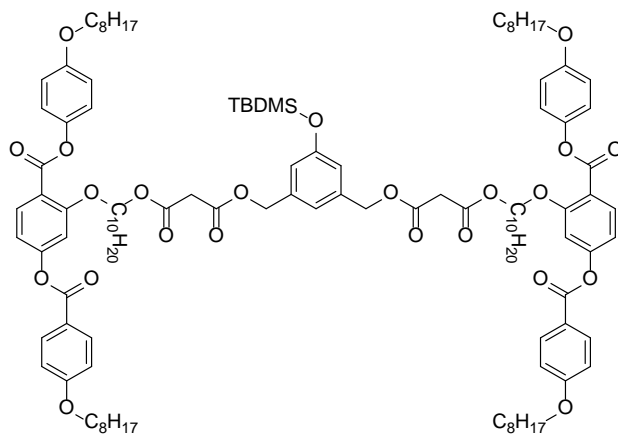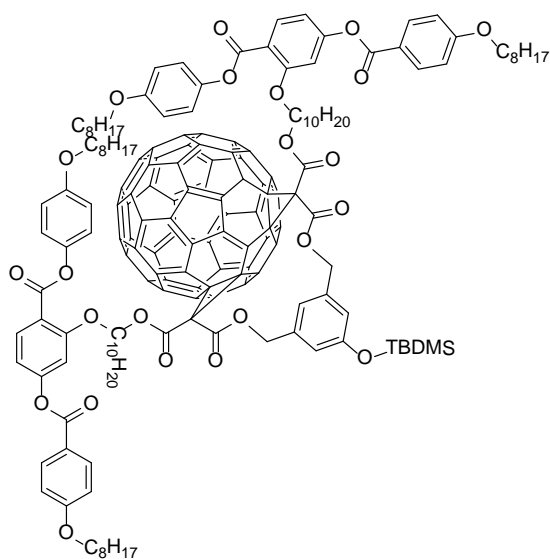

Compound 49bis

Compound 50

Designed structure of compound 51

Compound 52

Compound 53
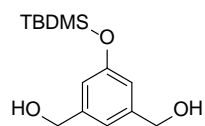
Compound A1

Compound A2

Compound A3
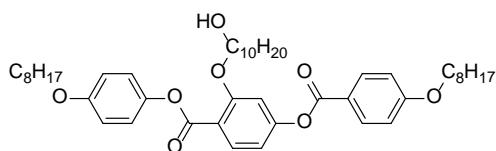
Compound A4

Compound A5

Compound A6

Kalman TOTH

Fonctionnalisation d' (endo)fullerène: de la science des matériaux aux applications biomédicales

Matériaux pour la science des matériaux

Nous avons synthétisé différentes dyades donneurs-accepteurs (D-A) π-conjuguées à base de fullerène pour des applications photovoltaïques dans lesquelles les unités D étaient soit des oligophenylenevinylenes (OPV) soit des oligophenyleneethynylene (OPE) et les unités A étaient le C60 ou un endofullerène du type Y3N@C80. Il y avait une exigence supplémentaire pour nos matériaux, à savoir qu'ils devaient s'auto-organiser en phases liquides-cristallines. Pour ce faire, toutes les unités D contenaient un promoteur mésogène afin d'induire le mésomorphisme de la dyade D- et donc de contrôler la morphologie des couches minces nécessaires à l'élaboraiton des cellules photovoltaïques grâce à une organisation supramoléculaire. En dehors de cela, nous avons étudié l'influence de la nature chimique du donneur (par exemple lyophile ou amphiphile), de la longueur des oligomères et de la multiaddition sur les propriétés photophysiques et sur l'auto-assemblage.

Nous avons synthétisé une dyade OPE-Y3N@C80 qui est le premier dérive mésomorphe et photosensible de ce type de métallofullerène endohédral.

Les applications biomédicales

Un dérivé dendritique hautement biocompatible de Gd3N@C80 a été synthétisé en tant qu'agent de contraste IRM de nouvelle génération (ne présentant pas de toxicité liée au ions Gd3+).

Mots clés: Fullerènes, Métallofullerènes endohédraux nitride trimétalliques, Liquides-cristalline, Photovoltaïques, Agent de contraste IRM

Materials for materials science

We have synthesized different π-conjugated system-fullerene dyads for photovoltaic applications, where the donor units were either oligophenylenevinylene (OPV) or oligophenyleneethynylene (OPE) derivatives and for the acceptor, C60 or Y3N@C80 was used. There was an additional requirement for our materials: liquid crystallinity. All the donor units contained a mesogenic promoter in order to induce mesomorphism in the D-A dyad and to control the morphology of the prepared film through supramolecular organization. Apart from that, we investigated the effect of the chemical nature of the donor moiety (ie. lyophilic or amphiphilic), the oligomeric length and multiaddition on the photophysical properties and on the self-assembly.

We have synthesized an OPE-Y3N@C80 dyad which is the first trimetallic nitride template endohedral metallofullerene derivative with mesomorphic and photoactive properties.

Biomedical applications

A tetraethylene glycol (TEG) dendron derivatized Gd3N@C80 adduct was synthesized as a potentially safe, new generation MRI contrast agent.

Key words: Fullerenes, Trimetallic nitride template endohedral metallofullerene, liquid crystal, photovoltaics, MRI contrast agent